UNIVERSIDAD DE CANTABRIA

ESCUELA DE DOCTORADO DE LA UNIVERSIDAD DE CANTABRIA
DOCTORADO EN *BIOLOGÍA MOLECULAR Y BIOMEDICINA*

TESIS DOCTORAL

Nuevas interacciones de la proteína MNT y su efecto en regulación transcripcional

PhD THESIS

Novel interactions of MNT protein and their effect on transcriptional regulation

---

Presentada por: **Judit Liaño Pons**

Dirigida por: **Prof. Javier León Serrano**

- 2019 -

Por la presente informo que JUDIT LIAÑO PONS ha completado su tesis doctoral, titulada: "**Nuevas interacciones de la proteína MNT y su efecto en regulación transcripcional"**

Este trabajo se ha realizado bajo mi dirección y en el mismo identifica una nueva interacción con el factor de transcripción MNT, implicada en oncogénesis con las proteína REL. También demuestra la autorregulación negativa de MNT y su capacidad de formar homodímeros que regulan la expresión de otros genes

Todos estos resultados son originales y obtenidos con la metodología apropiada.

Considero que esta Tesis está finalizada y lista para ser depositada y defendida, dentro del programa de doctorado de Biología Molecular y Biomedicina de la Universidad de Cantabria

Santander, 25 de junio de 2019

Firmado: Javier León Serrano

Catedrático de Bioquímica y Biología Molecular de la Universidad de Cantabria

Esta Tesis ha sido realizada en el Instituto de Biomedicina y Biotecnología de Cantabria (IBBTEC) perteneciente a la Universidad de Cantabria (UC) y al Consejo Superior de Investigaciones Científicas (CSIC), en Santander (Cantabria, España).

La financiación para la realización de esta Tesis doctoral ha sido proporcionada por el Ministerio de Educación y Ciencia (SAF2014-53526-R), (MINECO/FEDER, UE), (SAF2017-88026-R), (AEI/FEDER, UE).

El autor de esta Tesis ha disfrutado de una ayuda para la formación de profesorado universitario (FPU) (referencia FPU14/01786), concedida por el Ministerio de Educación y Formación Profesional.

Agradecimientos generales

Primero de todo, quiero agradecer enormemente a mi director de Tesis, Javier León, por apoyarme siempre y darme todas las oportunidades del mundo para que pudiera crecer como científica, pero también como persona. Gracias por tu confianza, por transmitirme tu curiosidad y pasión por la ciencia, por sacar siempre tiempo para mí y por esas conversaciones sobre todas las posibles e importantes funciones de MNT, con MAX y sin MAX. Siempre recordaré lo afortunada que he sido por tenerte a ti como director de Tesis.

Gracias también a M. Dolores Delgado por toda su ayuda durante estos años, por preocuparse siempre por nosotras y estar ahí para cualquier cosa que necesitáramos. Gracias además por la revisión y los consejos tan valiosos en la escritura de esta Tesis.

En definitiva, gracias, Javier y Dolo por crear un equipo tan bueno, una gran familia y un ambiente tan positivo en el que hacer ciencia es todo un placer.

Gracias también al resto de jefes de grupos vecinos por su ayuda directa o indirecta en la realización de este trabajo. Especialmente, gracias a los profesores del Departamento de Biología Molecular por hacerme un hueco en las clases de *Bioquímica* y *Molecular Biology*. Gracias a Nacho por toda la ayuda en los *lab meetings*, por su trabajo en el proyecto de MNT y por estar siempre dispuesto a resolver todas las dudas bioinformáticas.

Gracias, Anna Bigas y Lluís Espinosa por aceptarme en vuestro laboratorio y por ayudarme a avanzar en el mundo inexplorado de MNT en la ruta de NF-κB ("kappa" y no "k"). Muchas gracias a Carlota Colomer, por estar siempre dispuesta a resolver mis dudas y a planear mis experimentos.

I would also like to thank Peter J. Hurlin for allowing me to join his Lab for three months and share his knowledge about the MYC network with me. It was a great pleasure to discuss about MNT and to try to solve the unanswered questions about RAS. Thanks, Sara Ota, for all your help and for introducing me to the Shriners family. Thanks, Zhou, for the morning conversations about MNT, MYC and life.

LABORATORIO

Quiero agradecer a todas las personas que han pasado por el 01.01 y que han formado parte de esta gran familia.

Primero de todo, agradecer a MCar por dejarme el legado de MNT, por todo lo que me enseñaste y por todas esas conversaciones en las que nos emocionamos y creamos mil teorías sobre todo lo que puede estar haciendo MNT. Gracias por estar siempre ahí, tanto en el laboratorio como al otro lado del charco. Gracias también al resto del equipo MNT, Fabiana y Alba, que con vuestra ilusión conseguisteis aportar vuestro granito de arena a esta historia.

Después, me gustaría agradecer a Lucía y Ester por toda su ayuda, su motivación y por estar ahí siempre para compartir las ilusiones y las frustaciones. Formamos un gran equipo. Gracias a Lore por ser mi compañera de las mañanas y a Alex, por llenarnos de vida e ilusión el tiempo que estuviste por aquí.

Gracias, Lorena y Yelina. No sabéis lo que me alegro de poder haber compartido este camino con vosotras. Sin vuestro apoyo esto no habría sido lo mismo. Gracias a todo el equipo del café por ser mi familia del IBBTEC.

Me gustaría agradecer también a todos los grupos vecinos, especialmente a los Nachos y los Pieros, que siempre habéis proporcionado toda vuestra ayuda y habéis demostrado lo importante que es la cooperación en ciencia. Especialmente me gustaría agradecer a Lorena Agudo, por ser una gran persona y una gran científica, y por ayudarme siempre tanto.

LOS INICIOS

Gracias, Marta y Núria, por todo este camino en Biología desde la carrera. Siempre habéis estado ahí, sin importar la distancia o el tiempo sin vernos, con una gran sonrisa y un *Polysiphonia* para cada crisis.

También quiero agradecer a Alberto Bustillos, por enseñarme la ciencia en el Parc Científic de Barcelona, por esos primeros ChIPs y qPCRs y por su amistad.

MÁS ALLÁ DEL LABORATORIO

En primer lugar, muchas gracias a mis padres por apoyarme siempre en todas mis decisiones, por permitirme llegar hasta aquí y por confiar en mí y ayudarme

a resolver todos mis problemas. Mil gracias a mi hermana, Silvia, porque fue ella la que encontró a Javier León y sin esa maravillosa intuición, esta tesis no existiría.

Muchas gracias también a mis amigos fuera del laboratorio, que han escuchado mis historias con ilusión, imaginándose a MNT como una súper heroína. Gracias especialmente a Jimena por esa gran amistad que comenzó en Ecuador.

Finalmente, gracias a Shane por hacerme feliz en esta última fase de tesis y ser ese equilibrio que necesitaba.

Agradecimientos a colaboradores

Gracias a Mónica Molina Edesa y María Cruz Rodríguez González (Servicio de Secuenciación Masiva, IBBTEC, Santander) por su ayuda con el procesamiento y análisis del RNA-seq.

Gracias a Dreamgenics por el análisis del ChIP-seq y al Dr. Ignacio Varela (grupo de Análisis Genómico del Desarrollo Tumoral, IBBTEC, Santander) y a la Dra. Mª Carmen Lafita (Dept. of Cell Biology, University of Texas Southwestern Medical Center, Dallas, Texas) por los análisis adicionales.

Gracias a Sandra Zunzunegui (IBBTEC, Santander) por toda su ayuda en el laboratorio, especialmente con el clonaje de plásmidos.

Gracias al Dr. Víctor M. Campa (Servicio de Microscopía, IBBTEC, Santander) por su ayuda con la microscopía de fluorescencia, microscopía confocal y el análisis de imágenes.

Gracias al Dr. Peter J. Hurlin (Shriners Hospital for Children, Portland, Oregón) por proporcionarnos los plásmidos de MNT.

Gracias a Dra. Anna Bigas y Dr. Lluís Espinosa (Program in Cancer Research, Research Institute Hospital del Mar (IMIM), Barcelona) por las líneas celulares CEM y LoVo, y por el plásmido luciferasa IκBα-luc

Gracias al Dr. Miguel Ángel Lafarga y Dra. María Teresa Berciano (grupo de Biología Celular del Núcleo, Facultad de Medicina e IDIVAL, Santander) por la línea celular C6.

Gracias a la Dra. Montserrat Céspedes (Grupo de Genes y Cáncer, IDIBELL, Barcelona) por proporcionarnos la línea celular LU165.

Abbreviations

Abbreviations

aa	Amino acid
ALL	Acute Lymphoblastic Leukemia
BSA	Bovine serum albumin
bp	base pair
CDK	Cyclin-dependent kinase
cDNA	Complementary DNA
ChIP	Chromatin immunoprecipitation
ChIP-seq	Chromatin Immunoprecipitation sequencing
Ct	Cycle threshold
C-t	Carboxyl-terminal
CLL	Chronic Lymphocytic Leukemia
CML	Chronic myeloid leukemia
Co-IP	Co-immunoprecipitation
DAPI	4, 6´-diamino-2 phenylindole
DMEM	Dulbecco’s Modified Eagle Medium
DNA	Deoxyribonucleic acid
dNTP	Deoxyribonucleotide triphosphate
DTT	Dithiothreitol
EDTA	Ethylenediamine tetraacetic acid
EGTA	Ethylene glycol tetraacetic acid
EV	Empty vector
FBS	Fetal bovine serum
FDR	False discovery rate

GFP	Green fluorescent protein
GSEA	Gene set enrichment analysis
HDAC	Histone deacetylase
bHLHLZ	Basic helix-loop-helix leucine zipper
IB	Immunoblot
IF	Immunofluorescence
IP	Immunoprecipitation
IgG	Immunoglobulin G
IMDM	Iscove's Modified Dulbecco's Medium
kb	Kilobase
kDa	Kilodalton
KO	Knockout
LB	Lysogeny broth
M	Molar
MB	MYC box
MEF	Mouse embryonic fibroblast
NLS	Nuclear localization signal
NF-κB	Nuclear factor kappa-light-chain-enhancer of activated B-cells
NP-40	Tergitol-type NP-40 (nonyl phenoxypolyethoxylethanol)
PAGE	Polyacrilamide Gel Electrophoresis
PBS	Phosphate buffer saline
PCR	Polymerase chain reaction
PLA	Proximity ligation assay

PEI	Polyethylenimine
PEST	Peptide sequence rich in proline (P), glutamic acid (E), serine (S) and threonine (T)
qPCR	Quantitative PCR
R.L.U.	Relative luciferase units
RNA	Ribonucleic acid
RNAseq	RNA sequencing
r.p.m.	Revolutions per minute
RPMI	Roswell Park Memorial Institute culture medium
RPKM	Reads per kilobase per million reads
RT	Room Temperature
RT-qPCR	Reverse transcription and quantitative PCR
SCLC	Small cell lung cancer
SDS	Sodium Dodecyl Sulfate
shRNA	Short-hairpin RNA
shMNT	shRNA against MNT
shMAX	shRNA against MAX
shMLX	shRNA against MLX
shREL	shRNA against REL
TAE	Tris-acetate-EDTA buffer
TBS-T	Tris buffer saline –Tween 20
TE	Tris-EDTA buffer
TNFα	Tumor necrosis factor α
TSS	Transcription start site
WT	Wild-type

List of figures and tables

List of figures

Introduction

Materials and Methods

Results

Discussion

List of tables

Materials and Methods

Results

Annexes

Index

Index

Introduction

1. Introduction

1.1. The MYC-MAX-MXD-MLX network

The proto-oncogene *MYC* is a basic helix loop helix leucine zipper (bHLHLZ) transcription factor and a master regulator of several processes inside the cell, from transcription to protein biosynthesis, going through cell adhesion, cell cycle, metabolism and DNA repair (Conacci-Sorrell et al., 2014; Dang, 2012). MYC forms heterodimers with MAX and binds to E-boxes on the DNA. MYC is usually considered a transcriptional activator (Amati et al., 1992) but it can also repress some of its target genes (Schneider et al., 1997). On the other side of the network, we can find the MXD proteins MXD1, MXD2/MXI1, MXD3 and MXD4, MNT and MGA, which also bind to MAX and usually act as transcriptional repressors and MYC antagonists (Hurlin, Quéva and Eisenman, 1997; Hurlin *et al.*, 1999; Sommer *et al.*, 1999; Carroll *et al.*, 2018). MXD1, MXD4 and MNT can also interact with MAX-like protein X (MLX) (Billin et al., 1999; Meroni et al., 2000), which also binds to MLXIP (MONDOA) and MLXIPL (MONDOB/ChREBP), involved in nutrient sensing and metabolic stress (Diolaiti et al., 2015; Wilde and Ayer, 2015). These proteins and its interactions establish a complex network that regulates cell proliferation, differentiation and metabolism.

1.1.1. MYC family of proteins

MYC was discovered as the oncogene v-*myc* found in the retroviruses MC29, CMII, MH2 and OK10. Its name derives from the leukemia called **my**elo**c**ytomatosis that it caused in chickens. Later, its cellular form located in human chromosome 8q24 was found and named as c-*MYC* (*MYC* in HUGO nomenclature) (Duesberg and Vogtt, 1979; Sheiness and Bishop, 1979; Vennstrom et al., 1982). Then, two MYC paralogues were identified, *MYCN* and *MYCL*, which encode for N-MYC and L-MYC proteins, respectively (Kaye et al., 1988; Kohl et al., 1983; Nau et al., 1986; Stanton et al., 1986). Since MYC's

discovery, thousands of publications have proved its important and unique role in the cell, both in physiological and in pathological conditions.

N-MYC was first found in neuroblastoma, where it is amplified in 50% of the cases (Stanton et al., 1986). *MYCN* overexpression can also drive tumorigenesis of retinoblastomas, medulloblastomas, lymphoma, acute myeloid leukemia and small cell lung cancer (Rickman et al., 2018). On the contrary, L-MYC was found amplified or overexpressed in human small cell lung cancers (Nau et al., 1986; Romero et al., 2014). Both *MYCN* and *MYCL* display transforming cooperation with RAS (Barrett et al., 1992; Birrer et al., 1988; DePinho et al., 1987; Schwab et al., 1983; Yancopoulos et al., 1985) and appear amplified in 7% of tumors (Schaub et al., 2018). However, MYC is the most ubiquitously expressed and most involved in human cancer among the members of the family. For these reasons, MYC is going to be more extensively described in the following section.

1.1.2. MYC structure

MYC family members share a transcriptional activation domain (TAD) localized at the N-terminus and a bHLHLZ domain at the C-terminus. The TAD, in turn, is composed of four conserved regions named MYC Boxes (MB). MBI is mainly involved in the regulation of MYC protein stability. The ERK/MAPK and the PI3K/AKT pathways regulate the phosphorylation of two residues localized in MBI, Ser62 and Thr58, upon stimulatory signals. These phosphorylations control the stability of MYC protein (Kapeli and Hurlin, 2011; Sears, 2004). On the other side, MBII is crucial for MYC transcriptional transactivation function, as it mediates the interaction with several coactivators, such as TRAAP, GCN5, TIP60, TIP48, CBP/p300 or SKP2. Two more MBs have been identified though they are not localized at the TAD region. MBIII is involved in transcriptional repression through interaction with SP1 and/or MIZ-1. Furthermore, SIN3B was described to bind to MBIII and deacetylate MYC, causing its destabilization (Garcia-Sanz et al., 2014). MBIV contains the nuclear localization signal (NLS) and it is involved in DNA binding and apoptosis (Diolaiti et al., 2015; Poole and van Riggelen, 2017; Tu et al., 2015). The bHLHLZ domain is necessary for both binding to the DNA (through the basic domain and the helix 1) and interacting with MAX (through the helix 2

and the leucine zipper) (Amati et al., 1992; García-Gutiérrez et al., 2019; Prendergast et al., 1991). MYC structure is schematized in **Figure 1.1**.

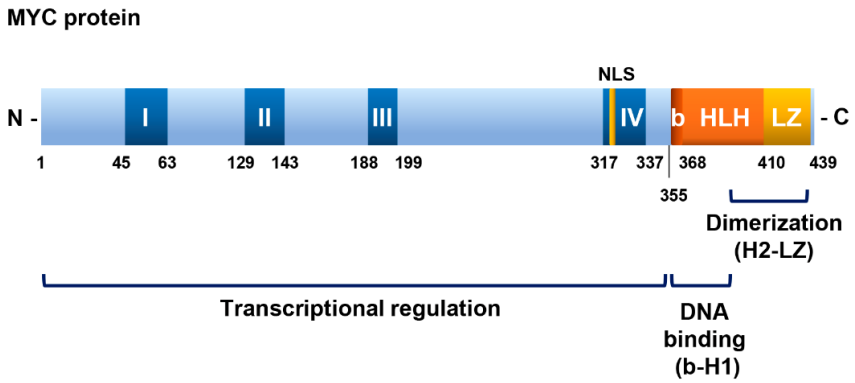

Figure 1.1. MYC protein structure. Schematic representation of the human MYC protein and its main conserved regions. I, II, III and IV refer to the MYC boxes (MB); NLS to the Nuclear Localization Signal and bHLHLZ to the basic helix-loop-helix leucine zipper domain.

1.1.3. MYC functions

Among the most important functions of MYC we can find the regulation of cell cycle progression, ribosome biogenesis, apoptosis, biomass accumulation, stemness and differentiation, regulation of the transcriptional pause release of RNA polymerase II or enhanced capping of nascent mRNA transcripts (Kalkat et al., 2017). This broad spectrum of cellular processes can be explained by the fact of MYC being bound to 10-15 % of human genes (Lüscher and Vervoorts, 2012). MYC main functions are summarized below and schematized in **Figure 1.2.**

a) Cell cycle

Different mitogenic signals (growth factors, cytokines, mitogens) can induce *MYC* expression, which in turn promotes G1-S transition. Among its target genes, MYC enhances the expression of genes that code for CDKs and Cyclins, like *CDK4* and *CCND2* (Cyclin D2), *CCNE1* (Cyclin E1) and *E2F* genes, while it counteracts the CDK inhibitors p21 and p27. Moreover, MYC upregulates genes involved in DNA replication and it binds to replication origins (Bretones et al., 2015; Dang, 2012; García-Gutiérrez et al., 2019; Grandori et al., 2000). MYC overexpression

is sufficient to shorten G1 phase and make quiescent cells enter cell cycle, diminishing the requirement for growth factors (Karn et al., 1989).

b) Apoptosis

MYC overexpression leads not only to an increase in proliferation but also drives apoptosis, which is thought to be a protective mechanism for the cell to avoid tumoral features. MYC induces apoptosis through both p53-dependent and independent pathways (Sakamuro et al., 1995). For instance, some MYC target genes are able to induce apoptosis (*ODC*, *CDC25A* or *LDH-A*). Mutations in the apoptotic pathways favor MYC-driven tumorigenesis, as it is the case of the loss of p53 or ARF (Dang, 1999; Grandori et al., 2000; Shim et al., 1998). In addition, MNT has turn out to counteract MYC's capacity to promote apoptosis in several models, being necessary for curbing MYC's hyperactivity (Campbell et al., 2017). Thus, it seems that the functions of the rest of the MYC-MAX-MXD-MLX network could also affect MYC's effect on apoptosis.

c) Cell growth and metabolism

As MYC can regulate genes involved in ribosome biogenesis and protein biosynthesis, it directly affects cell growth. This feature is clear in *Drosophila melanogaster*, where the deletion of dMyc affects larval growth and DNA endoreplication (Johnston et al., 1999; Pierce et al., 2004) and in human B-cells, in which overexpression of MYC results in the increase in cell size as a cause of enhanced protein synthesis (Iritani and Eisenman, 1999). The effects of MYC levels on cell growth could be explained by the regulation of several nucleolar and ribosomal proteins, as well as the RNA pol I (which synthesizes pre-rRNAs) and RNA pol III (which synthesizes tRNAs) (Grandori et al., 2000).

Regarding metabolism, cells with aberrant MYC expression are thoroughly dependent on metabolic activity and nutrients. In fact, glucose or glutamine withdrawal clearly triggers apoptosis in MYC-overexpressing cells (Dang, 2012; Shim et al., 1998; Yuneva et al., 2007). MYC is then a key factor for tumoral cells, as it sustains glycolysis and glutaminolysis in hypoxia conditions. In fact, MYC is

likely the major responsible for Warburg effect in tumors, being hexokinase 2 (HK2), lactate dehydrogenase A (*LDH-A*) or Enolase (ENO1) *bona fide* targets of MYC (Dang, 2012; Dang et al., 2008; O'Shea and Ayer, 2013; Shim et al., 1997). Moreover, MYC also regulates mitochondrial biogenesis (Li et al., 2005).

d) Differentiation

Upon cell differentiation, MYC levels usually decrease for allowing cell cycle exit and liberate the repression that it exerts on differentiation genes. In a tumoral cell, high levels of MYC could predispose it to a dedifferentiated phenotype. Several examples can be found in the literature, like MYC's blocking of erythroid differentiation by repression of *MXD1* and *GATA1* (Acosta et al., 2008) or the blocking of RAS-mediated differentiation of UR61 pheochromocytoma cells by repression of c-*JUN* (Vaque et al., 2008). In fact, MYC was described as one of the four factors able to induce pluripotent stem cells by Takahashi and Yamanaka (2006). However, even if it has not been so deeply studied, MYC can have a pro-differentiation role in other settings (Iavarone and Lasorella, 2014).

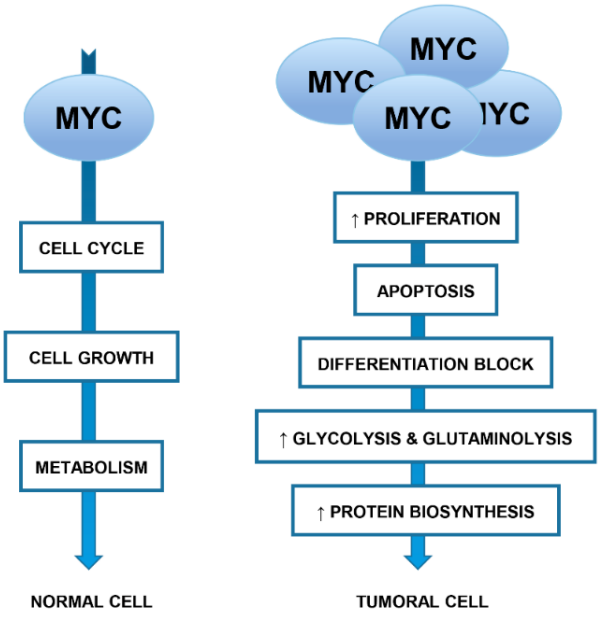

Figure 1.2. MYC cellular functions in physiological and pathological conditions. MYC sustains cell cycle, cell growth and metabolism, among other processes, in a normal cell. However, its levels are usually increased in tumoral cells, resulting in a higher proliferation rate, increased apoptosis, the blocking of differentiation processes and an enhanced metabolism.

1.1.4. MYC involvement in cancer

MYC is frequently altered in several types of tumors and it is believed to have a vital role in the initiation, progression and maintenance of the tumorigenic

process, as MYC induces cell proliferation, growth, angiogenesis and blocks cell differentiation. Indeed, *MYC* is overexpressed in 60–70% of human solid and hematopoietic tumors. In The Cancer Genome Atlas (TCGA), 28% of the samples had amplifications in at least one of the three *MYC* family genes (Kalkat et al., 2017; Poole and van Riggelen, 2017; Schaub et al., 2018; Vita and Henriksson, 2006).

Initially, the transforming ability of MYC was described in collaboration with another important oncogene, *RAS*, which is mutated in around 30% of human tumors (Hobbs et al., 2016). Several studies describe how these two oncoproteins cooperate to induce cell transformation *in vivo*, being actually the first proof of multi-step carcinogenesis (Land et al., 1983; Lee et al., 1985; Leone et al., 1997).

MYC deregulation in cancer can take place through different mechanisms, as gene amplification, translocation, transcriptional induction by altered cellular signaling or activation of its enhancers. Moreover, post-transcriptional modifications (phosphorylation, sumoylation, acetylation or ubiquitination) in MYC and deletions in the members of the MYC-MAX-MXD-MLX network can also alter MYC's function. On the contrary, mutations in *MYC* are not so usual though some affecting its stability have been described, particularly in lymphoma (Kalkat et al., 2017; Schaub et al., 2018).

1.2. MAX

MAX was first described as a partner and co-factor of MYC proteins to bind to DNA and regulate transcription. Then, it was described to form dimers with MXD1-4, MNT and MGA proteins. In contrast to the short life of its partners, MAX is a highly stable protein with a half-life of 24 h. This finding suggests that there is always a pool of MAX, ready to form the necessary dimers for the cell in every condition (Blackwood et al., 1992b, 1992a; Blackwood and Eisenman, 1992, 1991; Hurlin and Huang, 2006; Prendergast et al., 1991). Human *MAX* is localized in chromosome 14q22-24 and it gives rise to two protein isoforms by alternative splicing: p21MAX (21 kDa) and p22MAX (22 kDa). The 9 amino acids difference in their N-terminal domain changes their DNA binding affinity and,

consequently, allows them to have unique transcriptional and biological activities (Hurlin and Huang, 2006; Prochownik and VanAntwerp, 1993).

MAX can also form homodimers, which are unable to transactivate gene expression (Kato et al., 1992) and thus, can affect MYC function for which MAX is an obligate partner. The DNA-binding ability of the homodimers can be inhibited by phosphorylation of one or more serines in its N-terminal domain by casein kinase II (CKII). As this phosphorylation does not affect the function of MYC-MAX dimers, it can be a regulatory mechanism of the dynamics of gene regulation by MYC-MAX and MAX-MAX dimers (Berberich and Cole, 1992; Bousset et al., 1994, 1993; Hurlin and Huang, 2006).

1.2.1. MAX involvement in cancer

MYC-MAX dimers are involved in cell transformation, as bHLHLZ MAX deletion mutants are not oncogenically active. However, overexpression of *MAX* results in remarkable suppression of the co-transformation activity of the three members of MYC family, causing an increased cell cycle time and a reduced immortalization frequency. This is probably due to the competition between transcriptionally active heterodimers and inactive MAX homodimers and MAX-MXD repressive complexes that bind to common DNA binding sites (Conacci-Sorrell et al., 2014; Prochownik and VanAntwerp, 1993). Even if MAX is thought to be necessary for MYC transforming capacity, *MAX* is deleted in some cancers of neuroendocrine origin, as pheochromocytomas, paragangliomas, gastrointestinal stromal tumors and small cell lung cancer (Burnichon et al., 2012; Comino-Méndez et al., 2011; Pantaleo et al., 2017; Robledo, 2012). Moreover, a rat pheochromocytoma cell line (termed PC12) lacking a functional MAX protein was described by Hopewell and Ziff (1995). However, overexpression of *MYC* in this setting is able to block RAS-mediated differentiation of PC12 cells (Vaque et al., 2008). Besides, loss of dMax in *Drosophila melanogaster* has not as a severe phenotype as the one of dMyc deletion (Steiger et al., 2008). These findings suggest that MYC can carry out some functions in the absence of its partner MAX.

1.2.2. The UR61 cellular model

The UR61 cells derive from the U7 cell line, which in turn was established from the PC12. The PC12 cell line is a rat pheochromocytoma cell line that lacks a functional MAX, as mentioned above, and that differentiates into a neuronal-like phenotype with NGF. In these cells, a homozygous chromosomal rearrangement or translocation gives rise to a transcript that does not encode helix 2 and LZ domains of MAX. The resulting MAX protein is therefore unable to form complexes with any bHLHLZ protein (**Figure 1.3**).

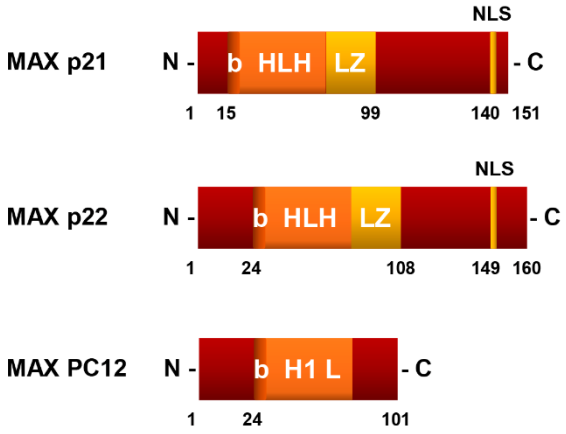

Figure 1.3. MAX protein structure. Images showing the structure and domains of the two spliced variants (p21 and p22) and the isoform present in PC12 cells. The latter is much smaller and does not have either the helix 2 or the leucine zipper domain. NLS, Nuclear Localization Signal; bHLHLZ, basic helix-loop-helix. leucine zipper.

U7 is a PC12-derived cell line that responds less to NGF (Burstein and Greene, 1982). UR61 derive directly from U7 after stable transfection of a mouse *N-RAS* (N-RAS Q61K) oncogene under the control of the long terminal repeat from mouse mammary tumor virus (LTR-MMTV). Upon dexamethasone treatment, this promoter is activated and RAS is induced, which finally leads to the neuronal differentiation of the cells (Guerrero et al., 1988). Afterwards, our laboratory generated two UR61 derivative cell lines: (i) URMax34 cells that express a wild type MAX protein in response to Zn_2SO_4, since the MAX gene is under the control of the metallothionein (MT) promoter and (ii) URMT cells that carry an empty construction as a control (Quintanilla, 2013).

1.3. The Proximal MYC Network

In order to understand how MYC participates in cell transformation, it is necessary to consider that it belongs to an extended network of bHLHLZ transcription factors, connected by MAX and MLX, which is quite conserved along metazoan evolution (Diolaiti et al., 2015; McFerrin and Atchley, 2011) (schematized in **Figure 1.4**). While MYC and MXD's half-lives are short (15-30 min), MAX and MLX remain more stable (6 to 24 h) (Billin et al., 1999; Blackwood and Eisenman, 1992), constituting the base partners for this proteins to carry out their functions. Regarding cancer, *MYC* genes are usually amplified and deletions are found in *MNT*, *MGA* and to a lesser extent, in the other *MXD*s, *MAX* and *MLX*, as a pan-cancer study recently showed. No exclusivity has been found between the mutations of *MYC* and the ones of the other members of the network. However, regarding the deletions, there is not usually loss of more than one copy. This may suggest that most of the proximal MYC network members are haploinsufficient (Schaub et al., 2018). More research in this network will open new insights into MYC function and it will provide new opportunities for counteracting MYC-driven tumorigenesis.

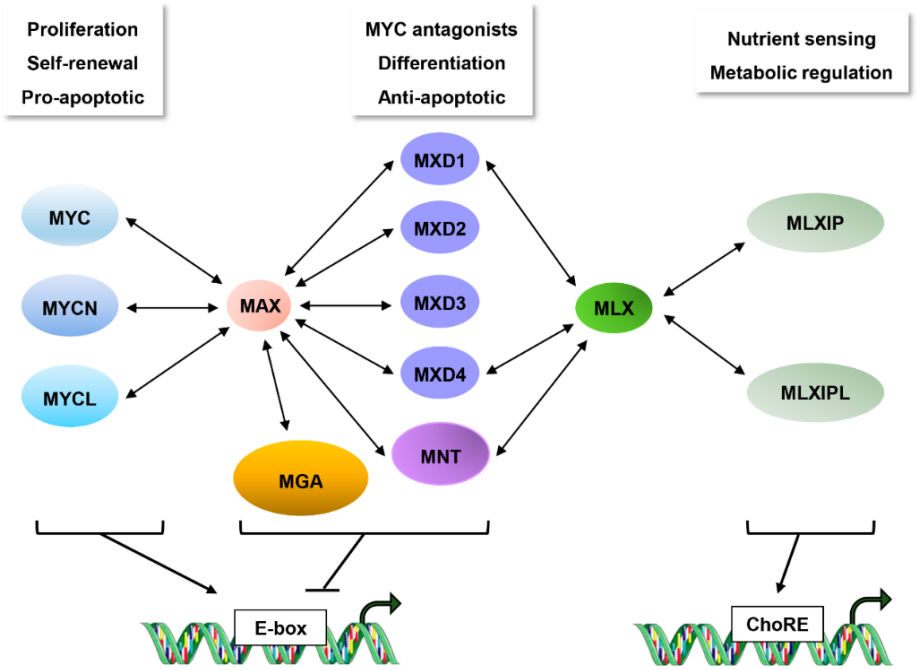

Figure 1.4. The MYC-MAX-MXD-MLX network and its functions. The double pointed arrows represent the interactions between members. MYC proteins bind to E-boxes y activate transcription, while MXD proteins usually act as transcriptional repressors. MLX-MLXIP(L) bind to Carbohydrate Response Element (ChoRE). Modified from Diolaiti *et al.*, 2015.

1.3.1. MXD1-4 and MGA

The MXD1-4 and MGA proteins are characterized by antagonizing MYC in dimers with MAX or in the case of MXD1 and MXD4, with MLX too. As they can repress some genes that are activated by MYC and compete for binding to MAX, they play an important role in MYC homeostasis. MYC-MAX and MXD1-MAX bHLHLZ crystal structures are shown in **Figure 1.5** together with the canonical and non-canonical E-boxes they can bind to (Grandori C. *et al*, 1996; Seitz *et al.*, 2011).

MXD1-4 were initially described as genes mostly expressed in differentiated cells, in which their levels increased while *MYC* levels shut down (Ayer and Eisenman, 1993; Hurlin et al., 1995; Koskinen et al., 1995; Vastrik et al., 1995). Then, *MXD2*/*MXI1* (MAX's Interactor 1) was found not only in growth-arrested cells but also in proliferating cells, from the central nervous system, epidermis and the myeloid lineage (Hurlin et al., 1995; Zervos et al., 1993). *MXD3* is also specifically expressed during S phase and it is important for cell proliferation (Barisone et al., 2012; Fox and Wright, 2003; Hurlin et al., 1995).

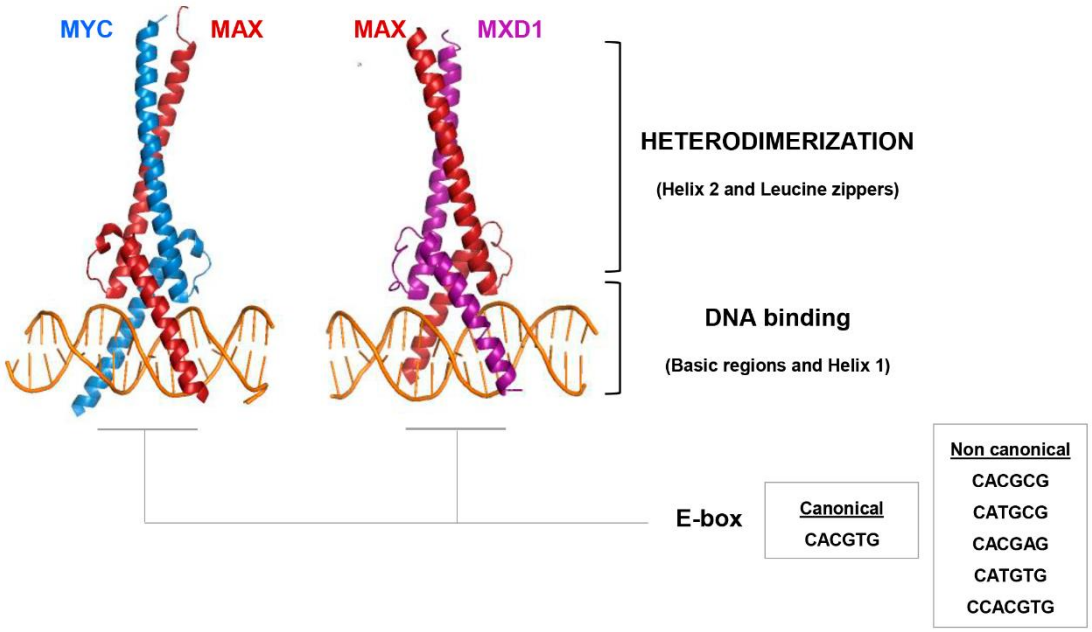

Figure 1.5. Crystal structures of the bHLHZ domains of MYC-MAX and MXD1-MAX. Image created with the PyMOL software 2.3.1 (Schrödinger), LLC with the structures PDB: INKP (MYC-MAX, right) and INLW (MXD1-MAX, left) resolved by Nair & Burley, 2003. The possible E-boxes MYC-MAX and MXD-MAX can bind to are listed below based on (Grandori C., Mac J., Siëbelt F., Ayer D.E., Eisenman, 1996; Seitz et al., 2011).

MGA (MAX's giant associated protein), is the biggest and less known protein of the network, is a dual specificity transcription factor with one bHLHLZ domain for heterodimerizing with MAX and binding to E-box sites and a T-box domain, first identified in Brachyury and characteristic of the TBX family. This uncommon feature lets it regulate both MAX-network and T-domain target genes, either as an activator or as a repressor (Hurlin et al., 1999; Ogawa et al., 2002; Washkowitz et al., 2015).

Regarding MYC antagonism, *MXD1-4* and *MGA* overexpression is sufficient for decreasing MYC and RAS co-transformation capacity (Cerni et al., 2002; Hurlin et al., 1999, 1995; Roussel et al., 1996; Schreiber-Agus et al., 1995; Vastrik et al., 1995). *MXD1-4* and *MGA* suffer deletions or inactivations in different types of cancers, which suggests their major potential role as tumor suppressors (Edelmann et al., 2012; Han et al., 2000; Kalkat et al., 2017; Paoli et al., 2013; Reddy et al., 2017; Romero et al., 2014; Schaub et al., 2018; Van Doorn et al., 2004; Vermeer et al., 2008).

1.3.2. MNT

MNT (MAX's Next Tango) has turn out to be a unique protein inside the MXD family, affecting MYC functions in several ways. It was first described by Hurlin et al. (1997) while trying to identify proteins that interacted with MAX. That same year, another group also published MNT's discovery, referring to it as ROX (Meroni et al., 1997).

MNT is bigger than the other MXD proteins and the most ubiquitously expressed, both in proliferating and differentiated cells. Interestingly, MNT is the only homolog from the MXD family in the *Drosophila melanogaster* genome (Loo et al., 2005). On the one side, the lack of *Mnt* in mice results in craniofacial defects, defective embryonic growth and death within several days after birth (Hurlin *et al.*, 2003; Toyo-oka *et al.*, 2004). In contrast, mice lacking *Mxd1*, *Mxd2* or *Mxd3* are viable (Hurlin and Huang, 2006). It can therefore be assumed that MNT function is not redundant with other members of the MXD family. On the other side, *MNT* overexpression embryos have also developmental defects and a

smaller size due to a decrease in cellularity (Hurlin et al., 1997). These data suggest that having a tight control of MNT protein levels is necessary for the correct function of the cells and, consequently, for the developmental process.

a) MNT structure and regulation

MNT is a 591-amino acid protein that contains along its structure (i) a coiled-coil α-helix structure for interaction with SIN3 (SID domain), (ii) an extremely proline-rich region, similar to the activation domains of other transcription factors like MYC, (iii) a bHLHLZ domain, for interaction with MAX and MLX and DNA-binding on E-boxes, and (iv) a proline and histidine-rich region at its C-terminal domain (Hurlin et al., 1997; Meroni et al., 2000, 1997). MNT structure and interaction with SIN3A, MAX and MLX is represented in **Figure 1.6**.

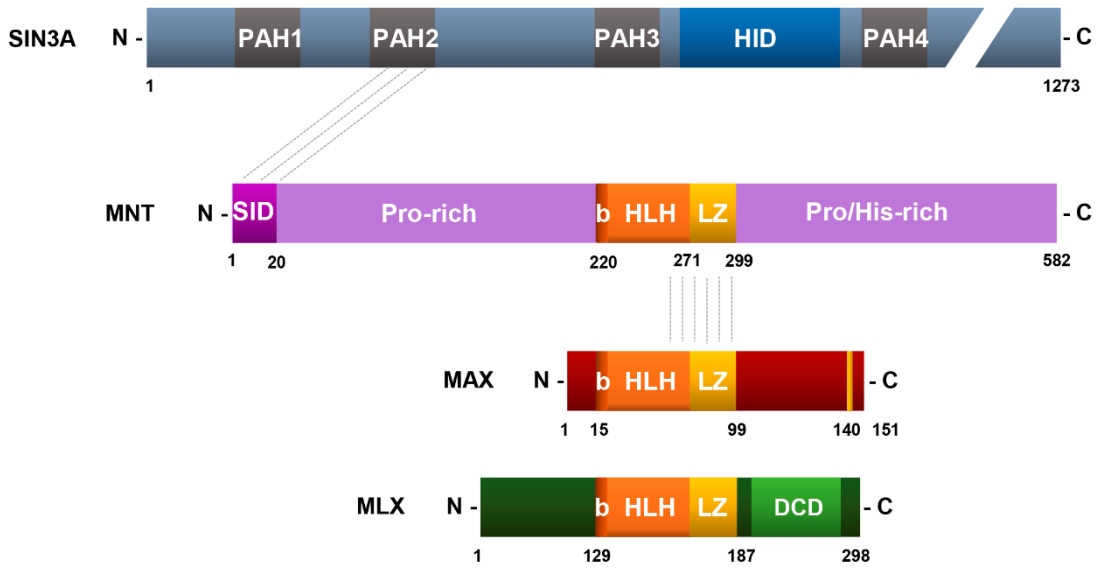

Figure 1.6. SIN3A, MNT, MAX and MLX protein structures. The grey bars connect the domains involved in each interaction. PAH, Paired Amphipathic Helix; HID, Histone Interaction Domain; SID, SIN3 Interaction Domain; Pro for proline and His for histidine; bHLHLZ, basic helix-loop-helix leucine zipper; DCD, Dimerization and Cytoplasmic localization Domain.

MNT has been described to interact with MAX and MLX but also to form homodimers through its bHLHLZ domain. However, the homodimerization was only analyzed by two-hybrid assays in yeasts and *in vitro* co-immunoprecipitation, and no binding to DNA was detected of the homodimers (Cairo et al., 2001; Hurlin et al., 1997; Meroni et al., 2000, 1997). MNT bHLHLZ domain is different to the

one of the MXD proteins, and MNT-MAX dimers show a higher preference for non-canonical CACGCG E-boxes though they can also bind to canonical CACGTG (Meroni et al., 1997). This difference in the DNA basic regions explains why MYC, MNT and the other MXDs share some target genes but they also have a subset of unique, non-overlapping group of target genes. MNT is usually a transcriptional repressor through its interaction with SIN3 and the recruitment of HDAC complexes, as described previously (Hurlin et al., 1997; Terragni et al., 2011; Yang and Hurlin, 2017).

MNT displays a half-life of 30-60 min and it appears as a doublet of 72-74 kDa, mostly nuclear (Hurlin et al., 1997; Meroni et al., 1997). The 72 kDa's form is the one detected in growth-arrested cells. The 74 kDa's form, on the contrary, is the prevalent one in serum-stimulated cells and it corresponds to hyperphosphorylated MNT. This phosphorylation is carried out by MKK/ERK kinases and it could impair the interaction with SIN3B and, consequently, MNT's transcriptional repressive function (Popov et al., 2005).

Little is known about the regulation of MNT expression. MNT is a target of the E6-associated protein (E6AP), an E3 ubiquitin ligase that induces its ubiquitination and degradation by the proteasome. This finding was observed in myeloid differentiation experiments, in which different agents (*e.g.*, all-trans retinoic acid, vitamin D3 or phorbol 12-myristate 13-acetate) downregulated E6AP and, consequently, reduced E6AP-mediated degradation of MNT (Kapoor et al., 2016).

b) MNT transcriptional repressor activity

The repressor ability of MXD1-4 and MNT is mainly achieved by the interaction with SIN3A and SIN3B. This interaction takes place through SIN3 second paired amphipathic helix (PAH2) domain and the mSIN3 Interaction Domain (SID) of the MXD proteins. SIN3A and B in turn recruit histone deacetylases (HDAC1 and HDCA2) through their Histone Interaction Domain (HID) or co-factors like N-CoR, SDS3, SAP30, SAP18, RBP1 or ING1/2 that work bridging and stabilizing the complex and/or enhancing the chromatin remodeling activities (**Figure 1.7**). The removal of acetyl groups on histones gives rise to a more closed chromatin

structure and, consequently, a transcriptional repression of their target genes (Ayer et al., 1995; Grzenda et al., 2009; Halleck et al., 1995; Heinzel et al., 1997; Laherty et al., 1997). This complex is key for MNT repressive function, as the SID deletion mutants of MNT are not able to either block MYC-dependent transformation nor cell cycle progression (Hurlin et al., 1997; Meroni et al., 1997).

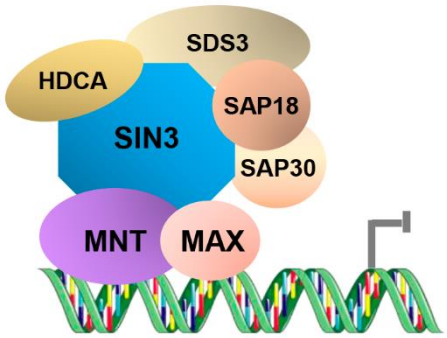

Figure 1.7. The MNT-MAX-SIN3 repressor complex. MNT-MAX dimers can repress transcription in a complex with SIN3A and B, which recruit different co-factors and histone deacetylases, generating a closed chromatin conformation around their target genes.

c) MNT as a MYC antagonist

MNT has been postulated to have the most general role as a MYC antagonist from all the MXD proteins. Conversely to them, MNT is ubiquitously expressed, and its levels are constant along the cell cycle. It can therefore be assumed that MNT-MAX dimers coexist with MYC-MAX dimers along all the cell phases. This antagonism is achieved at three different levels: (i) competition for binding to MAX (as MNT and MYC bind MAX with the similar affinities); (ii) competition between MNT-MAX and MYC-MAX for binding to the E-Boxes of their shared target genes; (iii) transcriptional repression of shared target genes that are normally activated by MYC-MAX (Hurlin et al., 2003, 1997). This antagonism has been demonstrated in diverse models and through different approaches, as summarized in the following lines.

Initial studies of the MNT-MYC antagonist were done by analyzing the phenotype of wild type mouse embryonic fibroblasts (MEFs) *versus* knockout for MNT ($MNT^{-/-}$ MEFs). First, $MNT^{-/-}$ MEFs were observed to proliferate faster and enter the S-phase prematurely. This was accompanied by an increase in *CDK4* and *CCNE1* (Cyclin E) and a decrease in *MYC*. Second, they showed an increase in apoptosis and efficiently escaped senescence. Third, they could be transformed by oncogenic RAS alone. This feature was specific for MNT, as reintroduction of

MNT into these MEFs dramatically slowed proliferation and reversed the anchorage-independent phenotype. Forth, deletion of *MYC* in MEFs caused proliferation arrest, which could be partially rescued by simultaneous deletion of *MNT* (Campbell et al., 2017; Hurlin et al., 2004, 2003; Link et al., 2012; Nilsson et al., 2004; Walker et al., 2005). Thus, *MNT* knockout could remarkably mimic *MYC* overexpression in MEFs.

Another example of this antagonism is the cell cycle entry. At the G_0 to G_1 transition, MYC is actively induced while MNT levels remain constant. This provokes a complex switching towards MYC-MAX dimers to favor the activation of cell cycle progression genes, such as *CDK4*, *CCND2* (Cyclin D2), *ODC* or *E2F2* (Hooker and Hurlin, 2006; Walker et al., 2005). This is consistent with the idea of MYC and MNT competing for available MAX. Moreover, both *MNT* overexpression or *MYC* loss blocks cell cycle entry, which indicates that MNT and MYC levels could determine the quiescent or proliferative state of the cell (Carroll *et al.*, 2018).

Next, conditional deletion of *MNT* in T-cells caused an increase in proliferation and apoptosis. Consequently, tumors were formed (although with a long latency), the T-cell development was disrupted and there was an enlargement of the secondary lymphoid organs. This was coupled with a modest increase in the expression of *CDK4* and cyclins (*D2*, *E1*, *A* and *B1*), and a slight downregulation of *BCL2* and *BCLXL*. The polarized differentiation of CD4+ T cells into T_{h1} (T helper cell type 1) caused inflammation and, consequently, predisposition to T-cell lymphoma (Dezfouli et al., 2006; Hooker and Hurlin, 2006; Link and Hurlin, 2014).

Studies in *Drosophila melanogaster* also reproduce the MYC-MNT antagonism found in mouse and human. In fact, dMnt and dMyc have opposing activities in cell growth (Loo et al., 2005). Moreover, there is an important overlap between dMyc, dMnt and dMax DNA binding regions, revealing the regulation of shared target genes. For instance, dMnt antagonized dMyc's growth stimulatory effects by downregulating pre-rRNA synthesis (Orian et al., 2005, 2003). Moreover, dMnt overexpression was able to rescue the viability and cell growth defects caused by deletion of dMyc (Pierce et al., 2008, 2004).

Regarding hypoxia, a common feature in tumors, we can observe another proof of MNT and MYC antagonism. During this process, there is an increase of HIF-1α and HIF-2α, which in turn induce the microRNA miR-210. miR-210 has been described to downregulate MNT in a cholestasis model and in cultured glioma cells. MNT downregulation caused a switch to MYC-MAX dimers and the activation of MYC-target genes. Consequently, tumoral cells can override cell cycle arrest and apoptosis by releasing MNT-MYC antagonism (Dang et al., 2008; Yang et al., 2009, 2014; Zhang et al., 2009).

MNT-MYC antagonism is also clear in a myeloid differentiation model described by Kapoor *et al.* (2016). Treating HL60 cells with differentiating agents, like all-trans retinoic acid, led to a decrease in E6AP and a loss of E6AP-mediated degradation of MNT. Increased levels of MNT can antagonize MYC and induce cell cycle arrest and myeloid differentiation.

d) MNT as a MYC cooperator

Despite of the evidences of MNT as a MYC antagonist and tumor suppressor, some recent studies suggest that MYC needs MNT for fully achieving its transformation potential. This can be explained by the pro-survival functions of MNT, which would antagonize the apoptosis caused by supraphysiological MYC levels. This is the case of T-cells, in which *MYC* overexpression leads to a higher proliferation rate of T-cells but also to a higher dependency on MNT. The increase in ROS and apoptosis is not even blocked by ectopic expression of *BCL-2*, suggesting the broader and more important role of MNT in T-cell lymphomagenesis (Link et al., 2012; Link and Hurlin, 2014). Another recent study also highlighted MNT's collaborative role with MYC, as MNT heterozygosity in vavP-MYC10 mice and Eμ-myc mice is able to slow down MYC-driven lymphomagenesis (Campbell et al., 2017).

The pro-survival role of MNT takes place also in the absence of MYC, as it was described in HO.15 *Myc*$^{-/-}$ Rat1a fibroblasts (Nilsson et al., 2004). This suggests that MNT controls some pathways independently of MYC but that its function can be affected by an altered MYC expression, probably indirectly through

competition for MAX or their binding to common target genes (Link et al., 2012; Wahlström and Henriksson, 2007; Walker et al., 2005).

In summary, having a balance between MYC and MNT is crucial for the correct functioning of cellular processes. In tumoral cells, MYC always needs some MNT for controlling the excess of apoptosis that it provokes and, consequently, for cell survival (**Figure 1.8**).

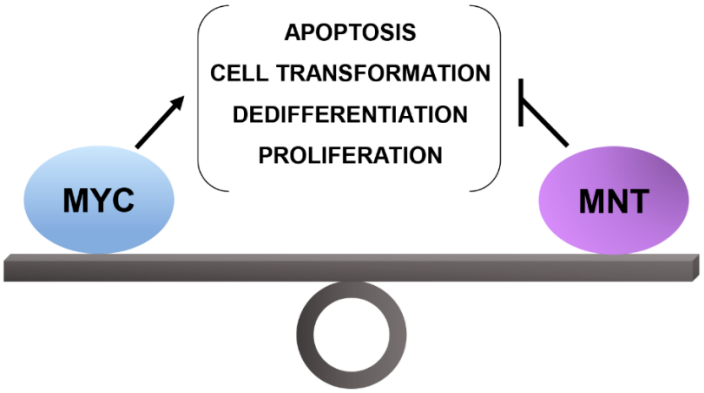

Figure 1.8. The balance of MYC and MNT for cell survival. Apoptosis, cell transformation, dedifferentiation and proliferation are induced by MYC and blocked by MNT. Altered levels of any of these proteins can have important consequences for the cell.

e) MNT involvement in cancer

Apart of its role as a MYC cooperator, other data suggests that MNT has functions favoring cancer progression. *MNT* locus is located in human 17p13.3, a hot spot for loss of heterozygosity (LOH) in several types of tumors, such as sporadic breast cancer, medulloblastomas or chronic lymphocytic leukemia (CLL) (Cvekl et al., 2004; Edelmann et al., 2012; Lo Nigro et al., 1998; Sommer et al., 1999). In a recent pan-cancer study with data from The Cancer Genome Atlas (TCGA), *MNT* deletion was found in the 10% of the cases (overall frequency) and in more than the 20% of liver hepatocellular carcinomas, lung adenocarcinomas, sarcomas and uterine carcinosarcomas (Schaub et al., 2018). Deletions were also found in acute leukemia (Guo et al., 2007) and a decrease in MNT levels in medulloblastomas, caused by the haploinsufficiency in chromosome 17p13.3 (Cvekl et al., 2004). MNT has been also related to Sézary Syndrome, a leukemic variant of cutaneous T-cell lymphoma (Vermeer et al., 2008). At the molecular

level, it usually shows a loss of *MNT* and/or *MXI1*, and a gain of *MYC* (Van Doorn et al., 2004; Vermeer et al., 2008).

Conditional deletion of *MNT* can lead to tumor formation, as it happens in mouse mammary epithelium (Hurlin et al., 2004; Toyo-oka et al., 2006) or in T-cells (Dezfouli et al., 2006). Therefore, it seems that the mechanisms that drive tumorigenesis in the absence of *MNT* could be similar to the ones associated with *MYC* overexpression. Nevertheless, *MNT* deficiency impairs MYC-driven tumorigenesis in other models (Campbell et al., 2017; Link et al., 2012), as mentioned above. This suggests that MNT can act either as a MYC antagonist or a cooperator of MYC.

1.3.3. MLX

MLX (MAX-like protein) was described while looking for new interactor proteins of MXD1 and MXD4 (Billin et al., 1999) and soon after of MNT (Cairo et al., 2001; Meroni et al., 2000). Its name comes from the high similarity with MAX based on different features: (i) broad expression in many tissues; (ii) long half-life; (iii) formation of transcriptional repressor heterodimers with MXD proteins; (iv) poor ability to homodimerize; (v) the lack of a TAD or SID and thus, transcriptional inactivity and (vi) an amino acid similarity of 50% of its bHLHLZ domain with the one of MAX (Billin et al., 1999; Hunt et al., 2015).

MLX gives rise to three spliced isoforms, named as MLXα (214 amino acids), MLXβ (244 amino acids) and MLXγ (298 amino acids). These isoforms are not tissue specific, but they differ in their subcellular localization, being MLXα and β predominantly cytoplasmic and MLXγ nuclear (Meroni et al., 2000; O'Shea and Ayer, 2013). Regarding the structure, MLX has a cytoplasmic localization and dimerization domain (DCD) at its C-terminus, not present in MAX. This domain allows its interaction with MLXIP (MONDOA) and MLXIPL (MONDOB or ChREBP), which are involved in regulating the cell response to different nutrients (Billin et al., 2000; Cairo et al., 2001; Diolaiti et al., 2015). MLXIP and MLXIPL have five Mondo Conserved Domains (MCR) in their N-terminus for nutrient detection and a transactivation domain (TAD) (**Figure 1.9**). Glucose drives the

nuclear accumulation of MLX:MLXIP and MLX:MLXIPL complexes and their binding to promoters on carbohydrate response elements (ChoRE) (Peterson et al., 2010). This motif consists of two E-boxes separated by five base pairs (CAYGYGnnnnnCRCRTG) (Shih et al., 1995) where two heterodimers could be binding to (Ma et al., 2007). Together, MLX and MLXIP proteins regulate genes from the glycolytic pathway to the fatty acid synthesis, as well as gluconeogenesis, glycogen synthesis, cholesterol metabolism, triglyceride formation and transport, different metabolic regulators and myogenesis and muscle regeneration (Hunt et al., 2015; Ma et al., 2006; Mattila et al., 2015).

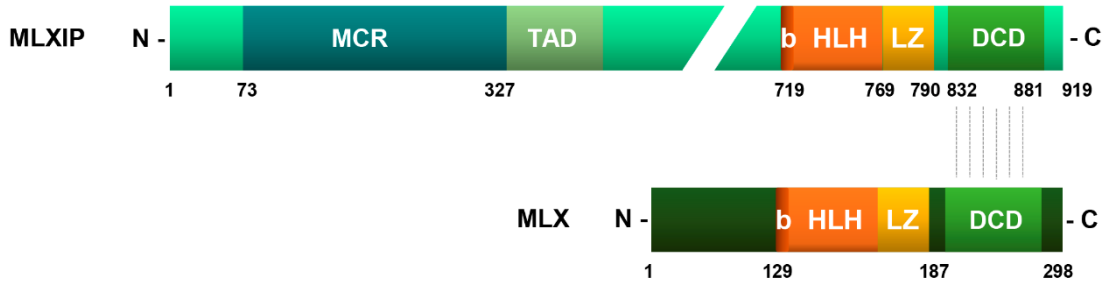

Figure 1.9. MLXIP and MLXγ protein structures. The grey bars connect the domains involved in the interaction. MCR, MONDO Conserved Region; TAD, Transcriptional Activation Domain; bHLHLZ, basic helix-loop-helix leucine zipper; DCD, Dimerization and Cytoplasmic localization Domain.

MLXIP and MLXIPL show a high similarity in their sequence and function. Nevertheless, there are some differences that could explain why their roles are not redundant. First, they differ in their phospho-acceptor sites implicated in their regulation by glucose, which are not conserved. Second, the highest expression of MLXIP is detected in skeletal muscle while MLXIPL is highly expressed in the liver. Third, MLXIP normally associates with the outer mitochondrial membrane as a peripheral protein, whereas MLXIPL is cytoplasmic (Peterson et al., 2010; Sans et al., 2006; Stoltzman et al., 2008). Finally, MLXIP regulates mainly glycolytic genes while MLXIPL can also bind to some key regulators of lipogenesis (Diolaiti et al., 2015).

Even if they have important roles in regulating the nutrients response, they do not seem involved in cell viability or differentiation during the embryonic development, as mice lacking *Mlx*, *Mlxip* or *Mlxipl* can survive without major

developmental defects (Diolaiti et al., 2015; Iizuka et al., 2004; O'Shea and Ayer, 2013).

a) Glucose uptake regulation by MLX and MLXIP

Glucose is an important source of energy for the cell and its metabolism is tightly regulated. MLX and the MLXIP proteins are in charge of the nutrients sensing and the adequate cellular response to them.

The process starts once the glucose enters the cell and it becomes phosphorylated by hexokinases to generate glucose-6-phosphate (G6P). G6P binds the MCR domain of MLXIP, inducing its nuclear accumulation, increasing its binding to promoters and the recruitment of histone acetyltransferases, enabling the activation of its target genes (Peterson et al., 2010). *TXNIP* (Thioredoxin Interacting Protein) or its paralogue *ARRDC4* are MLXIP-target genes (Stoltzman et al., 2008). TXNIP has been described as a possible tumor suppressor. Among its important functions inside the cell, TXNIP is able to inhibit thioredoxin (TRX, which regulates the internal redox homeostasis), to stabilize p27 inside the nucleus, to suppress mTOR activity and to block the glucose uptake. Thus, MLX-MLXIP dimers induce TXNIP and, consequently, create a negative feedback loop that avoids the excess of glucose inside the cell, and the evolution of pro-tumoral features (Zhou et al., 2011).

b) MLX and Mondo involvement in tumorigenesis

Altering the MLX-centered part of the network can impair diverse metabolic programs and the repression of MYC by the MXD proteins (O'Shea and Ayer, 2013; Schaub et al., 2018). Shallow deletions in *MLX* are present in around 5% of the tumors. *MLXIP* and *MLXIPL* also show deletions (3% and 8%, respectively) (Schaub et al., 2018). The MLX and MLXIP target gene *TXNIP* is also affected in cancer, showing a downregulation by hypermethylation of its promoter (e.g., in renal-cell carcinoma or leukemia) or by post-translational inhibition by miRNA (Zhou et al., 2011). The reduction in TXNIP causes a resistance to apoptosis and

an increase in GLUT1, allowing high levels of glucose necessary for the glycolysis and anabolic metabolism of the tumoral cells (Wu et al., 2013).

On the other side, overexpression of *MLXIP* can also be correlated with tumorigenesis, as it is described in acute lymphoblastic leukemia (Wernicke et al., 2012). This could be due to the important coordination of glucose sensing, glutamine utilization and the activation of metabolic programs that are important for tumoral cells, especially in the context of deregulated MYC. In fact, loss of *MLXIP* has been described to be synthetic lethal with deregulated MYC, as it impairs MYC and MLXIP co-regulation of metabolic genes (*LDHA*, *HKII*, *TXNIP*). Furthermore, *MLXIP* downregulation changes the balance of the MLX-centered network towards MXD-MLX dimers formation and its consequent repression of MYC-target genes (Carroll et al., 2015).

1.4. REL: a member from the NF-κB's family

c-REL (REL hereafter) is a transcription factor from the 'nuclear factor kappa-light-chain-enhancer of activated B-cells' (NF-κB). It was first described by homology with v-*rel*, the transforming gene of the avian reticuloendotheliosis virus (Brownell et al., 1987; Chen et al., 1983). Since then, several evidences have pointed out that REL is a key protein not only in B- and T-cell development but also in oncogenesis and other human diseases.

1.4.1. The NF-κB protein family

NF-κB's family includes a group of proteins that have been conserved, at least, from the phylum *Cnidaria* to humans and that control processes from immunity and development to oncogenesis. Inside the NF-κB's superfamily we can distinguish the REL and the NF-κB proteins, which share the REL homology domain (RHD) (**Figure 1.10**). This domain is necessary for nuclear localization, DNA binding, dimerization and interaction with the IκB proteins (Gilmore, 2006; Sen and Baltimore, 1986a, 1986b; Sullivan et al., 2007).

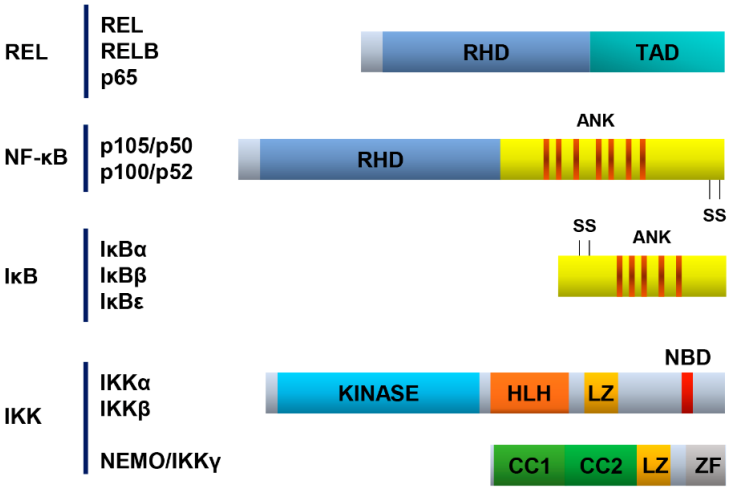

Figure 1.10. The NF-κB proteins. The REL and NF-κB subfamilies share the REL Homology Domain (RHD). The NF-κB and the IκB subfamilies have several ankyrin-repeats (ANK) that are marked in orange. TAD, Transcription Activation Domain; HLH, Helix-Loop-Helix; LZ, Leucine Zipper; CC, Coiled-Coil; NBD, NEMO-binding domain; ZF, zinc finger.

On the one hand, the REL subfamily is defined by their C-terminal transactivation domain (TAD) and it includes REL, RELB, p65 (encoded by *REL*, *RELB* and *RELA,* respectively). On the other hand, the NF-κB subfamily has several copies of ankyrin repeats (ANK) at their C-terminal domain that can inhibit REL proteins. It includes p100 and p105 (encoded by *NFKB1* and *NFKB2*, respectively). However, they do not always act as inhibitors, as they can go through proteolysis to generate forms without the ankyrin-repeats domain (p105 is cleaved to give p50 and p100 to p52). This way, p50 and p52 can form dimers with the REL proteins and regulate transcription.

In addition, belonging to the NF-κB's signaling network, we can find IκBα, β and ε (encoded by *NFKBIA*, *NFKBIB* and *NFKBIE respectively*) and IKKα/IKK1, IKKβ/IKK2 and IKKγ/NEMO (encoded by *CHUK*, *IKBKB* and *IKBKG,* respectively) (**Figure 1.10**). The IκB proteins retain REL dimers inactive in the cytoplasm thanks to their multiple ankyrin-repeats domains, which hide REL dimers nuclear localization signal (NLS) and interfere with their DNA-binding sequences. Furthermore, they also have two serine residues in their N-terminal halves that constitute a target for the IKKs. The IKK proteins can phosphorylate these serine residues, which target the IκBs for ubiquitination and degradation by the proteasome (Gilmore, 2006; Hayden and Ghosh, 2008; Kaltschmidt et al., 2018). Thus, IKK proteins finally release NF-κB activity. Aside from these deeply studied functions of the IκBs and the IKKs, they have additional and not so well

known functions inside the nucleus (reviewed in Espinosa, Bigas and Mulero, 2011).

All the members of the NF-κB's family are able to form dimers and regulate gene transcription by binding to κB sites of around 10 base pairs. The sequence has a loose consensus motif: 5' -GGGRNWYYCC-3' (R, A or G; N, any nucleotide; W, A or T; Y, C or T). This is the reason why these proteins have such a broad range of target genes (collected in the webpage bu.edu/nf-kb/). Furthermore, they are able to auto-regulate NF-κB's signaling, as *NFKBI*A (that codifies for IκBα), *RELA*, *RELB* and *REL* contain binding sites for p65, RELB and REL (Gilmore, 2006; Kaltschmidt et al., 2018).

1.4.2. REL structure and isoforms

Human *REL* is localized in chromosome 2p16.1, encoding a 587 amino acids protein with three main domains. First, the RHD domain is localized at its first 300 amino acids and it contains the NLS (290-295). Second, a transactivation inhibitory domain (RID) can be found between 323-422 amino acids. Deletion of the RID increases REL's binding to a κB site but it does not affect neither REL interaction with IκBs or REL-induced transformation of chicken spleen cells. Third, REL has a transactivation domain composed by two subdomains (TADI 424-490 and TADII 518-587), which are necessary for REL function as a transcriptional activator (Brownell et al., 1985; Gilmore and Gerondakis, 2011; Leeman et al., 2008).

Regarding REL splicing, two isoforms have been described: RELΔ9 and REL+Alu. In the case of RELΔ9, there is a deletion in exon 9 that results in a 564 amino acids protein (missing 308-330 amino acids), which has been detected in several lymphoma cell lines and in primary human DLBCL samples. Then, REL+Alu is a 619 amino acids protein with an Alu insertion (Brownell et al., 1989; Leeman et al., 2008). Both isoforms show a higher transactivation potential and an enhanced DNA binding.

In the case of mouse REL, only one isoform of 588 amino acids has been described. Its RHD shows a 84% similarity with the human and the C-terminus,

a 56% (Gilmore et al., 2001). The **Figure 1.11** shows the structure of the two main human REL isoforms and the mouse REL.

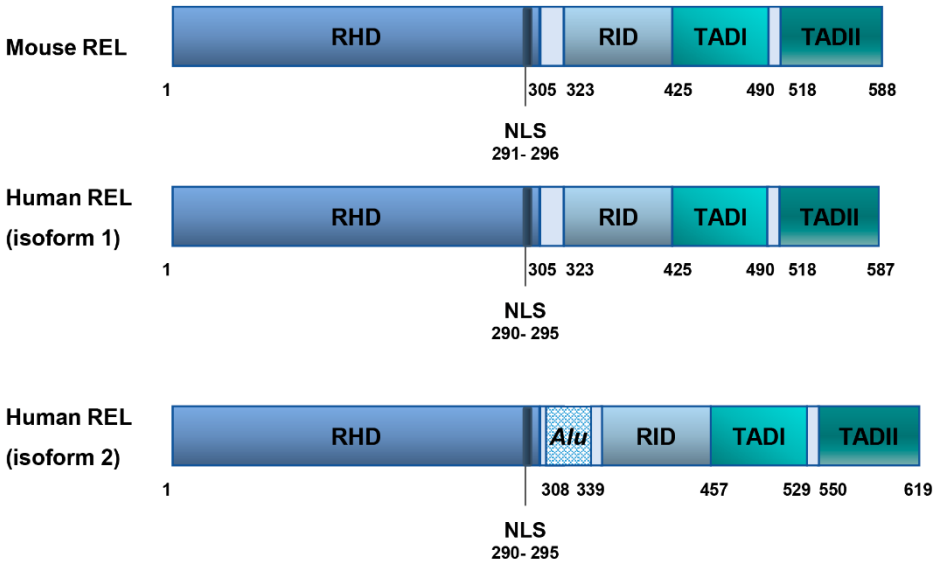

Figure 1.11. REL isoforms. The image shows the mouse REL (588 amino acids) and human isoform 1 (587 amino acids) and 2 (619 amino acids), which has an Alu insertion. RHD, REL Homology Domain; NLS, Nuclear Localization Signal; RID; REL Inhibitory Domain; TAD; Transcriptional Activation Domain.

1.4.3. REL activation

In basal conditions, REL is localized in the cytoplasm either as homodimers or as heterodimers with p50 or p65, which are sequestered by the IκB proteins (Gilmore and Gerondakis, 2011). REL translocation into the nucleus is induced through the canonical pathway by different stimuli, such as inflammatory cytokines (TNFα, IL-1), viruses, double-stranded RNA, bacterial products or physical and chemical stresses. These stimuli are able to activate the NEMO-IKKα-IKKβ complex, which suffers a conformational change and gets phosphorylated either by trans-autophosphorylation or by an upstream kinase. Then, active IKK phosphorylates IKKβ and NEMO, which provokes an opening in the complex that allows its inactivation by phosphatases. IKK also phosphorylates the IκB proteins (on Ser32 and Ser36 in the case of IκBα). Phosphorylated IκB is then recognized and polyubiquilated by an E3-ubiquitin ligase that contains the β-TrCP subunit, leading to its degradation by the 23S proteasome. After this, REL dimers can

translocate into the nucleus and regulate its target genes (**Figure 1.12**). One of its targets is *NFKBIA*, which codifies for IκBα. Once synthesized in the cytoplasm, IκBα can enter the nucleus and pull REL dimers away from the chromatin and back to their inactive state, generating a regulatory negative feedback loop (Hayden and Ghosh, 2008; Kanarek et al., 2010; Naugler and Karin, 2008).

REL optimal DNA-binding sequence is more variable (5' NGGRN(A/T)TTCC 3') than that of the other NF-κB's proteins (Kunsch et al., 1992). This suggests that REL has a greater degree of variation of its target sequences.

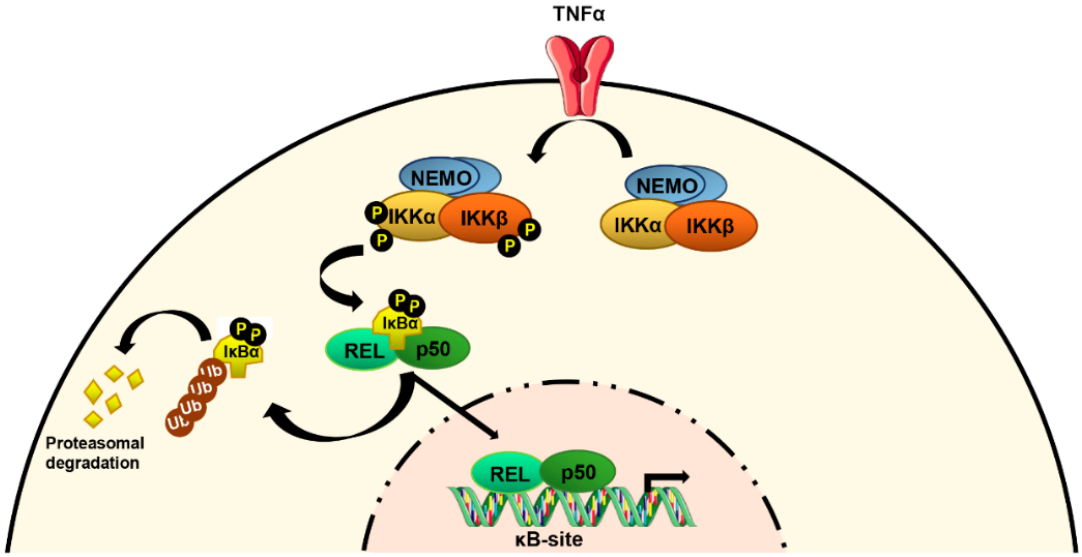

Figure 1.12. The canonical NF-κB activation pathway. Once TNFα (or other stimulus) binds its receptor on the membrane, the NEMO-IKK complex becomes phosphorylated and is able to phosphorylate IκBα, which is bound to REL-p50 dimers in the cytoplasm. This phosphorylation targets IκBα for ubiquitination and posterior proteasomal degradation. Finally, REL-p50 dimers are free to translocate into de nucleus and regulate their target genes by binding to κB sites on the DNA. Modified from Gilmore, 2006.

The non-canonical pathway is normally induced by other stimuli (e.g., lymphotoxin, CD40) and it involves IKKα and p100 processing into p52. Then, normally dimers of p52/RELB are the ones that translocate into the nucleus and initiate the transcription of different genes, such us cytokines, chemokines and the lymphoid organogenesis gene program (Naugler and Karin, 2008; Sun, 2017).

In addition to the classic activation pathways, REL has been described to be activated by direct phosphorylation, which involves IKKε and TANK-binding

kinase 1. REL phosphorylation disrupts the interaction with IκBα, so no degradation of IκBα is required (Harris et al., 2006).

1.4.4. REL diverse functions

Traditionally, the focus of the research on REL has been its role in the immune system. However, several findings support the idea that REL has a broader activity, affecting more biological processes in different organ systems.

As a general overview, *REL* knockout mice develop normally with no consequences on their hematopoietic cell development but they show some immunological defects: (i) decrease in B- and T-cell development, (ii) less activation in response to mitogenic stimuli, (iii) abnormal germinal center formation together and (iv) a decrease in marginal zone B-cells. Other processes such as hepatocyte wound healing, cognitive memory formation, cell cycle and epidermal homeostasis were also affected (Gilmore and Gerondakis, 2011; Priebe et al., 2018).

Although REL is not essential for hematopoiesis, it is key for the development of specialized functions in mature B- and T-cells. Indeed, REL is important for the evolvement of CD4 regulatory T lymphocytes (T_{reg}), by regulating *FOXP3*, and for the autocrine-dependent T-cell proliferation, by regulating *IL2* expression. Moreover, REL also controls the differentiation of CD4 T_h cells. Regarding the B-cells, REL is notably increased in the transition from a pre-B cell to a naïve mature B lymphocyte and it promotes proliferation and survival in mature B-cells. This can be explained taking into account its target genes: *E2F3*, *CCNE* (Cyclin E) and *MYC* and the pro-survival *BCL2A1* (A1/BLF-1) and *BCLXL*. REL is also necessary for B-cell antibody production and the efficient switching to IgG1 and IgE (Chen et al., 2000; Gilmore et al., 2004; Gilmore and Gerondakis, 2011). Among its target genes, *MYC* turns out to be interesting regarding this work. NF-κB's elements within the murine *Myc* gene were described upstream the P1 promoter and the exon 1. REL proteins were seen to bind to both of these sites and their overexpression (either p65 and p50 or REL) led to a transactivation of *MYC* promoter (La Rosa et al., 1994; Lee et al., 1985). Afterwards, additional

sites for REL binding were found in human together with a decrease in MYC levels upon *REL* knockdown (Gupta et al., 2018; Kaltschmidt et al., 2018; Slotta et al., 2017). This positive regulation of MYC by NF-κB leads to an increase in cell cycle progression.

Apart from the induction of MYC, REL can affect cell cycle through other mechanisms. This feature has been illustrated in models of *REL* knockdown or knockout, in HeLa cells (Slotta et al., 2017), keratinocytes (Lorenz et al., 2014), melanoma cell lines (Priebe et al., 2018) or tongue cancer cell lines (Gupta et al., 2018). In all the cases, the decrease in REL levels was followed by a decrease in cell proliferation and abnormalities in mitosis and cell cycle, such as delayed prometaphase, aberrant spindle formation, dysregulated Aurora A kinase activity or increase in the G_2/M phase. On the contrary, *REL* overexpression in HeLa cells lead to growth arrest in G_1/S, coupled with an increase in p21 and p53 and a decrease in CDK2 kinase activity (Bash et al., 1997). This can be explained by REL interaction with Cyclin E, which could interfere with CDK2/Cyclin E complexes and affect G_1/S transition (Chen and Li, 1998). Thus, REL levels must be tightly controlled for the correct progression of cell cycle.

Another important role of REL takes part in apoptosis, which is a type of programmed cell death required for the correct development and tissue homeostasis. NF-κB regulates apoptosis and, depending on the setting, it could finally induce or block it (Barkett and Gilmore, 1999). REL has been described as a direct transcriptional regulator of *BCLXL* and its homolog *BCL2A1* (BFL-1/A1). This way, it can block TNFα-induced cell death. However, REL does not affect *BCL-2* levels (Chen et al., 2000), suggesting that its regulation is not general for the BCL2 family. On the other side, REL can also induce the apoptotic program in other settings, by enhancing *DR4*, *DR5* and *BCL-Xs* and inhibiting *cIAP1*, *cIAP2* and *survivin/BIRC5* (Chen et al., 2003).

REL main functions are summarized in **Figure 1.13**.

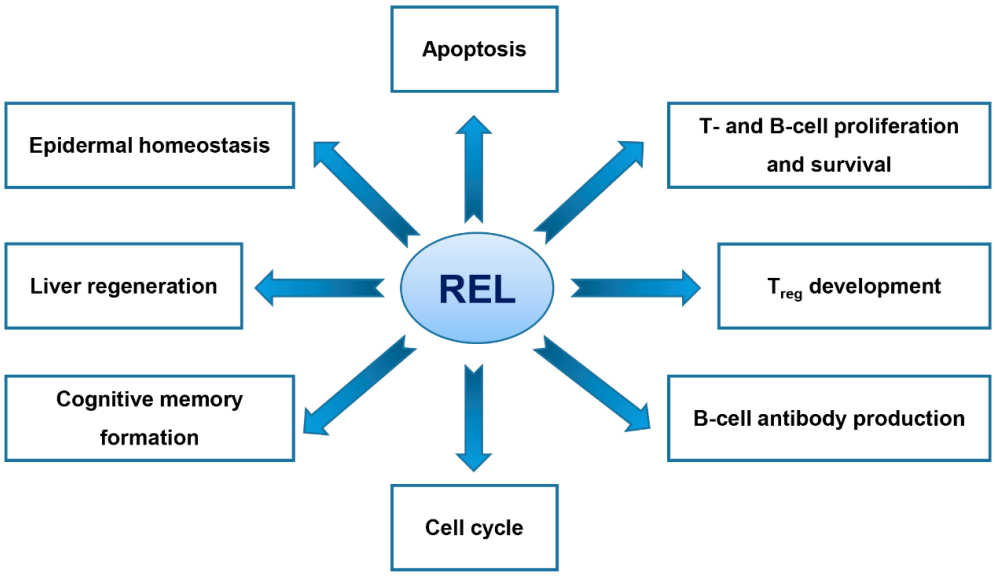

Figure 1.13. M**ain REL functions**. REL regulates general processes as apoptosis and cell cycle, but it also has specific roles in different cell systems (epidermis, liver, brain or immune system).

1.4.5. REL involvement in cancer

As *REL* was first described as the cellular homologue of v-*rel*, which causes lymphoma in birds (Brownell et al., 1987; Chen et al., 1983) and as the only NF-κB member with transforming ability (Gilmore et al., 2001), it was soon linked to the tumorigenic process. Although it does not always act as an oncogene, its importance in several lymphoid and solid tumors is unquestionably robust.

First, human *REL* gene is located at a chromosomal location (2p16) commonly amplified in a variety of B and T-cell malignancies, as Hodgkin's lymphoma (~46%) and non-Hodgkin's lymphomas (~15% for diffuse large B cell lymphoma (DLBCL), ~7% Burkitt's lymphoma) or natural killer T cell leukemia (~40%) and cutaneous CD30+ anaplastic large cell (~75%) lymphomas. This amplification normally correlates with increased nuclear REL and intensified NF-κB signaling. Moreover, lymphoma cell lines and DLBCL patient cells were observed to express the spliced hyperactive RELΔ9 isoform (Leeman et al., 2008). *REL* can be affected by translocation or mutation; for instance, the S525P mutant was found in B-cell lymphomas and it has a higher transforming activity *in vitro* (Gilmore and Gerondakis, 2011; Hunter et al., 2016).

Second, REL is also involved in solid tumors, which usually display an aberrant NF-κB signaling. In fact, *REL* overexpression is detected at a frequency of 8-2.5% in ovary, breast, colon, prostate, among other cancers (Slotta et al., 2017). Besides, *REL* overexpression can induce mammary tumors in mouse models of breast cancer (Romieu-Mourez et al., 2003). In other cases, NF-κB block is an advantage for tumoral cells, as it happens in MYC-dependent murine lymphoma cells (Klapproth et al., 2009). Mice lacking *Rel* were more prone to tumorigenesis, as it is described in a model of colitis-associated cancer (Burkitt et al., 2015).

Finally, REL can indirectly affect cancer progression through the regulation of inflammation and fibrosis, two key processes in tumorigenesis (Hunter et al., 2016).

Aims

2. Aims

Since its discovery, several studies have supported the importance of MNT for cell homeostasis and the control of MYC activities. Being the most divergent member of the MXD family, MNT is an essential and ubiquitous protein. However, little is known about how MNT is regulated and whether other proteins work in collaboration with MNT. This Thesis work has the objective to give an insight into MNT protein for the better understanding of its role in the MYC proximal network.

2.1. MNT as a regulator of the NF-κB pathway

Previous proteomic studies in our laboratory established a possible interaction between MNT and REL, an important member of the NF-κB pathway. We decided to study this interaction with the following objectives:

1) To confirm the interaction between MNT and REL in different rodent and human cell lines.
2) To investigate the presence of other NF-κB members in the complex with MNT.
3) To study the domain of MNT involved in the interaction with REL and the subcellular localization of the complexes.
4) To analyze the impact of the MNT-REL interaction on REL activity in NF-κB signaling.

2.2. MNT functions beyond MAX interaction

MNT functions have always been related to MAX. However, the discovery of *MAX* deletions in some tumors and in the rat PC12 cell line raised the possibility of MNT having MAX-independent functions. In the present work, using PC12-derived cells, we wanted to study possible MAX-independent functions of MNT in three objectives:

1) To study the formation of MNT-MLX heterodimers and MNT homodimers.
2) To test the MNT and MLX role in proliferation and gene regulation, including the direct binding to DNA.
3) To determine the autoregulation of MNT at the transcriptional and post-transcriptional levels.

2.3. Transcriptional regulation by MNT

MNT is an essential protein whose relevance has been attributed to its function as a MYC modulator. However, MNT transcriptional regulation in the absence of MAX and/or MLX and the pathways where it is involved have not been studied in deep. We decided then to approach these objectives:

1) To determine new MNT target genes through the analysis of the *MNT* knockout transcriptome in the HAP1 cell line.
2) To analyze the role of MAX and MLX in the regulation of new MNT-target genes.

Materials and Methods

3. Materials and methods

3.1. Cell culture

3.1.1. Cell lines and maintenance

The cell lines used in this work were grown in DMEM, RPMI-1640 or IMDM (Lonza), supplemented with 10 % (v/v) fetal bovine serum (Gibco™), 150 µg/mL of gentamicin (Lab. Normon) and 2 µg/mL ciprofloxacin. In the case of UR61-derived cell lines (URMT and URMax34) they were also supplemented with G418 at 250 µg/mL and Hygromycin B at 100 µg/mL (Gibco™). All the cell lines (listed in **Table 3.1**) were grown at 37 ºC in a humidified 5 % CO_2 atmosphere.

Cell densities were maintained below 80 % confluence by sub-culturing them at a ratio of 1:3 – 1:10. After aspirating cell culture media, cells were washed with 5-10 mL of PBS 1X (Phosphate Buffered Saline) and then detached using 1-2 mL of Trypsin-EDTA (Lonza). Finally, cells were collected with cell culture media, neutralizing trypsin activity.

3.1.2. Cell proliferation and viability assays

a) Cell counting

In order to have the correct confluence for each experiment, cells were counted using the NucleoCounter® NC-100™ system (Chemometec), following the manufacturer's instructions. In addition, the Neubauer chamber was used for some experiments, together with trypan blue (Invitrogen) for checking cell viability.

Table 3.1. Cell lines used in this Thesis work.

	Cell Line	Background	Culture medium	Origin/reference
Mouse	Neuro-2a	Neuroblastoma	DMEM 10 % FBS	A. Perez-Castillo (Olmsted et al., 2006)
Rat	C6	Glioma	DMEM 10 % FBS	M. Lafarga (Benda et al., 1968)
	U7	PC12 derivative clone	DMEM 10 % FBS	Laboratory collection (Burstein and Greene, 1982)
	UR61	PC12 derivative cell line (inducible N-RAS oncogene)	DMEM 10 % FBS	Laboratory collection (Guerrero et al., 1988)
	URMT	UR61 derivative cell line (inducible empty vector)	DMEM 10 % FBS	Laboratory collection (Quintanilla, 2013)
	URMax34	UR61 derivative cell line (inducible MAX gene)	DMEM 10 % FBS	Laboratory collection (Quintanilla, 2013)
Human	CEM	Acute lymphoblastic leukemia	RPMI 10 % FBS	A. Bigas/L. Espinosa (Foley et al., 1965)
	HAP1 WT	KBM7 derivative Chromic myeloid leukemia	IMDM 10 % FBS	Horizon™
	HAP1 MNT KO	HAP1 knockout for MNT	IMDM 10 % FBS	Horizon™
	HEK293T	Human embryonic kidney (SV40 T antigen constitutive expression)	DMEM 10 % FBS	Laboratory collection (Graham et al., 1977)
	HeLa	Cervical cancer	DMEM 10 % FBS	Laboratory collection (Gey et al., 1952)
	Jurkat	Acute T cell leukemia	RPMI 10 % FBS	Laboratory collection (Schneider et al., 1977)
	K562	Chronic myeloid leukemia	RPMI 10 % FBS	Laboratory collection (Lozzio and Lozzio, 1975)
	LoVo	Colorectal adenocarcinoma	DMEM 10 % FBS	A.Bigas/L. Espinosa (Drewinko et al., 1976)
	Lu165	Small Cell Lung Carcinoma	RPMI 10 % FBS	M. Sanchez Cespedes (Romero et al., 2014)
	MEC1	Chronic lymphocytic leukemia	RPMI 10 % FBS	ECACC (Stacchini et al., 1999)
	Raji	Burkitt's lymphoma	RPMI 10 % FBS	ATCC (Epstein et al., 1965, 1966)
	Ramos	Burkitt's lymphoma	RPMI 10 % FBS	Laboratory collection (Klein et al., 1975)

b) Clonogenic assays

First, cells were plated normally in six-well plates ($0.3 \cdot 10^6$ cells/well) after transfection or transduction (depending on the experiment). Once the experiment had finished, plates were washed twice with PBS 1X and stained with Crystal Violet solution for 15 min at room temperature (RT). Afterwards, several washes with water were done and the plates were left drying overnight. Finally, the plates were scanned for obtaining an image of the well and discolored with 10 % acetic acid for 10 min RT (in agitation). Then, the absorbance was measured at 620 nm in a spectrophotometer Multiskan FC (Thermo Scientific) in order to quantify the results.

- *Crystal Violet Solution: 1 % acetic acid, 1 % methanol, 1 % (w:v) crystal violet dye. Stored at RT and reusable.*

3.1.3. Drug treatments

Two drug treatments were carried out in this work. First, Zn_2SO_4 was used at 100 µM during 24 h to induce MAX gene expression in URMax34 and, as a control, in URMT cells. Second, human TNFα chemokine (Peprotech®) was used at 25 ng/mL during 30 min to activate the NF-κB pathway in UR61 and C6 cells.

- *Zn_2SO_4 Solution: dissolved in distilled water; stock solution: 75 mM; stored at 4 °C.*
- *TNFα: dissolved in 0.1 % BSA PBS 1X; stock solution: 100 µg/mL; stored at -20 ºC.*

3.2. Cell transfection

Cells were transfected following one of the three different transfection reagents and protocols described. The plasmids used are listed in **Table 3.2**.

Table 3.2. Plasmids used in this Thesis work. shRNA, short-hairpin RNA; aa, amino acids.

Name	Construct	Origin
pLKO.1 control	Empty vector	Sigma-Aldrich®
pLKO.1 – shScrambled (scrRNA)	Non-target shRNA control (SHC016-1EA)	Sigma-Aldrich®
pLKO.1 – sh-MNT-1 mouse/rat	shRNA against mouse/rat MNT mRNA (TRCN0000085733)	Sigma-Aldrich®
pLKO.1 – sh-MNT-1 human	shRNA against human MNT mRNA (TCR0000234788)	Sigma-Aldrich®
pLKO.1 – sh-MNT-2 human/mouse/rat	shRNA against human/mouse/rat MNT mRNA (TRCN0000235815)	Sigma-Aldrich®
pLKO.1 – sh-MAX-1 human/mouse/rat	shRNA against human/mouse/rat MAX mRNA (TRCN0000304477)	Sigma-Aldrich®
pLKO.1 – sh-MAX-2 human/mouse/rat	shRNA against human/mouse/rat MAX mRNA (TRCN0000231551)	Sigma-Aldrich®
pLKO.1 – sh-MLX-3 human/mouse/rat	shRNA against human/mouse/rat MLX mRNA (TRCN0000353574)	Sigma-Aldrich®
pLKO.1 – sh-MLX-5 human/mouse/rat	shRNA against human/mouse/rat MLX mRNA (TRCN0000329897)	Sigma-Aldrich®
pCMV-Sport6	Empty vector	Origene
pCMV-Sport6-MNT	Human MNT	Origene
pcDNA 3.1 Zeo	Empty vector	P.J. Hurlin
pcDNA 3 REL-flag human	Human REL with Flag-tag (N-t)	Addgene
pcDNA 3 REL-flag mouse	Mouse REL with Flag-tag (C-t)	Addgene
pcDNA 3.1 WT MNT-HA	Mouse MNT with HA-tag (C-t)	P.J. Hurlin
pcDNA 3.1 ΔbHLH MNT-HA	Mouse MNT with HA-tag (C-t) and a deletion of the bHLH domain (221-272 aa)	P.J. Hurlin
pcDNA 3.1 ΔNt_1 MNT-HA	Mouse MNT with HA-tag (C-t) and a deletion of the N-t domain (1-301 aa)	This thesis
pcDNA 3.1 ΔNt_2 MNT-HA	Mouse MNT with HA-tag (C-t) and a deletion of the N-t domain (1-273 aa)	This thesis
pcDNA 3.1 ΔCt_1 MNT-HA	Mouse MNT with HA-tag (C-t) and a deletion of the C-t and the SID domain (315-591 aa)	P.J. Hurlin
pME18F-MLX	Human MLX with Flag-tag (N-t)	D. Ayer (Billin et al., 1999)
Lv103	Empty vector	Genecopoeia
Lv103 MNT-GFP	Human MNT with GFP-tag (N-t) (EX-P0106-Lv103)	Genecopoeia
Lv158	Empty vector	Genecopoeia

	(EX-EGFP-Lv158)	
Lv158 MNT-flag	Human MNT with a Flag-tag (C-t) (EX-P0106-Lv158)	Genecopoeia
pRL-null	Renilla sp. luciferase reporter gene regulated by the T7 promoter	Promega
pNF-κB	Firefly sp. luciferase reporter gene regulated by 5 putative NF-κB regulatory elements	M. A. Piris (Martin et al., 2008)
pGL3 basic	Firefly sp. luciferase reporter gene with no promoter region	Promega
pGL3 IκBα-luc	Firefly sp. luciferase reporter gene with the promoter of NFKBIA (IκBα)	L. Espinosa
pBV-luc	Firefly sp. luciferase reporter gene with no promoter region	Addgene
pBV MNT-luc	*Firefly* sp. luciferase reporter gene regulated by 850 bp upstream the TSS of human *MNT*	Laboratory collection
pBV E-box 1 MNT-luc	*Firefly* sp. luciferase reporter gene regulated by 570 bp upstream the TSS of human *MNT*	This Thesis
pBV E-box 2 MNT-luc	*Firefly* sp. luciferase reporter gene regulated by 220 bp upstream the TSS of human *MNT*	This Thesis
pBV ΔE-box 2 MNT-luc	*Firefly* sp. luciferase reporter gene regulated by 220 bp upstream the TSS of human *MNT* with the E-box 2 deleted	This Thesis
pCMV-VSV-G	VSV-G-gene for the envelope lentiviral protein	Addgene
psPAX2	GAG and POL genes for the packaging lentiviral proteins	Addgene

3.2.1. Transfection with Polyethylenimine (PEI)

Cells were seeded for having a 60 % of confluence the day of the transfection. The DNA/PEI mixture was prepared in DMEM without serum and antibiotics. For a p60 plate, 3 µg of DNA were diluted in 100 µL of DMEM and 2.5 µg of PEI for each µg of DNA (7.5 µg of PEI for 5 µg of DNA) were diluted separately in other 100 µL of DMEM. Both tubes were mixed by vortexing and PEI dilution was added to the DNA mixture after 30 min of incubation RT. Meanwhile, the complete media of the plates was replaced by serum-free DMEM. Then, the mixture of DNA + PEI was added to the cells in a drop wise manner and gently homogenized by swirling. After 24 h, the media containing the DNA + PEI complexes was removed

and complete media was added to the cells. Finally, cells were harvested for analysis between 36-72 h after transfection.

PEI used for HEK293T, C6 cells.

- *PEI (Polysciences, Inc.): dissolved in distilled water; stock concentration 1 mg/mL, (pH: 7; Filtered with a 0.22 µm pore size sterile syringe filters) and stored at -20°C.*

3.2.2. Transfection by ScreenFect®A

As well as with PEI, cells were seeded for having a 60 % of confluence the day of the transfection. Then, 3 µg of total DNA were diluted in 120 µL of the dilution buffer and, in another tube, 18 µL of the reagent (6 times more than total µg of DNA) were diluted in 120 µL of the dilution buffer. Then, the two tubes were combined and mixed gently. After an incubation of 20 min RT, the mixture was added to the cells in a drop wise manner. After 24 h, the cell culture media was refreshed and cells were harvested for analysis between 36-72 h after transfection.

ScreenFect®A was used for LoVo cells.

3.2.3. Transfection by electroporation

Electroporation was performed with an Amaxa™ Nucleofector™ Device (Lonza), following the specific programs for each cell line that were already registered in the apparatus. Generally, $2 \cdot 10^6$ cells for each transfection were harvested, washed once with PBS 1X and resuspended in 100 µL Ingenio® Electroporation solution (MIRUS bio) together with 3 µg of total DNA. The mixture was placed in a cuvette (2 mm, VWR) for the electroshock. Afterwards, cells were resuspended in the corresponding media and seeded in plates. Cell culture media was refreshed 24 h after transfection. Finally, cells were harvested for analysis between 36-72 h after transfection.

Electroporation was used for UR61 cells.

3.3. Lentivirus infection

Cells were transduced with lentiviral particles for overexpressing or downregulating different genes. The plasmids used are listed in **Table 3.2**.

3.3.1. Lentiviral production

In order to produce the lentiviral particles, HEK293T cells were transfected using the PEI transfection method, with three different plasmids: (i) psPAX2, packaging plasmid encoding the HIV gag, pol, rev, and tat genes, (ii) pCMV-VSV-G, envelope plasmid encoding the VSV-G gene and (iii) transfer plasmid containing the LTR sequences, the psi packaging signal and the cDNA/shRNA of interest (normally a pLKO.1 vector, shown in **Figure 3.1**). The mixture of PEI + DNA (50 µg in a proportion of 6:19:25 µg) was added to each 150 mm Ø plate of HEK293T at a confluence of 70-80 %, which contained 15 mL of DMEM (without serum or antibiotics). After 12 h, the media was withdrawn and replaced by complete medium. 48 h and 72 h after transfection, the supernatant containing the lentiviral particles was collected, mixed and clarified by centrifugation at 1,500 rpm for 10 min. Then, this supernatant was filtered through a 45 µm pore size sterile syringe filter in order to remove possible cell debris.

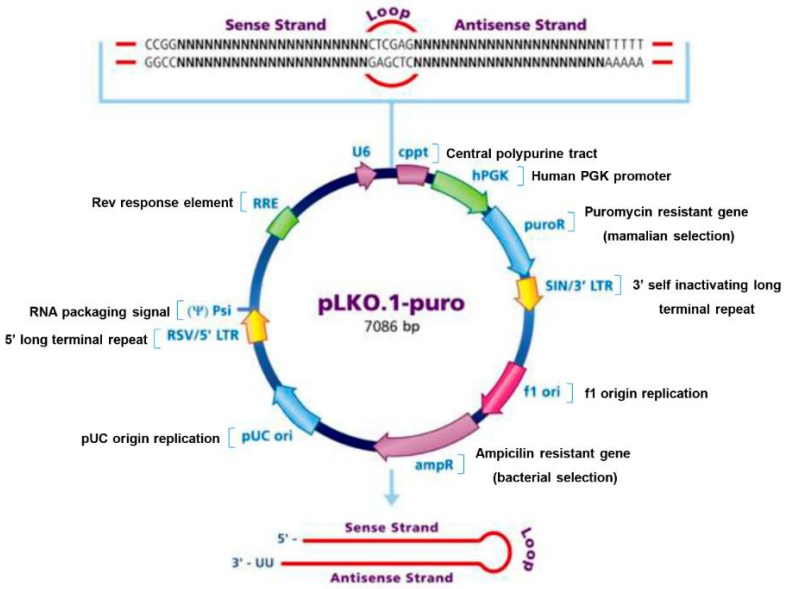

Figure 3.1: Scheme of the pLKO.1-puro vector used for gene knockdown. The specific vectors are listed in Table 3.2 and were ordered to Sigma-Aldrich®. Image modified from: https://www.sigmaaldrich.com/life-science/functional-genomics-and-rnai/shrna/library-information/vector-map.html.

3.3.2. Lentiviral concentration

Once the lentiviral-containing supernatants were clarified, Polyethylene Glycol 8000 (PEG8000, Fisher BioReagents) was added at a final concentration of 15 %-PEG8000 and homogenized gently by inversion. After an overnight incubation at 4 ºC, the mixture was centrifuged for 30 min at 1,500 xg 4 ºC. The obtained pellet was then resuspended in serum-free media (150 µL for each 15 mL), aliquoted and stored at -80 ºC.

- *PEG8000 (*Fisher BioReagents): *dissolved in PBS 1X; stock concentration 40 % (w/v); autoclaved; stored at RT.*

3.3.3. Lentivirus tittering

In order to determine the lentivirus titer, we seeded HeLa cells in a six-well plate ($2 \cdot 10^4$/well). Once attached, media was replaced by 1.5 mL of serum-free DMEM and 3 µg/mL of Polybrene® (Sigma-Aldrich) was added, together with different volumes of the concentrated lentivirus (normally 10 µL, 5 µL, 1 µL, 0.5 µL and 0.1 µL). After 12 h, 1.5 mL of complete media were added to each well and, 48 h after infection, the selective antibiotic (puromycin for all the viral particles used in this work, at 1 µg/mL) to select the infected cells. Media supplemented with puromycin was refreshed daily until the colonies had grown and remained separated from each other. Then, the media was removed and the plate washed twice with PBS 1X for posterior staining with Crystal Violet solution, as described in 3.1.2.b. Finally, the number of colonies was determined by counting, assuming that each one comes from one single cell infected by one single lentiviral particle. The titer was later calculated by: (x number of colonies/ y µL of virus) $\cdot$ 10^3 = C.F.U./mL.

3.3.4. Cell transduction

Once we had the virus produced and tittered, cells (normally $0.5 \cdot 10^6$ cells/p60) were resuspended 1 mL of serum-free media with the corresponding volume of lentiviral particles, together with Polybrene® (3-5 µg/mL) in a 1.5 mL Eppendorf

tube. After 1 h incubation at 37 ºC incubator and frequent mixing, the mixture was plated into a p60 with complete media. After 12 h, media was refreshed. If the experiment required a transient expression, cells were harvested 72 h after infection, while if cell selection was necessary, puromycin (0.3-1 µg/mL) was added 48 h after infection and the selection extended for the estimated days, depending on the experiment.

- *Polybrene (Sigma-Aldrich®): dissolved in distilled water; stock concentration: 5 mg/mL; stored at -20 °C.*

3.4. DNA and RNA analysis

3.4.1. Bacterial transformation and DNA plasmid purification

Plasmid DNA was transformed into heat-shock *E. coli* DH5α competent cells. The procedure started by thawing the DH5α cells in ice and mixing them with 100-200 ng of plasmid DNA. After an incubation of 30 min, a heat-shock of 20 s at 37 ºC was done. Then, bacteria were incubated in ice during two more minutes. Next, 1 mL of LB growth media was added to the transformed cells and incubated for 1 h at 37 ºC in an orbital shaking incubator. Finally, 100 µL of the bacteria were seeded on a LB agar plate containing the corresponding antibiotic selection (100 µg/mL ampicillin or 50 µg/mL kanamycin) and incubated overnight at 37 ºC.

Once single colonies were obtained from our transformation assay, normally three of them were selected and seeded on a separate LB agar plate and inoculated in 10 mL LB growth media, supplemented with antibiotic. After an overnight incubation at 37 ºC, LB media grown cells were centrifuged at 3,000 rpm for 10 min. Then, the cell pellet was processed with a GeneJet plasmid MiniPrep kit (Thermo Scientific).

Purified DNA plasmids were checked by enzymatic restriction digestion, using the corresponding restriction endonucleases (Fermentas) for each plasmid. To determine the preparation of the digestions, the Double Digest Calculator at the Thermo Scientific webpage was used. The digestions were run into an agarose

gel electrophoresis for analyzing the DNA fragments obtained. Agarose gel was prepared with low melting point agarose (Pronadisa) in 0.5 X TAE buffer to make a 0.8-1 % (w:v) agarose gel. Nucleic acid SYBR® Safe DNA Gel Stain (Invitrogen) was diluted 1:25,000 before gel solidification. DNA samples were mixed with 5X DNA loading buffer to a 1X final concentration and loaded into the gel. DNA fragments sizes were determined by using DNA size standards "1 Kb DNA ladder" or "100 bp DNA ladder" (Fermentas), run in a iMupid Mini gel Electrophoresis system for 30-40 min at 50-100 V, using 0.5 X TAE buffer. Finally, the gel was visualized in a Gel DocTM EZ Imager (Bio-Rad).

If the DNA plasmids had the correct fragments after digestion, bacteria were grown in a 250 mL LB growth matrass supplemented with antibiotic, in agitation and overnight at 37 ºC. The following day, 5 mL were centrifuged at 3,000 rpm for 10 min and resuspended in LB-glycerol (1:1) for preparing a stock to keep at -80 ºC. The rest of the culture was centrifuged at 6,000 rpm for 10 min and plasmid DNA was purified using the Plasmid Midi Kit (Qiagen), following manufacturer's instructions. Plasmid DNA concentrations were determined by measuring their absorbance at 260 nm in a microvolume spectrophotometer (Thermo ScientificTM NanoDrop 2000).

- *DNA loading buffer: 30 % Glycerol (Sigma-Aldrich®) diluted in distilled water (v/v); stock concentration: 5X; stored at 4 °C.*
- *TAE Buffer: 400 mM Tris; 200 mM acetic acid; 10 mM EDTA pH8; stock concentration: 10X pH 8.3; stored at RT.*

3.4.2. DNA cloning

a) MNT promoter luciferase vectors

Using the pBV MNT-luc, which was previously made in our laboratory (Lafita-Navarro, 2015), we built luciferase vectors containing only the E-box 1 or the E-box 2 of MNT promoter. The pBV MNT-luc contained 850 bp upstream the TSS of human MNT promoter, which sequence was obtained from the UCSC genome browser (http://genome.ucsc.edu/). Thus, we designed primers for amplifying

each region of interest. These primers contain the restriction enzyme recognition sequences that enabled the cloning of the fragments (**Figure 3.2**).

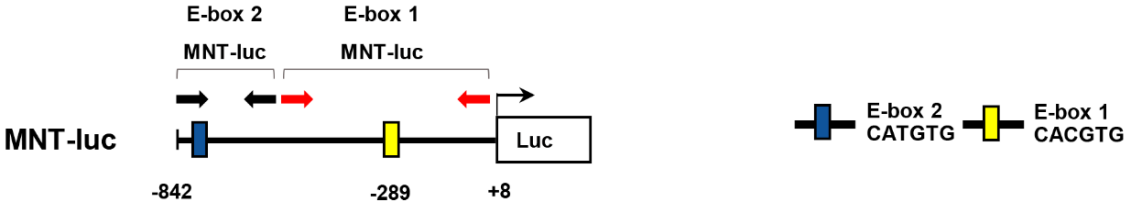

E-box 1 MNT-luc_**EcoRV** F :	TC**GATATC**ATGTGACCTGCAGACACTGG
E-box 1 MNT-luc_**HindIII** R:	TTG**AAGCTT**GCGACTGGAGACTGTCAAGA
E-box 2 MNT-luc_**EcoRV** F:	TC**GATATC**CAGTCTCTGCCATTCCCAAG
E-box 2 MNT-luc_**HindIII** R :	TG**AAGCTT**GGCACTGCCTCCCTTCTT

Figure 3.2: Scheme of the MNT promoter luciferase vector. The arrows represent the primers used in the cloning for each construct, which are listed below.

The procedure started with the digestion of the pBV-luc empty vector with EcoRV and HindIII and its treatment with alkaline phosphatase for avoiding a possible re-ligation. Second, 4 ng of pBV MNT-luc were amplified with the primers shown in **Figure 3.2** by PCR. PCR was performed with the Phusion High-Fidelity DNA Polymerase (ThermoScientific) following manufacturer's instructions and this protocol: 1 min at 98 ºC, (15 s at 98 ºC, 1 min at 90 ºC and 30 s at 72 ºC) x 30 cycles, 10 min at 72 ºC. Then, the digested vector and the products from the PCR were loaded into an agarose gel and run by electrophoresis. The corresponding bands were purified using the GeneJet Gel extraction kit (Thermo Scientific), following manufacturer's instructions. Purified digested vector and the PCR products were ligated using the T4 DNA ligase (Thermo Scientific). The reaction contained 1 µL of digested pBV-luc, 8 µL of the E-box 1 or 9 µL of the E-box 2 fragment (ratio Vector: Insert = 1:5 in mass), 2 µL 10X T4 DNA ligase buffer, 0.2 µL T4 DNA ligase (5 U/µL) and up to 20 µL DNAse-free water. The mix was incubated 1 h at 22 ºC following an enzyme inactivation step of 10 min at 65 ºC.

After ligation, 5 µL of the reaction was transformed into *E.coli* DH5α by the heat-shock method and tested by plasmid purification and digestion, as described in **3.4.1**.

b) MNT deletion constructs

In order to generate MNT constructs with deletions in different domains of the protein, we decided to start with the pcDNA 3.1 WT MNT-HA, from our collaborator P.J. Hurlin (Shriners Hospital for Children; Portland, USA). This plasmid contains the mouse MNT sequence together with a hemagglutinin (HA) tag at its C-terminal domain. By designing different primers, we generated two new constructs: ΔNt_1 and ΔNt_2 (**Figure 3.3**).

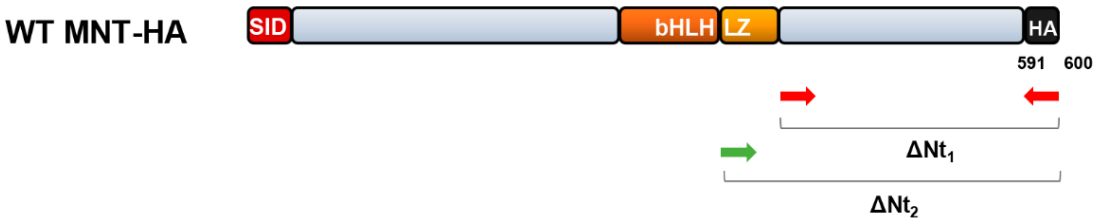

ΔNt_1 MNT-HA_**BamHI** F :	TC**GGATCC**ATGAAGCATGAGCTGAGTCAGTGG
ΔNt_1 MNT-HA _**EcoRI** R:	TG**GAATTC**TCAAGCGTAATCTGGAACATCGTA
ΔNt_2 MNT-HA_**BamHI** F :	TC**GGATCC**ATGTCCCTGAAGAGGAAGGAGAA
ΔNt_2 MNT-HA _**EcoRI** R:	TG**GAATTC**TCAAGCGTAATCTGGAACATCGTA

Figure 3.3: Scheme of the pcDNA 3.1. WT MNT-HA. The arrows represent the primers used in the cloning for each construct, which are listed below. SID for SIN3 Interaction Domain; bHLHLZ for basic-loop-helix leucine zipper domain; HA for hemagglutinin.

First, the pcDNA3.1 empty vector was digested with BamHI and EcoRI and treated with alkaline phosphatase for avoiding a possible re-ligation. Second, 0.2 µg of WT MNT-HA were amplified with the primers shown in **Figure 3.3** by PCR. PCR was performed with the Phusion High-Fidelity DNA Polymerase (ThermoScientific) following manufacturer's instructions and this protocol: 30 s at 98 ºC, (15 s at 98 ºC, 30 s at 57 ºC and 30 s at 72 ºC) x 35 cycles, 7 min at 72 ºC. Then, the digested vector and the products from the PCR were loaded into an agarose gel and run by electrophoresis. The corresponding bands were purified with the GeneJet Gel extraction kit (Thermo Scientific), following manufacturer's instructions. Purified digested vector and the PCR products were ligated using the T4 DNA ligase (Thermo Scientific) and following this equation: (100 ng vector · kb insert · 1/5) / kb vector = ng insert.

The mix was incubated 1 h at 22 ºC following an enzyme inactivation step of 10 min at 65 ºC. After ligation, 5 µL of the reaction was transformed to *E.coli* DH5α by the heat-shock method and tested by plasmid purification and digestion, as described in **3.4.1**.

3.4.3. RNA extraction and purification

RNA was purified from cell cultures using the TriReagent (Molecular Research Center), based on the guanidinium thiocyanate-phenol-chloroform extraction. Generally, $2 \cdot 10^6$ cells were harvested and lysed with 0.5 mL of TriReagent. After and incubation of 10 min RT, 100 µL of chloroform were added, mixed for 15 s and centrifuged at 12,000 rpm for 15 min at 4 ºC. Then, the upper phase was transferred to a new tube, where 250 µL of isopropanol were added, mixed and incubated for other 10 min RT. Next, the solution was centrifuged at 14,000 rpm for 10 min at 4ºC. The supernatant was discarded and the RNA pellet was washed with 75 % ethanol by vortexing. Then, the sample was centrifuged at 7,500 rpm for 5 min at 4 ºC and the supernatant was removed. Once completely dried, RNA was resuspended in 30 µL of water free of RNAses and its concentration was measured at 260 nm in a microvolume spectrophotometer (Thermo ScientificTM NanoDrop 2000).

3.4.4. Reverse transcription and quantitative polymerase chain reaction (RT-qPCR)

Reverse transcription was carried out with the iScript™ cDNA Synthesis Kit (Bio-Rad) from 1 µg of RNA, according to manufacturer's instructions in a total volume of 20 µL. The protocol for the reaction was the following: 5 min at 25 ºC, 20 min at 46 ºC and 1 min at 95 ºC.

Once the cDNA was obtained, we performed quantitative PCR. For each sample, the PCR mix consisted of 15 µL 2X SYBR® Select Master Mix (Applied Biosystems™); 0.2 µM of forward and reverse primer mix; 2 µL cDNA sample and up to 32 µL of water (used for two 15 µl duplicate reactions). PCRs were

carried out in a CFX Connect™ Real-Time PCR Detection System (Bio-Rad), following this protocol: 5 min at 95 ºC / (5 min at 95 ºC; 15 s at 57 ºC; 15 s at 72 ºC) x 40 / 1 min at 95 ºC. The mRNA expression was normalized to the housekeeping gene *RPS14* using the comparative Delta Ct (ΔCt) method:

$$\Delta Ct = 2^{\text{(Ct normalizing gene– Ct gene of interest)}}$$

The primers used for RT-qPCR are listed in **Table 3.3.** and were designed using the Primer 3 online software tool (http://bioinfo.ut.ee/primer3-0.4.0/). The parameters used are in line with the general PCR standards: length 18 to 22 bp, GC content 40 to 65 %, no secondary structures and T_m around 60°C.

Table 3.3. Primers used for RT-qPCR analysis.

	Gene	Primers Sequence (5' → 3')	Tm (ºC)
Rat	*BIRC5*	GCCTACAAGGAAGTGCAAGG GCGTCCTCATTCAGAAGCTC	60
	BRCA1	GCCTACAAGGAAGTGCAAGG GCGTCCTCATTCAGAAGCTC	60
	CCNG2	TGACCTTGATGGAGGCTACC CAGGGCCAAGAATCTATCCA	60
	CDK1	GCCAGTTCATGGATTCTTCG CCGAAATCTGCCAGTTTGAT	60
	CDK12	CCTCCCTCCCCTATTACCTG GTAATTGCCTTTGGCTCTGG	60
	CDKN1C	CTCTCCTAACGTGGCTCCTG GATGCCCAGCAAGTTCTCTC	60
	E2F6	CAGTGAAGGCTCCAGAGGAA AGAGGCCCCTACTCCATCAG	60
	ERCC6	GCGCTCTCTCAGACAGACAA GCACTGGGACTTTCTTCTCG	60
	FBXO32	CTACGATGTTGCAGCCAAGA GGCAGTCGAGAAGTCCAGTC	60
	MAX	CACCATAATGCACTGGAACG CTGGTGCGTATGGTTTTTCC	60
	MLX	CTCATGAGGGAGAGGACCAG GGACACCGATCACAATCTCC	60
	MNT	GAGAAGATTGCCACACAGCA GGACGATGGTTCAGCTTAGG	60
	PARPBP	TGGCGTGCTCATTGTAACTC CTCAGAGCGCAGAACAAGTG	60
	RPS14	CAAGGGGAAGGAAAAGAAGG GAGGACTCATCTCGGTCAGC	60
Human	*BCL2L1*	ACATCCCAGCTCCACATCAC	60

		AAGAGTGAGCCCAGCAGAAC	
	BMP2	TAGCAGTTTCCATCACCGAAT GACACCTTGTTTCTCCTCCAA	64
	CHMP4C	TGGCTTTGGTGATGACTTTG GACGACATGCCTGGTTTTCT	64
	FOXG1	GACGCAGACCTTGAGAACAAC TGCCAACTGAAACAACTTTCC	64
	GLIS3	GTTTGAAGGTTGCGAGAAGG GGGTCTGTGTAGCGTTTGGTA	60
	HECW2	CTTAGTGCGTGGCTTCTATGA AATGCTGGATGTGCCTGTAAC	60
	LIN28A	TGGGGGCTATTCTTTTGCTAT GCAGGTTGTAGGGTGATTCC	60
	MAPK10	GTGATTGACCCAGCAAAAAGA CATTGACAGACGAGGATGGAG	60
	MAX	TGTTGTTGTCGGTGACTTCC CATTATGATGAGCCCGTTTG	60
	MLX	TCAACGTGTTTCAAGGCATC AGGACGCCAATCACAATCTC	60
	MNT	AGCCAGTGGATGGACGTACT GACGATGGCTCAGCTTAGGT	60
	MYB	GCAGTGACGAGGATGATGAG TGTTCCATTCTGTTCCACCA	60
	MYC	TCGGATTCTCTGCTCTCCTC CCTGCCTCTTTTCCACAGAA	60
	NFKB1	CATCCCATGGTGGACTACCT ACAGTGCAGATCCCATCCTC	60
	NFKBIA	TGAAGAAAAGGCACTGACCA CTCACAGGCAAGGTGTAGGG	60
	NKX2-4	ACTGCGATTCAAAACGAACC CCACCTTTTCGCGTCATTTA	60
	REL	GAACGATTGGGAAGCAAAAG GGCACAGTTTCTGGAAAAGC	60
	RELA	GGCGAGAGGAGCACAGATAC CAGCCTCATAGAAGCCATCC	60
	RNF128	TTATTATTACGGCGGCAACTG ACTATCTCCATCAGGGCCAAT	60
	RPS14	TCACCGCCCTACACATCAAACT CTGCGAGTGCTGTCAGAGG	60
	SCARA3	GATGCCTTGTGCGTTACAGA AGGGCCAGGAAGAGGTAAAG	60
	THBS1	TGCCATCCGCACTAACTACA ATCAACAGTCCATTCCTCGTT	60
	WIPI1	GCCTCCAGTAACACCGAGAC AAAAGCCCTGTCCTGATGC	60

3.4.5. RNA-seq analysis

a) Library preparation and sequencing

First, total RNA (1-4 µg) of two samples (WT and MNT KO HAP1) and three replicates was obtained using TriReagent (Molecular Research Center), as described in 3.4.3., followed by RNA MiniQiagen kit purification and Ribozero treatment. The three replicates came from three independent RNA extractions carried out from cells harvested in three different days. This RNA was used to construct 250 bp-insert size mRNA libraries using Illumina TruSeq RNA Sample Prep Kit v2, following manufacturer's instructions. After quantification, quality control on a 2100 Agilent Bioanalyzer and normalization, a mix of four barcoded libraries per lane were submitted on a High-Seq 2000 Illumina sequencing platform following a 100 bp Paired-End protocol, obtaining a minimum of 30-40 million reads for each sample.

The libraries were prepared by M.C. Rodríguez González (Massive Sequencing Service – IBBTEC).

b) Data analysis

The RNA sequence reads obtained from each sample were aligned against human genome (UCSC hg19) using the TopHat 2.0.1 software that uses Tophat algorithm (Trapnell et al., 2009). Once sequence reads were aligned, Cufflinks software (Trapnell et al., 2012), DESeq2 (Love et al., 2014) and RNA-eXpress (Forster et al., 2013) were run to assemble the alignments into a parsimonious set of transcripts to test for differential expression. Transcripts abundances were estimated based on the number of reads per transcript. Estimated expression values were represented in RPKM units (**r**eads **p**er **k**ilobase per **m**illion reads) originally proposed by Mortazavi et al. (2008).

The analysis was carried out by M. Molina Edesa (Massive Sequencing Service – IBBTEC).

c) Functional analysis

RNA-seq results from the three softwares (Cufflinks, DESeq2 and RNA-eXpress) were compared with gene sets derived from the biological process gene ontology (based on MsigDB platform, http:software.broadinstitute.org/gsea/msigdb, (Liberzon et al., 2011). A FDR q-value below 0.05 was used.

Data obtained by Cufflinks was used for a Gene set enrichment analysis (GSEA) (Subramanian et al., 2005) and the pathways with a nominal p-value below 0.05 were considered as significative. Among them, the ones with a FDR q-value below 0.25 were highlighted.

3.5. Promoter analysis

3.5.1. Chromatin immunoprecipitation (ChIP)

Cells were grown until obtaining an 80 % confluence (normally, four 150 mm Ø cell plates, $20 \cdot 10^6$ cells/plate). Cells were washed twice with PBS 1X and fixed with 1 % formaldehyde-PBS 1X for 10 min RT in a shaker (gentle agitation). This step is key for cross-linking the proteins and the DNA. Then, glycine was added to a 125 mM final concentration and incubated for 5 min at 4 ºC in a shaker in order to stop the cross-linking reaction. Next, cells were washed twice with cold PBS 1X and harvested by scrapping in N/C Lysis Buffer 1 (1 mL/150 mm Ø plate), for purifying only the cell nuclei. After an incubation of 30 min at 4 ºC in a rotating wheel, the lysate was centrifuged 5 min at 1,500 rpm and resuspended in ChIP Lysis Buffer (500 µL/150 mm Ø plate). The lysate was also passed through a G20 needle syringe 4-5 times and homogenized by pipetting up and down on ice for 10 min. Next, cell lysates were sonicated to shear chromatin in sizes of 200 to 600 bp using the Bioruptor® Plus sonication device (Diagenode) for normally 10 cycles (30 s on and 30 s off). After sonication, cell lysates were centrifuged for 5 min at 14,000 rpm at 12ºC (the SDS precipitates easily at lower temperatures). Supernatants containing the sheared chromatin were collected and 30 µL was kept for checking the sonication efficiency. The rest of the lysate was preserved at -80 ºC.

Then, the 30 µL of chromatin sample were diluted with 170 µl of ChIP Dilution buffer, together with 12 µL of 5 M NaCl and 6 µL of 10 mg/mL RNAse A. The mix was incubated in agitation at 65 ºC overnight to reverse protein-DNA crosslinks and degrade RNA. The next day DNA fragments were purified with QIAquick PCR Purification Kit (Qiagen) following manufacturer's instructions and ran in a 1.5 % (w:v) agarose gel together with the "100 bp DNA ladder" standard. This purified DNA was kept at -20ºC as the input of the experiment.

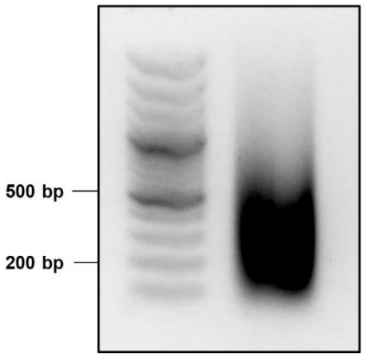

Figure 3.4. DNA from LoVo cells sonicated 10 cycles for ChIP assays. On the left, the 100 bp DNA ladder marker and on the right, the sample.

Once DNA fragmentation between 200 and 600 bp was achieved (an example is shown in **Figure 3.4**), 200 µL of the cell lysate (corresponding to $8 \cdot 10^6$ cells) were diluted 10 times with ChIP dilution buffer. Then, 3 µg of specific antibody or, as a mock control, unspecific immunoglobulins or water were added. The cell lysate-antibody mix was incubated rotating overnight at 4 ºC. The following day, protein G-bound magnetic beads "Dynabeads®-protein G" (Invitrogen) were used to capture the DNA-protein-antibody complexes, as they bind to the immunoglobulins constant regions (Fc). For each immunoprecipitation, 30 µL of "Dynabeads®-protein G" were washed with dilution buffer, collected using the DynaMag™ magnet (Invitrogen) and resuspended in 200 µL of dilution buffer. Then, they were added to the lysate-antibody and incubated for 30 min at 4 ºC in a rotating wheel. After incubation, beads-immunocomplexes were collected with the magnet and washes of 5 min at 4 ºC in rotation were done sequentially with 1 mL of the four different ChIP wash buffers: Low salt wash buffer, High salt wash buffer, LiCl wash buffer and TE wash buffer (x 2).

Finally, the immunocomplexes were separated from the beads with 200 µL of ChIP Elution Buffer and 12 µL of 5 M NaCl and 6 µL of 10 mg/mL RNAse A, overnight at 65 ºC in a shaker. Next day, 1 µL of 20 mg/ml proteinase K, 2 µL 0.5 M EDTA and 4 µL 1M Tris-HCl pH 6.8 were added and the mix was incubated for 3 h at 45 ºC in agitation to degrade proteins. Then, DNA was purified with QIAquick PCR Purification Kit (Qiagen) following manufacturer's instructions and eluted in 50 µL milli-Q water.

The results of the ChIP were obtained by qPCR (as described in 3.4.5.). In this case, 3 µL of eluted and input DNA (the latter previously diluted 1:10 in water) were used for quantitative PCR. Immunoprecipitated DNA was normalized to total DNA quantity in the lysate (input) using the comparative Delta Ct (ΔCt) method ($\Delta Ct=2^{(Ct\ Input - Ct\ DNA\ immunoprecipitated)}$) and then to DNA immunoprecipitated with unspecific IgGs or the beads. As a control of the qPCR, water was used as a negative control to detect possible amplification signals from contaminant DNA or primer dimers.

- *N/C Lysis Buffer 1: 10 mM HEPES pH 7; 10 mM KCl; 0.25 mM EDTA pH 8; 0.125 mM EGTA pH 8; 0.1 % (v:v) IGEPAL (Sigma- Aldrich); 1 mM DTT. 1:100 proteases inhibitor cocktail Set I (Calbiochem) and phosphatase inhibitor cocktail I (1:100; Sigma-Aldrich®) added just before use.*
- *ChIP Lysis Buffer: 50 mM Tris HCl pH 8; 10 mM EDTA; 1 % SDS. 1:100 proteases inhibitor cocktail Set I (Calbiochem) and phosphatase inhibitor cocktail I (1:100; Sigma-Aldrich®) added just before use.*
- *ChIP Dilution Buffer: 0.01 % SDS; 1.1 % Triton X-100; 1.2 mM EDTA; 20 mM Tris-HCl pH 8; 150 mM NaCl.*
- *Low salt wash buffer: 0.1 % SDS, 1.1 % Triton X-100, 2 mM EDTA, 20 mM Tris-HCl pH:8, 150 mM NaCl.*
- *High salt wash buffer: 0.1 % SDS, 1.1 % Triton X-100, 2 mM EDTA, 20 mM Tris-HCl pH 8, 500 mM NaCl.*
- *LiCl wash buffer: 0.25 M LiCl, 1 % IGEPAL (Sigma-Aldrich), 1 % sodium deoxycholate, 1 mM EDTA, 10 mM Tris-HCl pH 8.*
- *TE wash buffer: 10 mM Tris-HCl pH 7.5, 1 mM EDTA.*
- *ChIP elution buffer: 1 % SDS; 50 mM Tris-HCl pH 7.5.*

Table 3.4. Primers used for ChIP-PCR analysis. T_m = 60 ºC.

	Gene	Coordenates from TSS (bp)	Primers Sequence (5' → 3')
Rat	*BIRC5*	+318/+483	CTCTCCCCTCCCTTTACCTG CTCGTGAGCAAGGATCAACA
	BRCA1	+88/+310	CGGAAGAAAGGTGAGACAGC GGACTCCCTCACACATCCAT
	CDK1	-216/-54	GACGACATTGGAAGGAAAGC TGCACGTAGACGTTCAAAGG
	CDKN1C	-118/+223	GCGGTGTTGTTGAAACTGAA CTCGATCGTTTGTCCTGTCC
	E2F6	+303/+546	ACGAGGCACGTGTAGAGCTT ACAAAAGACGGATCCACCAG
	MNT promoter	-654/-478	CCGCTAATACGACCCTGAAG CCGGATTTTGTCTCTGTTCC
	MNT upstream	-1369/-1198	ATGGCTTCCACCAAAGTAGC CCTCTCTCAACCAACCGTCT
Human	*MNT* promoter	-842/-619	ATGTGACCTGCAGACACTGG GCGACTGGAGACTGTCAAGA
	MNT upstream	-4729/-4549	GAGTTCCGCTCTGTTTGCTT GCTGCAGGATGAAGAGGAAA
	NFKBIA	-743/-937	GTGCCCAGAAGTAGGCTCAC TGGGGAAACTGCTGAATAGG
	NFKBIA	-275/-476	CCAGCCATCATTTCCACTCT CCTGCACCCTGTAATCCTGT
	NFKBIA	-67/-316	AGAAGGCTCACTTGCAGAGG GGAATTTCCAAGCCAGTCAG
	NFKBIA	+171/+343	AGAAGGAGCGGCTACTGGAC ACTTACGAGTCCCCGTCCTC
	NFKBIA	+801/+1003	GCCAGGAACACTCAGCTCAT CCATGGTCAGTGCCTTTTCT
	NFKBIA	+1959/+2176	CTTGGGTGCTGATGTCAATG CCCCACACTTCAACAGGAGT
	TXNIP	-156/+51	TCCAGAGCGCAACAACCAT AAGCAGGAGGCGGAAACGT

3.5.2. ChIP-seq

For ChIP-seq analysis, DNA was obtained following the protocol in 3.5.1. Single-end 51 bp ChIP-seq data from 3 replicate experiments (anti-MNT URMT) and 3 input samples were generated by HiSeq. Alignment and peak detection were performed using the ENCODE (phase-3) transcription factor ChIP-seq pipeline specifications (Consortium, 2012). Reads were aligned to the rat reference genome (assembly Rnor_6.0) using BWA (Li and Durbin, 2009), removing

duplicates with PICARD (Picard Toolkit 2018, http://broadinstitute.github.io/picard) and filtering all reads with a quality score < 30. Peaks were called using SPP (Kharchenko et al., 2008) and input samples as background samples. Enrichment and quality measures were computed with Phantompeakqualtools (Landt et al., 2012). Reproducibility of peaks identified from the 3 replicate experiments was measured using IDR with a threshold of 0.1 and peaks with a q-value < 0.7 were considered significant. Peak annotation was performed with Homer (http://homer.ucsd.edu/homer/motif/motifDatabase.html) (Heinz et al., 2010).

The analysis was carried out by DREAMgenics (Oviedo, Spain). The HOMER data were obtained by Ignacio Varela (Genomic analysis of tumour development, IBBTEC).

3.5.3. Luciferase reporter assays

The analysis of the promoter's activity upon overexpression or knockdown of the gene of interest was performed using luciferase reporter assays.

Generally, $2 \cdot 10^6$ cells were transfected with a mix of DNA plasmids specific for each experiment. First, the firefly (*Photinus pyralis;* 1 µg) luciferase gene reporter vector carrying a 5' transcription regulatory sequence or a control vector without any specific transcription regulatory sequence. Second, "pRL-null" Renilla (*Renilla reniformis*; 0.5 µg) luciferase gene construct that is constitutively expressed and it is used as control of transfection efficiency. Third, the specific gene/short hairpin sequence or control constructs that we wanted to use for each experiment (1.5 µg).

Luciferase reporter assays were carried out with the Dual-Luciferase Reporter (DLR) System (Promega). Briefly, cells were harvested and lysed with 100 µL PLB (Passive Lysis Buffer) diluted in distilled water, and incubated 30 min in ice. Then, cell lysates were frozen at -80 ºC for 30 min to increase the lysis efficiency. Cell lysates were thawed and centrifuged 15 min at 14,000 rpm and supernatants were collected for the assay. For each condition, 20 µL of cell lysate were loaded

into a 96-well plate (in duplicates). Next, 100 µL of Luciferase Assay Reagent (LARII) containing the firefly luciferase substrate (luciferin) was added and luminescence was measured within 1 min after addition. After quantifying luminescence, Firefly luciferase reaction was quenched with 100 µL of Stop&Glo® Reagent that also contains the Renilla luciferase substrate (coelenterazine) so that starts the second luciferase reaction. Luminescence from both luciferase reactions was measured with the Glomax Multi-detection System (Promega). Firefly luminescence values were normalized against Renilla luminescence values, as they constitute a control of the transfection for each sample. The mean of the duplicates was done, and values were relativized against the empty vector (control). The results were finally represented as Relative Luciferase Units (R.L.U.).

3.6. Protein analysis

3.6.1. Western Blot

Cell lysis for protein analysis by immunoblot was carried out by washing them once with 1X PBS and then harvesting them in 100 µL of 1% NP-40 lysis buffer by scrapper. After 30 min of incubation and mixing once every 5 min in ice, samples were sonicated 10 cycles in Bioruptor® Plus sonication device (Diagenode) (30 s on and 30 s off) and centrifuged 20 min at 14,000 rpm and 4 ºC. Supernatants were collected and quantified by the Qubit Assay Kit in a Qubit 3.0 Fluorometer, following manufacturer's instructions. Generally, 100 µg of protein were mixed with SDS-PAGE loading buffer and separated by SDS-PAGE electrophoresis.

Then, the volume from the lysate corresponding to 100 µg of protein was mixed with 5X-SDS-PAGE loading buffer and heated at 95 ºC for 5 min. Then, samples were run on a SDS-PAGE gel (8-12 % acrylamide/bis-acrylamide, depending on the molecular weight of the analyzed proteins) in a Mini Protean III cuvette (Bio-Rad) with running buffer at 120-160 V. Once the electrophoresis finished, proteins

were transferred to a nitrocellulose membrane (AmershamProtran Supported 0.45 NC, GEHealthcare Life Sciences) in a Mini-Trans Blot cell (Bio-Rad) at 400 mA for 40 min, using transfer buffer. Next, the membrane was incubated with TBS supplemented with 1 % of non-fat dry milk (w/v) or 4% BSA (w/v) for 1 h RT for blocking. After three washes of 10 min with TBS-T, the membrane was incubated with the primary antibody in TBS-T supplemented with 1-4 % BSA (w/v) overnight at 4ºC. Then, other three washes of 10 min with TBS-T were accomplished and the membrane was incubated with the secondary antibody conjugated to IRDye680 or IRDye800 fluorochromes (Li-COR Biosciences), diluted 1:15,000 in TBS-T 1 % BSA (w/v). Finally, the membrane was washed three times for 10 min with TBS-T and scanned using an Odyssey Infrared Imaging Scanner (Li-COR Biosciences). The antibodies used for immunoblot analysis are shown in **Table 3.5**.

- *1% NP40 lysis buffer: 50 mM Tris-HCl pH8, 1 % NP40 (v/v), 150 mM NaCl, 1 mM EDTA, 10 mM NaF, supplemented with protease inhibitor cocktail Set I (1:100; Calbiochem), phosphatase inhibitor cocktail I (1:100; Sigma-Aldrich®) and 0.2 % SDS immediately before using; stock concentration: 1 %; stored at 4 °C.*
- *5X-SDS-PAGE loading buffer: 100 mM Tris-HCl pH6.8, 5 % β-mercaptoethanol (v/v), 5 % SDS (w/v), 0.1 % bromophenol blue (w/v), 50 % glycerol (v/v); stock concentration: 5X; stored at -20 °C.*
- *Coomassie Brillant Blue solution: 0.025 % Coomassie Brilliant Blue R-250 (w/v), 40 % methanol (v/v) and 10 % (v/v) glacial acetic acid; stock concentration: 1X; stored at room temperature protected from light.*
- *Running buffer: 25 mM Trizma pH8.3, 192 mM glycine and 0.1 % SDS (w/v); stock concentration: 1X; stored at room temperature.*
- *Transfer buffer: 25 mMTris pH8.3, 192 mM glycine and 10 % methanol (v/v); stock concentration: 1X; stored at room temperature.*
- *TBS: 20 mM Tris-HCl pH7.5, 150 mM NaCl; stock concentration: 1X; stored at room temperature.*
- *TBS-T: 0.05 % Tween 20 (v/v) diluted in TBS; stock concentration: 1X; stored at room temperature.*

Table 3.5. **Primary and secondary antibodies used in this Thesis work.** aa, amino acids; IB, immunoblot; IF, immunofluorescence; IP, immunoprecipitation.

Primary antibodies				
Antibody	**Immunogen**	**Type**	**Origin (reference)**	**Technique and dilution**
β-actin	C-terminus (human)	Goat polyclonal	Santa Cruz Biotech. (I-19, sc-1616)	IB (1:1000)
BCL-XL	Residues surrounding Asp61 of human Bcl-xL	Rabbit monoclonal	Cell Signaling (54H6, -2764)	IB (1:1000)
Cyclin A2	FL (human)	Rabbit polyclonal	Santa Cruz Biotech. (H-432, sc-751)	IB (1:1000)
GFP	GFP from *Aequorea victoria*	Rabbit polyclonal	Invitrogen (A-11122)	IB (1:1000); IP
HA	Influenza virus hemagglutinin (HA) epitope	Mouse Monoclonal	Genecopiea (CGAB-HA-0050)	IP
HA	Influenza virus hemagglutinin (HA) epitope	Rat monoclonal	Roche (3F10)	IB (1:2000)
IκBα	C-terminus (human)	Rabbit polyclonal	Cell Signaling (#4812)	IB (1:1000)
IgG	-	Rabbit polyclonal	Cell Signaling (#2729)	IP; ChIP
IgG	-	Mouse polyclonal	Santa Cruz Biotech. (sc-2025)	IP; ChIP
MAX	C-terminal (human)	Rabbit polyclonal	Santa Cruz Biotech. (C-17, sc-197)	IB (1:1000); ChIP
MLX	17-42 aa (human)	Mouse monoclonal	Santa Cruz Biotech. (F12, sc-393086)	IB (1:1000) IP; ChIP
MLXIP	MLXIP fusion protein Ag4519	Rabbit polyclonal	Proteintech (13614-1-AP)	IF (1:200)
MNT	226-361 aa (human)	Rabbit polyclonal	Santa Cruz Biotech. (M-132, sc-769)	IB (1:1000); IF (1:200); IP; ChIP

MNT	1-50 aa (human)	Rabbit polyclonal	Novus (NBP2-04052)	IB (1:1000); IP; ChIP
MNT	532-582 aa (human)	Rabbit polyclonal	Novus (NBP2-04053)	IB (1:1000); IP; ChIP
MYC	1-262 aa (human)	Rabbit polyclonal	Santa Cruz Biotech. (N-262, sc-764)	IB (1:1000)
MYC	Full protein (human)	Mouse monoclonal	Santa Cruz Biotech. (C-33, sc-42)	IF (1:50)
MYC	N-terminal (human)	Rabbit polyclonal	Cell Signaling (#9402)	IB (1:3000)
p65	C-terminus (human)	Goat polyclonal	Santa Cruz Biotech. (C-20, sc-372-G)	IB (1:1000), IF (1:200), IP
Anti-p105/p50	N-terminus (human)	Rabbit polyclonal	Cell Signaling (#3035)	IB (1:1000); IP
Anti-REL	N-terminus (human)	Rabbit polyclonal	Santa Cruz Biotech. (N, sc-70)	IB (1:1000) IF (1:200), IP, ChIP
Anti-REL	143-184 aa (human)	Mouse monoclonal	Santa Cruz Biotech. (D-6, sc-373713)	IB (1:500)
Anti-PARP1	764-1014 aa (human)	Rabbit polyclonal	Santa Cruz Biotech (H-250, sc-7150)	IB (1:1000)
Anti-RhoGDI	N-terminal (human)	Rabbit polyclonal	Santa Cruz Biotech (A-20, sc-360)	IB (1:1000)
Anti-SIN3B	172-228 aa (mouse)	Mouse monoclonal	Santa Cruz Biotech (H-4, sc-13145)	IB (1:1000)
Anti-Survivin	1-142 aa (human)	Rabbit polyclonal	Santa Cruz Biotech (FL-142, sc-10811)	IB (1:1000)
Anti-α-tubulin	149-448 aa (human)	Rabbit polyclonal	Santa Cruz Biotech. (H300, sc-5546)	IB (1:1000)

Secondary antibodies				
Antibody	**Immunogen**	**Type**	**Origin (reference)**	**Technique and dilution**
Anti-Goat IRDye®680	Goat heavy and light immunoglobulins chains	Donkey polyclonal	Li-Cor Biosciences (926-68074)	IB (1:10000)
Anti-Goat IRDye®800	Goat heavy and light immunoglobulins chains	Donkey polyclonal	Li-Cor Biosciences (926-32214)	IB (1:10000)
Anti-Mouse IRDye®680	Mouse heavy and light immunoglobulins chains	Donkey polyclonal	Li-Cor Biosciences (926-68072)	IB (1:10000)
Anti-Mouse IRDye®800	Mouse heavy and light immunoglobulins chains	Donkey polyclonal	Li-Cor Biosciences (926-32212)	IB (1:10000)
Anti-Rabbit IRDye®680	Rabbit heavy and light immunoglobulins chains	Donkey polyclonal	Li-Cor Biosciences (926-68073)	IB (1:10000)
Anti-Rabbit IRDye®800	Rabbit heavy and light immunoglobulins chains	Donkey polyclonal	Li-Cor Biosciences (926-32213)	IB (1:10000)
Anti-Rabbit FITC	Rabbit heavy and light immunoglobulins chains	Goat polyclonal	Jackson InmunoResearch laboraotries (111-095-045)	IF (1:200)

3.6.2. Subcellular fractionation

Generally, $6 \cdot 10^6$ cells were washed in PBS 1X twice and lysed in 200 µL of N/C Lysis Buffer 1. Using a scrapper, the cells were harvested and incubated in ice for 30 min (mixing every 5 min). Cell lysates were centrifuged for 5 min at 1,500 rpm 4 ºC. Supernatant containing the cytoplasmic fraction was collected and centrifuged again at 14,000 rpm 4 ºC for removing possible debris. Then, the nuclei-containing pellet was resuspended in 200 µL of N/C Lysis Buffer 2 and incubated for 30 min in ice (mixing every 5 min). Nuclei lysates were centrifuged 20 min at 4 ºC maximum speed in a microcentrifuge. Both lysates were collected and kept at -80 ºC until use. To verify the enrichment of the fractions, RhoGDI and SIN3B were used as controls for cytoplasm and nucleus, respectively. Coomassie blue stain was used as a protein loading control.

- *N/C Lysis Buffer 1: 10 mM HEPES pH 7; 10 mM KCl; 0.25 mM EDTA pH 8; 0.125 mM EGTA pH 8; 0.1 % (v:v) IGEPAL (Sigma- Aldrich); 1 mM DTT. 1:100 proteases inhibitor cocktail Set I (Calbiochem) and phosphatase inhibitor cocktail I (1:100; Sigma-Aldrich®) added just before use.*
- *N/C Lysis Buffer 2: 20 mM HEPES; 400 mM NaCl; 0.25 mM EDTA; 1.5 mM $MgCl_2$; 0.5 mM DTT. 1:100 proteases inhibitor cocktail Set I (Calbiochem) and phosphatase inhibitor cocktail I (1:100; Sigma-Aldrich®) added just before use.*

3.6.3. Co-immunoprecipitation

Co-immunoprecipitation assays were carried out in order to study protein-protein interactions. Firstly, cells were collected, washed once with 1 mL of 1X PBS and then resuspended in a non-denaturing lysis buffer. Cell lysate was passed through a G20 needle syringe 4-5 times and incubated in rotation for 30 min at 4 ºC. Secondly, the cell lysate was clarified by centrifugation for 20 min at 14,000 rpm 4 ºC. Thirdly, the protein supernatant was incubated overnight at 4 ºC with 30 µL of Gammabind Sepharose Beads (Amersham Pharmacia Biotech) and 3 µg of antibody. The beads were previously washed three times with 1 mL of lysis buffer for 5 min rotating at 4 ºC. 50 µl of cell lysate was stored as the input. Next day, the beads-antibody-protein complexes were collected by centrifugation for 1 min at 4,000 rpm and washed four times with 1 mL of wash buffer for 5 min at 4 ºC, in rotation. Finally, the pellet was resuspended in 60 µL 1 X SDS-PAGE loading buffer, then heated at 95 ºC for 10 min and centrifuged at 4,000 rpm for 1 min. Finally, the samples were run into a SDS-PAGE gel for immunoblot analysis (10 µL of input and 18 µL of the IP), as described previously.

$6 \cdot 10^6$ cells were used for each protein immunoprecipitation assay. The growing media was refreshed the day before the assay.

- *IP Lysis Buffer:* 50 mM Tris-HCl pH 7.5, 150 mM NaCl, 0.5-1 % NP-40 (v/v), 1 mM EDTA pH 8, 0.5 M EGTA, supplemented with protease inhibitor cocktail Set *I (Calbiochem) (1:100) and phosphatase inhibitor cocktail I (1:100; Sigma-Aldrich®) added just before use.*
- *IP Wash buffer: 50 mM Tris-Hcl pH 7.5, 150 mM NaCl, 0.25 % NP-40 (v/v).*
- *1 X SDS-PAGE loading buffer: 20 mM Tris-HCl pH 6.8, 1 % β-mercaptoethanol (v/v), 1 % SDS (w/v), 0.02 % bromophenol.*

3.6.4. Immunofluorescence

Cells that were previously attached to a glass cover slip (10 mm Ø) were washed with 1 X PBS and fixed with a 4 % (v/v) paraformaldehyde 1X PBS for 15 min, in order to cross-link proteins. After three washes (5 min each) with 1X PBS, cells were permeabilized and blocked 30 min RT. Primary antibody was diluted 1:200 in antibody dilution buffer and added to the samples, which were incubated overnight at 4 ºC in a wet chamber. After three washes with 1X PBS, secondary antibody conjugated to FITC or Tx-Red fluorochromes (Jackson InmunoResearch laboratories Inc.) was diluted 1:500 in blocking buffer and incubated during 1 h RT (wet chamber, in dark). After three washes with 1X PBS, the cover slips were mounted with ProLong Gold Antifade Mountant (Life Technologies) with a DAPI nuclear stain incorporated. Finally, samples were observed at a Zeiss IMAGER M1 fluorescence microscope or at a confocal microscope (Leica SP5 TCS) and the images were processed with ImageJ software.

The antibodies solutions were freshly prepared in the day. The washing steps were carried out in agitation at RT.

- *Permeabilization and blocking buffer: 1 % (v/v) Triton X-100, 3 % BSA (w/v) in 1 X PBS.*
- *Antibody dilution buffer: 3 % (w:v) BSA, 0.1 % (v:v) Triton X-100 in PBS.*

3.6.5. Proximity Ligation Assay (PLA)

The proximity ligation assay is a technique for the detection of protein-protein interactions *in vivo*. Through an immunodetection we can know if two proteins are so closed together (between 0 and 40 nm) that we assume that they are interacting. Moreover, it gives us information about the subcellular compartment where the interaction is taking place.

The PLA was performed with Duolink® *in situ* Red Starter kit Mouse/Rabbit (Sigma-Aldrich®) (**Figure 3.5**). First, cells were seeded in cover slips (10 mm Ø) and fixed with 4 % (v/v) paraformaldehyde 1 X PBS for 15 min RT. Three washes with PBS 1X were done and then the cells were permeabilized and blocked for 30 min RT. Afterwards, the samples were incubated with a solution containing the two antibodies against our proteins of interest, which have to be produced in different species. The incubation was done overnight in a wet chamber at 4 ºC. After primary antibody incubation, 3 washes of 10 min with buffer A (from the kit) were performed. Meanwhile, oligonucleotide-conjugated secondary antibodies solution (PLA probe anti-Rabbit PLUS and anti-Mouse MINUS, Sigma-Aldrich®) was prepared in the homemade antibody dilution buffer and incubated 20 min at RT. Then, the samples were incubated with the secondary antibody solution for 1 h in a wet chamber at 37 ºC. Next, they were washed two times with buffer A (10 min each) and incubated with the ligation solution for 30 min at 37ºC. This step is necessary for the hybridization of the oligonucleotide probe that will form a DNA circle. After that, two washes with buffer A of 2 min each were done and the amplification solution was added to the samples and incubated for 90 min in a wet and dark chamber at 37 ºC. If the proteins are close enough and, consequently, the antibodies that are bound to them, this step will amplify the DNA through rolling circle DNA amplification, introducing red fluorescent probes. After this, samples were washed twice with buffer B (from the kit) for 10 min and stored overnight with buffer B 0.01X at 4ºC. The following day, samples were mounted with Duolink® In Situ Mounting Medium with DAPI (4 µL for cover slip).

Finally, the result was checked in a Zeiss IMAGER M1 fluorescence microscope. Images were acquired and analyzed with the ImageJ software.

All the solutions were freshly prepared in the day (including buffer A and B solutions). The washing steps were carried out in agitation at RT.

- *Permeabilization and blocking buffer: 1 % (v/v) Triton X-100, 3 % BSA (w/v) in 1 X PBS.*
- *Antibody dilution buffer: 3 % (w:v) BSA, 0.1 % (v:v) Triton X-100 in PBS.*

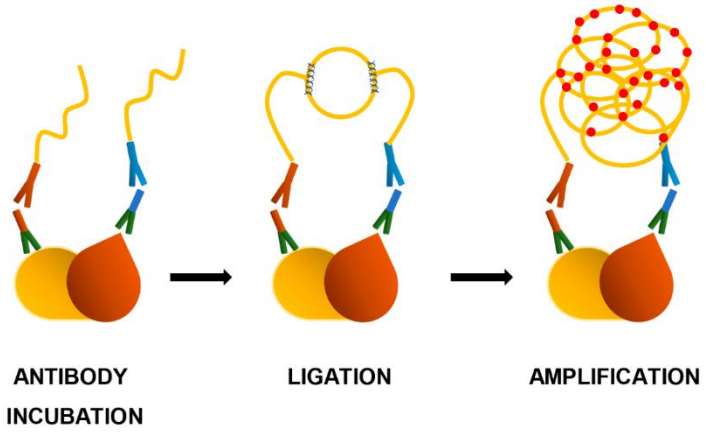

Figure 3.5. Scheme of the main steps of the Proximity Ligation Assay. After an incubation with the primary and the secondary antibodies, a ligation step allows the hybridization of the oligonucleotides that are amplified in the final step, where fluorescent probes are introduced for the posterior detection of the interaction.

3.7. Statistical analysis

Results were presented as the mean of 3 to 10 determinations, with error bars representing the S.E.M.

Student's t-test was used to evaluate the significance of differences between control and experimental groups. Generally, a *P*-value of less than 0.05 was considered as significant and shown as an asterisk (*) in the graphs, or with two (**) if it was less than 0.01.

Results

4. Results

4.1. MNT as a regulator of the NF-κB pathway

4.1.1. MNT and REL interaction

Up to now, MNT functions have been linked to MAX, as it is the main and most studied partner of the MYC and the MXD proteins. However, as different cell lines and tumors have been found with deletions in *MAX* (Comino-Méndez et al., 2011; Hopewell and Ziff, 1995; Romero et al., 2014), we wondered whether MNT was carrying out some of its functions in a MAX-independent manner. For this, a proteomic study was performed in our laboratory (Lafita-Navarro, PhD Dissertation 2015) using MAX-deficient UR61 cells, which derive from the PC12 rat pheochromocytoma cell line. URMax34 (UR61 cells carrying a MAX-inducible construct by Zn_2SO_4) and URMT (UR61 carrying the empty vector) were transfected with a MNT overexpressing construct in order to ensure higher amounts of the protein. Then, 12 h post-transfection, the cells were treated with 100 µM Zn_2SO_4 for 24 h and lysed for the immunoprecipitation assay. MNT was immunoprecipitated by triplicate for each cell line. After MNT immunoprecipitation, our collaborators from the Alex von Kriegsheim's group (Systems Biology Ireland, Conway Institute, Dublin) analyzed the immunoprecipitated proteins by mass spectrometry.

The results showed eleven proteins that were immunoprecipitated in URMT and forty-seven in URMax34. Five proteins were shared between the two sets (REL, CCDC6, AMPD2, QSER1 and TPP2), meaning that they would bind to MNT whether MAX is present or not. A summary of the process is shown in **Figure 4.1.**

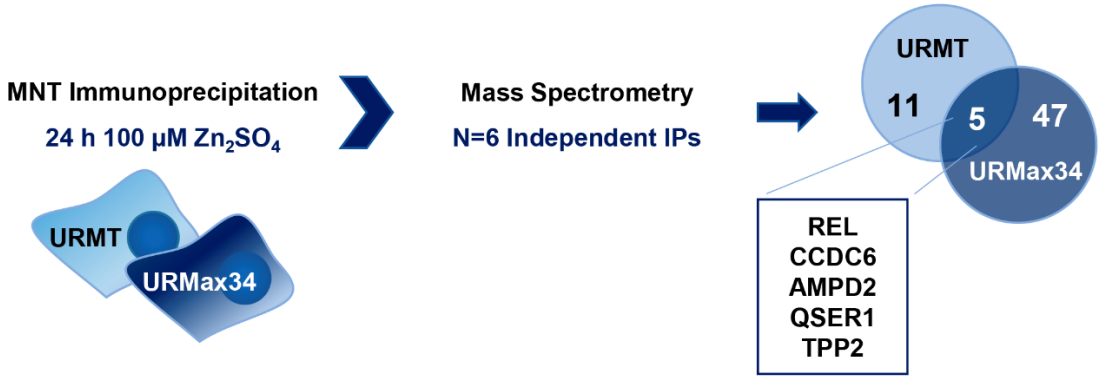

Figure 4.1. Proteomic study of MNT immunoprecipitates. URMT and URMax34 cells were treated with 100 µM Zn_2SO_4 for 24 h and lysed for posterior MNT immunoprecipitation. Six independent immunoprecipitations were analyzed by mass spectrophotometry and 5 proteins were found bound to MNT in URMT and URMax34. Work carried out by M.C. Lafita-Navarro and Alex von Kriegsheim.

Among the proteins detected bound to MNT, we selected REL as the main focus of this research project. REL is a transcription factor from the NF-κB family that is involved in several biological processes and has a role in tumorigenesis (Gilmore and Gerondakis, 2011). Thus, we wanted to confirm this interaction and ask for the functional implication of MNT and REL interaction in the cell.

First of all, we analyzed the data published in The Cancer Genome Atlas Program (TCGA) for REL and MNT. As it can be observed in **Figure 4.2**, the mutations of *REL* and *MNT* are mostly exclusive among the samples compiled in TCGA. Therefore, it could conceivably be hypothesized that MNT and REL are involved in a common pathway.

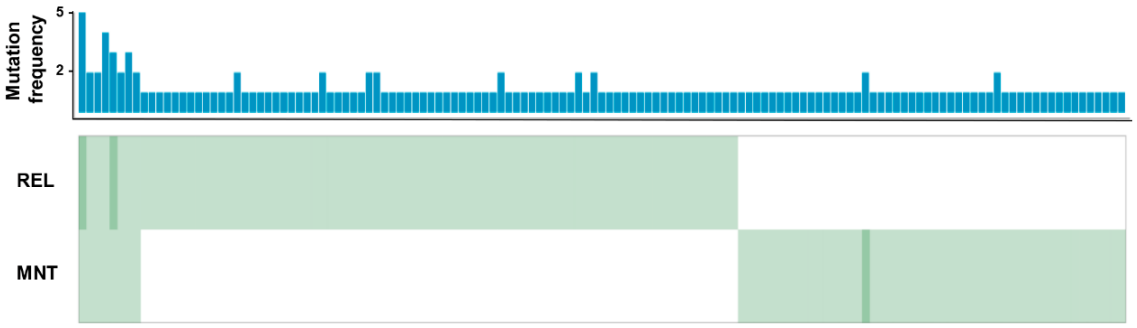

Figure 4.2. The Cancer Genome Atlas Program (TCGA) data for REL and MNT. Individual cases and their corresponding mutation frequency along the X-axis, and our selected genes displayed on the left of the grid (Y-axis). Dark green bands correspond to the cases displaying more than one type of mutation.

Next, we decided to check the expression of MNT and REL in different cell lines by RT-qPCR. As REL is remarkably involved in the immune system homeostasis, we chose a few human cell lines from the B- and T-cell lineage (CEM, Jurkat, Raji, K562, Ramos, MEC1, CEM). Moreover, we checked the expression in LoVo (from colorectal adenocarcinoma) and Lu165 (from small cell lung cancer). The latter is a human cell line that lacks MAX, as it happens with the UR61 cell line (Romero et al., 2014). The expression levels of *NFKBI* (p50) and *NFKBIA* (IκBα) and *RELA* (p65) were also checked. All these genes were expressed in the selected cell lines but we did not find a clear correlation between their mRNA levels (**Figure 4.3**).

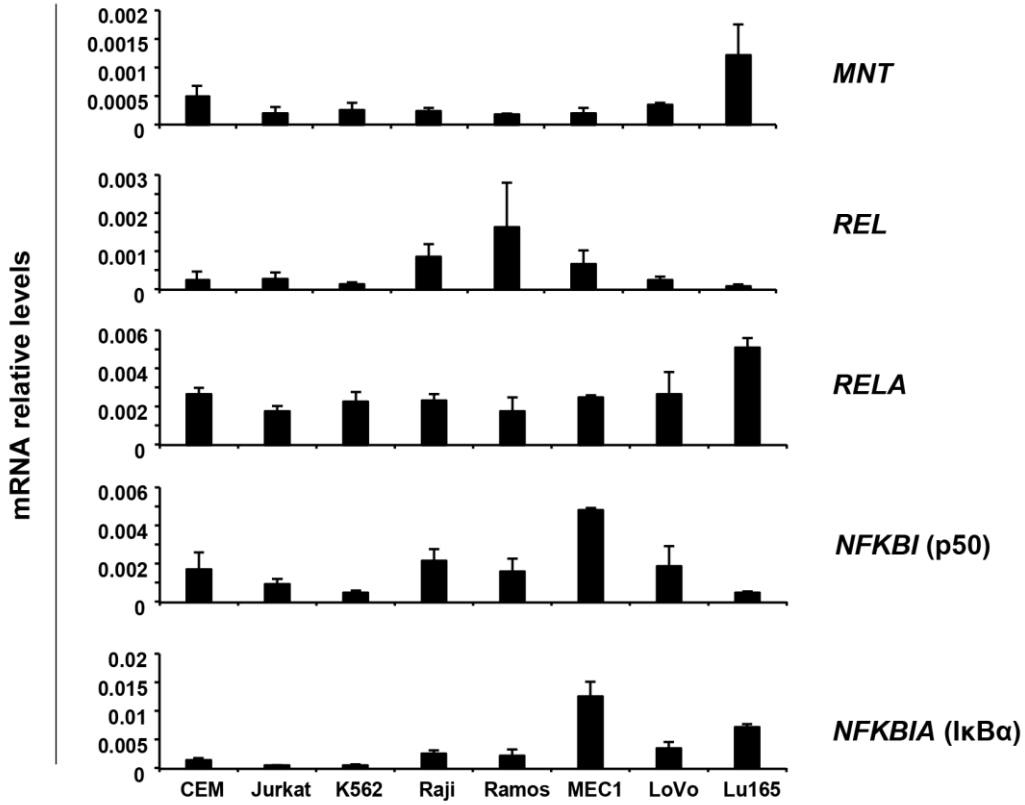

Figure 4.3. MNT and NF-κB members' expression. Graph showing the mRNA levels of *MNT*, *REL*, *RELA*, *NFKBI* and *NFKBIA* in different cell lines relative to RPS14. The data are represented as the mean ±S.E.M. from three independent RNA extractions.

Thirdly, we analyzed the protein levels of MNT, REL, IκBα, together with MYC, MAX and MLX by immunoblot. We took some of the B- and T-cell lineage cell lines mentioned before and HAP1 cells, which derive from KMB-7 cell line. These cells constitute a good model to study MNT functions, as we have the wild-type

and the *MNT* knockout HAP1. All the proteins were detected in all the cell lysates (**Figure 4.4 A**). After quantification, we observed an inverse correlation between MNT and REL protein levels (**Figure 4.4 B**).

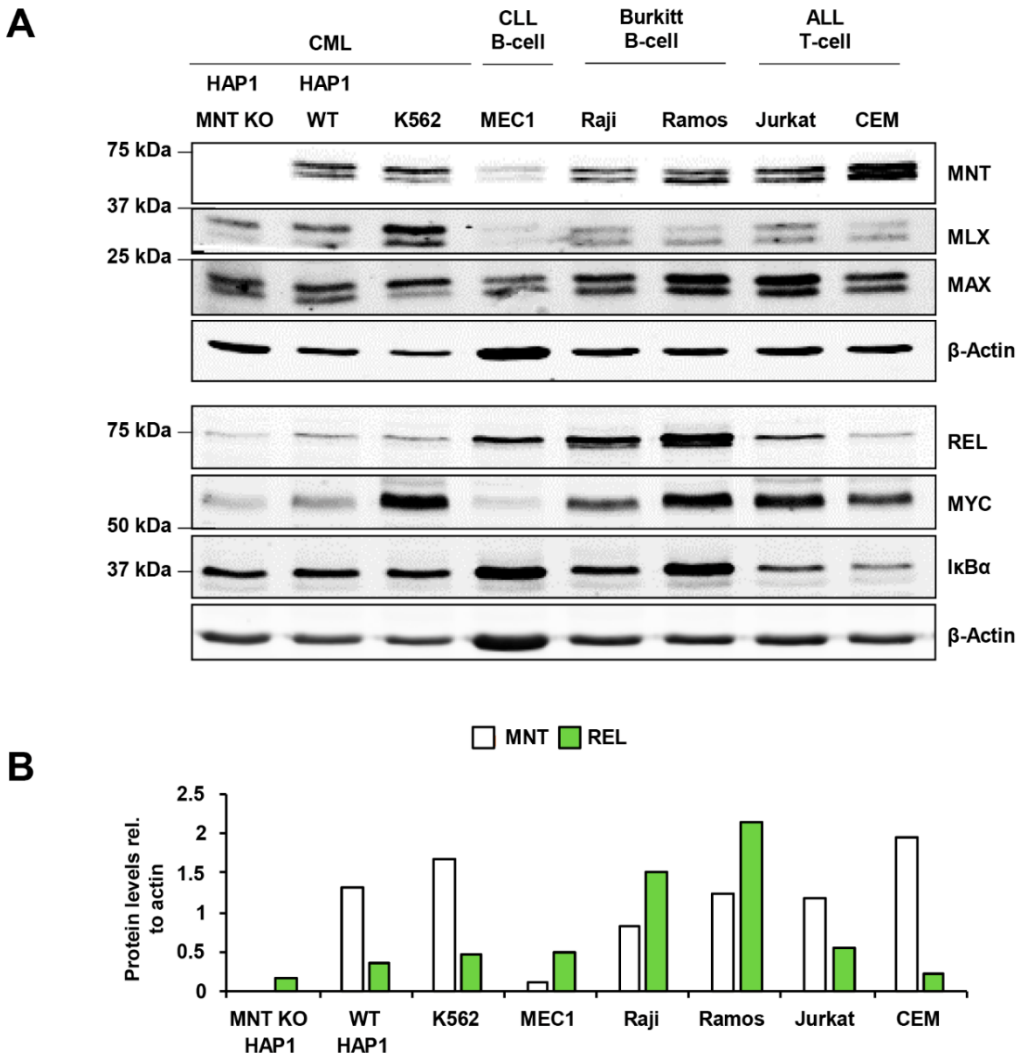

Figure 4.4. MNT and NF-κB members' protein levels. (A) Immunoblot for MNT, MLX, MAX, REL, MYC, IκBα. β-actin levels were determined as protein loading control. CML, chronic myeloid leukemia; CLL, chronic lymphocytic leukemia; ALL, acute lymphoblastic leukemia. (B) Quantification of MNT and REL protein levels relative to β-actin levels.

Then, we tested the MNT-REL interaction found in the proteomic study by co-immunoprecipitated assays (co-IP), in UR61 cells and other rat, mouse and human cell lines. Using a non-ionic "soft" buffer, cells were lysed and immunoprecipitated with anti-MNT or a non-specific IgG as a negative control. After doing the immunoblot of the immunoprecipitated complexes, we detected the co-IP of REL in the PC12-derived cell lines, U7, URMT and URMax34 (**Figure 4.5 A**). URMax34 immunoprecipitation was performed after 24 h treatment with

Zn^{2+} (to induce MAX expression) and the lysate was incubated also with anti-MAX antibodies. As it can be observed in the immunoblot, REL was found bound to MNT and not to MAX, suggesting that REL does not form part of the MNT-MAX complex. Moreover, we found REL co-IP in rat glioma C6 and mouse neuroblastoma Neuro-2a cell lines. As a proof of concept, we immunoprecipitated URMT and C6 lysates with anti-REL antibodies for discarding that the interaction was an artefact of the MNT antibody. As it can be observed, MNT co-immunoprecipitated with REL. In other cell lines, this co-IP was not so well detected (not shown).

To assess the interaction between MNT and REL in human, several cell lines from different tissues were grown and lysed for co-IP studies. However, the interaction was only detected in LoVo (from colon adenocarcinoma) and CEM (from acute lymphoblastic leukemia), as shown in **Figure 4.5 B**.

REL is generally found in homodimers or heterodimers with p65 or p50 (Gilmore and Gerondakis, 2011). For this reason, we wondered whether there was any p65 or p50 in the MNT-REL complex. In order to do this, we took LoVo cells and performed co-immunoprecipitation assays first with the endogenous proteins (**Figure 4.6 A**). We used antibodies against MNT (052 that recognizes the first 50 amino acids of MNT and 053, which binds to the 532-582 amino acids of MNT), REL, p65 and p105/p50. The blot shows the REL co-IP in the anti-MNT^{052} immunoprecipitates, together with the co-IP of MAX (as a positive control). No p65 or p50 were found in the MNT-immunoprecipitated complex. In the case of REL IP, we did not detect the co-IP of MNT, nor p65 or p50. However, REL did co-immunoprecipitate with p65 and p50. Then, we overexpressed MNT and REL in LoVo cells and performed the co-immunoprecipitation assay 48 h after transfection (**Figure 4.6 B**). We detected MNT-REL, REL-p50 and REL-p65 complexes but again no p65 or p50 bound to MNT.

Altogether, these data show that MNT and REL interact in different cell lines. As no p50 or p65 were detected bound to MNT, the complex may be composed by REL homodimers or REL bound to other unknown protein(s) (**Figure 4.6 C**).

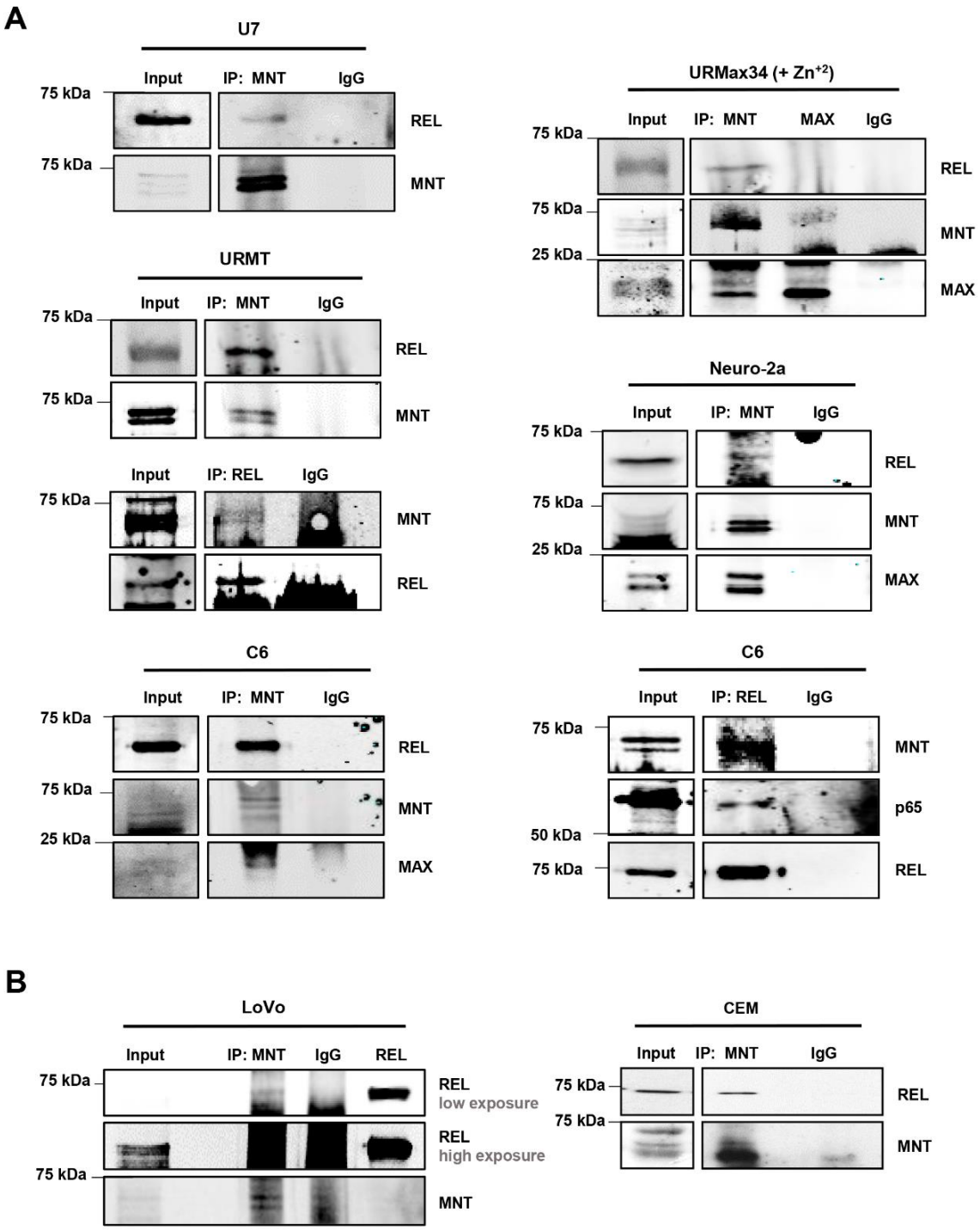

Figure 4.5. MNT and REL interact in several cell lines. (A) Co-immunoprecipitations assays in rat cell lines (U7, URMT, URMax34 after 24 h treatment with 100 µM Zn^{+2}, C6) and mouse Neuro-2a. (B) Co-immunoprecipitation assays in LoVo and CEM human cell lines. IP, Immunoprecipitation. All the IPs performed with untransfected cells. MAX blot as a positive control for MNT IP (in C6 and Neuro-2a).

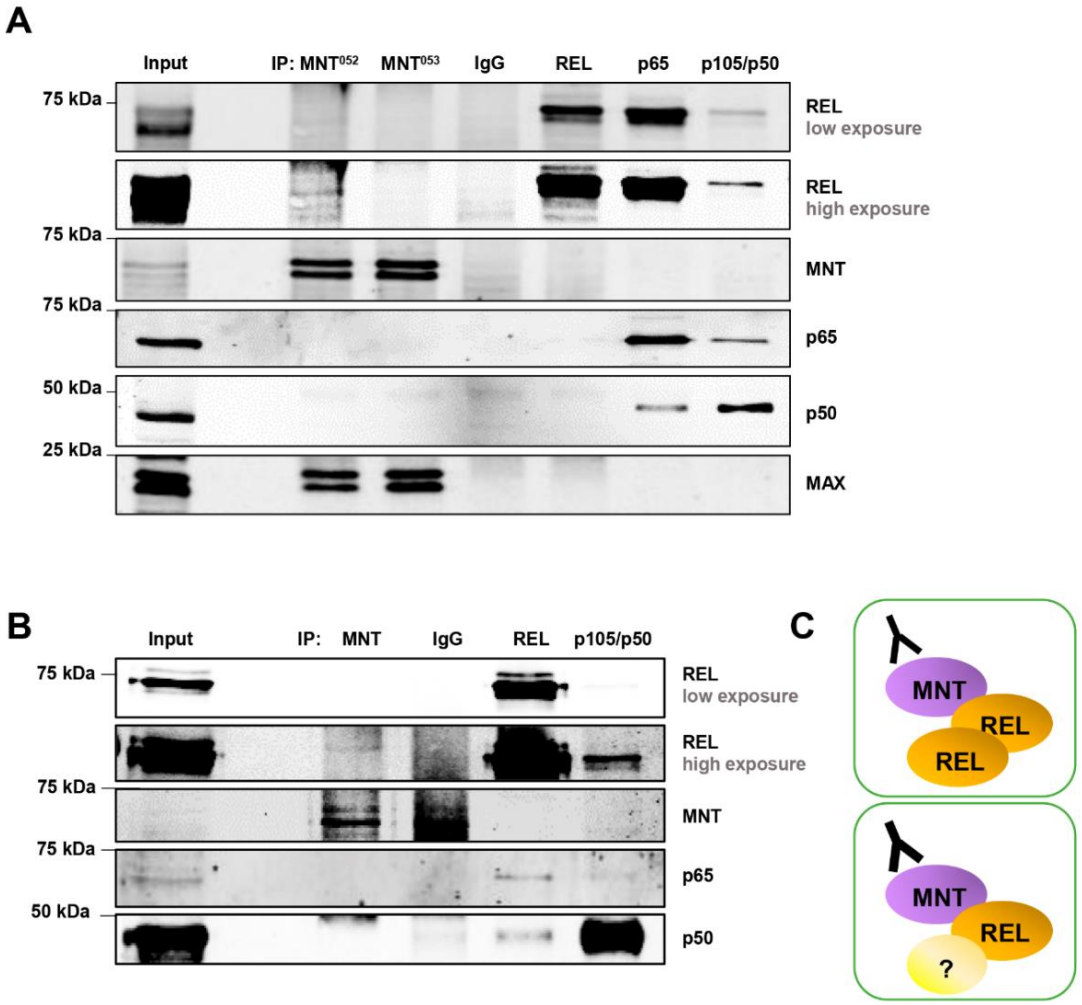

Figure 4.6. MNT interacts with REL but not with p50 or p65. (A) Co-immunoprecipitation of REL and MNT in untransfected LoVo cells. (B) Co-immunoprecipitation assay in LoVo cells 48 h after transfection with MNT and REL human overexpression vectors (pCMV MNT and pcDNA3.1. human REL-flag). IP, Immunoprecipitation; MNT^{052}, antibody against the 50 first amino acids of MNT protein; MNT^{053}, antibody against the 532-582 amino acids of MNT protein. (C) Working hypothesis with two options: (i) MNT bound to REL homodimers, (ii) MNT bound to REL and other yet unknown protein(s).

Next, we wanted to confirm the interaction between MNT and REL through another technique. For this, we carried out a Proximity Ligation Assay (PLA). This method represents a parallel approach to the co-IP assays, and it allows us to detect the interaction *in vivo* by fluorescent dots and the cell compartment where it occurs. First, we performed the assay in LoVo cells, where we obtained a positive signal for MNT and REL (**Figure 4.7**). As a positive control, we tested REL and p65 interaction and as a negative control, MNT and MYC. Then, we took C6 cells and overexpressed MNT and REL, in order to increase the signal and be able to see it better. As expected, we got more positive dots all around the cell

(**Figure 4.8**). This time we used MYC-MAX and REL-MYC as positive and negative controls, respectively.

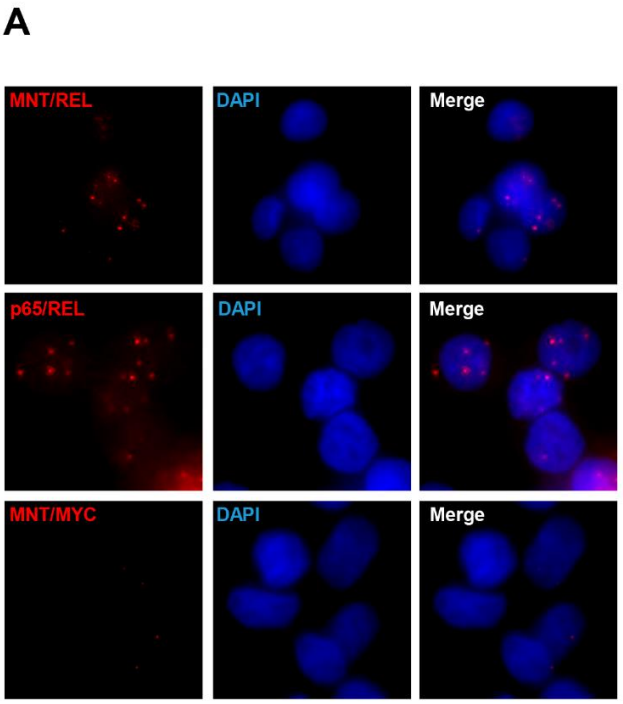

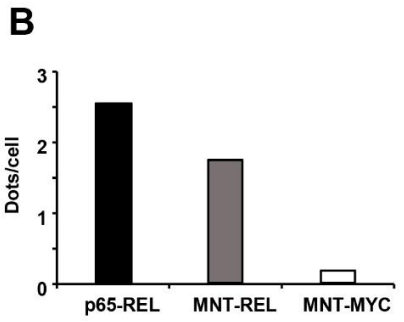

Figure 4.7. MNT and REL interaction in LoVo cells by PLA. Proximity Ligation Assay performed in LoVo cells (untransfected cells). (A) Images of the assay: PLA positive signal in red and DAPI as a nuclear marker. (B) Quantification of a minimum of 10 cells for each condition by ImageJ. p65-REL used as positive control and MNT-MYC for negative control.

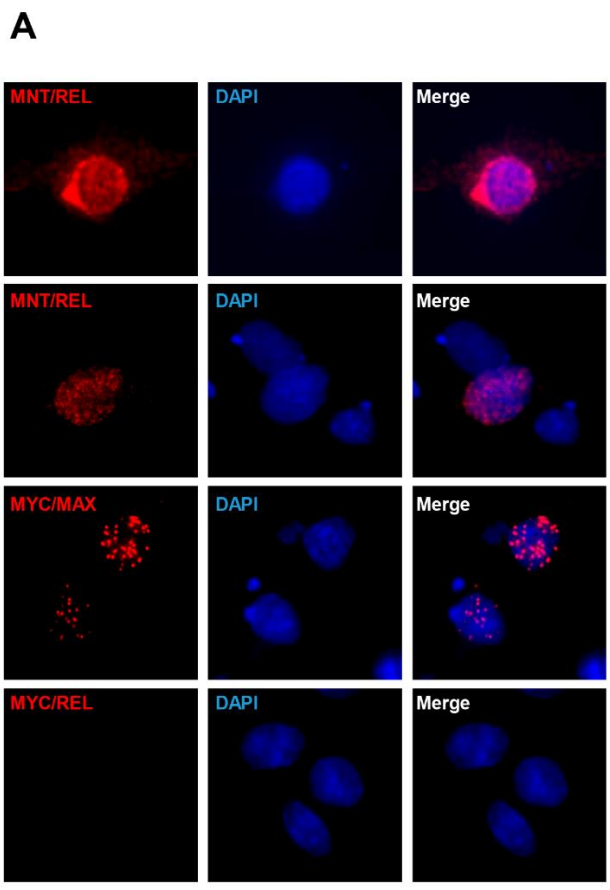

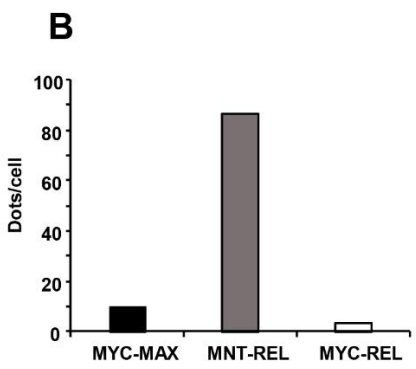

Figure 4.8. MNT and REL interaction in C6 cells by PLA. Proximity Ligation assay performed in C6 cells 48 h after transfection with WT MNT-HA and REL-flag overexpressing vectors. (A) Images of the assay: PLA positive signal in red and DAPI as a nuclear marker. (B) Quantification of a minimum of 10 cells per condition by ImageJ. MYC-MAX as positive control and MYC-REL as a negative control.

So as to clarify the localization of MNT-REL complexes, we carried out a nucleus-cytoplasm fractionation and posterior co-immunoprecipitation assay. For this, we used C6 cells in basal conditions and after 30 min of stimulation with TNFα. As it can we observed in **Figure 4.9 A**, REL is mostly cytoplasmic in basal conditions but it is translocated into the nucleus after NF-κB activation. Even if MNT is mostly nuclear, a small amount was immunoprecipitated from the cytoplasm, where we detected REL bound to MNT. Once REL was activated, the MNT-REL complex was also detected in the nuclear compartment. A summary of these results is schematized in **Figure 4.9 B**.

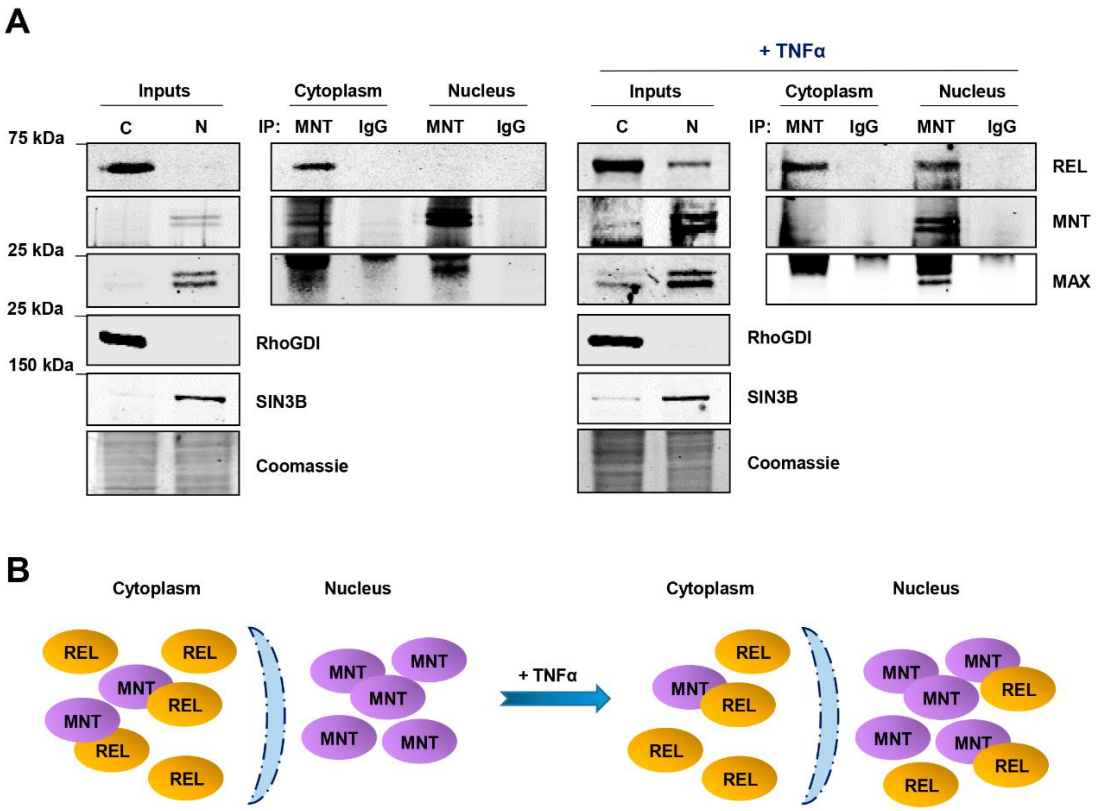

Figure 4.9. MNT and REL complexes can be found in both the nucleus and the cytoplasm. (A) C6 cells were lysed following the nucleus/cytoplasm fractionation protocol, both in basal conditions or 30 min after treatment with TNFα (100 ng/mL) and immunoprecipitated with an anti-MNT antibody or the IgG (the latter as a negative control). The presence of REL, MNT and MAX was determined in the immunoprecipitates by immunoblot. RhoGDI and SIN3B were analyzed as cytoplasm and nucleus markers, respectively. Coomassie blue as protein loading control for the inputs. (B) Scheme summarizing the obtained results.

Finally, to evaluate the domain of MNT that is interacting with REL, we took advantage of some MNT deletion mutants. The ΔbHLH and ΔCt_1 MNT-HA were made by our collaborators from P.J. Hurlin group, while ΔNt_1 and ΔNt_2 MNT-HA

were made in our laboratory (**Figure 4.10 A**). We transfected each of these constructs together with wild-type (WT) mouse REL into C6 cells. C6 were lysed and subjected to a co-IP assay 48 h after the transfection. Interestingly, REL appeared bound to ΔbHLH, ΔNt_1 and ΔNt_2 mutants but not to ΔCt_1 MNT-HA (**Figure 4.10 B, C**). Although further studies need to be performed, these results suggest the implication of the C-terminal domain of MNT in its interaction with REL.

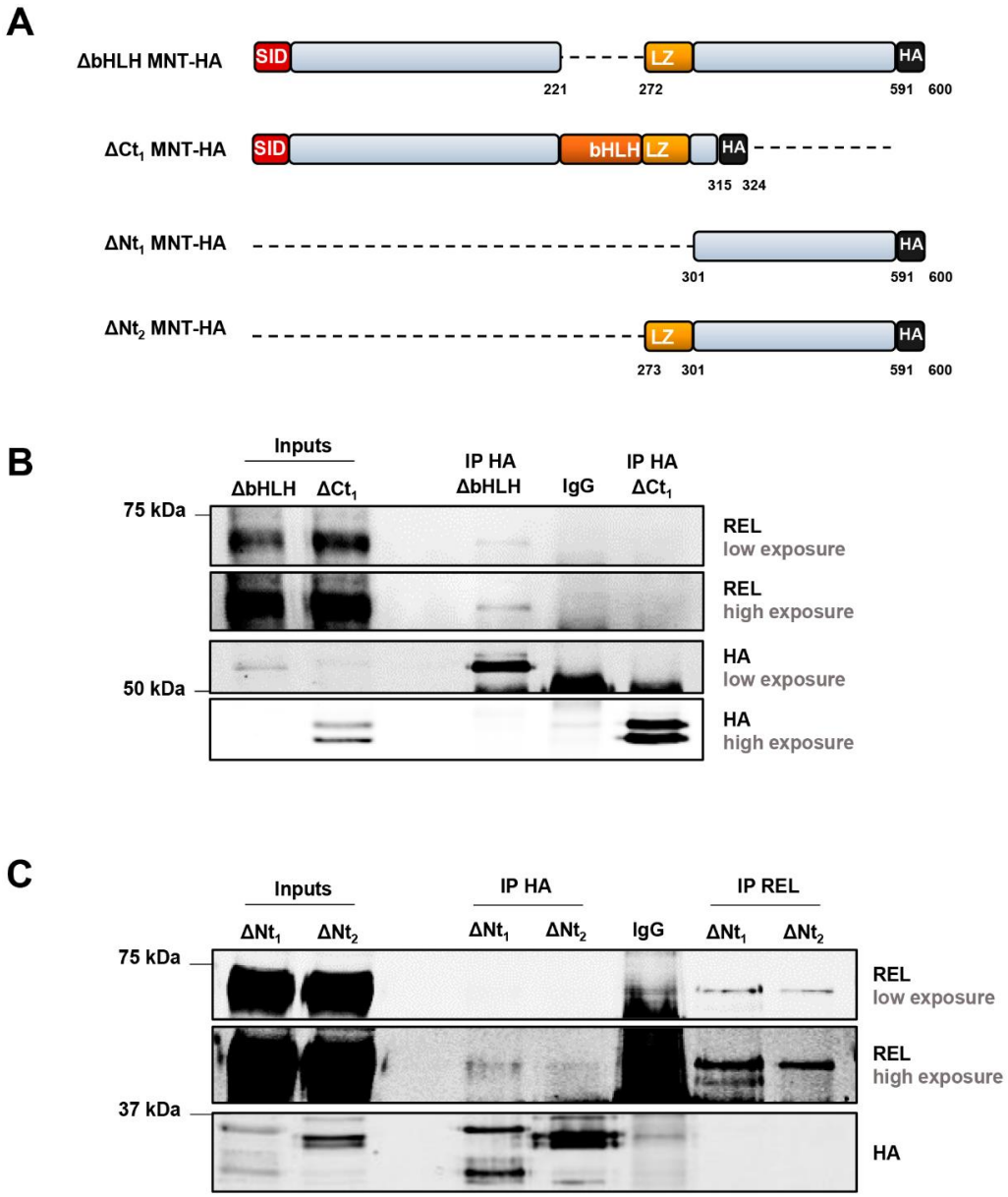

Figure 4.10. MNT could be interacting with REL through its C-terminal domain. (A) Schematic representation of the different MNT deletion construct used for the co-IP assays. (B) C6 cells 48 h after transfection with REL-flag (mouse) and ΔbHLH or ΔCt_1 MNT-HA were immunoprecipitated with anti-HA antibodies (IgG as negative control). (C) C6 cells 48 h after transfection with REL-flag (mouse) and ΔNt_1 or ΔNt_2 were immunoprecipitated with anti-HA antibodies (IgG as negative control). REL and HA were analyzed by immunoblot.

In summary, MNT and REL interaction was detected in some cell lines. The complex, which seemed not to have p50 or p65 as a part of it, was found both in the cytoplasm and in the nucleus.

4.1.2. MNT effect on NF-κB signaling

After confirming MNT and REL interaction, we started wondering which the role of MNT on NF-κB pathway was. By silencing or overexpressing MNT, we analyzed its effect on the subcellular localization of NF-κB dimers and on NF-κB targets.

NF-κB dimers translocate into the nucleus upon the activation of the pathway (Gilmore, 2006), so we wanted first to know if MNT was interfering with this process. Taking advantage of the short-hairpin RNA technology, we knocked down *MNT* in LoVo cells and performed immunofluorescence assays for REL and p65. As a negative control we used a shScrambled shRNA (scrRNA), which carries a random sequence that does not target any gene. Interestingly, MNT depletion provoked a change in REL subcellular distribution but not in p65. REL got accumulated in the nucleus with a compact pattern around the nucleolus (**Figure 4.11 A**). On the contrary, p65 remained in the cytoplasm whether MNT levels were normal or reduced (**Figure 4.11 B**). An immunoblot confirming the correct achievement of *MNT* knockdown is shown in **Figure 4.11 C**.

These results revealed a possible role of MNT on NF-κB signaling as a specific consequence of its interaction with REL.

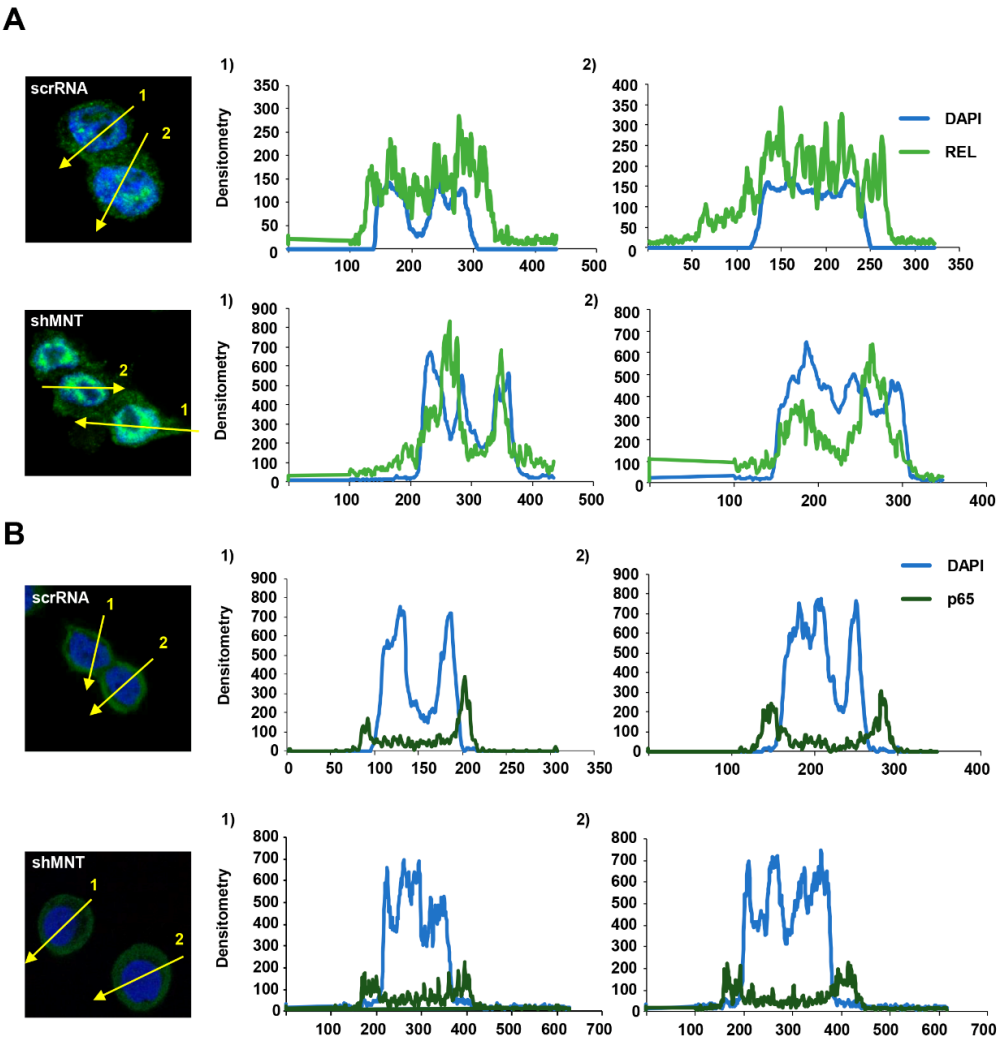

Figure 4.11. *MNT* knockdown causes a translocation of REL into the nucleus. Immunofluorescence of LoVo cells that were infected with lentiviral particles carrying a shRNA against MNT (shMNT) or a scrambled shRNA (scrRNA), and selected with puromycin (1 µg/mL) for 72 h. (A) REL immunofluorescence and (B) p65 immunofluorescence. DAPI used as a nucleus marker. The signal was quantified with the ImageJ software. (C) Immunoblot of the cells used for the immunofluorescence showing the MNT knockdown efficiency. α-Tubulin was determined as a protein loading control.

The next step for unraveling MNT role in NF-κB function was checking its effect on NF-κB transcriptional activity. For this, we opted to perform luciferase assays with NF-κB constructs: one of them carrying 5 κB binding sites (5x κB-Luc) and another one under the control of the IκBα promoter (IκBα-Luc), which is a *bona fide* target of NF-κB (Iwai et al., 2005) (**Figure 4.12 A**).

First, we analyzed the luciferase activity in LoVo cells after knocking down MNT with shRNAs, compared to the controls (scrRNA). Interestingly, the luciferase activity of both constructs was significantly increased upon *MNT* knockdown (**Figure 4.12 B**). Second, we repeated the experiment but this time overexpressing *MNT* in LoVo cells. Despite that less significant changes were obtained, the tendency of the luciferase activity was the opposite compared to the *MNT* knockdown (**Figure 4.12 C**).

Overall, the results obtained in the immunofluorescence and the luciferase assays suggest a possible negative correlation between MNT and the NF-κB pathway.

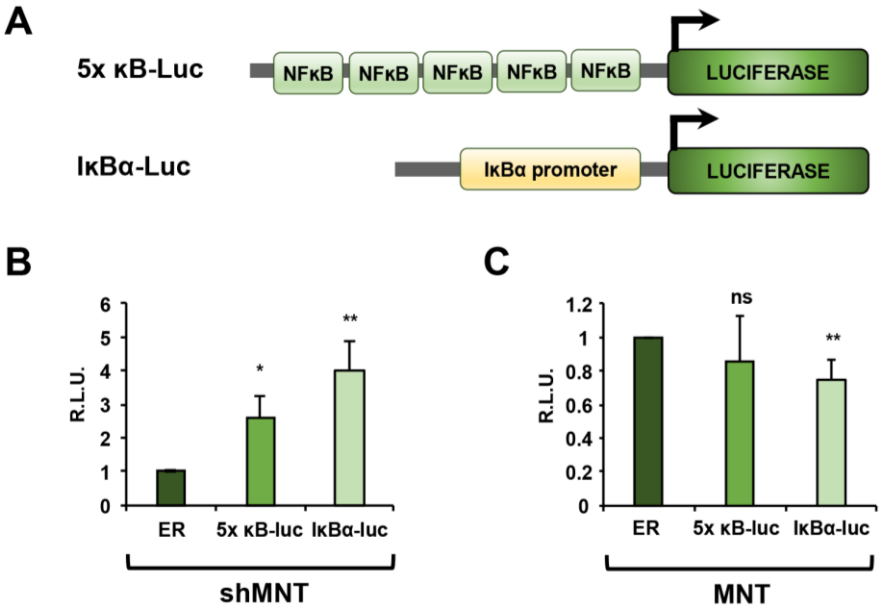

Figure 4.12. *MNT* knockdown provokes an activation of the NF-κB pathway. (A) Schematic representation of luciferase reporters driven by five (5x κB-Luc) NF-κB binding sites, or the human *NFKBIA* (IκBα) promoter (IκBα-Luc) used in this work. (B) Luciferase assays in LoVo cells, infected with lentiviral particles carrying a shRNA against MNT (or a scrambled shRNA as a control, scrRNA), selected with puromycin (1 µg/mL) for 72 h and then transfected with the luciferase vectors. (C) Luciferase assays in LoVo cells, 48 h after transfection with a MNT overexpressing vector or its corresponding empty vector, and the luciferase constructs. Results are expressed in relative luciferase units (R.L.U.) after normalizing each condition first to the luciferase empty reporter (ER) and then to the scrRNA (B) or the empty vector of MNT (C). The data are shown as the mean ± S.E.M. of 3 (B) or 4 independent experiments (C). * P <0.05; ** P <0.01; ns: non-significant.

Next, we determined the mRNA levels of *NFKBIA* (IκBα), *BCL2L1* (BCL-XL) and *NFKB1* (p105/p50) by RT-qPCR 48 h after transfection of LoVo cells with a MNT

overexpressing vector. *NFKBIA* and *BCL2L1* are two genes described to be induced by REL. On the contrary, *NFKB1* is not a REL target gene (Chen et al., 2000; Gilmore and Gerondakis, 2011). This experiment was performed in basal conditions and after 30 min induction with TNFα (25 ng/mL) (**Figure 4.13 A**). The results show a repression of REL target genes, *NFKBIA* and *BCL2L1,* after MNT overexpression. *NFKB1* expression levels did not change upon the increase in MNT protein levels. Then, after the direct activation of the pathway by TNFα, there were not significant changes in the expression levels of either of the genes analyzed. This may suggest that the effect of MNT is abolished once a strong signal activates the NF-κB pathway.

Following this, we knocked down *MNT* again in LoVo cells and checked the protein levels of IκBα and BCL-XL by immunoblot (**Figure 4.13 B**). The results showed the increase in IκBα and BCL-XL protein levels after MNT decrease, even if REL levels were also surprisingly reduced.

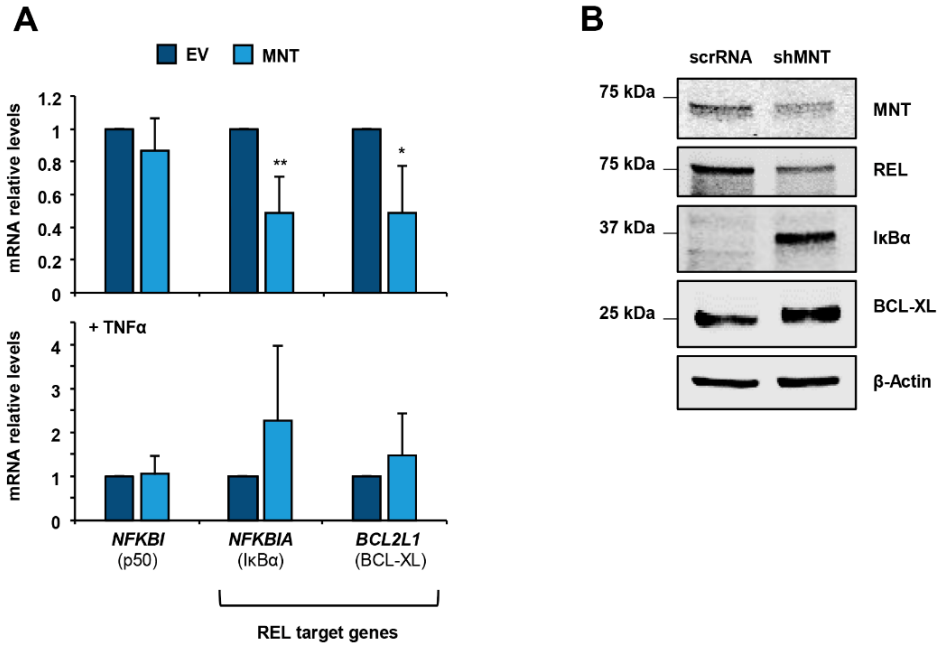

Figure 4.13. MNT can repress *NFKBIA* and *BCL2L1*, two REL target genes. (A) mRNA levels of LoVo cells 48 h after transfection with a MNT overexpressing construct or its corresponding empty vector (EV) relative to RPS14 (upper panel) and after TNFα (25 ng/mL) treatment for 30 min (lower panel). The data are shown as the mean ± S.E.M. of 3 independent experiments * P <0.05; ** P <0.01. (B) Protein levels of LoVo cells 72 h after infection with lentiviral particles carrying a shRNA against MNT or a scrambled shRNA (scrRNA), as a control. β-Actin used as a protein loading control.

Based on the changes obtained in IκBα RNA and protein levels upon changes in MNT total abundance, we wondered if MNT directly regulates IκBα gene. For this, we first checked the ChIP-seq data published in the ENCODE project (genome-euro.ucsc.edu/), using the human assembly GRChg19 from February 2009. Selecting *NFKBIA* and looking for MNT, MYC and MAX binding in the K562 cell line, we observed two peaks from the transcription start site (TSS) to exon 2. As MNT seemed to be repressing IκBα in our previous experiments and it is described that MNT represses transcription through its interaction with SIN3, we looked for the binding peaks of SIN3A and SIN3B. The data published for SIN3A and SIN3B correspond to the lymphoblastoid cell line GM78 and human embryonic stem cells H1ES, respectively. SIN3A and SIN3B also bind to *NFKBIA* (**Figure 4.14**).

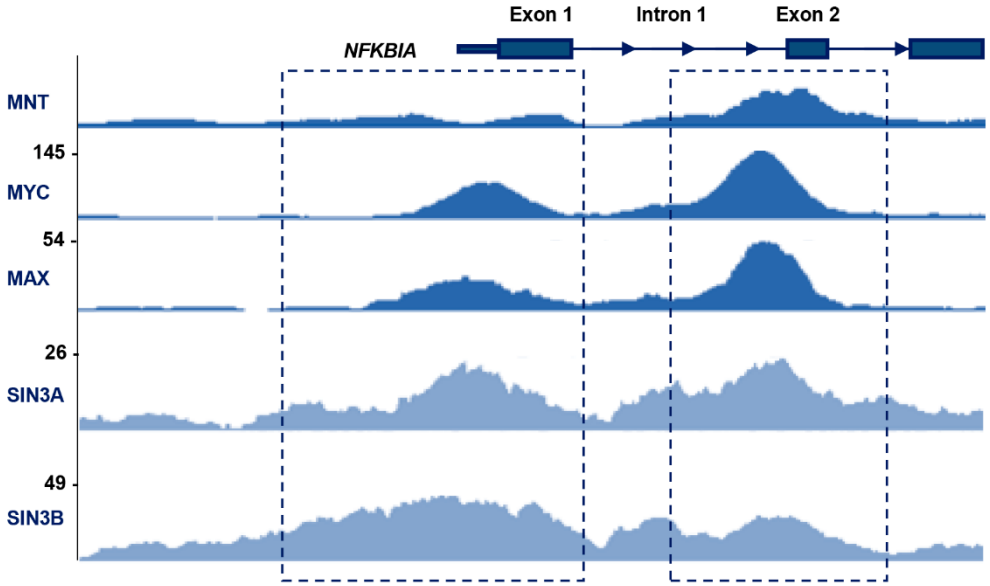

Figure 4.14. MNT, MYC, MAX and SIN3 binding to *NFKBIA* gene. Schematic representation of human *NFKBIA* (IκBα) promoter showing the peaks for MNT, MYC, MAX (K562 cell line), SIN3A (GM78) and SIN3B (H1ES) as published by the ENCODE project (genome-euro.ucsc.edu/).

Afterwards, we went back to our LoVo cell line and carried out ChIP experiments for MNT and REL. For this, we designed primers for mapping *NFKBIA* gene from around -1000 bp TSS to +1000 bp TSS. The position of the tested amplicons is represented in **Figure 4.15 A**. The ChIP of MNT shows its binding to *NFKBIA* gene (**Figure 4.15 B**). As a positive control for anti-MNT ChIP we used *TXNIP* and *MNT* -842, and as a negative control, a region upstream *MNT* promoter (MNT

-4729 bp). *TXNIP* is an already described direct target of MNT (Terragni et al., 2011) and MNT -842 is the region where MNT autoregulates its own promoter, as seen previously in our laboratory (Lafita-Navarro, PhD dissertation 2015). Next, we performed the ChIP of REL and observed its binding to *NFKBIA* gene (**Figure 4.15 C**). Interestingly, both MNT and REL had a maximum binding at +171/+343 bp from the TSS of *NFKBIA*. This result suggests that MNT and REL are regulating *NFKBIA* together. Further research will clarify if this regulation is a result of a complex formed by MNT and REL.

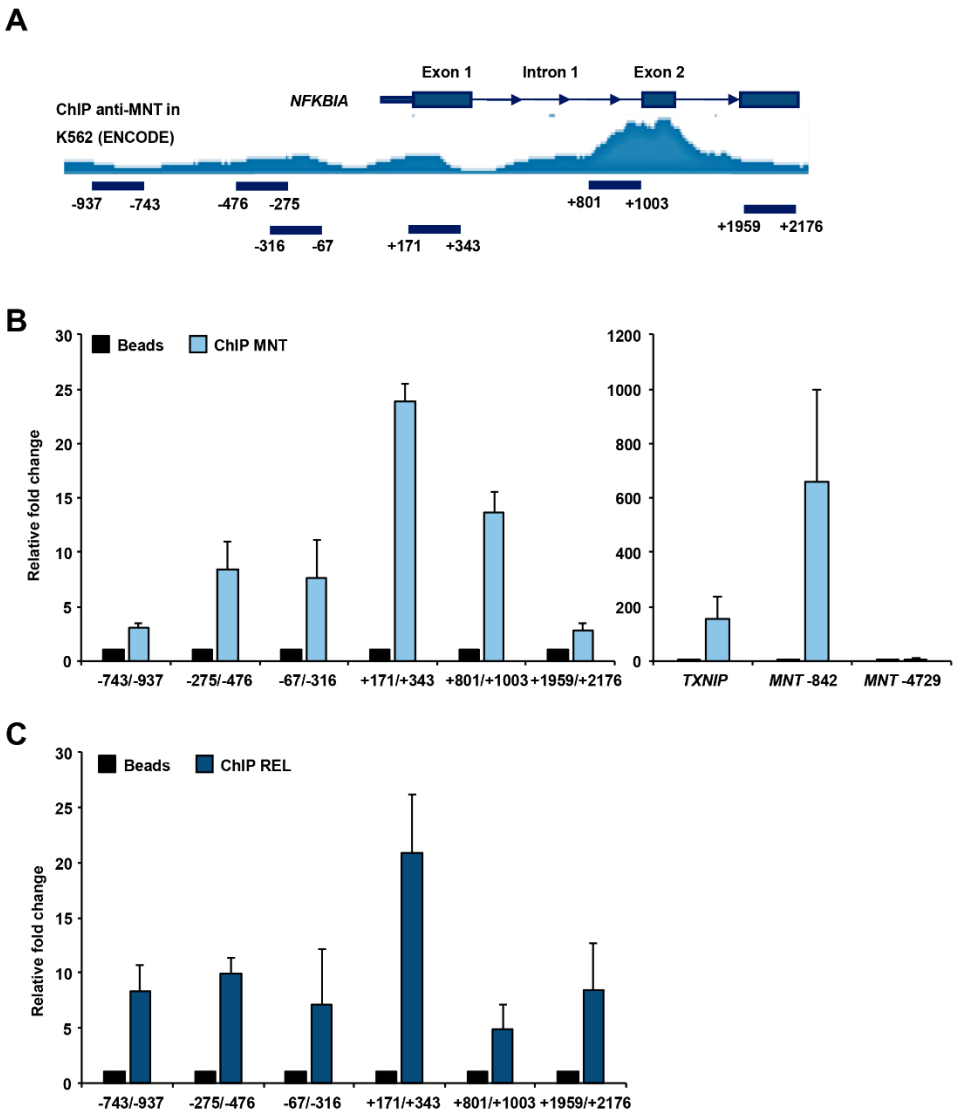

Figure 4.15. MNT and REL bind to *NFKBIA* gene in LoVo cells. (A) Schematic representation of human *NFKBIA* (IκBα) promoter showing the peaks for MNT binding in K562 cell line, from the ChIP-seq published by the ENCODE project. The bars show the amplicons analysed by ChIP-PCR. (B) ChIP with an antibody anti-MNT in LoVo cells. *TXNIP* and *MNT* -842 used as positive controls and a region upstream MNT promoter, as a negative control. (C) ChIP with an antibody against REL in LoVo cells. The data are shown as the mean ± S.E.M. of 3 independent experiments.

4.2. MNT beyond MAX interaction

4.2.1. MNT interacts with MLX in UR61 cells

UR61 cells express a small isoform of MAX that is not functional, as it has a deletion that includes bHLHLZ domain. This deletion in MAX impedes its interaction with any other bHLHLZ protein, meaning that MYC and the MXD proteins are working without their well-known partner (Hopewell and Ziff, 1995). Thus, we wondered if the lack of MAX in UR61 cells was compensated by MLX, in order to maintain MNT's activity in the cell. MNT has previously been described to interact with MLX (Cairo et al., 2001; Meroni et al., 2000), although the role of this interaction has not been deeply studied before.

Firstly, we transfected MLX-Flag into URMT cells or the corresponding empty vector (EV) and 48 h later, lysates were immunoprecipitated with anti-MLX and anti-MNT antibodies. The immunoprecipitates were analyzed by immunoblot and the data demonstrated that MNT interacted with MLX in UR61 cells in both conditions. As expected, the amount of MLX in the immunoprecipitates was higher in the MLX-overexpressed condition (**Figure 4.16 A**). We next studied this interaction in URMax34 cells treated with Zn^{2+} to induce MAX expression. The immunoblot results showed that MNT and MLX also interacted in the presence of MAX, although the interaction was much weaker after MAX induction. Thus, the data suggest that, at least in our experimental conditions, there is a preference of MNT to form dimers with MAX rather than with MLX (**Figure 4.16 B**). To confirm the MNT-MLX interaction in URMT cells, we used a HA-tagged MNT mutant with a deletion of the bHLH domain of mouse MNT, termed ΔbHLH MNT-HA (**Figure 4.16 C**). Members of the MYC-MAX-MXD-MLX network stablish interactions through the bHLH domain (Diolaiti et al., 2015). Thus, we transfected URMT cells with wild-type MNT (WT MNT-HA) or ΔbHLH MNT-HA and 48 h later, lysed and immunoprecipitated with anti-HA antibodies. As predicted, MLX appeared bound to WT MNT but not to ΔbHLH MNT, being this a good control for our experimental approach **(Figure 4.16 D**).

Next, we wondered whether the interaction between MNT and MLX was taking place in the cytoplasm or in the nucleus. MNT is generally nuclear (Hurlin et al.,

1997), although part of it is found in the cytoplasm of UR61 cells, probably as a consequence of the lack of MAX (Lafita-Navarro, 2015). MLX, on the contrary, is distributed along the cytoplasm (MLX α and β isoforms) and the nucleus (mostly MLX γ isoform). Taking advantage of the nucleus-cytoplasm fractionation method and the immunoblot, we found that MLX was present in cytoplasm and, at a lesser extent, in the nucleus of URMT cells. MNT was detected both in cytoplasm and nucleus. SIN3B and RhoGDI were used as nucleus and cytoplasm markers, respectively, and the Coomassie blue staining of the gel after transfer, as a protein loading reference (**Figure 4.16 E**). Next, we prepared these nuclear and cytoplasmic fractions of URMT cells for immunoprecipitation with anti-MNT and anti-MLX antibodies. The results showed that MNT and MLX co-immunoprecipitated in both nuclear and cytoplasmic fractions (**Figure 4.16 F**).

As an alternative approach, we performed two independent proximity ligation assays in URMT cells and checked the interaction between MNT and MLX. As it is shown in **Figure 4.17 A**, the assay detected the MNT-MLX interaction, being the fluorescent dots distributed along nucleus and cytoplasm. This is in accordance to the co-IPs presented in **Figure 4.16 F**, confirming that MNT-MLX dimers can be found both in the nuclear and the cytoplasmic compartments. As a positive control of the assay we chose the well-described interaction between MLXIP-MLX (Cairo et al., 2001). As a negative control, we used MNT-MAX, as the MAX present in URMT cells is unable to interact with any bHLHLZ protein (Hopewell and Ziff, 1995). The quantification of the assay is represented in **Figure 4.17 B**.

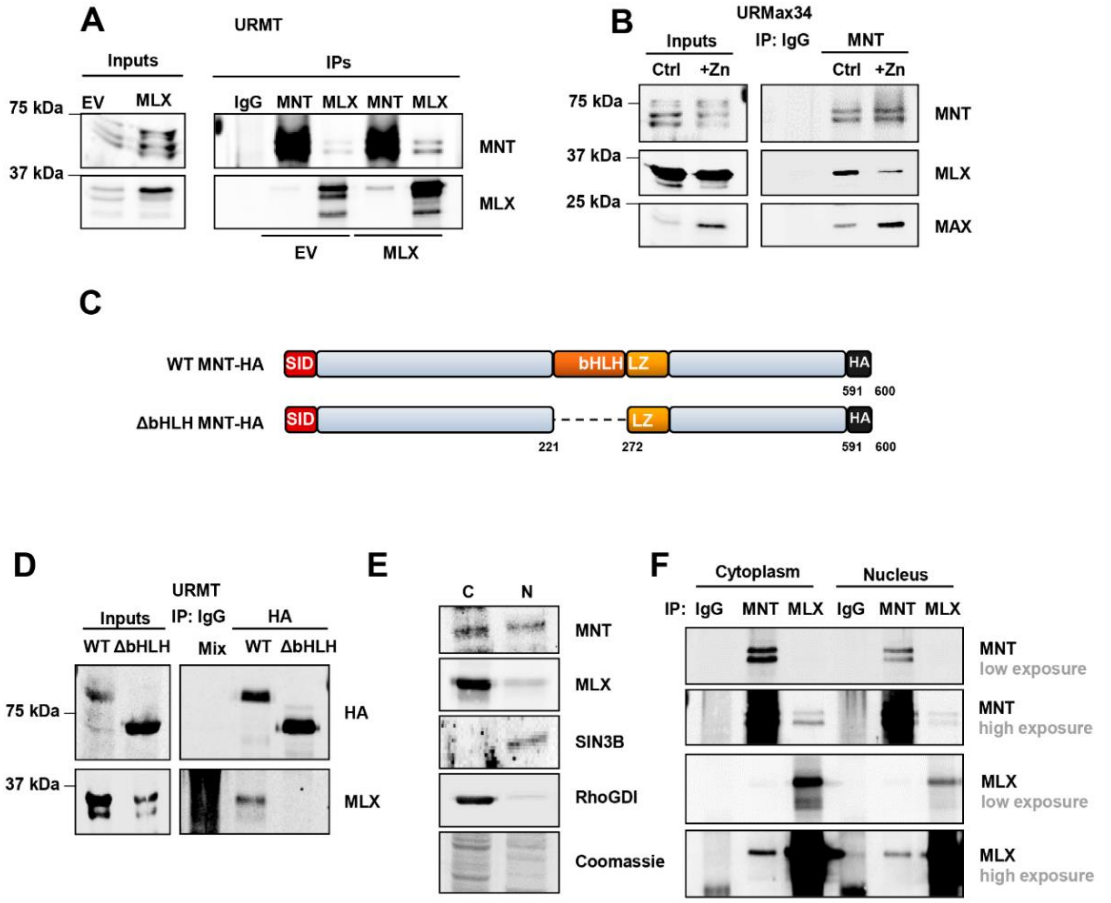

Figure 4.16. MNT interacts with MLX in UR61 cells. (A) Co-IPs of URMT cells 48 h after transfection with a MLX expression vector or the empty vector (EV: pcDNA3), using anti-MNT or anti-MLX antibodies, as well as unspecific IgG. (B) Co-IPs of URMax34 cells 48 h after transfection with a MLX expression vector and 24 h treatment with 100 µM Zn^{2+}. Lysates were immunoprecipitated with anti-MNT antibodies and, as a control, a mixture of lysates from cells treated and untreated with Zn^{2+} was immunoprecipitated with unspecific IgG. (C) Schematic representation of the wild-type (WT) and the deletion mutant ΔbHLH MNT-HA used in subsequent experiments. The SID (Sin3 Interacting Domain), bHLH, LZ domains, HA tag and amino acids of the murine protein are indicated. (D) URMT cells were co-transfected with a vector expressing MLX and the constructs shown in (C) as indicated at the top. IP performed with an anti-HA antibody 48 h after transfection. As a control, lysates (a mixture of lysates from cell transfected with WT MNT and ΔbHLH MNT) were also immunoprecipitated with unspecific IgGs. (E) MLX localization in UR61 cells. “N” for nuclear and “C” for cytoplasmic extracts. SIN3B and RhoGDI (ARHGDIA) were used as nuclear and cytoplasmic markers, respectively, and the Coomassie Blue staining of the gel after transfer as a protein loading control. (F) Co-IP in URMT cells 48 h after transfection with a MLX expression vector and nucleus/cytoplasm fractionation with anti-MNT or anti-MLX antibodies. The levels of MNT and MLX in the immunoprecipitates were assayed by immunoblot and reproduced in two independent experiments.

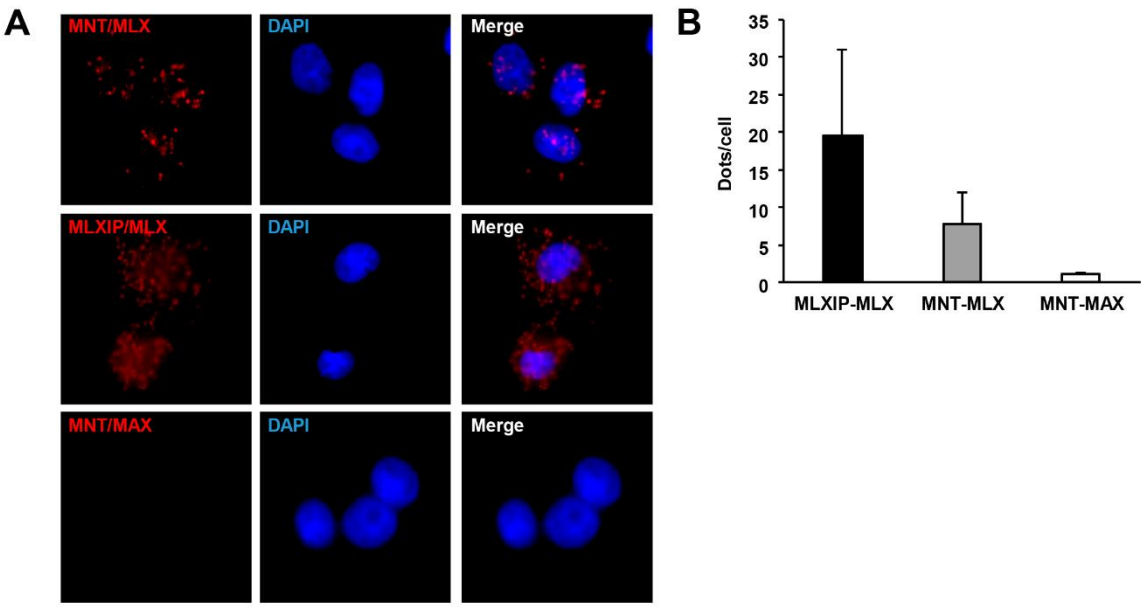

Figure 4.17. MNT and MLX interaction in URMT cells by PLA. (A) Images of the proximity ligation assay performed in URMT cells (untransfected cells): PLA positive signal in red and DAPI as a nuclear marker. (B) Quantification of a minimum of 100 nucleus per condition in two independent experiments by ImageJ. The error bars correspond to the S.E.M. obtained after the two experiments. MLXIP-MLX used as positive control and MNT-MAX for negative control.

4.2.2. MNT forms homodimers in UR61 cells

Homodimerization has not been described for the members of the MYC-MAX-MXD family except for MAX and MLX (Kato et al., 1992; Meroni et al., 2000), and also MNT, with recombinant proteins and in two-hybrid experiments (Hurlin et al., 1997; Meroni et al., 1997). However, MNT homodimerization in animal cells has not been reported so far.

After confirming MNT-MLX interaction, we wondered if MNT was also working as a homodimer in the absence of MAX in two models: HEK293T and UR61 cells. We first co-transfected HEK293T cells with GFP-MNT and Flag-MNT constructs and immunoprecipitated the lysates with an anti-GFP antibody. The immunoblot analysis demonstrated the presence of the smaller Flag-MNT protein in the material immunoprecipitated with anti-GFP. This result confirmed the ability of MNT to form homodimers in animal cells. As expected, both GFP-MNT (higher band) and Flag-MNT (lower band) were detected when the immunoblots were analyzed with an anti-MNT antibody (**Figure 4.18 A**).

Next, we tested MNT homodimerization in UR61 cells. URMT cells were infected with lentiviral particles containing the GFP-MNT gene, immunoprecipitated with the anti-GFP antibody, and the immunoprecipitates analyzed by immunoblot with anti-MNT and anti-GFP antibodies. As it is not possible to overexpress MNT in UR61 (see section 4.3.2) we treated the cells with bortezomib to ensure enough MNT levels. The results from the co-IP showed that endogenous MNT was present in the immunoprecipitates with anti-GFP (**Figure 4.18 B**). As MNT dimerization depended on the bHLHLZ domain in yeast two hybrid assays (Hurlin et al 1997, Meroni et al 1997), we wondered whether bHLH was involved in the homodimerization of MNT in our system. We transfected HEK293T cells with the MNT-HA construct that lacks the bHLH region (ΔbHLH MNT) (**Figure 4.16 C**), or the corresponding wild-type, together with GFP-MNT constructs. Then, we carried out immunoprecipitations with anti-HA antibodies to immunoprecipitate only the HA-tagged proteins. As expected, the immunoblot analysis revealed that ΔbHLH MNT was unable to interact with GFP-MNT (**Figure 4.18 C**). The same experiment was performed in URMT cells and the same result was obtained, i.e, GFP-MNT bound to wild-type MNT-HA but not to the ΔbHLH form (**Figure 4.18 D**). Thus, MNT forms homodimers through its bHLH domain in both human and rat cell lines, whether MAX is present or not.

Then, we wondered whether MNT homodimerization was affected by MAX presence or not. For this, URMax34 cells were transfected with GFP-MNT and treated (+Zn) or not (Ctrl) with Zn^{2+} for 24 h to induce MAX. The levels of MAX and MLX after the immunoprecipitation assay were determined by immunoblot and the results showed that at least in our experimental conditions, when both MAX and MLX are expressed, MNT preferentially binds to MAX than to MLX or MNT (**Figure 4.18 E**).

Altogether, the results suggest that MNT can form homodimers or heterodimers with MLX, whereas after MAX induction in URMax34, MNT mainly forms heterodimers with MAX.

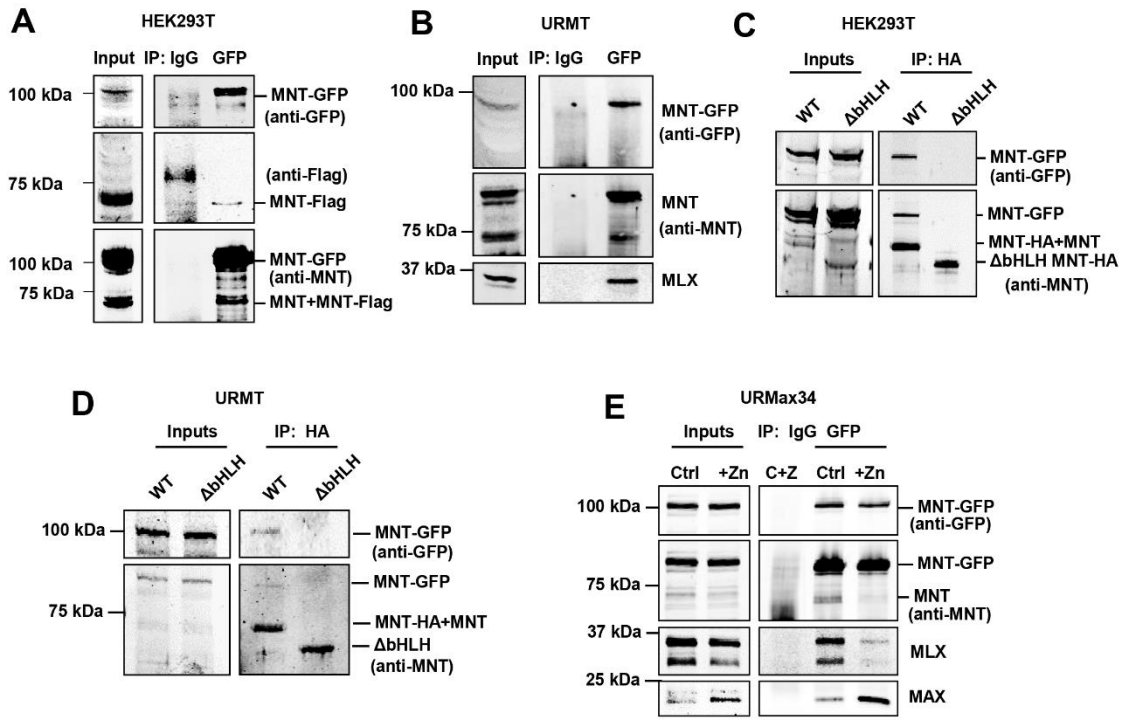

Figure 4.18. MNT homodimerizes in the presence and absence of MAX. (A) Co-IP in HEK293T 24 h after co-transfection with GFP-MNT and MNT-Flag expression vectors, using the anti-GFP antibody or an unspecific IgG as a negative control. The results were reproduced in two independent immunoprecipitations. (B) Co-IP in URMT cells that had been infected with lentivirus encoding a MNT-GFP and 72 h later transfected with MNT-Flag and treated with 15 nM bortezomib for 12 h before harvesting. 48 h after transfection lysates were prepared and immunoprecipitated with anti-GFP antibody. The results were reproduced in two independent experiments. (C) Co-IP in HEK293T cells 24 h after transfection with MNT-GFP and expression vectors for WT MNT or ΔbHLH MNT (Figure 4.16 C) as indicated at the top of each lane. An anti-HA antibody was used for the IP. The results were reproduced in two experiments. (D) URMT cells were infected with lentivirus encoding a GFP-MNT and 72 h later transfected with expression vectors for wild-type (WT) MNT or ΔbHLH as indicated at the top of each lane. 48 h after transfection, an IP with anti-HA was performed to pull down the transfected MNT proteins. (E) URMax34 cells were transfected with a MNT-GFP expression vector and 48 h after transfection cells were left untreated or treated with 100 µM Zn^{2+} for 24 h. IP performed with an anti-GFP antibody. As a control, a mixture of lysates from cells treated and untreated with Zn^{2+} was immunoprecipitated with unspecific IgG. The results were reproduced in three independent immunoprecipitations**.**

4.2.3. MNT and MLX in cell proliferation

Once formation of MNT-MLX and MNT-MNT dimers was confirmed in UR61 cells, we were interested in knowing if both MNT and MLX had a role in cell proliferation. Using short-hairpin RNAs, we knocked down *MNT* and *MLX* and checked proliferation and survival markers (Cyclin A2 and Survivin) by immunoblot. Interestingly, both markers diminished after *MNT*, *MLX* or both *MNT* and *MLX*

knockdown (**Figure 4.19 A**). In parallel, we performed clonogenic assays by selecting the cells for 15 days with puromycin. Knocking down *MNT*, *MLX* or both provoked a decrease in UR61 proliferation, being this a proof of the importance of these two proteins for the cell function (**Figure 4.19 B**).

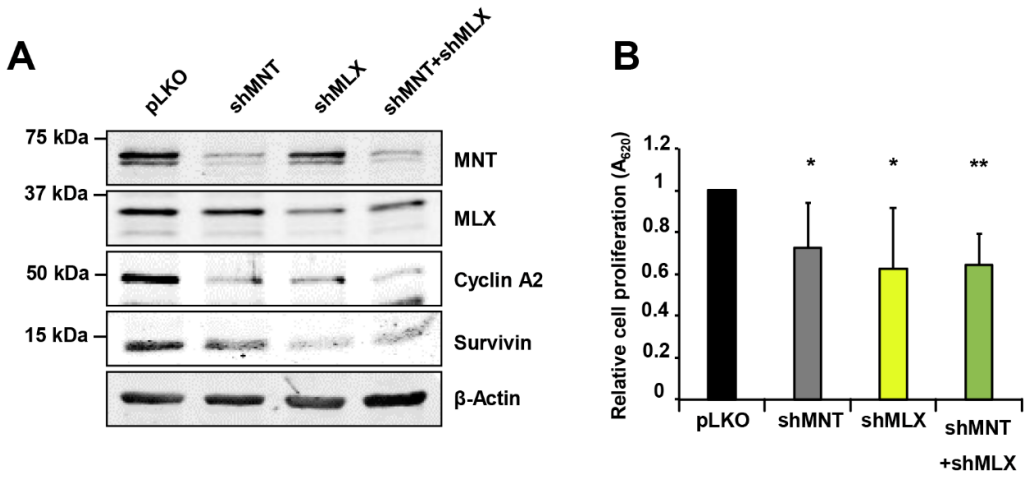

Figure 4.19. MNT and MLX downregulation inhibits UR61 cell proliferation. (A) URMT cells were transfected with shMNT and shMLX, or the empty vector (pLKO) as indicated at the top. 5 days after selection with puromycin, the cell lysates were subjected to immunoblot to detect MNT and MLX. Cyclin A2 and survivin were determined as control for proliferation and β-actin as protein loading control. (B) Cell proliferation determined by crystal violet staining in URMT cells transfected with the indicated short hairpin vectors. After 15 days of puromycin selection the colonies were stained with crystal violet and the dye was solubilized and quantified by absorbance at 620 nm. * *P* <0.05; ** *P* <0.01. Data show mean values ± S.E.M. from four independent experiments.

4.2.4. MNT regulates gene expression in the absence of MAX

Once we confirmed that MNT forms homodimers and heterodimers with MLX in UR61 MAX-deficient cells, we studied if MNT was also able to regulate transcription. For this, Lafita-Navarro (PhD Dissertation 2015) carried out a RNA-seq upon MNT depletion in cells with and without MAX in our laboratory. URMT and URMax34 cells were transfected with the short-hairpin RNA construct against the rat MNT gene (shMNT-1) or the empty vector (pLKO) as a control in two different biological replicates. These analyses revealed that MNT regulates transcription in the absence of MAX, as 281 genes were regulated upon MNT depletion in MAX-deficient URMT cells. In the case of MAX-expressing cells, 537 were the genes affected by MNT depletion. Comparing both sets of differentially

expressed genes, 158 were shared between URMT and URMax34 after *MNT* depletion: 27% up-regulated and 73% down-regulated.

Taking this data into account, we selected a few genes that were differentially expressed upon *MNT* knockdown and were related to cell cycle and DNA repair mechanisms: *E2F6, PARPBP, BIRC5, CDK1, BRCA1* and *CDKN1C*. URMT and URMax34 cells were then transfected with shRNAs against *MNT*, *MLX* or both. Gene expression was studied by RT-qPCR 48 h after transfection and 24 h of treatment with Zn^{+2} (**Figure 4.20, upper panel URMT, lower panel URMax34**). *MNT* and *MLX* levels were checked in order to know if the knockdown had worked. The results showed a statistically significant decrease in the expression of *E2F6, PARPBP, BIRC5, CDK1, BRCA1* and an increase of *CDKN1C* upon MNT depletion, both in URMT and URMax34 cells. This results are in line with the data from the RNA-seq experiments (Lafita-Navarro, PhD Dissertation 2015). The knockdown of *MLX* instead, had a milder effect, affecting only *CDK1* and *BRCA1*, which were downregulated in the case of URMT cells. Interestingly, *CDK1* and *BRCA1* were not downregulated further after both *MNT* and *MLX* knockdown. These results suggest that both MNT-MNT and MNT-MLX dimers could be regulating the transcription of these genes.

Subsequently, we were interested in knowing if the transcriptional changes observed after *MNT* and *MLX* silencing were a consequence of a direct regulation by these two proteins. For this reason, we took URMT and URMax34 cells after 24 h stimulation with Zn^{2+} and carried out a ChIP with antibodies against MNT or MLX. Then, we checked the binding to the regions that showed a peak for MNT in the K562 ChIP-seq published by the ENCODE project. The primers for amplifying these regions in the rat genome were designed and the presence of E-boxes in the amplicons was confirmed in all but *BRCA1* (**Table 4.1**). In the MAX-deficient URMT cells, we identified a positive binding of MNT to *BIRC5, CDK1, BRCA1*. Among these regions, MLX was bound to *BIRC5* and *BRCA1* (**Figure 4.21**).

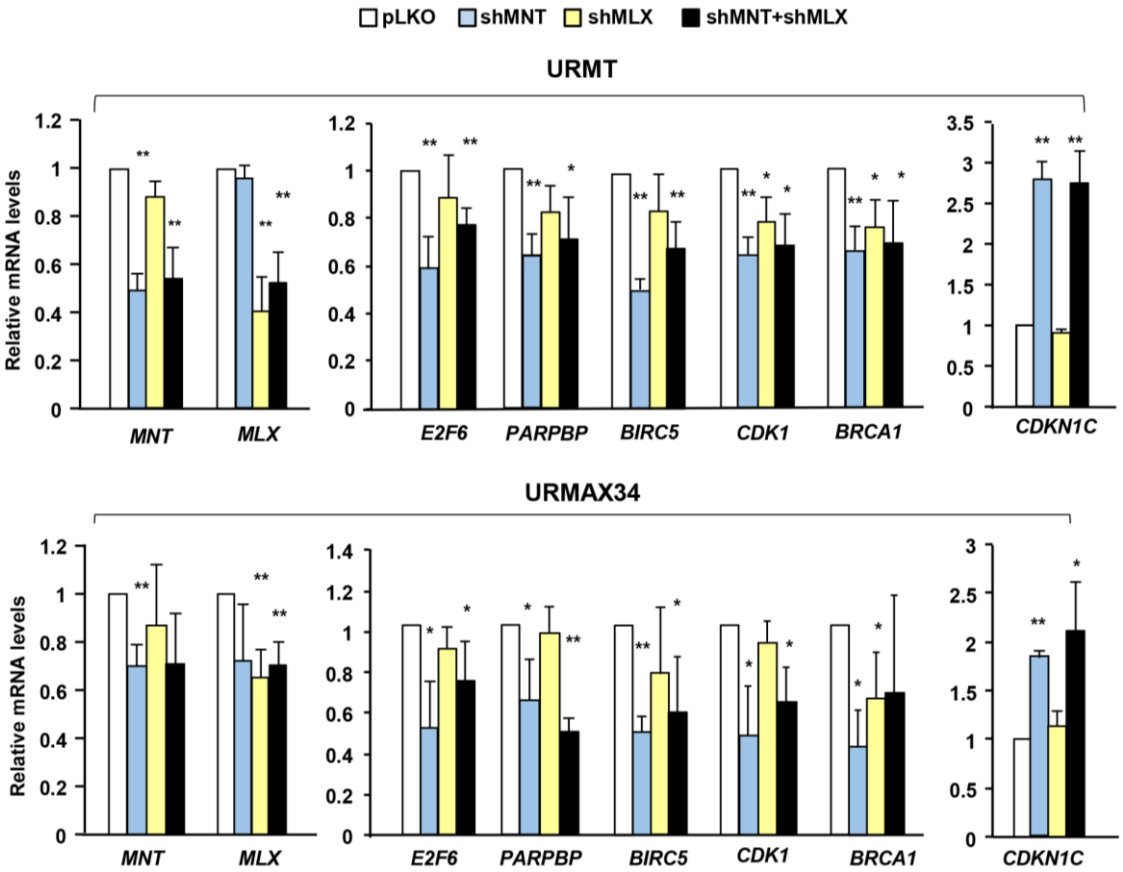

Figure 4.20. Gene expression changes in *MNT* and *MLX* knockdown cells. (A) mRNA expression regulation due to *MNT* and *MLX* silencing in genes selected after the RNA-seq data analysis. URMT (upper panel) and URMax34 cells (lower panel) were transfected with a mixture of shMNT-1 and shMNT-2 or/and shMLX constructs as indicated. Cells were treated for further 24 h with 100 µM Zn^{+2} 48 h after transfection, total RNA was prepared and mRNA levels of the indicated genes were determined by RT-qPCR. The data are represented as mean ±S.E.M. from three independent transfection experiments. In all cases, * *P* <0.05.; ** *P* <0.01.

Table 4.1. Genes found to have a peak for MNT binding in the K562 ChIP-seq published in the ENCODE project. The position of the peaks and their E-boxes are shown, together with the corresponding regions analyzed in rat and the E-boxes identified around the amplicons.

Gene	Peak MNT ChIP-seq ENCODE Project (human K562)		Analyzed sequence in rat genome	
	Position	E-boxes	Amplicon	E-boxes
E2F6	-202/+574 bp	**CACGTG** +109 and +534 bp	+303/+546	**CACGTG** +309
BIRC5	-335/+365	**CACGCG** -149 bp	+318/+483	**CACGCG** -216 bp **CACGAG** +303 bp and +477 bp **CATGTG** +727 bp
CDK1	-298/+270 +783/+1413	**CACGTG** +1157 bp	-216/-54	**CCACGTG** +207 bp
BRCA1	-295/+231	None	+88/+310	None
CDKN1C	-118/+512	**CACGAG** +890	-118/+223	**CACGAG** +401

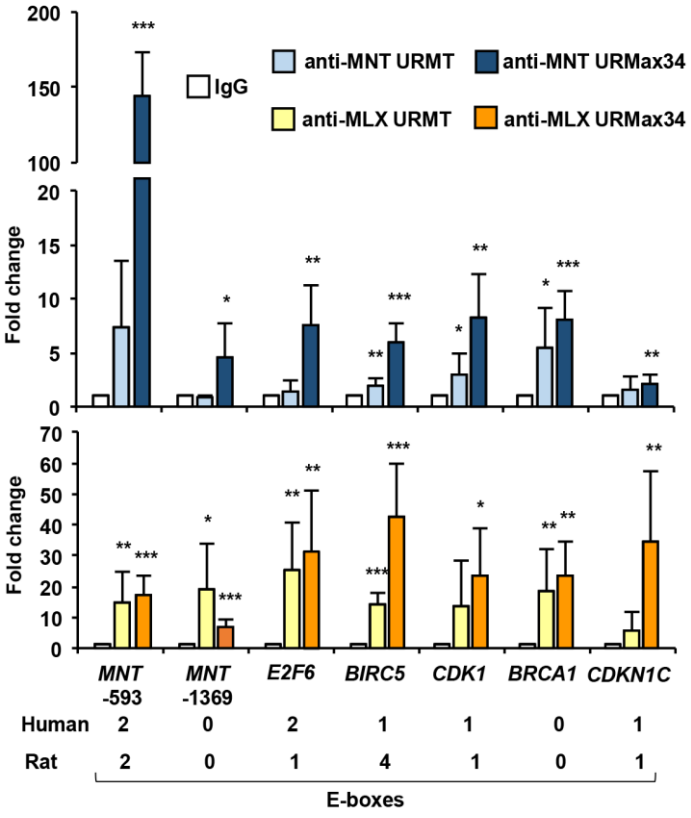

Figure 4.21. MNT and MLX binding to the DNA in URMT and URMax34 cells. ChIP with anti-MNT (upper panel) and anti-MLX (lower panel) antibodies of URMT and URMax34 cells, both treated with 100 μM Zn^{+2} for 24 h. The binding of MNT and MLX were analyzed in the amplicons listed in **Table 4.1** by qPCR. The data are means ± S.E.M. from 3 independent experiments. * *P* <0.1; ***P* <0.05; *** *P* <0.01. The E-boxes found in the regions bound by MNT in human K562 (ENCODE) and the E-boxes in rat genome are specified below and explained in **Table 4.1**.

Then, we also performed a ChIP-PCR with an anti-MAX antibody in the same genes looking at the same amplicons. MAX binding was analyzed in both URMax34 and URMT cells (the latter cell line, which is MAX-deficient, as a negative control). The results showed that MAX was bound to all promoters but the signal in *BIRC5* and *BRCA1* was not statistically significant (**Figure 4.22**).

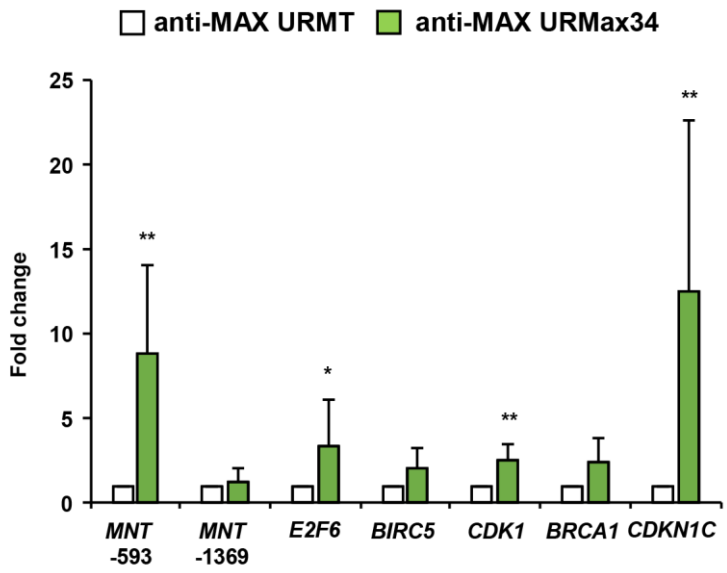

Figure 4.22. MAX binding to DNA in URMax34 *versus* URMT cells. ChIP with anti-MAX antibody of URMax34 cells relative to URMT, both treated with 100 μM Zn^{+2} for 24 h. Data determined by qPCR on the amplicons listed in **Table 4.1**. Represented as means ± S.E.M. from 3 independent experiments. * *P* <0.1; ** *P* <0.05; *** *P* <0.01.

Next, we wanted to explore further the direct regulation of gene expression carried out by MNT. For this, we performed a ChIP-seq experiment with an antibody against MNT in triplicates in MAX-deficient URMT cells. In general, we did not observe a large number of regions bound to MNT (**Annex 1**). However, some of the peaks were quite clear and consistent among the replicates, such as *FBXO32*/*Atrogin-1, CCNG2*, *CDK12, ERCC6* or *MNT* promoter (**Figure 4.23 A**). As we wanted to know if MNT binding to these genes implied an effect on their expression, we knocked down *MNT* in URMT and URMax34 cells through short-hairpin constructs and checked their expression by RT-qPCR. The results showed that upon *MNT* knockdown, the mRNA expression of *FBXO32/Atrogin-1, CCNG2* and *ERCC6* increased, indicating that MNT binds to their promoters to repress their expression even in the absence of MAX (**Figure 4.23 B**).

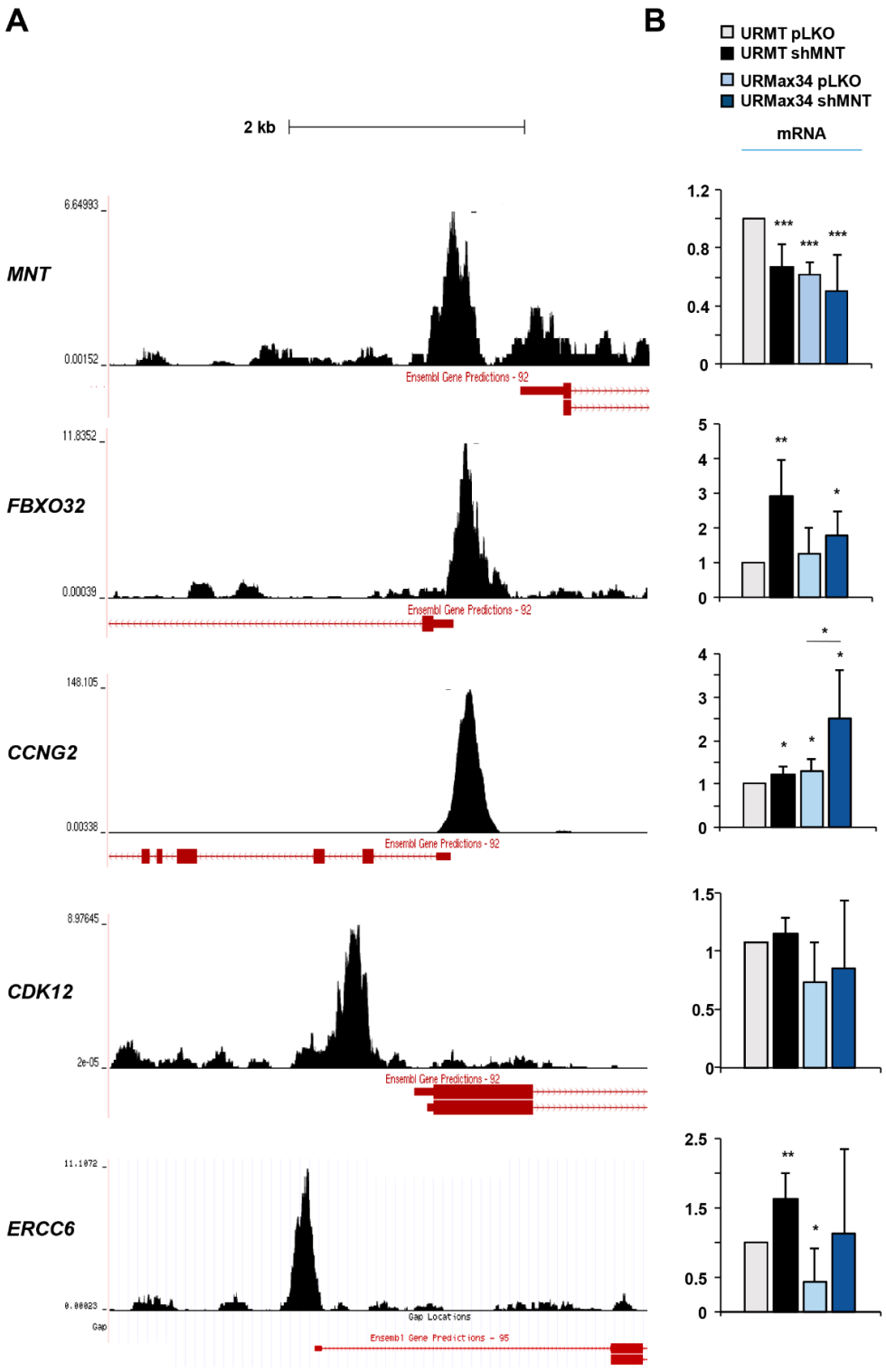

Figure 4.23. **MNT binds to the DNA in the absence of MAX.** (A) MNT ChIP-seq peaks found on the *MNT*, *FBXO32*, *CCNG2*, *CDK12* and *ERCC6* promoters in URMT cells, using the UCSC Genome Browser on Rat Jul. 2014 (RGSC 6.0/rn6) assembly. The image shows the peaks of one of the three replicates of the assay. (B) Expression of *MNT*, *CCNG2*, *CDK12* and *ERCC6* in URMT and URMax34 48 h after transfection with shMNT-2 or pLKO constructs and 24 h of treatment of Zn^{+2}. Data obtained by RTqPCR (left panel) was normalized with S14 and relativized to URMT pLKO. Data obtained in the RNA-seq (right panel). Represented as a mean ±S.E.M. of three independent transfection experiments. * *P* <0.1; ** *P* <0.05, *** *P* <0.01.

Ontology analysis of the genes obtained in our ChIP-seq experiments revealed that MNT-bound genes are involved in cell cycle, DNA replication and regulation of gene expression (**Figure 4.24**). We then analyzed if there were any DNA motifs that significantly appeared in the regions bound by MNT. The results revealed that MNT was bound to regions with E-boxes in the absence of MAX. Surprisingly, MNT was also bound to regions containing DNA binding motifs for forkhead transcription factors, SMAD, VDR and TBXT (**Table 4.2**).

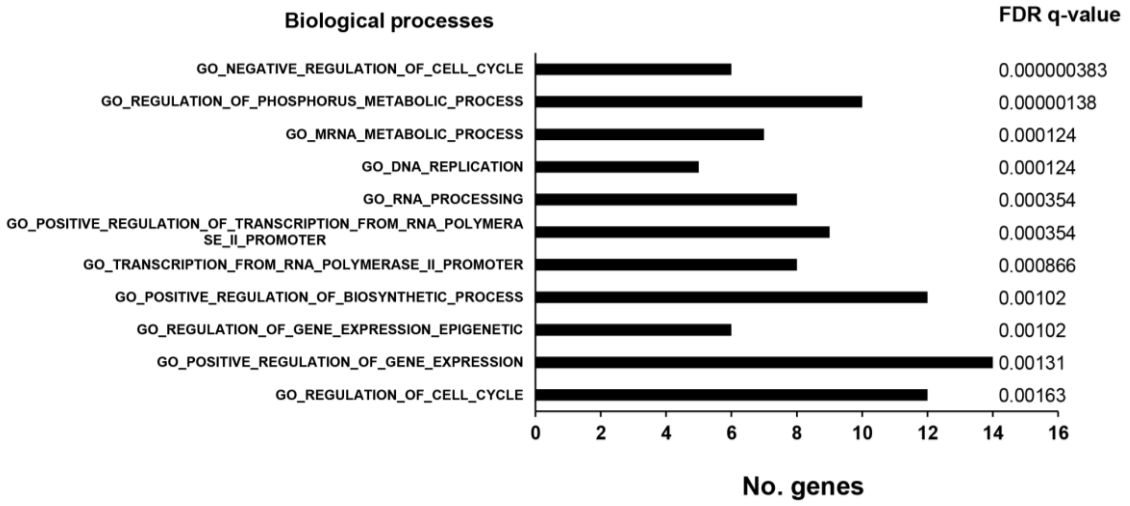

Figure 4.24. **Gene ontology analysis of MNT-bound genes are involved in cell cycle, DNA replication and regulation of expression**. The genes where MNT was found to be significantly bound (FDR <0.1) within -/+ 3 Kb of their TSS in our ChIP-seq experiment were analyzed with the MsigDB platform (http://software.broadinstitute.org/gsea/msigdb) using the biological processes gene sets. The 11 top enriched pathways according to FDR value are represented in the graph. The bioinformatic analysis was carried out by Dr. M Carmen Lafita-Navarro, Southwestern Medical Center, Dallas.

Altogether, these findings about MNT and MLX's role in gene regulation without MAX have led to the identification of genes directly regulated by MNT-MNT or MNT-MLX dimers. As the studied genes are involved in cell cycle and DNA repair, this could explain why MNT is such a key protein for the cell biology.

Table 4.2. HOMER enriched results for known sequence motifs on MNT immunoprecipated DNA regions on rat genome. The 10 motifs with higher scores are shown. The ChIP-seq data from **Annex 1** was analyzed by the HOMER algorithm (homer.ucsd.edu/homer/motif/motifDatabase.html) using the rat genome Rnor_6.0 version as reference. The bionformatic analysis has been carried out by Dr. Ignacio Varela, IBBTEC.

Sequence	Factor	Log P-value	q-value	No. of targets
	FOXP1	-6.512e+00	0.6148	77
	FOXA2	-5.496e+00	0.8490	164
	SMAD2	-5.441e+00	0.8490	30
	FOXO3	-5.428e+00	0.8490	121
	VDR	-5.235e+00	0.8490	31
	RXR	-5.011e+00	0.8490	135
	E-box 1	-5.006e+00	0.8490	12
	E-box 2	-4.881e+00	0.8490	43
	EWS-FLI-4.672	-4.672	0.8490	86

4.3. MNT regulation at the mRNA and protein levels

4.3.1. MNT regulation of its own promoter

MNT is an essential protein for the cell and several evidences from our group and others demonstrate its key role in cell proliferation and survival (Hurlin et al., 2003; Lafita-Navarro, PhD Dissertation 2015; Toyo-oka et al., 2004). Considering MNT's role in curbing the excessive MYC activity, we hypothesized that MNT levels must be tightly controlled to assure the correct development of the biological processes.

Previous results in our laboratory using the URMT and the URMax34 cells as the main model of study, showed that MNT levels are higher and are distributed between nucleus and cytoplasm in the absence of MAX. However, when MAX expression is induced, MNT total levels diminish, and MNT is mostly localized in the nucleus. It has also been demonstrated that MNT-MAX dimers bind to the MNT promoter to autorepress MNT transcription (Lafita-Navarro, PhD Dissertation 2015), which is also supported by the ChIP-seq data shown previously in **Figure 4.23**. These results prompted us to study the MNT-MAX regulation of MNT. We first performed luciferase assays with MNT promoter, which has two E-boxes 1 kb upstream the transcriptional start site. One of them is canonical (CACGTG, named E-box 1) and the other one is non-canonical (CATGTG, named E-box 2) and they are conserved among rat, mouse and human (**Figure 4.25 A**).

In order to study MNT regulation of its promoter, we took a luciferase reporter carrying the 850 bp upstream region of the transcription start site from the human MNT gene, which was previously made in our laboratory. The construct was termed MNT-Luc (**Figure 4.25 B**). Then, HEK293T cells (which express MAX) were transfected with the MNT-Luc and MNT expression vectors (or the corresponding empty vectors). The obtained results showed that MNT overexpression led to a reduction in the luciferase activity (**Figure 4.25 B, left panel**), suggesting that MNT-MAX dimers negatively regulate the *MNT* promoter. Then, we wondered which of the two E-boxes was contributing more to the MNT-mediated negative autoregulation. Thus, we constructed two reporters containing

each of the E-boxes, termed E-box 2 MNT-Luc (containing the last 220 bp of the MNT-Luc reporter which includes the E-box 2) and E-box 1 MNT-Luc (containing the first 570 bp of the MNT-Luc reporter and including the E-box 1) (**Figure 4.25 B**). Surprisingly, only the E-box 2 MNT-Luc construct was repressed upon MNT overexpression and the E-box 1 MNT-Luc was not affected at all.

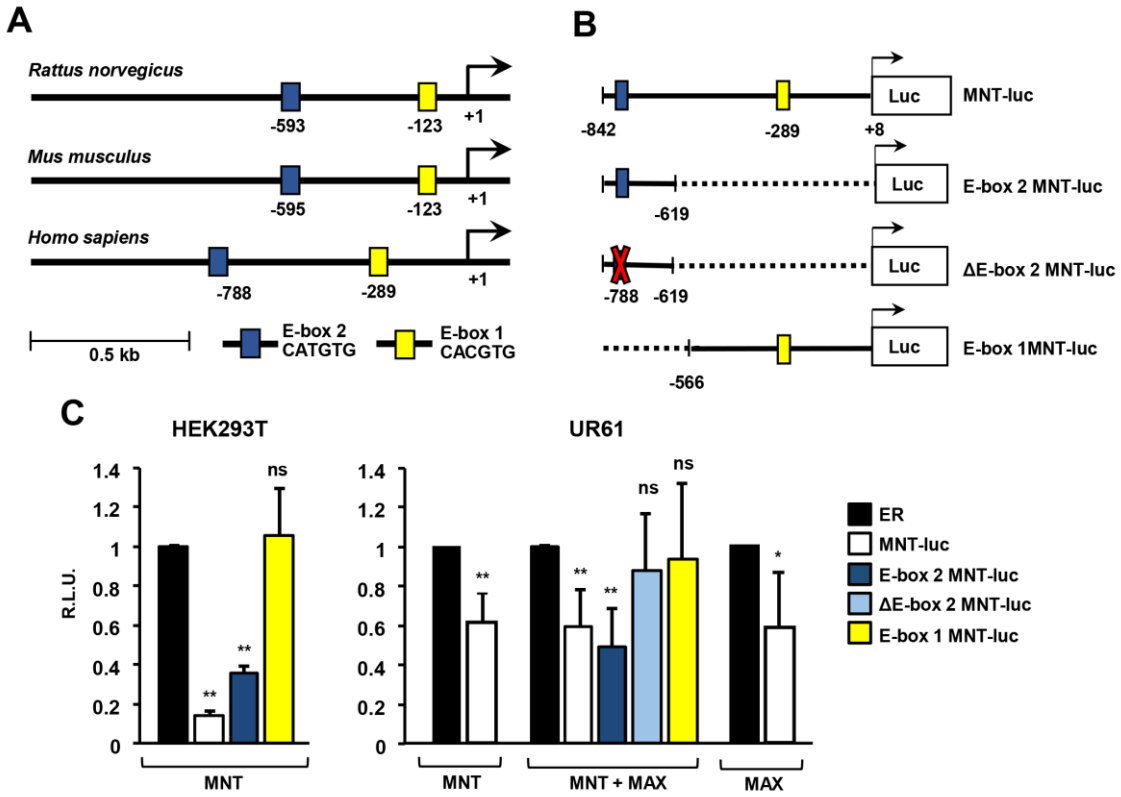

Figure 4.25. MNT regulates its own promoter. (A) Schematic representation of human, rat and mouse MNT promoters showing two conserved E-boxes. The coordinates correspond to the 5' nucleotide of each E-box, using the UCSC genome browser (http://genome.ucsc.edu/, release GRCh37/hg19). (B) Schematic representation of luciferase reporters driven by human MNT promoter used in this work. (C) Luciferase assays in HEK293T and UR61, 24 h or 36 h after transfection, respectively. Results are expressed in relative luciferase units (R.L.U.) after normalizing each condition first to the luciferase empty reporter (ER) and then to the empty vector of MNT and/or MAX. The data are shown as the mean ±S.E.M. of 9 (for MNT-luc) or 4 independent transfections (for the rest of experimental points). **P* <0.01; ***P* <0.005; ns: non-significant.

Subsequently, we also investigated the activity of the MNT promoter in the MAX-deficient UR61 cells. UR61 cells were transfected with the MNT-Luc vector together with MNT and MAX expression vectors. The results also showed a decrease in the luciferase activity although less than in HEK293T cells (**Figure 4.25 C, right panel**). The overexpression of MNT alone in UR61 cells also led to

a decrease in the luciferase activity of MNT-Luc, suggesting that MNT can downregulate *MNT* promoter in UR61 cells in the absence of MAX. The repressive effect of MNT was stronger in HEK293T cells than in UR61 cells, which may be explained by the limited overexpression of MNT protein achieved in transfected UR61 cells (shown below). In the case of the other constructs, co-transfection of *MNT* and *MAX* resulted in a decrease in the activity of E-box 2 MNT-Luc but not of E-box 1 MNT-Luc, in accordance with the results obtained in HEK293T. We next constructed a reporter with a deletion of the -788 E-box (ΔE-box 2 MNT-Luc) and the results showed that in UR61 cells, MNT had no effect on the activity of the mutant reporter (**Figure 4.25 C, right panel**), confirming that E-box 2 CATGTG, mapping at –788, was the one involved in the autoregulation of MNT promoter.

4.3.2. MNT protein levels are modulated by MAX

Previous results obtained in our laboratory (Lafita-Navarro, PhD Dissertation 2015) together with the data above, suggested that MNT and MAX control MNT levels by direct binding to MNT promoter on E-box 2 and its consequent repression. Then, we analyzed MNT protein levels in URMT versus URMax34 cells after treatment with Zn^{+2} and transfected with a MNT expression vector or its corresponding empty vector (EV). As it can be observed in **Figure 4.26 A**, MNT levels were higher in MAX-deficient cells (URMT) and even if we introduced MNT expression DNA to overexpress it, we were not able to increase MNT protein levels. The results showed that MAX-expressing URMax34 cells showed much less MNT in the empty vector condition and we were able to overexpress MNT. Afterwards, we transfected URMT cells with MNT, MAX or MNT+MAX expressing vectors, for discarding the possibility of a side-effect from the selected clones of the URMax34 cells. As shown in **Figure 4.26 B**, the results obtained were quite similar as we were only able to overexpress MNT when MAX was present. These constructs were co-transfected with a GFP vector, which expression was analyzed by western blot as a control of transfection.

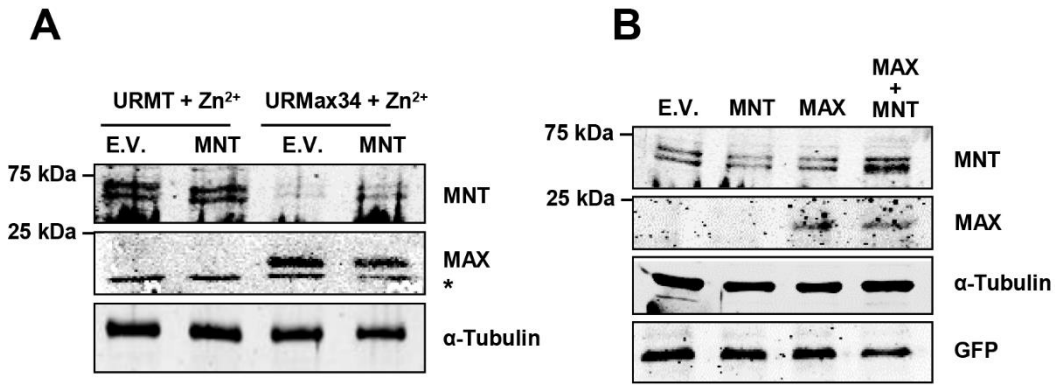

Figure 4.26. MNT levels depend on MAX (A) URMT or URMax34 cells were treated with Zn^{2+} to induce MAX (in URMax34 cells) and transfected with a MNT expression vector or the empty vector (E.V., pCMVSport6-MNT). The levels of MNT and MAX were analyzed by immunoblot 48 h after transfection. The asterisk marks an unspecific band. The levels of α-tubulin were also determined as a protein loading control. (B) UR61 cells were transfected with MNT and MAX expression vectors (pCMV-Sport6-MNT and pCEFL-MAX respectively) as indicated at the top, as well as the corresponding empty vectors. In each case a GFP expression vector was also co-transfected. The levels of MNT and MAX were analyzed by immunoblot 48 h after transfection. The α-tubulin was used as a protein loading control and GFP as a transfection control.

As previous experiments in our laboratory showed an accumulation of MNT after treatment with the proteasome inhibitor bortezomib, we wondered whether MNT had any PEST sequence. PEST sequences are polypeptide sequences enriched in proline (P), glutamic acid (E), serine (S) and threonine (T) that target proteins for rapid destruction (Rechsteiner and Rogers, 1996). After analyzing MNT amino acid sequence, we detected two potential PEST (61-121 and 319-349 amino acids) and one poor PEST (142-156) (http://www.bioinformatics.nl/emboss-explorer/). We transfected WT MNT and different MNT deletion mutants into URMT and checked if we were able to overexpress any of them (**Figure 4.27 A**). Thus, **Figure 4.27 B** shows that ΔSID, ΔNt_2 and ΔCt_1 MNT mutants were overexpressed, in contrast to WT and ΔbHLH MNT. This can be explained by the fact that ΔNt_2 and ΔCt_1 MNT lack some PEST sequences, so they may be less prone to degradation. On the contrary, ΔSID contains all three PEST sequences and even so, its overexpression was achieved, suggesting that interaction with SIN3B or other mechanisms may also contribute to MNT regulation.

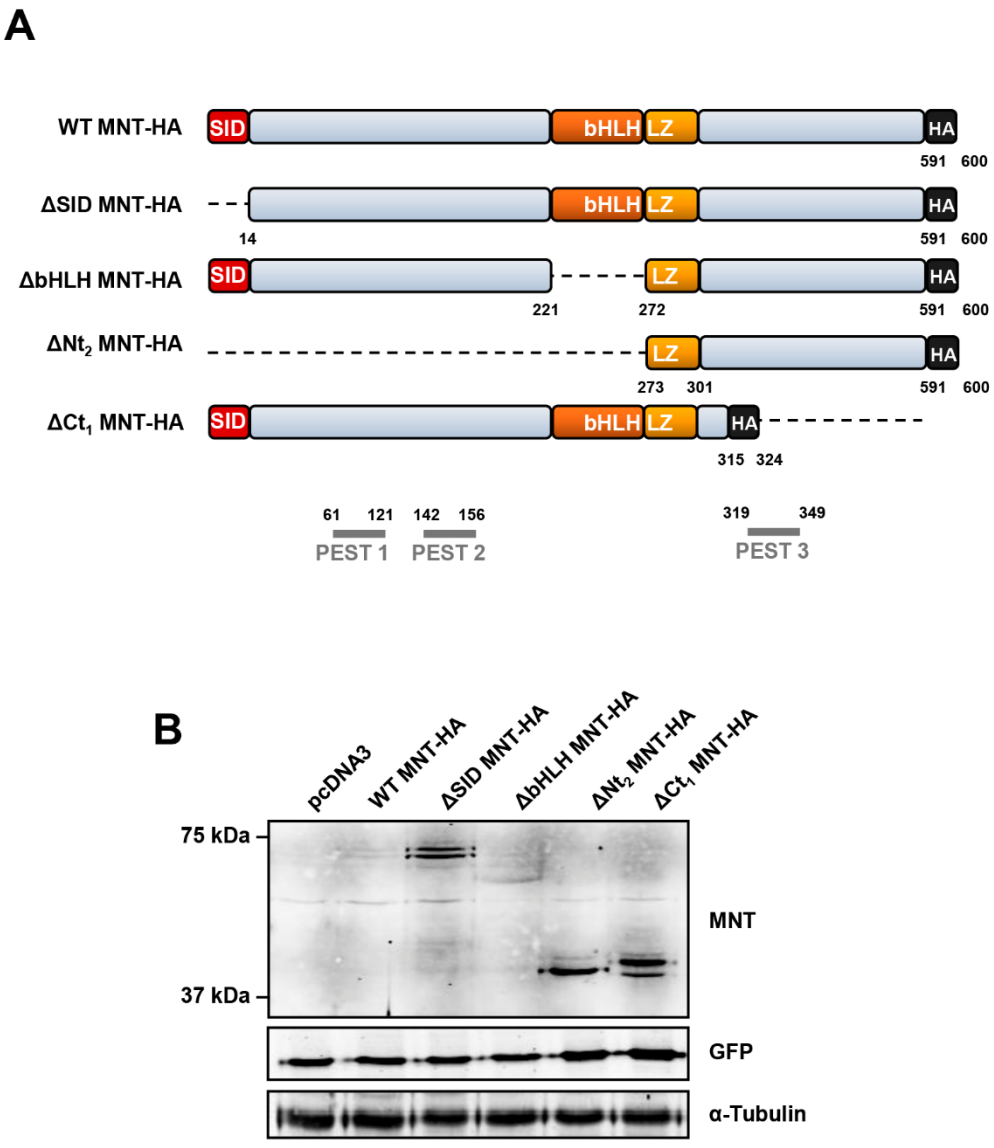

Figure 4.27. MNT protein stability may depend on PEST sequences. (A) Schematic representation of WT MNT and the deletion MNT constructs used in this work. (B) URMT cells lysates 48 h after transfection with the constructs shown in A. GFP as a transfection control and tubulin, as a protein loading control.

4.4. Transcriptional regulation by MNT: in the search of new target genes

4.4.1. *MNT* knockout in the HAP1 cellular model

MNT is a transcription factor that generally represses its target genes by its association with SIN3 proteins, which in turn recruit histone deacetylases and different cofactors, resulting in a more compacted chromatin structure (Hurlin et al., 1997; Yang and Hurlin, 2017). Although it is clear that MNT plays a crucial role in cell biology, we still do not understand how MNT carries out its functions. This is the reason why we decided to go deeper in the study of MNT through a new model of *MNT* knockout cells.

The model used in this project was the HAP1 cell line. HAP1 cells derive from KBM-7, a chronic myelogenous leukemia (CML) cell line. HAP1 cells are characterized by being near-haploid, adherent cells with a fibroblast-like morphology (Essletzbichler et al., 2014). The fact that these cells are near-haploid makes them a good model for performing the knockout (KO) of the gene of interest (in this case, *MNT*) by CRISPR/Cas9 (Ran et al., 2013).

MNT KO and WT HAP1 cells were obtained from the Horizon company. The CRISPR/Cas9 procedure produced an insertion of 4 nucleotides in MNT's sequence that caused a frameshift, abolishing MNT protein synthesis in HAP1 cells (**Figure 4.28**).

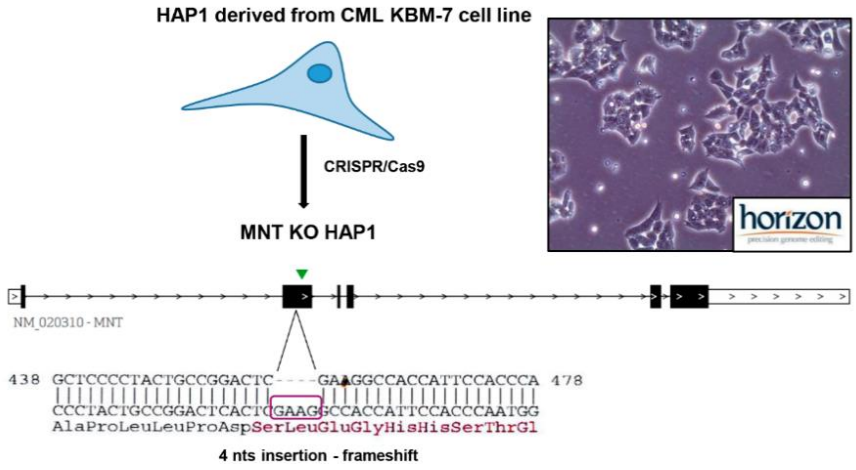

Figure 4.28. Generation of the HAP1 MNT KO cell line. CRISPR/Cas9 system for knocking out *MNT* in HAP1 cells (Horizon). An insertion of 4 nucleotides was made, generating a frameshift. The image of the cells was obtained in https://www.horizondiscovery.com/cell-lines/all-products/isogenic-cell-lines/hap1-cells.

HAP1 cells were grown in our laboratory and MNT protein levels were tested by immunoblot, confirming that the cells are *MNT* knockout (**Figure 4.29 A, B**). In addition, MYC, MAX and MLX protein levels were analyzed. The results showed a decrease in these proteins upon *MNT* knockout. Cyclin A2 and survivin, which are markers of proliferation and survival, did not show major changes between the two conditions. Afterwards, we tested the expression of *MNT*, *MAX*, *MLX* and *MYC* by RT-qPCR at the mRNA level. *MNT*, *MAX* and *MLX* did not change significantly upon *MNT* knockout. However, it is interesting to note that MYC expression did decrease, which suggests that MNT deletion affects MYC levels at the transcriptional and post-transcriptional level (**Figure 4.29 C**).

Finally, we assayed the proliferation rate by plating the WT and KO cells and staining them with Crystal Violet 24 h after seeding (day 1) and four days after seeding (day 4). The results showed that MNT KO HAP1 cells proliferated much faster than their wild type countermates (**Figure 4.29 D**), suggesting that in these cells, MNT limits cell proliferation.

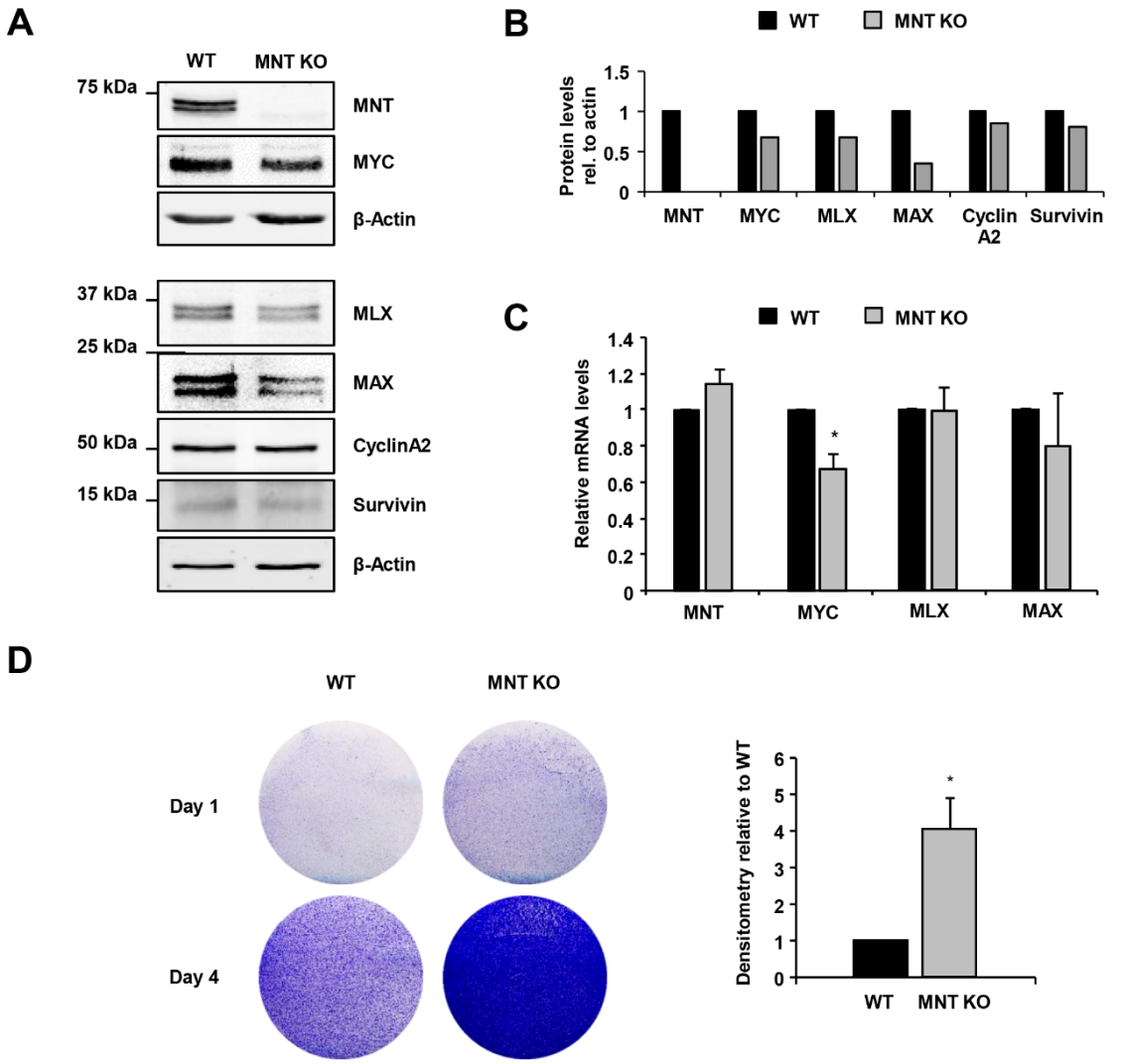

Figure 4.29. MNT KO *versus* WT HAP1 cell features. (A) Immunoblot of MNT, MYC, MLX and MAX from total WT and MNT KO HAP1 cell lysates. Cyclin A2 and Survivin as proliferation and survival markers. β-actin levels as protein loading control for each gel. (B) Quantification of the immunoblot of MYC, MLX, MAX, Cyclin A2 and Survivin relative to β-actin levels. (C) mRNA levels of *MNT*, *MAX*, *MLX* and *MYC* relative to *RPS14* (housekeeping gene) and WT HAP1. Error bars correspond to S.E.M. from three independent experiments * *P* <0.05. (D) Proliferation assay of MNT KO and WT HAP1 cells: images of the cells dyed with cristal violet solution 1 and 4 days after seeding. The quantification of two independent experiments is shown on the right, error bars correspond to S.E.M. and * *P* <0.1.

4.4.2. *MNT* knockout causes several changes at the transcriptional level

Next, we carried out a RNA-seq of MNT KO *versus* WT HAP1 cells. For this, we extracted RNA in triplicates (for each one, cells harvested and RNA extracted independently in three different days) and sequenced it using the Illumina platform. Then, three softwares (Cufflinks, DESeq2 and RNA eXpress) were used as described in the Materials and Methods' section of this Thesis work. By comparing the two conditions, we were able to observe the changes in the pattern of gene expression, as shown in the heatmap of **Figure 4.30 A**. Then, we represented the $\log_2$ fold changes attributable to a given variable over the mean of normalized counts for all the samples, what is named a MA-plot (**Figure 4.30 B**). This graph shows the non-significant changes in black dots and the significant ones in red (with a *P*-value <0.1). Points that fall out of the window are plotted as open triangles pointing either up or down. Next, we considered significant those genes that had a q-value <0.05 and a $0.7<\log_2$ ratio<-0.7. The Venn diagram of **Figure 4.30 C** shows the significant genes obtained with each of the softwares: 1173 with RNA eXpress, 950 with Cufflinks and 572 with DESeq2. From these, 460 genes were found significantly regulated in MNT KO *versus* WT by the three softwares (**Annex 2**). We selected 13 genes for further validation studies: *LIN28A*, *HECW2*, *MAPK10*, *MYB*, *NKX2-4*, *THBS1*, *WIPI1*, *SCARA3*, *GLIS3*, *RNF128*, *CHMP4C*, *FOXG1* and *BMP2* (**Figure 4.30 C**). By looking at the $\log_2$ ratio of these 460 genes, we classified them in up-regulated (49 %) and down-regulated (51 %) after *MNT* knockout. This result suggests that MNT could work as a transcriptional activator or a repressor at the same level in HAP1 cells (**Figure 4.30 D**).

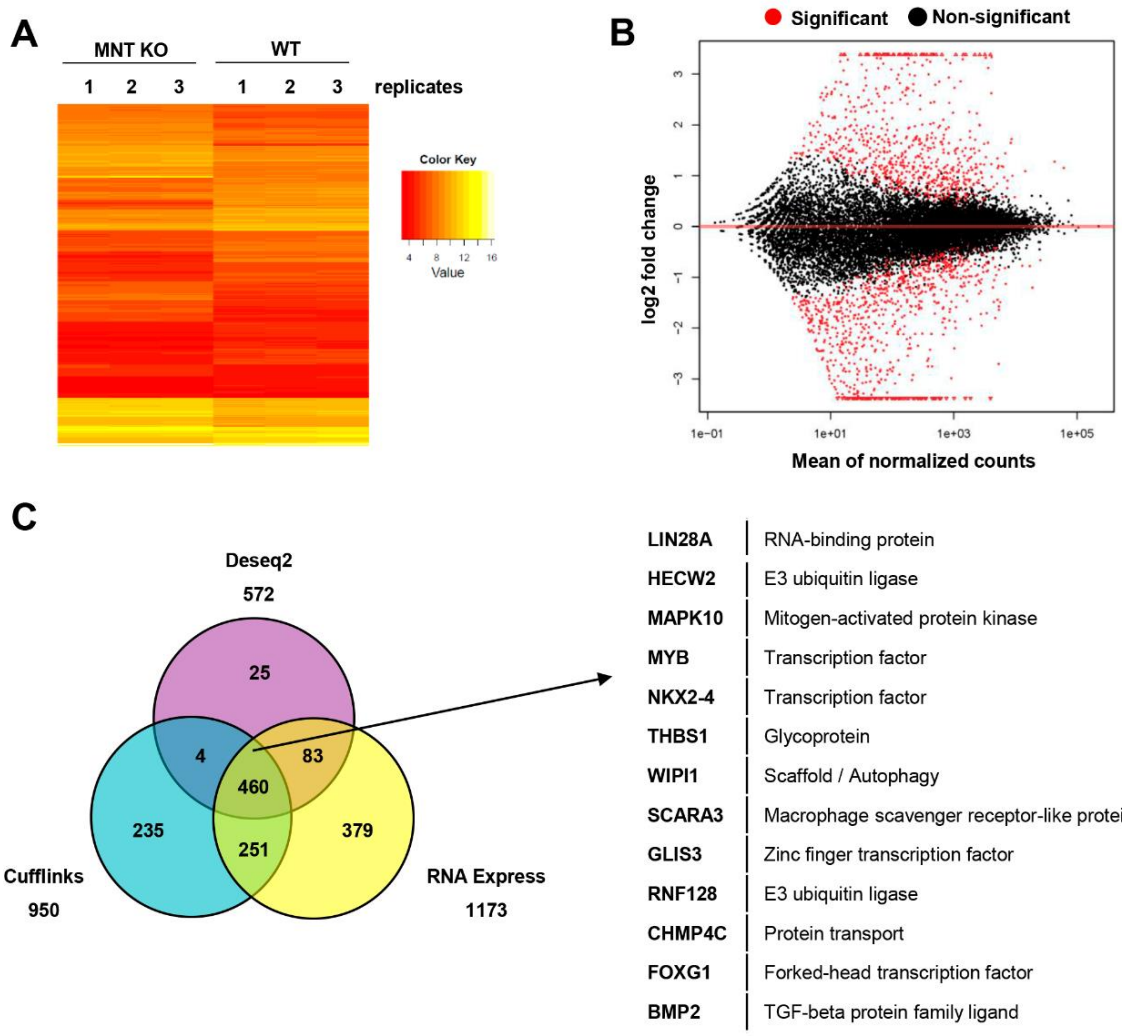

Figure 4.30. RNA-seq MNT KO *versus* WT HAP1 cells. (A) Heat map corresponding to the changes in expression for each of the three replicates of each condition (DESeq2). (B) MA-plot (DESeq2) showing log_2 fold changes attributable to a given variable over the mean of normalized counts for all the samples in the DESeqDataSet. Points in red if the adjusted p value is less than 0.1 (significant). Points which fall out of the window are plotted as open triangles pointing either up or down. (C) Venn diagram showing the number of genes deregulated in MNT KO vs. Control using three different analysis. The table shows the genes selected for validation. (D) Percentage of genes up- and downregulated upon MNT KO.

Following this, the list of differentially regulated genes upon *MNT* knockout were compared with the gene sets derived from the biological process gene ontology (based on MsigDB platform, http://software.broadinstitute.org/gsea/msigdb, (Liberzon et al., 2011). The resulting most enriched sets corresponded to

development, cell response to stimulus, cell differentiation, biological adhesion, cell proliferation and regulation of gene expression (**Table 4.3**)

Table 4.3. Gene Ontology of MNT-regulated genes. The genes showing expression changes in the MNT KO vs. WT HAP1 cells (**Annex 2**) were analyzed with the MsigDB platform (http://software.broadinstitute.org/gsea/msigdb). Ten of the most enriched pathways found in the analysis are represented in the table.

MNT KO *vs.* WT HAP1					
GO pathway	**Genes in set (K)**	**Genes in overlap (k)**	**k/K**	**p-value**	**FDR q-value**
Regulation of multicellular organismal development	1672	86	0.0514	1.84E-37	1.09E-33
Neurogenesis	1402	79	0.0563	4.38E-37	1.29E-33
Regulation of cell differentiation	1492	79	0.0529	3.31E-35	4.89E-32
Tissue development	1518	78	0.0514	7.23E-34	8.55E-31
Cellular response to organic substance	1848	82	0.0444	3.57E-31	3.52E-28
Response to external stimulus	1821	81	0.0445	7.39E-31	6.25E-28
Cell development	1426	72	0.0505	9.31E-31	6.89E-28
Biological adhesion	1032	62	0.0601	1.36E-30	8.94E-28
Regulation of cell proliferation	1496	70	0.0468	6.38E-28	3.78E-25
Positive regulation of gene expression	1733	71	0.0410	6.58E-25	2.43E-22

In order to go further in our biological analysis of the RNA-seq, we performed a GeneSet Enrichment Analysis (GSEA) (Subramanian et al., 2005) with the data obtained by Cufflinks. Different gene set databases were used for trying to figure out if the changes in gene expression caused by MNT KO correlated with an up-regulation or down-regulation of a certain pathway. The results with a nominal p-value <0.05 are shown in **Annex 3**. From these, some interesting pathways (mainly with a FDR q-value <0.25) are represented in **Figure 4.31**. Among them,

the genes characteristic of a downregulated response to UV, angiogenesis and TGFβ signaling were positively enriched in MNT KO cells *versus* WT. On the contrary, ion channel transport, tight junction interactions, IL6/JAK/STAT3 signaling, transport of vitamins, nucleosides and related molecules and the $T_{h1}T_{h2}$ pathway genes were negatively enriched in the MNT KO condition.

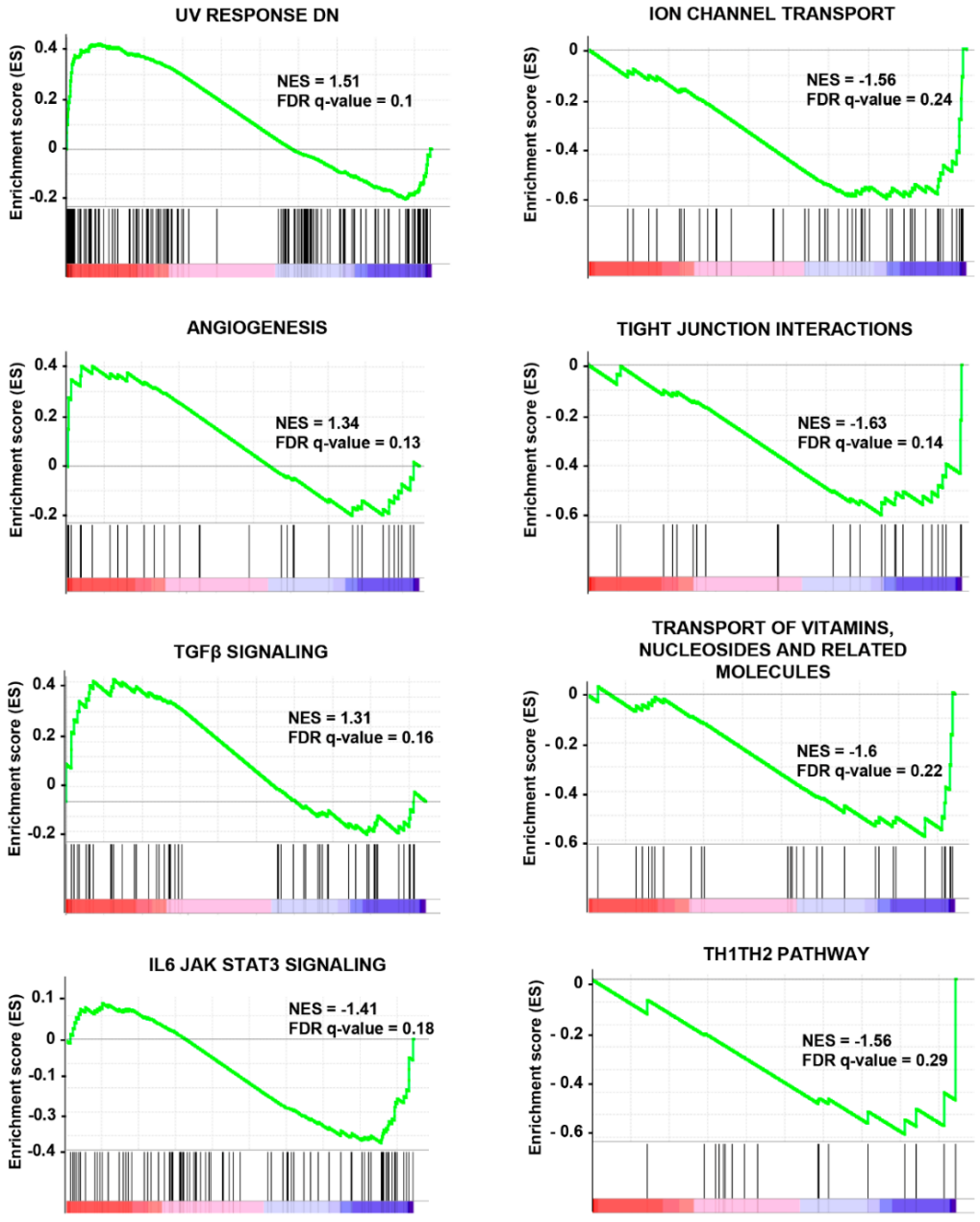

Figure 4.31. Gene Set Enrichment Analysis (GSEA) of the MNT KO *versus* the WT HAP1 transcriptome. These plots showing "UV response downregulated", "Ion channel transport", "Angiogenesis", "Tight Junction Interactions", "TGFβ Signaling", "Transport of vitamins, nucleosides and related molecules", "IL6 JAK STAT3 Signaling" and "TH1TH2 Pathway" pathways enriched in the genes regulated upon *MNT* knockout in HAP1 cells compared to the WT HAP1. Normalized Enriched Score (NES) and the False Discovery Rate (FDR) q-value are shown for each gene set.

Afterwards, *LIN28A*, *HECW2*, *MAPK10*, *MYB*, *NKX2-4*, *THBS1*, *WIPI1*, *SCARA3*, *GLIS3*, *RNF128*, *CHMP4C*, *FOXG1* and *BMP2,* which showed a severe change upon *MNT* knockout and were interesting genes for us, were used for validating the RNA-seq. First, we extracted new RNA from MNT KO and WT HAP1 cells in triplicates and checked the expression of these thirteen genes by RT-qPCR. **Figure 4.32** shows the mean of the log_2 ratio obtained in the three softwares of each of these genes (upper panel) and the mRNA relative levels obtained with new samples by RT-qPCR (lower panel). Since the results from the two analysis were similar, we were able to confirm the data obtained by RNA-seq.

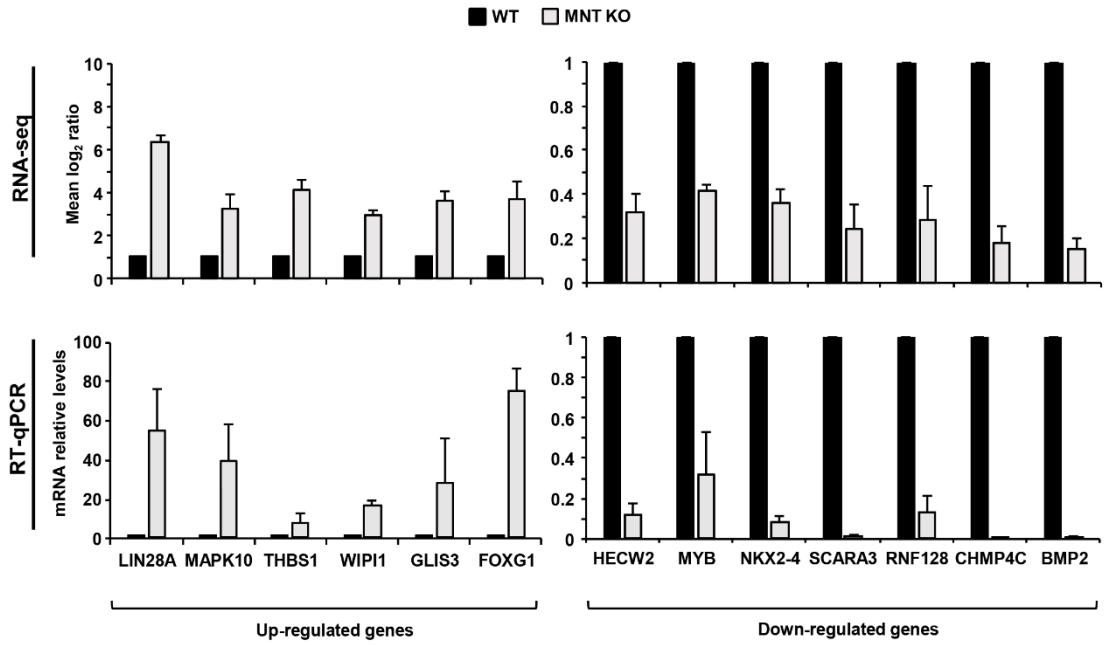

Figure 4.32. RNA-seq validation. Upper panel: mean of the log_2 ratio results obtained from the analysis of the RNAseq with Cufflinks, DESeq2, RNAeXpress comparing the FPKMs of MNT KO and WT HAP1. Lower panel: validated genes by RT-qPCR (three independent RNA preparations), relative to RPS14. Error bars correspond to S.E.M. from three independent experiments.

4.4.3. MAX and MLX regulate some of the MNT target genes

As MNT is described to form homodimers (this Thesis, section **4.2.2**) or heterodimers with MAX and MLX (Cairo et al., 2001; Hurlin et al., 1997; Meroni et al., 2000, 1997), we wondered if the mRNA levels of these selected genes

changed upon *MAX* or *MLX* knockdown. In order to answer this question, we produced lentiviral particles containing two different short-hairpin RNAs (shRNAs) for human *MAX* and *MLX* or a scrambled shRNA (scrRNA), as a control. Firstly, MNT KO and WT HAP1 cells were infected with lentivirus carrying the shRNAs against *MAX* and 72 h after infection, protein and RNA were purified and analyzed. **Figure 4.33 A** shows the protein levels of MNT and MAX by immunoblot. MAX levels were diminished around 80 %, which confirmed the efficiency of our shRNAs. Then, mRNA expression from WT HAP1 cells was checked by RT-qPCR and also confirmed the decrease in *MAX*. On the contrary, *MNT* levels increased in the shMAX condition, which agrees with previous results from our group (Lafita-Navarro, PhD Dissertation 2015). Then, the selected genes were classified depending if their levels were not affected by *MAX* knockdown (*LIN28A*, *FOXG1*, *NKX2-4*, *SCARA3*) (**Figure 4.33 B**), up-regulated (*MAPK10*, *GLIS3*, *HECW2*, *RNF128*) or down-regulated (*THBS1*, *WIPI1*, *MYB*, *CHMP4C*, *BMP2*) (**Figure 4.33 C**). As *MAPK10*, *GLIS3*, *MYB*, *CHMP4C*, *BMP2* changed with the shMAX in the same direction as with the *MNT* KO, we decided then to check the mRNA levels of these genes in MNT KO HAP1 cells shMAX *versus* scrRNA. Interestingly, the results showed that *MYB*, *CHMP4C* and *BMP2* were not further affected by *MAX* knockdown, comparing MNT KO + shMAX with MNT KO + scrRNA (**Figure 4.33 D**). These data suggest that *MYB*, *CHMP4C* and *BMP2* could be regulated by MNT-MAX dimers, as deleting MNT, MAX or both triggers the same effect.

Secondly, we followed the same procedure for figuring out if MLX was involved in the regulation of gene expression together with MNT. *MLX* knockdown was confirmed by immunoblot and an efficiency of 80-90 % was achieved (**Figure 4.34 A**). In this case, MNT protein levels decreased upon *MLX* knockdown but not *MNT* mRNA levels (**Figure 4.34 A and B**). Next, the selected genes were classified depending if their levels were not affected (*FOXG1*, *HECW2*, *NKX2-4*), up-regulated (*LIN28A*, *MAPK10*, *GLIS3*, *THBS1*) or down-regulated (*WIPI1*, *MYB*, *SCARA3*, *RNF128*, *CHMP4C*, *BMP2*) upon *MLX* knockdown. Among them, *LIN28A*, *MAPK10*, *GLIS3*, *THBS1, MYB*, *SCARA3*, *RNF128*, *CHMP4C* and *BMP2* were deregulated in the same direction as *MNT* knockout. Then, we knocked down *MLX* in MNT KO HAP1 cells too and analyzed the expression of

these genes. The results showed that *MAPK10*, *GLIS3* and *THBS1* were up-regulated and *SCARA3*, *RNF128*, *CHMP4C* and *BMP2* down-regulated, whether we delete *MNT*, *MLX* or both. We concluded then that these three genes could be regulated by MNT-MLX dimers.

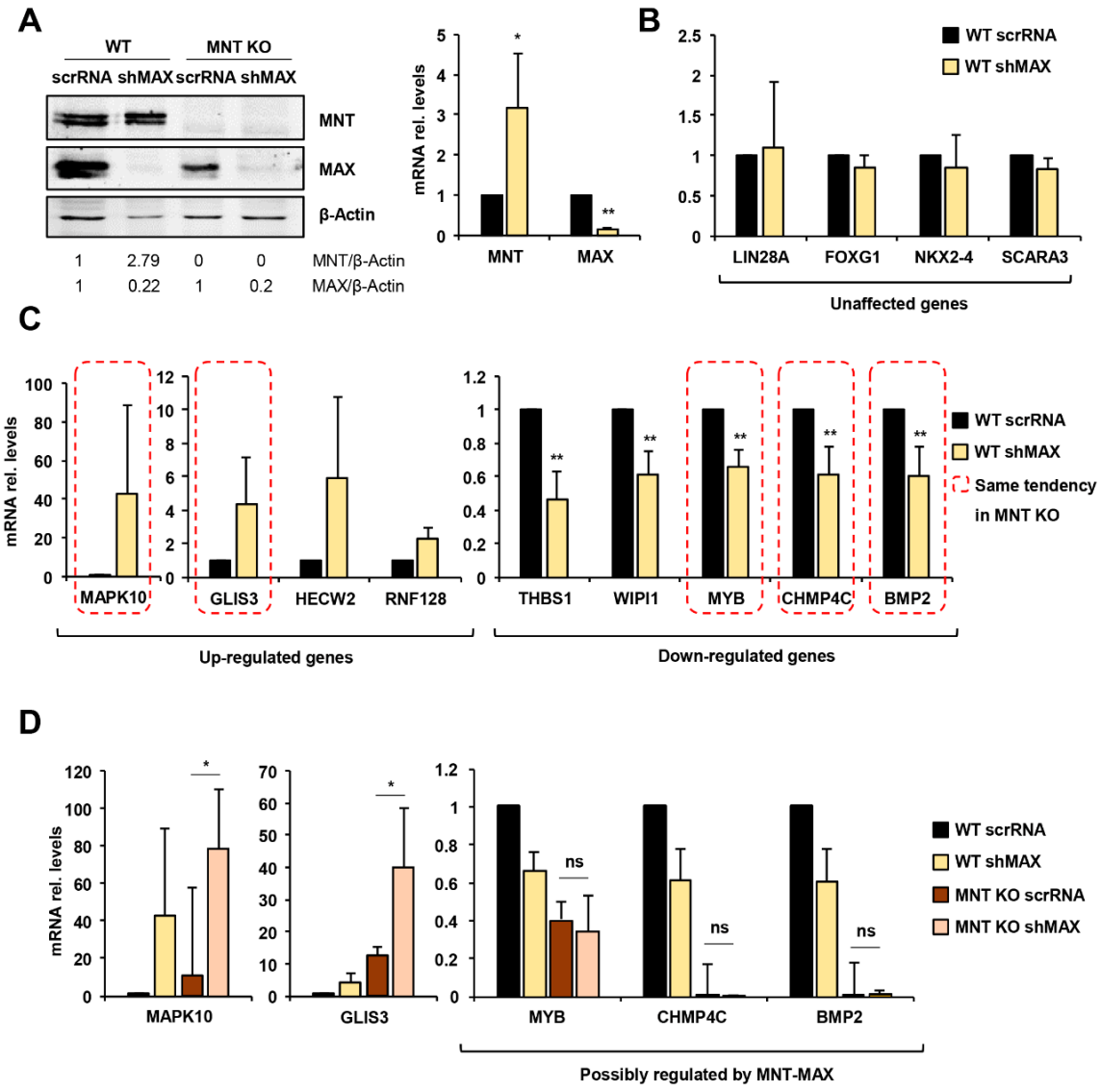

Figure 4.33. MAX role in the regulation of gene expression. (A) *MAX* knockdown analysis in MNT KO and WT cells by immunoblot and RT-qPCR. (B) RT-qPCR results of the genes that were not affected upon *MAX* knockdown in WT HAP1 shMAX vs. shScramble (scrRNA). (C) RT-qPCR results of the genes up- or down-regulated upon *MAX* knockdown in WT scrRNA. (D) RT-qPCR results of the knockdown of *MAX* in WT and MNT KO HAP1 cells. All protein and RNA extracts were obtained 72 h after infection with lentivirus carrying shMAX constructs or shScramble (scrRNA). Error bars from S.EM. of three independent experiments. * *P* <0.05; ** *P* <0.01; ns: non-significative.

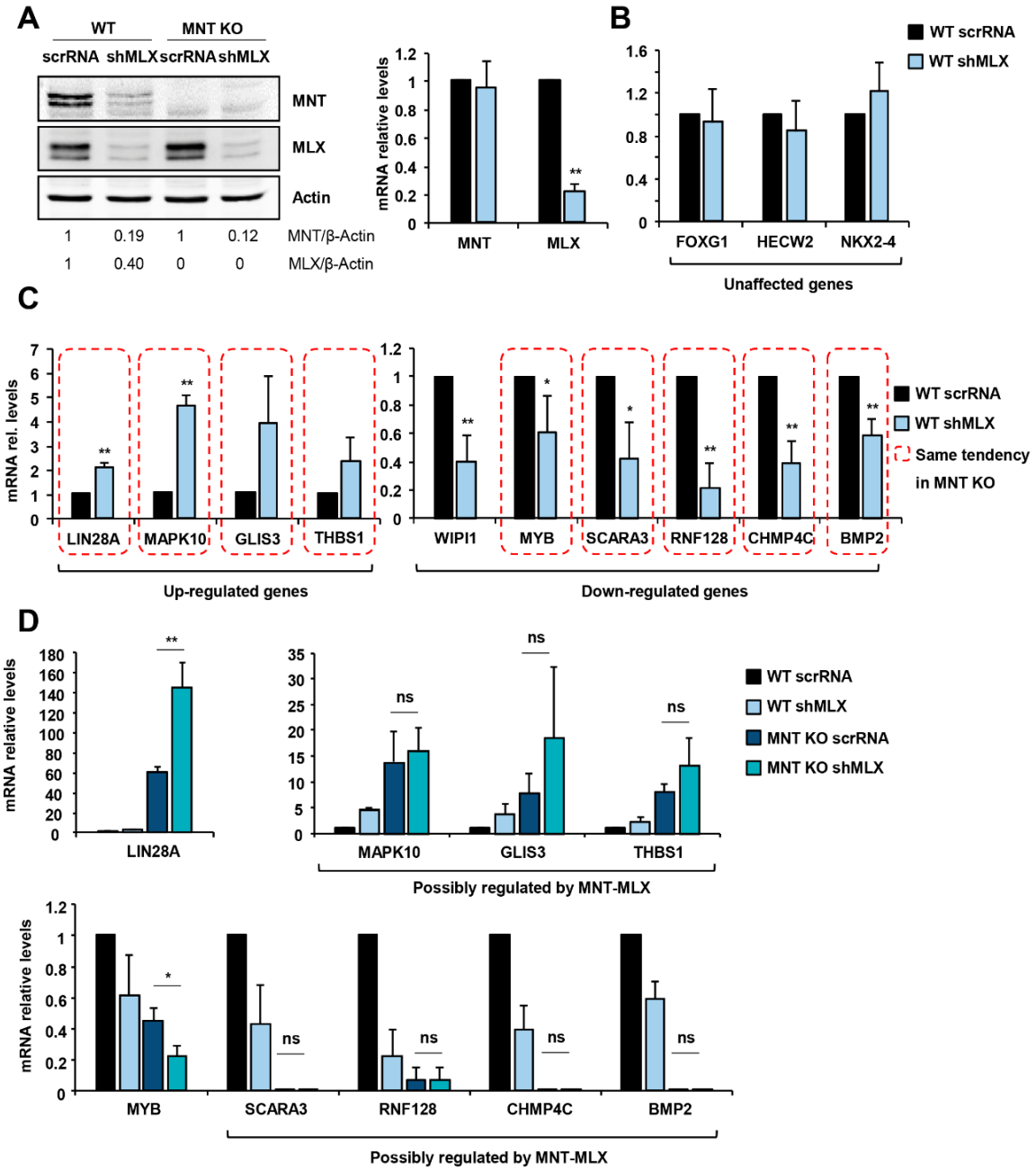

Figure 4.34. MLX role in the regulation of gene expression. (A) *MLX* knockdown analysis in MNT KO and WT cells by immunoblot and RT-qPCR. (B) RT-qPCR results of the genes that were not affected upon *MLX* knockdown in WT HAP1 shMLX vs. shScramble (scrRNA). (C) RT-qPCR results of the genes up- or down-regulated upon *MLX* knockdown in WT scrRNA. (D) RT-qPCR results of the knockdown of *MLX* in WT and MNT KO HAP1 cells. Protein and RNA extracts 72 h after infection with lentivirus carrying shMLX constructs or shScramble (scrRNA). Error bars from S.EM. of three independent experiments. * *P* <0.05; ** *P* <0.01; ns: non-significative.

A summary of the obtained results is presented in **Figure 4.35**. However, as both *MAX* and *MLX* knockdowns affected MNT levels, the conclusions of these experiments should be read with caution.

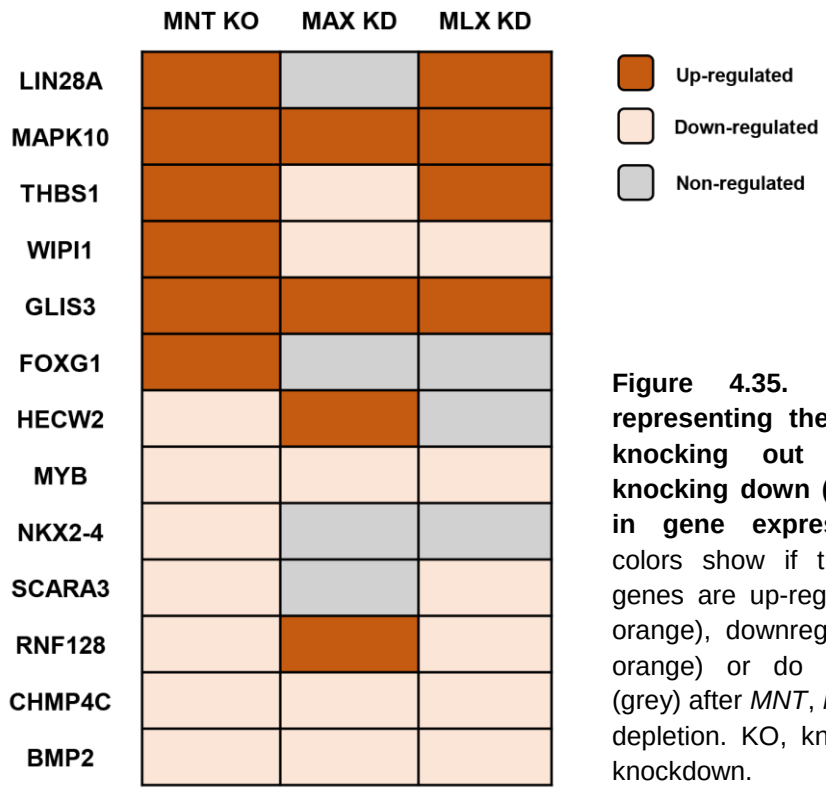

Figure 4.35. Heat map representing the results of knocking out (*MNT*) or knocking down (*MAX*, *MLX*) in gene expression. The colors show if the selected genes are up-regulated (dark orange), downregulated (light orange) or do not change (grey) after *MNT*, *MAX* or *MLX* depletion. KO, knockout; KD, knockdown.

4.4.4. MNT new direct target genes

After analyzing the changes in gene transcription produced by *MNT* knockout, we wondered if MNT was binding directly to any of these genes. For this we used the ENCODE project and analyzed the binding of MNT, MAX and MYC to the genes selected for validation. It is noteworthy that the ChIP-seqs published in this platform were performed in K562, which are chronic myeloid leukemia cells, as the HAP1 cells.

The data of the ChIP-seq showed that MNT binds to *LIN28A*, *WIPI1*, *FOXG1*, *CHMP4C*, *HECW2* and *MYB* genes (**Figure 4.36**). The peaks are detected in the near promoter (maximum -2 kb from TSS) or in the first intron of the gene. The only exception is *HECW2*, which has a peak of MNT binding around -5 kb from TSS. In the case of MYC and MAX, they can also be found bound to these genes, with the exception of MAX in *HECW2*. MNT, MYC and MAX were bound to these genes in the same regions in most of the times, suggesting a possible antagonistic regulation between MNT-MAX/MNT-MNT and MYC-MAX. However,

as there is not any available ChIP-seq of MLX in K562, further research needs to be done in order to figure out if MNT truly regulates these genes in a direct way and whether it is as a homodimer or as a heterodimer with MAX or MLX.

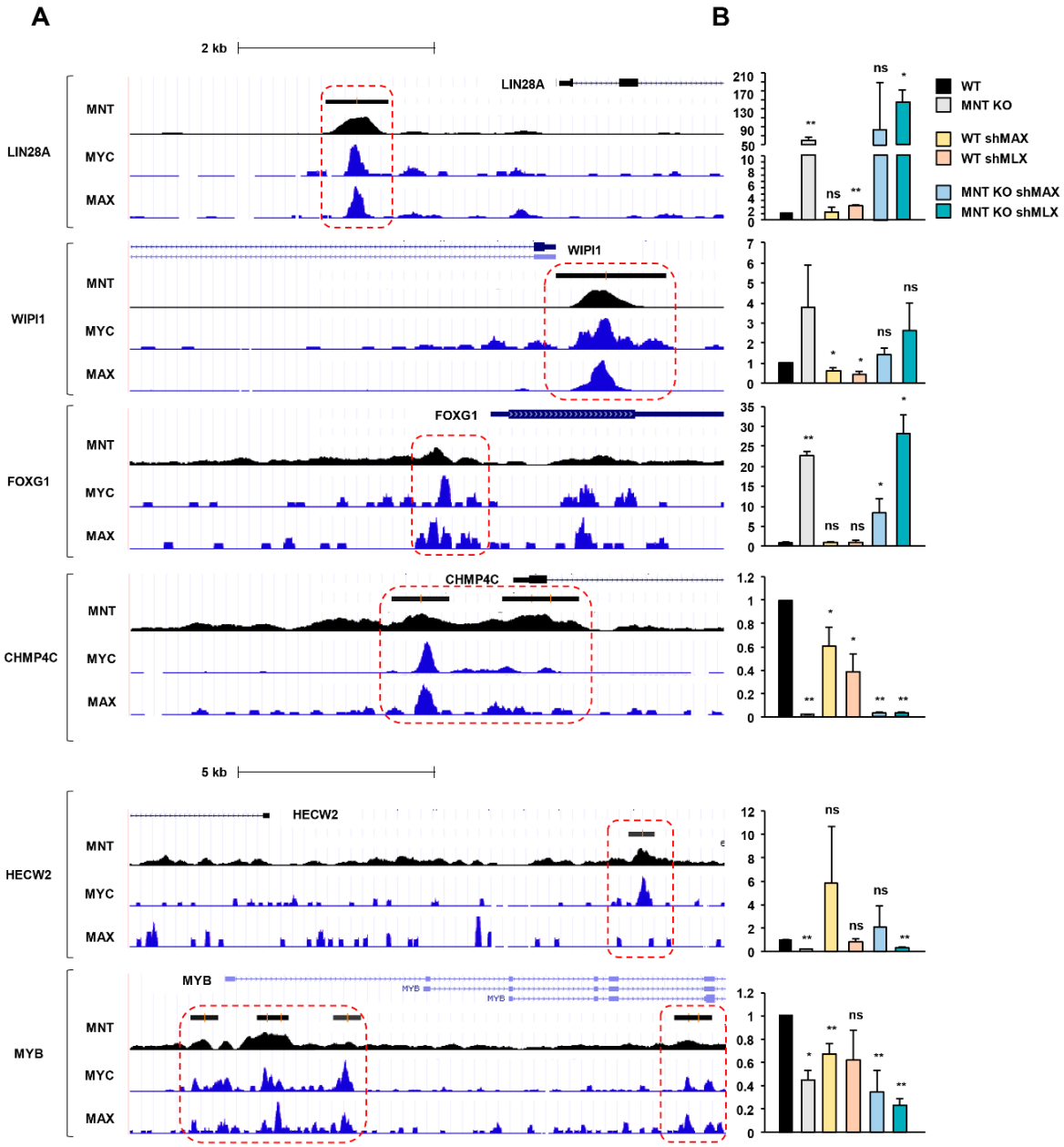

Figure 4.36. MNT, MYC and MAX binding to the RNA-seq selected genes. (A) Schematic representation of human *LIN28A*, *WIPI1*, *FOXG1*, *CHMP4C*, *HECW2*, *MYB* promoters showing the peaks for MNT, MYC and MAX in human K562 cell line as published by the ENCODE project. (B) mRNA levels of each gene upon MNT KO and MAX or MLX depletion. Error bars from S.EM. of three independent experiments. * *P* <0.05; ** *P* <0.01; ns: non-significative.

The working hypothesis based on the data presented in this work is shematized in **Figure 4.37**. The genes are clasified first according to their activation/repression by MNT, second depending if they can be regulated by MNT-MAX or MNT-MLX and third, whether they show a peak of MNT binding in the ENCODE project. Thus, MNT-MAX would activate directly *MYB and CHMP4C*; MNT-MLX, *CHMP4C* and MNT homodimers would regulate directly *HECW2* (activation) and *LIN28A*, *WIPI1* and *FOXG1* (repression).

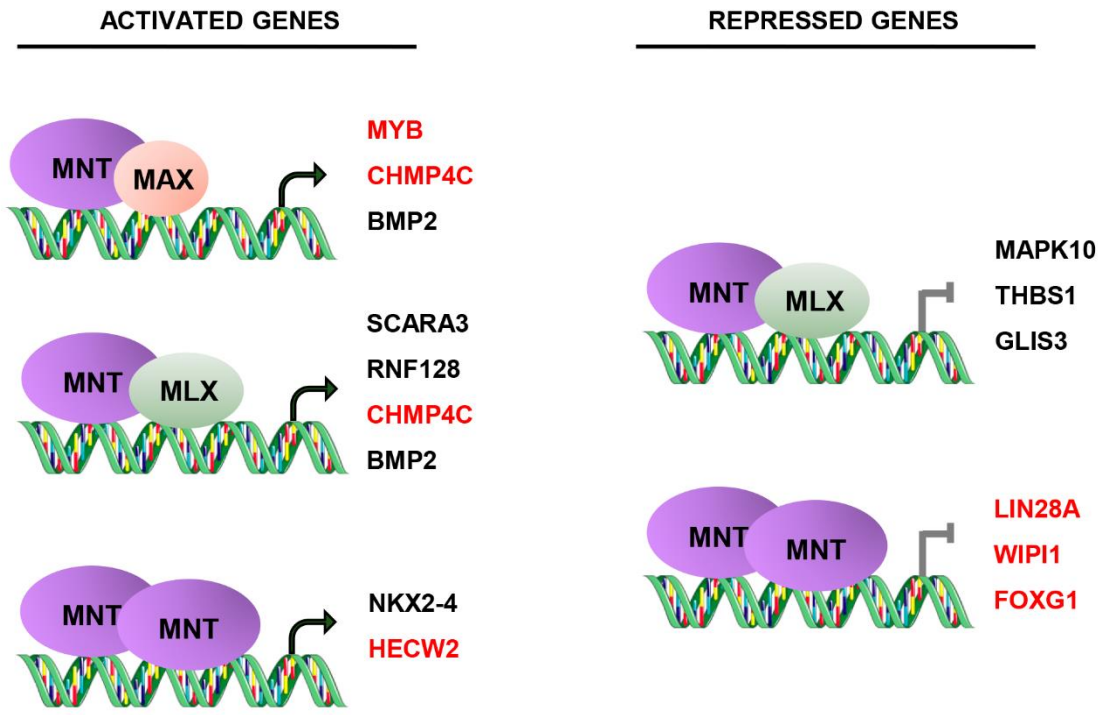

Figure 4.37. Working hypothesis of MNT gene regulation. The scheme represents the possible regulation of the genes selected for validating the RNA-seq of HAP1 cells. In red, the genes possibly regulated directly by MNT-MAX, MNT-MLX or MNT-MNT, based on the ENCODE ChIP-seq results.

Discussion

5. Discussion

5.1. MNT as a regulator of the NF-κB pathway

In the first part of this Thesis, we report several novel findings that place MNT in the regulation of one of the most important signaling pathways for the cell: the NF-κB pathway. First, MNT and REL interact in some mouse, rat and human cell lines, and this complex can be found in both cytoplasm and nucleus. Second, *MNT* knockdown triggers REL translocation into the nucleus, the activation of NF-κB pathway and the increase in two REL-target proteins: IκBα and BCL-XL. Meanwhile, *MNT* overexpression provokes a repression in NF-κB pathway and in the mRNA levels of *NFKBIA* (IκBα) and *BCL2L1* (BCL-XL). Third, MNT and REL bind to *NFKBIA* gene, having a maximum binding at a region mapping +171/+343 from the TSS. These results widen our knowledge of MNT beyond MAX interaction and provide a new connection between the MYC and the NF-κB oncogenic pathways.

5.1.1. MNT and REL protein levels vary among cell lines

As REL was found bound to MNT in the proteomic analysis of MNT immunoprecipitates, both in MAX-deficient (URMT) and MAX-expressing (URMax34) cells (Lafita-Navarro, PhD Dissertation 2015), we decided first to analyze REL and MNT mutations in cancer, together with their mRNA and protein levels in different cell lines.

First, the TCGA data mostly showed mutual exclusivity between MNT and REL mutations in human cancer. It seems likely that MNT and REL play a role in the same pathway and that mutations in the two of them do not increase the fitness of tumors. This mutual exclusivity in the presence of mutations is also observed, for instance, between *MYC* and the oncogenic drivers *PTEN*, *BRAF*, *PIK3CA* and *APC* (Schaub et al., 2018).

Afterwards, we chose some cells derived from leukemias and lymphomas, as REL is described to have an important role in these malignancies (Hunter et al., 2016). We also used one from colon adenocarcinoma (LoVo) and another one from small cell lung cancer (Lu165), which is MAX-deficient (Romero et al., 2014). Thus, mRNA levels of *MNT*, *REL*, *RELA* (p65), *NFKBI* (p105/p50) and *NFKBIA* (IκBα) were observed to vary among the tested cell lines although we did not find a clear correlation between them. Regarding protein levels, MNT was detected in all the analyzed cell lines, which agrees with the ubiquitously of its expression already described, both in differentiated and proliferating cells (Hurlin et al., 2003). MNT is detected as a 75 kDa's doublet and the upper band corresponds to a MNT phosphorylated form (Popov et al., 2005). REL protein levels were highest in Burkitt's lymphoma cell lines, which is in accordance with the REL amplifications that are commonly found in this malignance (Gilmore and Gerondakis, 2011). The inverse correlation observed between MNT and REL in most of the cell lines suggests a crosstalk between these two proteins.

5.1.2. MNT and REL interact in different cell lines

After studying a diverse panel of cell lines, MNT and REL interaction was confirmed in rat U7 (UR61's parental cell line), URMT, URMax34 and C6, mouse Neuro-2a and human LoVo and CEM cells by co-immunoprecipitation assays. This interaction is independent of MAX, as it takes place in both MAX-deficient and MAX-expressing cell lines. In fact, REL was not found in MAX immunoprecipitates, suggesting that REL does not form a complex with MNT-MAX heterodimers but only with MNT. MNT and REL interaction was also confirmed by proximity ligation assays in LoVo (untransfected) and C6 (MNT and REL overexpressed) cells. The fact that we did not detect MNT-REL interaction in other cell lines may indicate that the interaction is weak and possibly dependent on certain characteristics of the cell. It is also conceivable that an auxiliary protein not detected in our proteomic studies is required for the interaction, which expression may vary among cell types. Moreover, this interaction seems not to be so strong in human cell lines. This could be due to the amino acid difference between mouse and human REL (Gilmore et al., 2001), that could make a difference in the binding, or to the presence of an auxiliary protein in humans, as a bridge between MNT and REL. If this were true,

it would affect the efficiency of the co-immunoprecipitation and the proximity ligation assays, leading to a difficult detection of MNT and REL interaction.

REL is described to form homodimers or heterodimers with two members of the NF-κB pathway: p65 or p50 (Gilmore and Gerondakis, 2011). However, we did not detect either p65 or p50 bound to MNT, not even when we overexpressed MNT in LoVo cells. As a complementary approach, we immunoprecipitated p65 and p50 and found REL, as expected, but not MNT bound to them. Thus, these results indicate that MNT binds specifically to REL. Whether REL is in homodimers or bound to other unknown protein(s) inside the complex, remains unknown.

Afterwards, we were interested in the subcellular localization of the interaction, as it could give us a clue of the functional role of MNT-REL complex. NF-κB proteins are in the cytoplasm under basal conditions, bound to the IκBs, which hide their nuclear localization signal. The reception of a stimulatory signal (like TNFα) triggers the IκB degradation and the translocation of NF-κB dimers to the nucleus (Gilmore, 2006; Hayden and Ghosh, 2008; Kanarek et al., 2010; Naugler and Karin, 2008). Taking this into account, we carried out a fractionation lysis into cytoplasm and nucleus in C6 cells, both in basal and after TNFα stimulation. As expected, REL was cytoplasmic in basal conditions and part of it translocated into the nucleus extracts after TNFα treatment (Pimentel-Muiños et al., 1995), while MNT was localized mainly in the nucleus in both conditions (Hurlin, Quéva and Eisenman, 1997). Interestingly, REL was found bound to MNT in cytoplasmic extracts in basal conditions, even if the amount of MNT in cytoplasm was minimum. Upon NF-κB signaling activation, REL was detected in both nuclear and cytoplasmic MNT immunoprecipitates. These results offer unprecedented evidence for a possible function of MNT-REL complex in the nucleus (possibly as a transcriptional regulator complex) and in the cytoplasm (likely as a retention mechanism of REL dimers in the cytoplasm under basal conditions).

Finally, we were curious about the domain of MNT that is involved in the interaction with REL. For this reason, we transfected C6 cells with a REL expression vector and different MNT deletion constructs. Interestingly, the co-IP of REL was detected with all MNT constructs except the ΔCt_1 MNT-HA mutant. This construct lacks the C-terminal region of MNT but retains the bHLHLZ domain. As described by Meroni

et al., (1997), the C-terminal region of MNT is rich in prolines, which normally have a structural role and more probabilities to be involved in protein-protein interactions (**Figure 5.1**) (Kay et al., 2000). This agrees with the result showing that REL is found in MNT immunoprecipitates when using an antibody recognizing the first 50 amino acids of MNT but not when using an antibody recognizing the C-terminal domain of MNT. The binding of the antibody to this region may disrupt the interaction, thus affecting the final result.

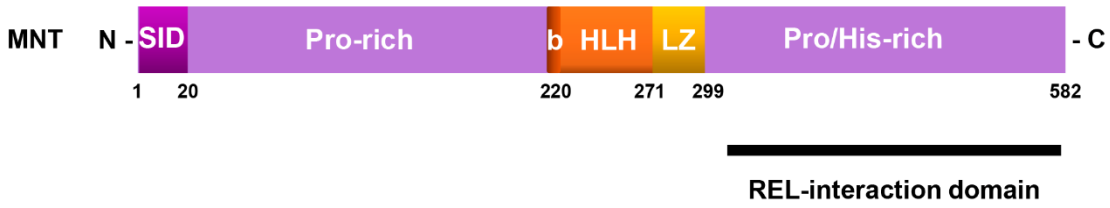

Figure 5.1. MNT interacts with REL through the C-terminal region. The C-terminal region characterized by being proline and histidine rich is necessary for MNT-REL interaction. SID, SIN3 Interaction Domain; Pro, proline and His, histidine; bHLHLZ, basic helix-loop-helix leucine zipper.

5.1.3. MNT levels affect the NF-κB pathway

Once MNT-REL interaction was confirmed, we chose LoVo for further studies as they are adherent, easily-transfectable cells and one of the human cell lines where we found MNT-REL interaction.

First, we knocked down *MNT* and observed a surprising change in REL subcellular distribution by immunofluorescence assays. REL accumulated in the nucleus, excluding the nucleolus. This localization is commonly observed when NF-κB pathway is active (Kaltschmidt et al., 2018). This change in the subcellular localization after *MNT* knockdown was not observed for p65, suggesting that the change in REL was a consequence of the MNT specific interaction with REL.

Second, we knocked down *MNT* and analyzed the activity of two luciferase constructs. One of them included an artificial promoter containing five κB-binding sites and the other one the *NFKBIA* (IκBα) promoter. The latter is a *bona fide* NF-

κB target gene (Iwai et al., 2005; Kaltschmidt et al., 2018). Interestingly, *MNT* knockdown provoked an increase in the luciferase activity of both constructs, which is in accordance with previous results in our laboratory, in UR61 and HeLa cells (Lafita-Navarro, PhD Dissertation 2015). We also overexpressed *MNT* and observed a repression of the constructs, although the result was not as clear as with the knockdown strategy. As MNT is already expressed at significant levels in the cells under assay, the result can be explained by the fact that endogenous MNT is enough to control NF-κB activity.

Third, we analyzed the effect of MNT on the mRNA levels of two REL-target genes (*NFKBIA* and *BCL2L1*, which encode for IκBα and BCL-XL, respectively) and a non REL-target gene (*NFKBI*, which encodes for p105/p50) (Chen et al., 2000; Iwai et al., 2005). Their expression was reduced upon *MNT* overexpression. Then, we induced the NF-κB pathway with TNFα in order to see if the repression carried out by MNT was still taking place and we found that the repressive effect of MNT was abolished after TNFα treatment. This is possibly due to the strong activation of the NF-κB signaling triggered by TNFα that cannot be counteracted by MNT. It can be assumed then that MNT's role in NF-κB pathway is not dominant under strong stimulatory signals. Thus, MNT might be acting as a limiter of NF-κB activity in the absence of the specific activators of the pathway. Forth, we checked REL, IκBα and BCL-XL protein levels after *MNT* knockdown. In accordance to the mRNA data, we observed the increase in both IκBα and BCL-XL after *MNT* depletion. On the one hand, REL protein levels decreased. This could be due to a possible degradation induced by the disruption of MNT-REL complexes and the consequent destabilization of REL. On the other hand, the increase in IκBα and BCL-XL would be due to the abolishment of MNT retention of REL dimers, which are able to translocate into the nucleus and activate their target genes. This hypothesis is schematized in **Figure 5.2**.

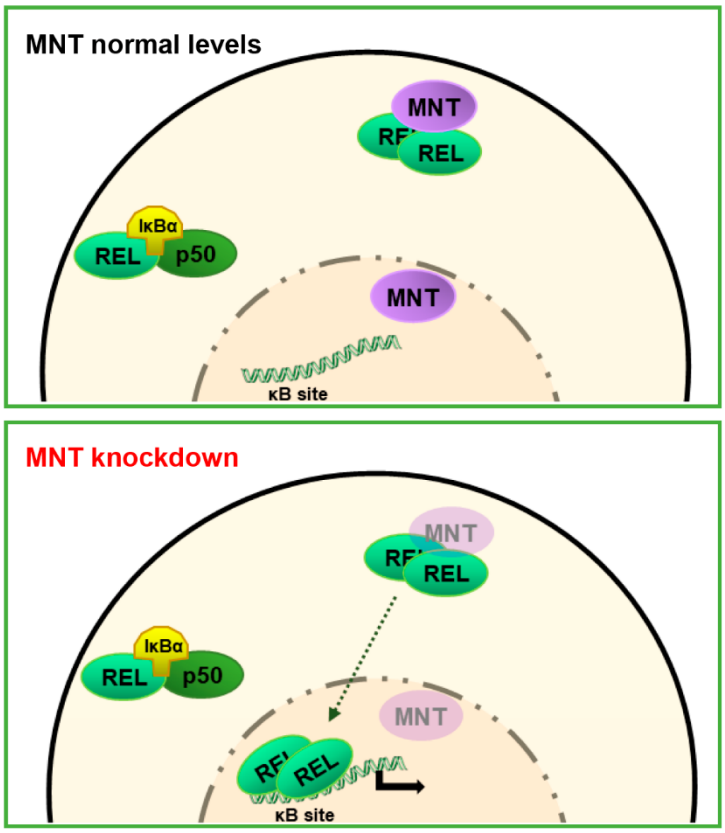

Figure 5.2. MNT affects REL function. When MNT levels are not altered, REL dimers would be sequestered in the cytoplasm by IκBα and MNT (upper panel). However, when *MNT* levels are knocked down, some of the REL dimers translocate into the nucleus, bind to κB target sequences and activate the transcription of REL-target genes, such as *NFKBIA* and *BCL2L1*.

5.1.4. *NFKBIA* (IκBα) is a MNT direct target gene

The results obtained in this work pointed to the possibility of MNT being a repressor of the NF-κB and, possibly, of IκBα. IκBα is one of the inhibitor members of the NF-κB family, which binds to the NF-κB members under the absence of stimulatory signals (Gilmore, 2006). Once a stimulus is detected by the cell, the NF-κB pathway is activated and IκBα degraded. However, NF-κB also induces a negative feedback loop that leads to the transcription of *NFKBIA* (IκBα). The newly synthesized IκBα enters the nucleus and shuttles NF-κB dimers back to the cytoplasm to terminate transcription (Hayden and Ghosh, 2008; Kanarek et al., 2010; Naugler and Karin, 2008; Sun et al., 1993). If the stimulus is constant, NF-κB DNA-binding activity appears and disappears every 30-60 min and it is accompanied by the degradation and resynthesis of IκBα. This is the reason why analyzing IκBα levels is a good method to study the transcriptional activity of NF-κB (Bottero et al., 2003).

The ENCODE project data showed MNT binding to *NFKBIA* in a K562 cells ChIP-seq (genome.ucsc.edu). As MNT is described to be a transcriptional repressor through its binding to SIN3, we also decided to check the binding of SIN3A and SIN3B (Hurlin, Quéva and Eisenman, 1997). The results showed that indeed SIN3A and SIN3B also bind to *NFKBIA* (in this case the available data was in GM78 and H1ES cell lines, respectively), suggesting that the effects observed in *NFKBIA* (IκBα) could be due to a direct regulation by a MNT-SIN3 complex. MYC and MAX also bind to *NFKBIA* gene in the same regions, implying a possible antagonism between MNT-MAX and MYC-MAX (Yang and Hurlin, 2017). ChIP assays confirmed the binding of MNT and REL to *NFKBIA* gene in LoVo cells, which had a coincident maximum peak at +171/+343. This advocates to a possible regulation of this gene by a MNT-REL complex. The fact that MNT can bind and repress *NFKBIA,* possibly through its interaction with REL, opens a new level of regulation of the NF-κB pathway. MNT may form a repressive complex with REL and repress genes that are normally activated by REL (model schematized in **Figure 5.3**).

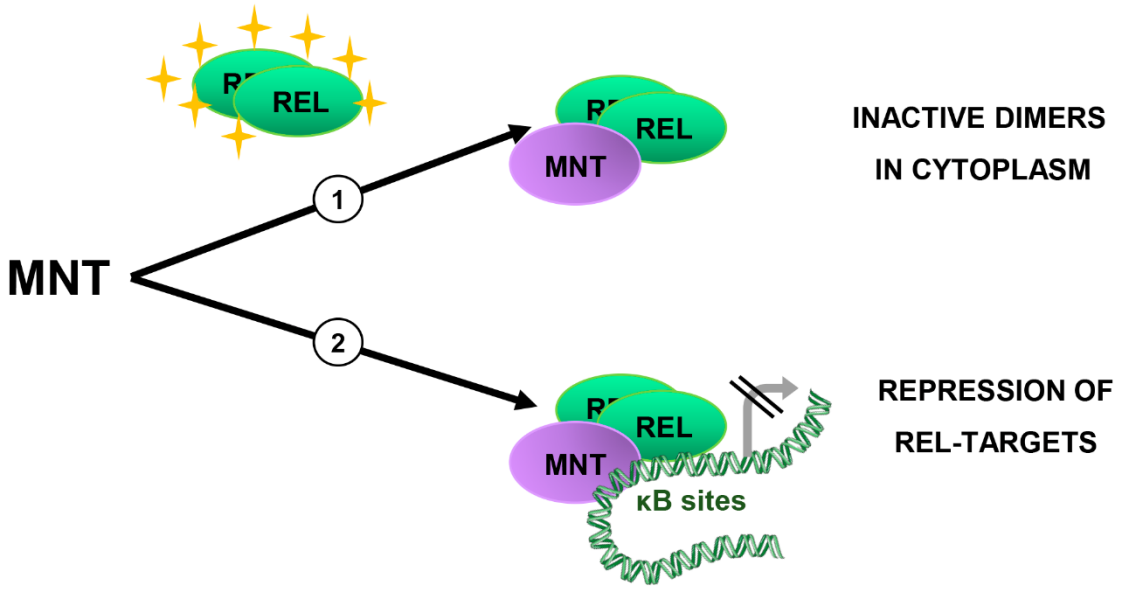

Figure 5.3. Model of the MNT regulation of NF-κB signaling. Our results indicate that MNT would be regulating NF-κB signaling by retaining REL dimers in the cytoplasm (function 1) and by forming a complex with REL in the nucleus that would repress the genes that are normally activated by REL dimers (function 2).

MNT pro-survival role has been extensively described but the exact mechanism responsible for that remains unknown (Campbell et al., 2017; Dezfouli et al., 2006; Hurlin et al., 2003; Link et al., 2012). Here we describe the novel connection between MNT and the NF-κB pathway, which is also key in regulating cell homeostasis. In some settings, REL can induce apoptosis and affect cell proliferation (Bash et al., 1997; Chen et al., 2003). It can therefore be assumed that blocking REL function, first by retaining it in the cytoplasm and second by the repression of REL-target genes, would be a way for MNT to control NF-κB, reduce apoptosis and maintain cell proliferation. Moreover, it has been described that NF-κB proteins, including REL, induce MYC expression by direct binding to *MYC* gene (Gupta et al., 2018; Kaltschmidt et al., 2018; Slotta et al., 2017). Considering the MYC-MNT antagonism, it would be possible that MNT could control MYC levels through the inhibition of REL functions. Furthermore, loss of *MNT* in T-cells leads to a disruption of T-cell development and a polarized differentiation of CD4+ T-cells into T_{h1} cells (Dezfouli et al., 2006). As REL is also important for T_{h1} cell differentiation, it would be possible that the consequences of MNT on the immune system are related to its interaction with REL (Dezfouli et al., 2006; Link et al., 2012; Pai and Ho, 2002; Visekruna et al., 2012).

In summary, MNT-REL interaction opens a new path to the understanding of MNT wide functions in different cellular pathways and organ systems. Further research will definitely increase our knowledge about MNT and, consequently, about MYC biology in physiological and pathological conditions.

5.2. MNT functions beyond MAX interaction

This second part of the Thesis work had the objective of clarifying how MNT works in the absence of MAX. For this we chose the UR61 cellular model and studied MNT interactions and its transcriptional activity. First, the presented results show that MNT is able to form homodimers and heterodimers with MLX through the bHLH domain. Second, MNT and MLX are required for optimum proliferation even in the absence of MAX. Third, MNT is able to regulate gene expression in the absence of MAX by direct binding to the DNA. Finally, MNT levels are tightly

controlled inside the cell at the mRNA level (MNT negatively regulates its own promoter) and at the protein level (by proteasomal degradation).

MAX was originally defined as an obligate dimerization partner of MYC, MNT, MXD1-4 and MGA (Diolaiti et al., 2015). Despite this, work carried out in the PC12 model and in *Drosophila* indicates that MYC can also function in a MAX-independent manner (Steiger et al., 2008; Vaque et al., 2008). Regarding MNT, we have shown here that its depletion impairs cell proliferation and that it is able to regulate gene expression in MAX-deficient UR61 cells. To our knowledge this is the first report on a MAX-independent function of a MXD protein and it made us wonder how MNT was carrying out its functions.

5.2.1. MNT forms homodimers and heterodimers with MLX in the absence of MAX

We confirmed that MNT could be carrying its functions through MNT-MLX heterodimers and MNT homodimers in the absence of MAX. MNT has already been described to interact with MLX (Cairo et al., 2001; Meroni et al., 2000). However, MNT homodimerization has only been described by *in vitro* and yeast two-hybrid experiments (Hurlin et al., 1997; Meroni et al., 1997). Thus, our results are the first proof of MNT homodimerization in animal cells. Moreover, the fact that MAX induction provokes a decrease in the amount of MLX bound to MNT, together with a decrease in MNT homodimers, adds complexity to an already complex network. This suggests a possible competition between MAX and MLX and it represents the first evidence of a functional crosstalk between de two arms of the MYC proximal network (Carroll and Diolaiti, 2016; Diolaiti et al., 2015). Moreover, previous work in our laboratory demonstrates an increase in cytoplasmic MNT in MAX-depleted cells (Lafita-Navarro, PhD Dissertation 2015). As a relevant fraction of MLX is cytoplasmic, and MNT and MLX complexes are detected in both cytoplasm and nucleus, this interaction could explain the increase in cytosolic MNT in MAX-deficient cells. The model is depicted in **Figure 5.4**.

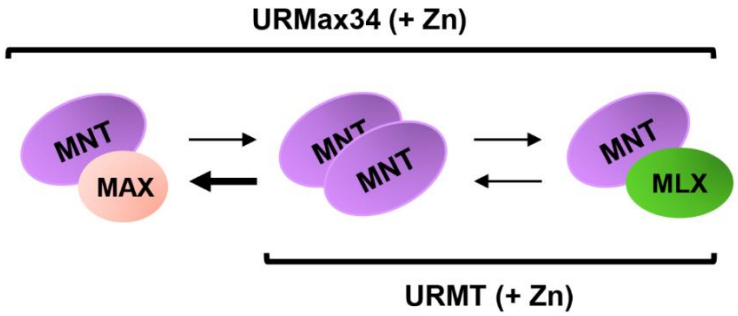

Figure 5.4. MNT forms homodimers and heterodimers in UR61 cells. MNT forms homodimers and heterodimers with MLX in URMT cells (MAX-deficient). However, upon MAX induction (URMax34 + Zn), the balance is displaced towards MNT-MAX dimers.

5.2.2. MNT regulates gene transcription in the absence of MAX

Based on the RNA-seq performed in UR61 cells, we selected some of the genes that significantly changed upon MNT depletion and that were not affected by MAX presence (Lafita-Navarro, PhD Dissertation 2015). By depleting *MNT* and *MLX* in UR61 cells we tried to figure out which genes could be regulated by MNT-MLX or MNT-MNT. In fact, co-depletion of *MLX* and *MNT* does not modify the effect of *MNT* depletion on genes as *CDKN1C/p57*, *BIRC5/Survivin*, *CDK1*, *E2F6*, *BRCA1*, *PARPBP*. Furthermore, ChIP-seq and ChIP-PCR analyses show that MNT binds to some genes in MAX-deficient cells that are regulated by MNT (*BIRC5/Survivin*, *CDK1*, *BRCA1*, *ERCC6*, *FBXO32*), supporting the possibility of a direct regulation by MNT homodimers. The genes that did not show a binding of MNT could be indirectly regulated by MNT (*CDKN1C*, *E2F6*). CDK1 is the only essential CDK protein for cell cycle progression in animal cells (Santamaría et al., 2007). In addition, BIRC5/Survivin is a critical protein for cell survival and mitosis (Altieri, 2015; Wheatley and Altieri, 2019) and we have also confirmed its regulation by MNT in URMT cells at the protein level. Thus, the MNT-dependent regulation of both genes helps to explain the anti-proliferative effect of *MNT* knockdown in MAX-deficient cells. Altogether, the data suggest that MNT can regulate transcription as a MNT-MNT homodimer or as a heterodimer with MLX or with another not yet identified protein. The analysis of bound regions in our ChIP-seq experiments also revealed the presence of sites for forkhead transcription factors (FOXP1, FOXA2, FOXO3) in agreement with the reported

coordinated regulation between MNT and FOXO of some cell cycle control genes (Terragni et al., 2011).

According to our results, MNT homodimers or MNT-MLX heterodimers would be regulating cell cycle and DNA repair checkpoint genes in a MAX-independent manner for correct survival and proliferation of the cells. The model based on these observations is presented in **Figure 5.5**.

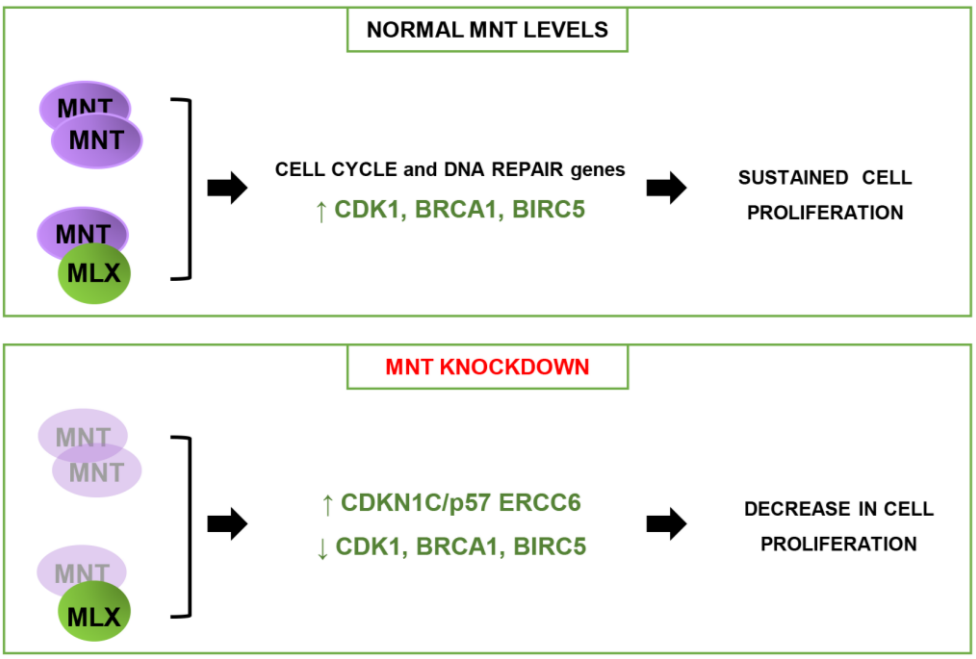

Figure 5.5. Model of the biological roles of MNT independent of MAX in UR61 cells. With physiological MNT levels, MNT homodimers and MNT-MLX heterodimers are enhancing cell cycle progression through direct regulation of *CDK1* and *BIRC5*, and DNA repair through *BRCA1*-dependent mechanisms. However, upon *MNT* knockdown, this regulation is impaired, with a decrease in *CDK1*, *BIRC5* and *BRCA1* and increased levels of *CDKN1C* and *ERCC6*. This would cause a cell cycle arrest and the activation of *ERCC6*-dependent DNA repair mechanisms.

5.2.3. MNT regulation at the mRNA and the protein levels

Previous reports suggest that MNT functions as a "MYC buffer", curbing excessive MYC activity that would lead to cell transformation. For instance, *in vivo MNT* knockdown antagonizes MYC-driven lymphomagenesis (Campbell et al., 2017; Link et al., 2012) whereas *MNT* silencing leads to MYC-like phenotypes (Hurlin et al., 2003; Nilsson et al., 2004; Walker et al., 2005). The data of this work indicate that there is a tight control of MNT expression. On the one hand, luciferase reporter experiments showed that MNT represses its own promoter

(mainly through E-box 2 in collaboration with MAX). Our ChIP-seq assays showed that MNT binds to its own promoter. On the other hand, the presence of PEST sequences along MNT protein and the analysis of expression of different MNT deletion constructs suggest that there is an additional level of regulation at the protein level.

Therefore, MNT seems to be tightly controlled by transcriptional and post-transcriptional mechanisms (**Figure 5.6**). These controls suggest that MNT plays a critical function in cell biology. Given the relevance of MNT in the modulation of MYC activity and its central position between the MYC-MAX and MLX-MONDO networks, the activities and regulation of MNT are a key issue on MYC-dependent tumorigenesis.

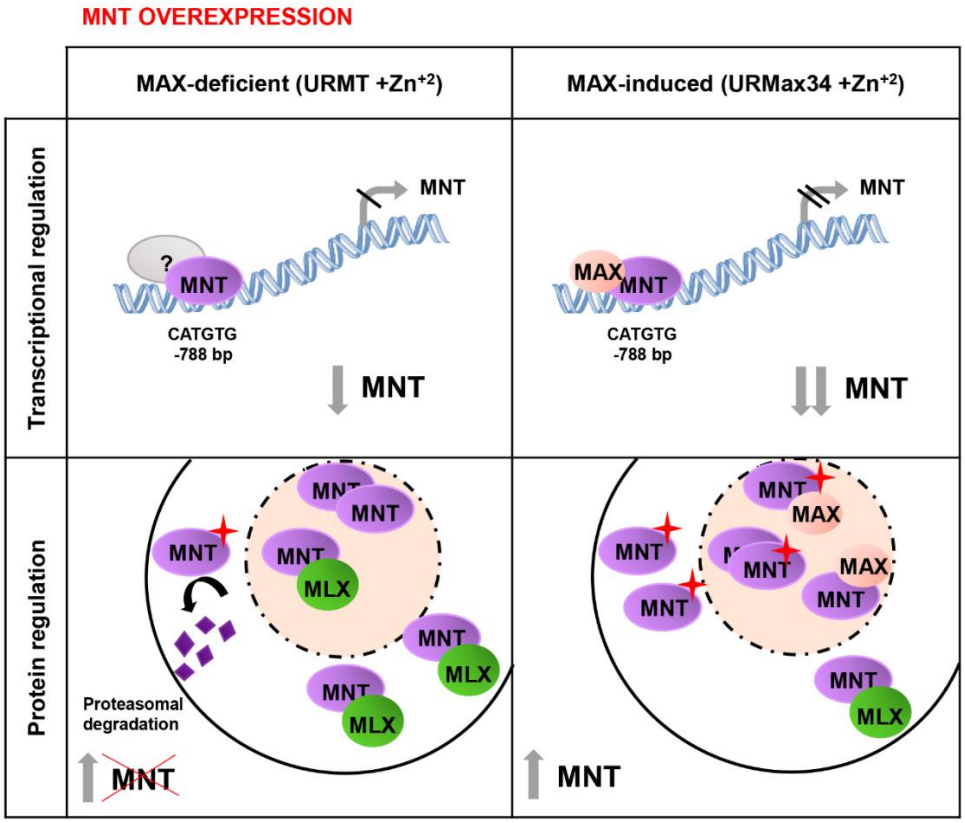

Figure 5.6. MNT levels are tightly regulated in UR61 cells. MNT is regulated at the transcriptional level (upper panel) and at the protein level (lower panel), after MNT overexpression. First, MNT binds to its own promoter (on the E-box localized 788 upstream the TSS), which causes its repression. This binding is increased upon MAX induction (URMax34 +Zn) and the repression is higher, resulting in lower levels of MNT protein in the cell. Second, as MNT levels in MAX-deficient cells (URMT +Zn) are maximum, the transfected MNT (marked with a red star) is degraded by the proteasome. This impedes MNT overexpression in these cells. On the contrary, MNT protein levels are lower in URMax34 cells and the exogenous MNT is not degraded, which allows MNT overexpression with respect to untrasfected cells.

5.3. Transcriptional regulation by MNT

Despite the unquestionable important role of MNT for cell biology, there are still several holes in our understanding of MNT function. By studying the transcriptome of MNT KO *versus* MNT WT HAP1 cells, we confirmed that MNT is a key transcriptional regulator: half activator and half repressor. In addition, we identified new MNT target genes and classified them based on their regulation by MNT-MAX, MNT-MLX or possible MNT homodimers. Finally, we proposed some genes as direct MNT target genes, based on the data available in the ENCODE project (genome-euro.ucsc.edu) as *LIN28A*, *HECW2*, *FOXG1*, *MYB*, *WIPI1* and *CHMP4C*.

5.3.1. *MNT* knockout affects MYC levels and enhances proliferation

First of all, we analyzed different features of the MNT KO cells. Protein levels confirmed the correct achievement of the knockout and showed the decrease in MYC, MAX and MLX. However, only the mRNA levels of *MYC* were affected by *MNT* knockout. This suggests a possible dependence of MYC expression for MNT. This has already been described in whole embryo lysates and mouse embryonic fibroblasts, in which *Mnt* knockout led to a decrease in both mRNA and protein MYC levels, without affecting their proliferation rate (Hurlin et al., 2003; Toyo-oka et al., 2004). MAX and MLX protein decrease may be a consequence of degradation after disruption of their complexes with MNT.

Regarding cell proliferation, MNT KO HAP1 cells proliferated much faster than their wild type countermates although they did not differ in Cyclin A and Survivin levels, which are proliferation and survival markers. This increased proliferation is consistent with other published studies where *MNT* silencing leads to MYC overexpression-like phenotypes. For instance, in mouse embryonic fibroblasts (Hurlin et al., 2003; Nilsson et al., 2004; Walker et al., 2005), in T-cells (Dezfouli et al., 2006; Link and Hurlin, 2014) and in myeloid HL60 cells (Kapoor et al., 2016). Still, MNT depletion does not always imply an increase in proliferation. It is noteworthy that the effect of *MNT* depletion in HAP1 cells is not reproduced in UR61. In the latter model, *MNT* knockdown leads to a decrease in proliferation

and survival, and this is in accordance with other studies (Campbell et al., 2017; Link and Hurlin, 2014). This abounds in the “gatekeeper” role of MNT controlling the effects of MYC and likely other genes critical for the proliferative balance of the cells. There is still work to do in order to fully understand MYC and MNT antagonism and cooperation in different models.

5.3.2. MNT is a key transcriptional regulator – half activator, half repressor

The RNA-seq of MNT KO *versus* WT HAP1 demonstrated the important role of MNT in transcriptional regulation. From the 460 genes that significantly changed upon *MNT* KO, around 50 % were up-regulated and the other 50 %, downregulated. Most part of the literature describe MNT as a repressor that works in association with SIN3 proteins. In fact, MNT-SIN3 interaction is key for the repressive function of MNT, as the deletion of the SID domain converts MNT in an activator (Hurlin, Quéva and Eisenman, 1997). However, Meroni *et al.*, (1997) detected also a transactivation activity of MNT in HeLa cells, although the mechanism is still undetermined. Thus, MNT is a transcription factor that can both activate and repress transcription.

Among the genes affected by MNT KO, ontology analysis revealed that pathways such as development, proliferation, differentiation, regulation of gene expression, biological adhesion or response to stimulus were affected. Most of these pathways have already been linked to MNT. In fact, *Mnt* KO mice are born severely runted, especially with craniofacial abnormalities. These mice are also smaller and die soon after birth (Hurlin et al., 2003; Toyo-oka et al., 2004), which demonstrates the key role of MNT in development. In addition, MNT is a transcription factor, so it regulates gene expression (Hurlin, Quéva and Eisenman, 1997; Meroni *et al.*, 1997). MNT is involved in proliferation as a MYC antagonist, thus repressing genes already described as MYC target genes like *CDK4*, *CCNE1* (Cyclin E) or *E2F2* (Hurlin et al., 2003; Walker et al., 2005). In addition, MNT has been described to induce differentiation in the HL60 promyeloblasts (Kapoor et al., 2016). Although the biological adhesion or the

response to stimulus have not been described before, the other pathways altered by MNT KO are in accordance with the available literature about MNT.

Next, GSEAs analysis revealed more specific pathways affected by *MNT* KO. For instance, angiogenesis, ion channel transport, UV response or TGFβ and IL6/JAK/STAT3 signaling. These results provide new evidence of the involvement of MNT in cell homeostasis and its role in cancer. Furthermore, the $T_{h1}T_{h2}$ differentiation pathway was another pathway obtained, although not as significant as the other pathways (FDR q-value of 0.29). We considered this important, as Dezfouli et al., (2006) stated the existence of a polarized differentiation of CD4+ T-cells into T_{h1} cells in a model of MNT-deficient T-cells.

5.3.3. MNT new target genes

After selection of a few genes that significantly changed upon *MNT* KO and the study of their expression changes after *MAX* or *MLX* depletion, together with the available data of the ENCODE project, we proposed some MNT direct target genes: *LIN28A*, *HECW2*, *FOXG1*, *MYB*, *WIPI1* and *CHMP4C*. These genes are regulated upon *MNT* depletion and MNT is found bound to their regulatory regions.

LIN28A is a RNA-binding protein that post-transcriptionally downregulates the let-7 microRNA family, which in turn triggers the overexpression of their targets (e.g. *MYC*, *RAS*, *HMGA2*, *BLIMP-1*). Thus, it is considered as a potential oncogene (Balzeau et al., 2017; Wang et al., 2015). LIN28A also participates in brain development by the induction of proliferation of the neural progenitor cells (Yang et al., 2015).

WIPI1 is a WD40-repeat protein that works as a scaffold and regulator of the autophagosome formation (Bakula et al., 2018, 2017).

HECW2 is an E3 ubiquitin ligase that plays an important role in the proliferation, migration and differentiation of neural crest cells as a regulator of glial cell line-derived neurotrophic factor (GDNF)/RET signaling (Wei et al., 2015). Mutations in this gene cause neurodevelopmental delay and hypotonia (Berko et al., 2017).

In addition, HECW2 is degraded by APC/C-Cdh1 during mitotic exit, being a regulator of the transition from metaphase to anaphase (Lu et al., 2013).

MYB is a transcription factor involved in several pathways, as the regulation of hematopoiesis, and its overexpression is associated with the block in cellular differentiation. Thus, MYB is considered an oncoprotein, which participates in tumorigenesis of leukemia, breast and colon cancer (Mitra, 2018).

CHMP4C is a member of the chromatin-modifying protein/charged multivesicular body protein (CHMP) family and a component of the endosomal sorting complex required for transport III (ESCRT-III). This complex is involved in the degradation of surface receptor proteins and the formation of endocytic multivesicular bodies by membrane deformation and vesicle invagination (Saksena et al., 2007).

FOXG1 is a Forkhead Box G1 factor involved in brain development, required for survival of postmitotic granule neurons (Dastidar et al., 2011; Kumamoto and Hanashima, 2017). Moreover, it has been described the repression of *FOXG1* by MYC/MIZ-1 in medulloblastoma (Vo et al., 2016). The finding of MNT bound to or in the vicinity of DNA target sequences for forkhead factors in our ChIP-seq experiment in UR61 cells and previous literature (Terragni et al., 2011) confirms the link between MNT and the FOX proteins. The fact that FOXG1 is upregulated upon *MNT* knockout in the absence of either MLX or MAX suggests that it could be regulated by homodimers MNT-MNT in HAP1 cells.

Altogether, the proposed MNT target genes have functions that are in accordance with different biological processes MNT has already been linked to (Yang and Hurlin, 2017). For instance, the regulation of potential oncogenes (*LIN28A*, *MYB*) is related with MNT role in tumorigenesis. Next, autophagocitosis driven by WIPI1, which is repressed by MNT, could be related to MNT's pro-survival function. Moreover, MNT's importance in brain development would be due to the regulation of important genes, such as *LIN28A*, *FOXG1* and *HECW2*, which have roles in proliferation and differentiation of neuronal cells. Finally, CHMP4C and its role in vesicle formation would allow MNT to regulate transport of nutrients and signaling pathways by the internalization of receptors. In our view, these results

constitute an initial step towards the understanding of MNT function as a key protein in the MYC proximal network.

The MNT targets that have been described in this work and their functions are schematized in **Figure 5.7**.

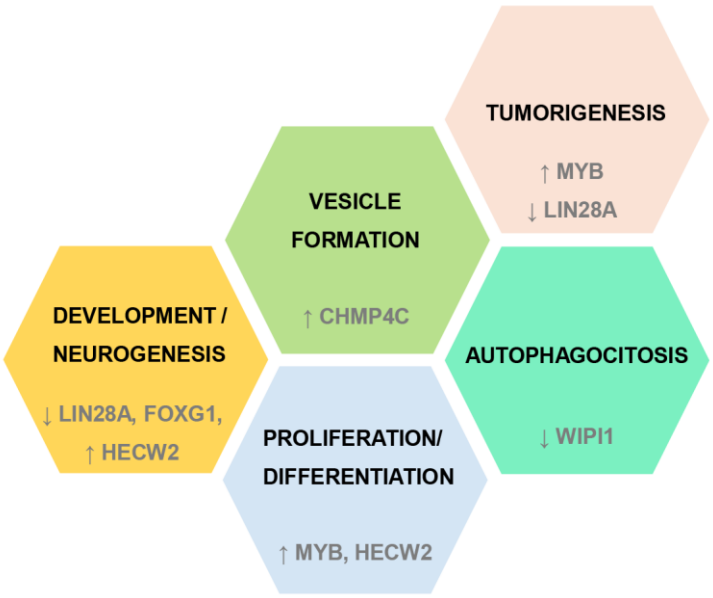

Figure 5.7. MNT new target genes and their functions. MNT binds to and regulates the transcription of *LIN28A*, *HECW2*, *FOXG1*, *MYB*, *WIPI1* and *CHMP4C*. Their main functions are shown in each of the hexagons.

As a final conclusion, our work provides an insight into MNT protein and widens our knowledge about its functions and its interactions. MNT regulates multiple processes that maintain cell homeostasis. MNT plays a key role in the MYC proximal network constituting a link between the MAX and the MLX arms. Understanding the specific functions of each of the members of the network and how their balance affects MYC functions will certainly provide new opportunities for counteracting MYC in tumorigenesis.

Conclusions

6. Conclusions

1) MNT interacts with REL in some mouse (Neuro-2a), rat (U7/UR61, C6) and human (LoVo, CEM) cell lines, both in the cytoplasm and the nucleus, independently of MAX.
2) MNT depletion triggers REL translocation, the activation of NF-κB signaling and the increase in two REL targets: IκBα and BCL-XL.
3) MNT represses *NFKBIA* (encoding IκBα) by direct binding to the gene regulatory regions. The maximum peak is detected at +171/+343 from the TSS and it concurs with the peak of REL on *NFKBIA* gene.
4) MNT forms homodimers and heterodimers with MLX through the bHLH domain in UR61 cells.
5) MNT-MLX dimers are localized both in the cytoplasm and the nucleus.
6) MNT and MLX are required for optimum proliferation in the absence of MAX.
7) MNT regulates gene expression of genes involved in cell cycle and DNA repair in the absence of MAX.
8) MNT binds directly to *BIRC5*, *CDK1* and *BRCA1* (to activate transcription) and to *FBXO32*, *CCNG2* and *ERCC6* (to repress transcription).
9) MNT binds to E-boxes and to forkhead transcription factor motifs in the absence of MAX.
10) MNT negatively autoregulates its promoter through E-box 2 (CATGTG), at 788 bp upstream the TSS, in collaboration with MAX.
11) MNT is in excess in MAX-deficient cells and cannot be overexpressed.
12) MNT knockout HAP1 cells proliferate faster even if MYC levels are reduced.
13) MNT regulates gene transcription as an activator and as a repressor, in MNT-MAX, MNT-MLX or MNT-MNT dimers, affecting several cellular processes, including development, proliferation, differentiation or response to external stimulus.

Bibliography

7. Bibliography

Acosta JC, Ferra N, Bretones G, Blanco R, Richard C, Connell BO, Sedivy J, Delgado MD, Leo J. 2008. Myc Inhibits p27-Induced Erythroid Differentiation of Leukemia Cells by Repressing Erythroid Master Genes without Reversing p27-Mediated Cell Cycle Arrest. *Mol Cell Biol* 28:7286–7295. doi:10.1128/MCB.00752-08.

Altieri DC. 2015. Survivin - The inconvenient IAP. *Semin cell Dev Biol* 39:91–96. doi:10.1016/j.semcdb.2014.12.007.

Amati B, Dalton S, Brooks MW, D LT, Evan GI, Land H. 1992. Transcriptional activation by the human c-Myc oncoprotein in yeast requires interaction with Max. *Nature* 359:423–426.

Ayer DE, Eisenman RN. 1993. A switch from Myc:Max to Mad:Max heterocomplexes accompanies monocyte/macrophage differentiation. *Genes Dev* 7:2110–2119.

Ayer DE, Lawrence QA, Eisenman RN. 1995. Mad-max transcriptional repression is mediated by ternary complex formation with mammalian homologs of yeast repressor Sin3. *Cell* 80:767–776. doi:10.1016/0092-8674(95)90355-0.

Bakula D, Müller AJ, Proikas-Cezanne T. 2018. WIPI3 and WIPI4 β-propellers are scaffolds for LKB1-AMPK-TSC signalling circuits in the control of autophagy. *Autophagy* 14:1082–1083. doi:10.1038/ncomms15637.

Bakula D, Müller AJ, Zuleger T, Takacs Z, Franz-Wachtel M, Thost AK, Brigger D, Tschan MP, Frickey T, Robenek H, Macek B, Proikas-Cezanne T. 2017. WIPI3 and WIPI4 β-propellers are scaffolds for LKB1-AMPK-TSC signalling circuits in the control of autophagy. *Nat Commun* 8. doi:10.1038/ncomms15637.

Balzeau J, Menezes MR, Cao S, Hagan JP. 2017. The LIN28/let-7 Pathway in Cancer. *Front Genet* 8:1–16. doi:10.3389/fgene.2017.00031.

Barisone GA, Ngo T, Tran M, Cortes D, Shahi MH, Nguyen T, Perez-lanza D, Matayasuwan W, Dı E. 2012. Role of MXD3 in Proliferation of DAOY Human Medulloblastoma Cells. *PLoS One* 7. doi:10.1371/journal.pone.0038508.

Barkett M, Gilmore TD. 1999. Control of apoptosis by Rel/NF-kappaB transcription factors. *Oncogene* 18:6910–6924. doi:10.1038/sj.onc.1203238

Barrett J, Birrer MJ, Kato GJ, Dosaka-Akita H, Dang1 C V. 1992. Activation Domains of L-Myc and c-Myc Determine Their Transforming Potencies in Rat Embryo Cells. *Mol Cell Biol* 12:3130–3137. doi:10.1128/MCB.12.7.3130.

Bash J, Zong WX, Gélinas C. 1997. c-Rel arrests the proliferation of HeLa cells and affects critical regulators of the G1/S-phase transition. *Mol Cell Biol* 17:6526–6536.

Benda P, Lightbody J, Sato G, Levine L, Sweet W. 1968. Differentiated Rat Glial Cell Strain in Tissue Culture. *Science* 161:370–371. doi:10.1126/science.161.3839.371.

Berberich SJ, Cole MD. 1992. Casein kinase II inhibits the DNA-binding activity of Max homodimers but not Myc/Max heterodimers. *Genes Dev* 6:166–176. doi:10.1101/gad.6.2.166.

Berko ER, Cho MT, Eng C, Shao Y, Sweetser DA, Waxler J, Robin NH, Brewer F, Donkervoort S, Mohassel P, Bönnemann CG, Bialer M, Moore C, Wolfe LA, Tifft CJ, Shen Y, Retterer K, Millan F, Chung WK. 2017. De novo missense variants in HECW2 are associated with neurodevelopmental delay and hypotonia. *J Med Genet* 54:93–99. doi:10.1136/jmedgenet-2016-103943.

Billin a N, Eilers a L, Coulter KL, Logan JS, Ayer DE. 2000. MondoA, a novel basic helix-loop-helix-leucine zipper transcriptional activator that constitutes a positive branch of a max-like network. *Mol Cell Biol* 20:8845–8854. doi:10.1128/MCB.20.23.8845-8854.2000.

Billin AN, Eilers AL, Queva C, Ayer DE. 1999. Mlx, a Novel Max-like BHLHZip Protein That Interacts with the Max Network of Transcription Factors. *J Biol Chem* 274:36344–36350.

Birrer MJ, Segal S, Degreve JS, Kaye F, Sausville EA, Minna JD. 1988. L-myc Cooperates with ras To Transform Primary Rat Embryo Fibroblasts. *Mol Cell Biol* 8:2668–2673.

Blackwood EM, Eisenman RN. 1992. Regulation of Myc:Max complex formation and its potential role in cell proliferation. *Tohoku J Exp Med* 168:195–202.

Blackwood EM, Eisenman RN. 1991. Max: A Helix-Loop-Helix Zipper Protein That Forms a Sequence-Specific DNA-binding Complex with Myc. *Science* 251:1211–1217.

Blackwood EM, Kretzner L, Eisenman RN. 1992a. Myc and Max function as a nucleoprotein complex. *Curr Opin Genet Dev* 2:227–235.

Blackwood EM, Lüscher B, Eisenman RN. 1992b. Myc and Max associate in vivo. *Genes Dev* 6:71–80.

Bottero V, Imbert V, Frelin C, Formento J-L, Peyron J-F. 2003. Monitoring NF-κB transactivation potential via real-time PCR quantification of IκBα gene expression. *Mol diagnostics* 7:187–194.

Bousset K, Henriksson M, Luscher-Firzlaff JM, Litchfield DW, Luscher B. 1993. Identification of casein kinase II phosphorylation sites in Max: effects on DNA-binding kinetics of Max homo- and Myc/Max heterodimers. *Oncogene* 8:3211–3220.

Bousset K, Oelgeschlager MH, Henriksson M, Schreek S, Burkhardt H, Litchfield DW, Luscher-Firzlaff JM, Luscher B. 1994. Regulation of transcription factors c-Myc, Max, and c-Myb by casein kinase II. *Cell Mol Biol Res* 40:501–511.

Bretones G, Delgado MD, León J. 2015. Myc and cell cycle control. *Biochim Biophys Acta* 1849:506–516. doi:10.1016/j.bbagrm.2014.03.013

Brownell E, Mathieson B, Young H a, Keller J, Ihle JN, Rice NR. 1987. Detection of c-rel-related transcripts in mouse hematopoietic tissues, fractionated lymphocyte populations, and cell lines. *Mol Cell Biol* 7:1304–9. doi:10.1128/MCB.7.3.1304.

Brownell E, Mittereder N, Rice NR. 1989. A human rel proto-oncogene cDNA containing an Alu fragment as a potential coding exon. *Oncogene* 4:935–942.

Brownell E, O'Brien SJ, Nash WG, Rice N. 1985. Genetic characterization of human c-rel sequences. *Mol Cell Biol* 5:2826–2831.

Burkitt MD, Hanedi AF, Duckworth CA, Williams JM, Tang JM, O'Reilly LA, Putoczki TL, Gerondakis S, Dimaline R, Caamano JH, Mark Pritchard D. 2015. NF-κB1, NF-κB2 and c-Rel differentially regulate susceptibility to colitis-associated adenoma development in C57BL/6 mice. *J Pathol* 236:326–336. doi:10.1002/path.4527.

Burnichon N, Cascoń A, Schiavi F, Morales NP, Comino-Méndez I, Abermil N, Inglada-Pérez L, De Cubas AA, Amar L, Barontini M, De Quirós SB, Bertherat J, Bignon YJ, Blok MJ, Bobisse S, Borrego S, Castellano M, Chanson P, Chiara MD, Corssmit EPM, Giacchè M, De Krijger RR, Ercolino T, Girerd X, Gómez-Garćia EB, Gómez-Graña Á, Guilhem I, Hes FJ, Honrado E, Korpershoek E, Lenders JWM, Letón R, Mensenkamp AR, Merlo A, Mori L, Murat A, Pierre P, Plouin PF, Prodanov T, Quesada-Charneco M, Qin N, Rapizzi E, Raymond V, Reisch N, Roncador G, Ruiz-Ferrer M, Schillo F, Stegmann APA, Suarez C, Taschin E, Timmers HJLM, Tops CMJ, Urioste M, Beuschlein F, Pacak K, Mannelli M, Dahia PLM, Opocher G, Eisenhofer G, Gimenez-Roqueplo AP, Robledo M. 2012. MAX mutations cause hereditary and sporadic pheochromocytoma and paraganglioma. *Clin Cancer Res* 18:2828–2837. doi:10.1158/1078-0432.CCR-12-0160.

Burstein DE, Greene LA. 1982. Nerve growth factor has both mitogenic and antimitogenic activity. *Dev Biol* 94:477–482. doi:10.1016/0012-1606(82)90364-5.

Cairo S, Merla G, Urbinati F, Ballabio A, Reymond A. 2001. WBSCR14, a gene mapping to the Williams-Beuren syndrome deleted region, is a new member of the Mlx transcription factor network. *Hum Mol Genet* 10:617–627. doi:10.1093/hmg/10.6.617.

Campbell KJ, Vandenberg CJ, Anstee NS, Hurlin PJ, Cory S. 2017. Mnt modulates Myc-driven lymphomagenesis. *Cell Death Differ* 1–10. doi:10.1038/cdd.2017.131.

Carroll PA, Diolaiti D. 2016. A novel role for the extended MYC network in cancer cell survival. *Mol Cell Oncol* 3:e1026528. doi:10.1080/23723556.2015.1026528.

Carroll PA, Diolaiti D, McFerrin L, Gu H, Djukovic D, Du J, Cheng PF, Anderson S, Ulrich M, Hurley JB, Raftery D, Ayer DE, Eisenman RN. 2015. Deregulated Myc Requires MondoA/Mlx for Metabolic Reprogramming and Tumorigenesis. *Cancer Cell* 27:271–285. doi:10.1016/j.ccell.2014.11.024

Carroll PA, Freie BW, Mathsyaraja H, Eisenman RN. 2018. The MYC transcription factor network: balancing metabolism, proliferation and oncogenesis. *Front Med* 1–14. doi:10.1007/s11684-018-0650-z.

Cerni C, Skrzypek B, Popov N, Sasgary S, Schmidt G, Larsson L-G, Luscher B, Henriksson M. 2002. Repression of in vivo growth of Myc/Ras transformed tumor cells by Mad1. *Oncogene* 21:447–459. doi:10.1038/sj/onc/1205107.

Chen C, Edelstein LC, Gélinas C. 2000. The Rel/NF-kappaB family directly activates expression of the apoptosis inhibitor Bcl-x(L). *Mol Cell Biol* 20:2687–95. doi:10.1128/MCB.20.8.2687-2695.2000.

Chen E, Li CCH. 1998. Association of Cdk2/cyclin E and NF-κB complexes at G1/S phase. *Biochem Biophys Res Commun* 249:728–734. doi:10.1006/bbrc.1998.9224.

Chen ISY, Wilhelmsen KC, Temin HM. 1983. Structure and Expression of c-rel, the Cellular Homolog to the Oncogene of Reticuloendotheliosis Virus Strain T. *J Virol* 45:104–113.

Chen X, Kandasamy K, Srivastava RK. 2003. Differential Roles of RelA (p65) and c-Rel Subunits of Nuclear Factor kB in Tumor. *Cancer Res* 63:1059–1066.

Comino-Méndez I, Gracia-Aznárez FJ, Schiavi F, Landa I, Leandro-García LJ, Letón R, Honrado E, Ramos-Medina R, Caronia D, Pita G, Gómez-Graña Á, Cubas AA De, Inglada-Pérez L, Maliszewska A, Taschin E, Bobisse S, Pica G, Loli P, Hernández-Lavado R, Díaz JA, Gómez-Morales M, González-Neira A, Roncador G, Rodríguez-Antona C, Benítez J, Mannelli M, Opocher G, Robledo M, Cascón A, Gómez-Graña A, de Cubas A a, Inglada-pérez L, Maliszewska A, Taschin E, Bobisse S, Pica G, Loli P, Hernández-lavado R, Díaz JA, Gómez-Morales M, González-Neira A, Roncador G, Rodríguez-Antona C, Benítez J, Mannelli M, Opocher G, Robledo M, Cascón A. 2011. Exome sequencing identifies MAX mutations as a cause of hereditary pheochromocytoma. *Nat Genet* 43:663–667. doi:10.1038/ng.861.

Conacci-Sorrell M, McFerrin L, Eisenman RN. 2014. An overview of MYC and its interactome. *Cold Spring Harb Perspect Med* 4:a014357. doi:10.1101/cshperspect.a014357.

Consortium TEP. 2012. An integrated encyclopedia of DNA elements in the human genome. *Nature* 489:57–74. doi:10.1038/nature11247.

Cvekl A, Zavadil J, Birshtein BK, Grotzer MA, Cvekl A. 2004. Analysis of transcripts from 17p13.3 in medulloblastoma suggests ROX/MNT as a potential tumour suppressor gene. *Eur J Cancer* 40:2525–2532. doi:10.1016/j.ejca.2004.08.005.

Dang C V. 2012. MYC on the path to cancer. *Cell* 149:22–35. doi:10.1016/j.cell.2012.03.003.

Dang C V. 1999. c-Myc Target Genes Involved in Cell Growth, Apoptosis, and Metabolism. *Mol Cell Biol* 19:1–11.

Dang C V., Kim J, Gao P, Yustein J. 2008. The Interplay Between MYC and HIF in the Warburg Effect. *Nat Rev Cancer* 8:51–56.

doi:10.1007/2789_2008_088.

Dastidar SG, Landrieu PMZ, D'Mello SR. 2011. FoxG1 Promotes the Survival of Postmitotic Neurons. *J Neurosci* 31:402–413. doi:10.1523/jneurosci.2897-10.2011.

Delgado MD, León J. 2010. Myc Roles in Hematopoiesis and Leukemia. *Genes Cancer* 1:605–616. doi:10.1177/1947601910377495.

DePinho RA, Hatton KS, Tesfaye A, Yancopoulos GD, Alt FW. 1987. The human myc gene family: structure and activity of L-myc and an L-myc pseudogene. *Genes Dev* 1:1311–1326. doi:10.1101/gad.1.10.1311.

Dezfouli S, Bakke A, Huang J, Wynshaw-Boris A, Hurlin PJ. 2006. Inflammatory Disease and Lymphomagenesis Caused by Deletion of the Myc Antagonist Mnt in T Cells. *Mol Cell Biol* 26:2080–2092. doi:10.1128/MCB.26.6.2080-2092.2006.

Diolaiti D, McFerrin L, Carroll PA, Eisenman RN. 2015. Functional interactions among members of the MAX and MLX transcriptional network during oncogenesis. *Biochim Biophys Acta* 1849:484–500. doi:10.1016/j.bbagrm.2014.05.016.

Drewinko B, Romsdahl MM, Yang LY, Trujlilo JM. 1976. Establishment of a Human Carcinoembryonic Antigen-producing Colon Adenocarcinoma Cell Line1. *Cancer Res* 36:467–475.

Duesberg PH, Vogtt PK. 1979. Avian acute leukemia viruses MC29 and MH2 share specific RNA sequences: Evidence for a second class of transforming genes (gel electrophoresis of RNA/RNA-cDNA hybridization/fingerprinting of oligonucleotides/group-specific and specific sequences of defect 76:1633–1637.

Edelmann J, Holzmann K, Miller F, Winkler D, Buhler A, Zenz T, Bullinger L, Kuhn MWM, Gerhardinger A, Bloehdorn J, Radtke I, Su X, Ma J, Pounds S, Hallek M, Lichter P, Korbel J, Busch R, Mertens D, Downing JR, Stilgenbauer S, Dohner H. 2012. High-resolution genomic profiling of chronic lymphocytic leukemia reveals new recurrent genomic alterations. *Blood* 6:4783–4794. doi:10.1182/blood-2012-04-423517.

Epstein BYMA, Henle G, Achong BG, Ch B, Barr YM. 1965. Morphological and biological studies on a virus in cultured lymphoblasts from Burkitt's lymphoma. *J Exp Med* 121:761–770.

Epstein MA, Achong BG, Barr YM, Zajac B, Henle G, Henle W. 1966. Morphological and virological investigations on cultured Burkitt tumor lymphoblasts (strain Raji). *J Natl Cancer Inst* 37:547–559.

Espinosa L, Bigas A, Mulero MC. 2011. Alternative nuclear functions for NF-κB family members. *Am J Cancer Res* 1:446–59.

Essletzbichler P, Konopka T, Santoro F, Chen D, Gapp B V., Kralovics R, Brummelkamp TR, Nijman SMB, Bürckstümmer T. 2014. Megabase-scale deletion using CRISPR/Cas9 to generate a fully haploid human cell line. *Genome Res* 24:2059–2065. doi:10.1101/gr.177220.114.

Foley GE, Lazarus H, Farber S, Uzman BG, Boone BA, McCarthy RE. 1965. Continuous culture of human lymphoblasts from peripheral blood of a child with acute leukemia. *Cancer* 18:522–529.

Forster SC, Finkel AM, Gould JA, Hertzog PJ. 2013. RNA-eXpress annotates novel transcript features in RNA-seq data. *Bioinformatics* 29:810–812. doi:10.1093/bioinformatics/btt034.

Fox EJ, Wright SC. 2003. The transcriptional repressor gene Mad3 is a novel target for regulation by E2F1. *Biochem J* 370:307–313.

García-Gutiérrez L, Delgado MD, León J, García-Gutiérrez L, Delgado MD, León J. 2019. MYC Oncogene Contributions to Release of Cell Cycle Brakes. *Genes (Basel)* 10:244. doi:10.3390/genes10030244.

Garcia-Sanz P, Quintanilla A, Lafita MC, Moreno-Bueno G, García-Gutierrez L, Tabor V, Varela I, Shiio Y, Larsson LG, Portillo F, Leon J. 2014. Sin3b Interacts with Myc and decreases Myc levels. *J Biol Chem* 289:22221–22236. doi:10.1074/jbc.M113.538744.

Gey GO, Coffman WD, Kubicek MT. 1952. Tissue culture studies of the proliferative capacity of cervical carcinoma and normal epithelium. *Cancer Res* 12:264–265.

Gilmore TD. 2006. Introduction to NF-κB: players, pathways, perspectives. *Oncogene* 25:6680–6684. doi:10.1038/sj.onc.1209954.

Gilmore TD, Cormier C, Jean-Jacques J, Gapuzan ME. 2001. Malignant transformation of primary chicken spleen cells by human transcription factor c-Rel. *Oncogene* 20:7098–7103. doi:10.1038/sj.onc.1204898.

Gilmore TD, Gerondakis S. 2011. The c-Rel Transcription Factor in Development and Disease. *Genes Cancer* 2:695–711. doi:10.1177/1947601911421925.

Gilmore TD, Kalaitzidis D, Liang M-C, Starczynowski DT. 2004. The c-Rel transcription factor and B-cell proliferation: a deal with the devil. *Oncogene* 23:2275–2286. doi:10.1038/sj.onc.1207410.

Graham FL, Smiley J, Nairn R. 1977. Characteristics of a Human Cell Line Transformed by DNA from Human Adenovirus Type 5. *J Gen Virol* 36:59–72. doi:10.1099/0022-1317-36-1-59.

Grandori C., Mac J., Siëbelt F., Ayer D.E., Eisenman RN. 1996. Myc-Max heterodimers activate a DEAD box gene and interact with multiple E box-related sites in vivo. *EMBO J* 15:4344–57.

Grandori C, Cowley SM, James LP, Eisenman RN. 2000. The Myc/Max/Mad Network and the Transcriptional Control of Cell Behavior. *Ann Rev cell Dev* 16:653–699.

Grzenda A, Lomberk G, Zhang JS, Urrutia R. 2009. Sin3: Master scaffold and transcriptional corepressor. *Biochim Biophys Acta - Gene Regul Mech* 1789:443–450. doi:10.1016/j.bbagrm.2009.05.007.

Guerrero I, Pellicer A, Burstein DE. 1988. Dissociation of c-FOS from ODC expression and neuronal differentiation in a PC12 subline stably transfected

with an inducible N-RAS oncogene. *Biochem Biophys Res Commun* 150:1185–1192.

Guo X, Pan L, Zhang X, Suo X, Niu Z, Zhang J, Wang F, Dong Z, Da W, Ohno R. 2007. Expression and mutation analysis of genes that encode the Myc antagonists Mad1 , Mxi1 and Rox in acute leukaemia. *Leuk Lymphoma* 48:1200–1207. doi:10.1080/10428190701342018.

Gupta Shilpi, Kumar P, Kaur H, Sharma N, Gupta Sunita, Saluja D, Bharti AC, Das B. 2018. Constitutive activation and overexpression of NF-kB/c-Rel in conjunction with p50 contribute to aggressive tongue tumorigenesis. *Oncotarget* 9:33011–33029. doi:10.18632/oncotarget.26041.

Halleck MS, Pownall S, Harder KW, Duncan AMV, Jirik FR, Schlegel RA. 1995. A widely distributed putative mammalian transcriptional regulator containing multiple paired amphipathic helices, with similarity to yeast SIN3. *Genomics* 26:403–406. doi:10.1016/0888-7543(95)80229-F.

Han S, Park K, Kim HY, Lee MS, Kim HJ, Kim YD, Yuh YJ, Kim SR, Suh HS. 2000. Clinical implication of altered expression of Mad1 protein in human breast carcinoma. *Cancer* 88:1623–1632. doi:https://doi.org/10.1002/(SICI)1097-0142(20000401)88:7<1623::AID-CNCR17>3.0.CO;2-W.

Harris J, Oliere S, Sharma S, Sun Q, Lin R, Hiscott J, Grandvaux N. 2006. Nuclear Accumulation of cRel following C-Terminal phosphorylation by TBK1/IKK. *J Immunol* 177:2527–2535. doi:10.4049/jimmunol.177.4.2527.

Hayden MS, Ghosh S. 2008. Shared Principles in NF-kB Signaling. *Cell* 132:344–362. doi:10.1016/j.cell.2008.01.020.

Heinz S, Benner C, Spann N, Bertolino E, Lin YC, Laslo P, Cheng JX, Murre C, Singh H, Glass CK. 2010. Simple combinations of lineage-determining transcription factors prime cis-regulatory elements required for macrophage and B cell identities. *Mol Cell* 38:576–89. doi:10.1016/j.molcel.2010.05.004.

Heinzel T, Lavinsky RM, Mullen T, Soderstrom M, Lahertyll CD, Torchia J, Yang W, Branl G, Ngo SD, Davie JR, Seto E, Eisenmanll RN, Rose DW, Glass CK, Rosenfeld MG. 1997. A complex containing N-CoR, mSin3 and histone deacetylase mediates transcriptional repression. *Nature* 387:43–48.

Hobbs GA, Der CJ, Rossman KL. 2016. RAS isoforms and mutations in cancer at a glance. *J Cell Sci* 129:1287–1292. doi:10.1242/jcs.182873.

Hooker CW, Hurlin PJ. 2006. Of Myc and Mnt. *J Cell Sci* 1198:208–216. doi:10.1242/jcs.02815.

Hopewell R, Ziff EB. 1995. The nerve growth factor-responsive PC12 cell line does not express the Myc dimerization partner Max. *Mol Cell Biol* 15:3470–3478.

Hunt LC, Xu B, Finkelstein D, Fan Y, Carroll PA, Cheng PF, Eisenman RN, Demontis F. 2015. The glucose-sensing transcription factor MLX promotes myogenesis via myokine signaling. *Genes Dev* 29:2475–2489. doi:10.1101/gad.267419.115.

Hunter JE, Leslie J, Perkins ND. 2016. c-Rel and its many roles in cancer: an old story with new twists. *Br J Cancer* 114:1–6. doi:10.1038/bjc.2015.410.

Hurlin PJ, Huang J. 2006. The MAX-interacting transcription factor network. *Semin Cancer Biol* 16:265–274. doi:10.1016/j.semcancer.2006.07.009.

Hurlin PJ, Quéva C, Eisenman RN. 1997. Mnt, a novel Max-interacting protein is coexpressed with Myc in proliferating cells and mediates repression at Myc binding sites. *Genes Dev* 11:44–58. doi:10.1101/gad.11.1.44.

Hurlin PJ, Queva C, Koskinen PJ, Steingrimsson E, Ayer DE, Copeland NG, Jenkins NA, Eisenman RN. 1995. Mad3 and Mad4 : novel Max-interacting transcriptional repressors that suppress c-myc dependent transformation and are expressed during neural and epidermal differentiation. *EMBO J* 14:5646–5659.

Hurlin PJ, Steingrimsson E, Copeland NG, Jenkins NA, Eisenman RN. 1999. Mga, a dual-specificity transcription factor that interacts with Max and contains a T-domain DNA- binding motif. *EMBO J* 18:7019–7028.

Hurlin PJ, Zhou Z, Toyo-oka K, Ota S, Walker WL, Hirotsune S, Wynshaw-boris A. 2003. Deletion of Mnt leads to disrupted cell cycle control and tumorigenesis. *EMBO J* 22:4584–4596.

Hurlin PJ, Zhou ZQ, Toyo-Oka K, Ota S, Walker WL, Hirotsune S, Wynshaw-Boris A. 2004. Evidence of Mnt-Myc antagonism revealed by Mnt gene deletion. *Cell Cycle* 3:97–99. doi:638 [pii].

Iavarone A, Lasorella A. 2014. Myc and differentiation: going against the current. *EMBO Rep* 15:324–325.

Iizuka K, Bruick RK, Liang G, Horton JD, Uyeda K. 2004. Deficiency of carbohydrate response element-binding protein (ChREBP) reduces lipogenesis as well as glycolysis. *Proc Natl Acad Sci U S A* 101:7281–7286. doi:10.1073/pnas.96.22.12737.

Iritani BM, Eisenman RN. 1999. c-Myc enhances protein synthesis and cell size during B lymphocyte development. *Proc Natl Acad Sci* 96:13180–13185.

Iwai K, Lee BR, Hashiguchi M, Fukushima A, Iwashima M. 2005. IkB-α-specific transcript regulation by the C-terminal end of c-Rel. *FEBS Lett* 579:141–144. doi:10.1016/j.febslet.2004.11.060.

Johnston LA, Prober DA, Edgar BA, Eisenman RN, Gallant P. 1999. Drosophila myc Regulates Cellular Growth during Development. *Cell* 98:779–790.

Kalkat M, Melo J De, Hickman KA, Lourenco C, Redel C, Resetca D, Tamachi A, Tu WB, Penn LZ. 2017. MYC Deregulation in Primary Human Cancers. *Genes (Basel)* 8. doi:10.3390/genes8060151.

Kaltschmidt B, Greiner J, Kadhim H, Kaltschmidt C. 2018. Subunit-Specific Role of NF-κB in Cancer. *Biomedicines* 6:44. doi:10.3390/biomedicines6020044.

Kanarek N, London N, Schueler-Furman O, Ben-Neriah Y. 2010. Ubiquitination and Degradation of the Inhibitors of NF-kB. *Cold Spring Harb Perspect Biol* 2:1–16.

Kapeli K, Hurlin PJ. 2011. Differential Regulation of N-Myc and c-Myc Synthesis, Degradation, and Transcriptional Activity by the Ras/Mitogen-activated Protein Kinase Pathway. *J Biol Chem* 286:38498–38508. doi:10.1074/jbc.M111.276675.

Kapoor I, Kanaujiya J, Kumar Y, Thota JR, Bhatt MLB, Chattopadhyay N, Sanyal S, Trivedi AK. 2016. Proteomic discovery of MNT as a novel interacting partner of E3 ubiquitin ligase E6AP and a key mediator of myeloid differentiation. *Oncotarget* 7:7640–7656. doi:10.18632/oncotarget.6156.

Karn J, Watson J V, Lowe AD, Green SM, Vedeckis W. 1989. Regulation of cell cycle duration by c-myc levels. *Oncogene* 4:773–787.

Kato GJ, Lee WMF, Chen L, Dang C V. 1992. Max: functional domains and interaction with c-Myc. *Genes Dev* 6:81–92.

Kay BK, Williamson MP, Sudol M. 2000. The importance of being proline: the interaction of proline-rich motifs in signaling proteins with their cognate domains. *FASEB J* 14:231–41.

Kaye F, Battey J, Nau M, Brooks B, Seifter E, De Greve J, Birrer M, Sausville E, Minna J. 1988. Structure and expression of the human L-myc gene reveal a complex pattern of alternative mRNA processing. *Mol Cell Biol* 8:186–195. doi:10.1128/MCB.8.1.186.

Kharchenko P V, Tolstorukov MY, Park PJ. 2008. Design and analysis of ChIP-seq experiments for DNA-binding proteins. *Nat Biotechnol* 26:1351–1359. doi:10.1038/nbt.1508.

Klapproth K, Sander S, Marinkovic D, Baumann B, Wirth T, Dc W. 2009. The IKK2/NF-κB pathway suppresses MYC-induced lymphomagenesis. *Blood* 114:2448–2458. doi:10.1182/blood-2008-09-181008.

Klein G, Giovanella B, Westman A, Stehlin JS, Mumford D. 1975. An EBV-Genome-Negative Cell Line Established from an American Burkitt Lymphoma; Receptor Characteristics. EBV Infectibility and Permanent Conversion into EBV-Positive Sublines by in vitro Infection. *Intervirology* 5:319–334. doi:doi: 10.1159/000149930.

Kohl NE, Kanda N, Schreck RR, Bruns G, Latt SA, Gilbert F, Alt FW. 1983. Transposition and amplification of oncogene-related sequences in human neuroblastomas. *Cell* 35:359–367. doi:10.1016/0092-8674(83)90169-1.

Koskinen PJ, Ayer DE, Eisenman RN. 1995. Ras Cotransformation by Mad Is Mediated by Multiple Interactions. *Cell Growth Differ* 6:623–629.

Kumamoto T, Hanashima C. 2017. Evolutionary conservation and conversion of Foxg1 function in brain development. *Dev Growth Differ* 59:258–269. doi:10.1111/dgd.12367.

Kunsch C, Ruben SM, Rosen CA. 1992. Selection of optimal kappa B/Rel DNA-binding motifs: interaction of both subunits of NF-kappa B with DNA is required for transcriptional activation. *Mol Cell Biol* 12:4412–4421. doi:10.1128/mcb.12.10.4412.

La Rosa FA, Pierce JW, Sonenshein GE. 1994. Differential regulation of the c-

myc oncogene promoter by the NF-kappa B rel family of transcription factors. *Mol Cell Biol* 14:1039–1044. doi:10.1128/MCB.14.2.1039.

Lafita-Navarro MC. 2015. New biological functions of MXD1 and MNT, proteins of the MYC-MAX-MXD network. Universidad de Cantabria.

Laherty CD, Yang W, Sun J, Davie JR, Seto E, Eisenman RN. 1997. Histone Deacetylases associated with the mSin3 Corepressor mediate Mad Transcriptional Repression. *Cell* 89:349–356.

Land H, Parada LF, Weinberg RA. 1983. Tumorigenic conversion of primary embryo fibroblasts requires at least two cooperating oncogenes. *Nature* 304:596–602.

Landt SG, Marinov GK, Kundaje A, Kheradpour P, Pauli F, Batzoglou S, Bernstein BE, Bickel P, Brown JB, Cayting P, Chen Y, DeSalvo G, Epstein C, Fisher-Aylor KI, Euskirchen G, Gerstein M, Gertz J, Hartemink AJ, Hoffman MM, Iyer VR, Jung YL, Karmakar S, Kellis M, Kharchenko P V, Li Q, Liu T, Liu XS, Ma L, Milosavljevic A, Myers RM, Park PJ, Pazin MJ, Perry MD, Raha D, Reddy TE, Rozowsky J, Shoresh N, Sidow A, Slattery M, Stamatoyannopoulos JA, Tolstorukov MY, White KP, Xi S, Farnham PJ, Lieb JD, Wold BJ, Snyder M. 2012. ChIP-seq guidelines and practices of the ENCODE and modENCODE consortia. *Genome Res* 22:1813–31. doi:10.1101/gr.136184.111.

Lee WMF, Schwab M, Westaway D, Varmus HE. 1985. Augmented Expression of Normal c-myc Is Sufficient for Cotransformation of Rat Embryo Cells with a Mutant ras Gene. *Mol Cell Biol* 5:3345–3356.

Leeman JR, Weniger M a, Barth TF, Gilmore TD. 2008. Deletion analysis and alternative splicing define a transactivation inhibitory domain in human oncoprotein REL. *Oncogene* 27:6770–6781. doi:10.1038/onc.2008.284.

Leone G, DeGregori J, Sears R, Jakoi L, Nevins JR. 1997. Myc and Ras collaborate in inducing accumulation of active cyclin E/Cdk2 and E2F. *Nature* 387:422–426.

Li F, Wang Y, Zeller KI, Potter JJ, Wonsey DR, Donnell KAO, Kim J, Yustein JT, Lee LA, Dang C V. 2005. Myc Stimulates Nuclearly Encoded Mitochondrial Genes and Mitochondrial Biogenesis. *Mol Cell Biol* 25:6225–6234. doi:10.1128/MCB.25.14.6225.

Li H, Durbin R. 2009. Fast and accurate long-read alignment with Burrows-Wheeler transform. *Bioinformatics* 26:589–595. doi:10.1093/bioinformatics/btp698.

Liberzon A, Subramanian A, Pinchback R, Thorvaldsdóttir H, Tamayo P, Mesirov JP. 2011. Molecular signatures database (MSigDB) 3.0. *Bioinformatics* 27:1739–1740. doi:10.1093/bioinformatics/btr260.

Link JM, Hurlin PJ. 2014. The activities of MYC, MNT and the MAX-interactome in lymphocyte proliferation and oncogenesis. *Biochim Biophys Acta - Gene Regul Mech* 21–23. doi:10.1016/j.bbagrm.2014.04.004.

Link JM, Ota S, Zhou Z, Daniel CJ, Sears RC, Hurlin PJ. 2012. A critical role for

Mnt in Myc-driven T-cell proliferation and oncogenesis. *Proc Natl Acad Sci* 109:19685–19690. doi:10.1073/pnas.1206406109.

Lo Nigro C, Venesio T, Reymond A, Meroni G, Alberici P, Cainarca S, Enrico F, Stack M, Ledbetter DH, Liscia DS, Ballabio A, Carrozzo R. 1998. The Human ROX Gene: Genomic Structure and Mutation Analysis in Human Breast Tumors. *Genomics* 282:275–282.

Loo LWM, Secombe J, Little JT, Leni-Sue Carlos L-S, Yost C, Cheng P-F, Flynn EM, Edgar BA, Eisenman RN. 2005. The Transcriptional Repressor dMnt Is a Regulator of Growth in Drosophila melanogaster. *Mol Cell Biol* 25:7078–7091. doi:10.1207/S15327841MPEE0404_1.

Lorenz VN, Schön MP, Seitz CS. 2014. c-Rel downregulation affects cell cycle progression of human keratinocytes. *J Invest Dermatol* 134:415–22. doi:10.1038/jid.2013.315.

Love MI, Huber W, Anders S. 2014. Moderated estimation of fold change and dispersion for RNA-seq data with DESeq2. *Genome Biol* 15:550. doi:10.1186/s13059-014-0550-8.

Lozzio C, Lozzio B. 1975. Human Chronic Myelogenous Leukemia Cell-Line with Positive Philadelphia Chromosome. *Blood* 45:321–334.

Lu L, Hu S, Wei R, Qiu X, Lu K, Fu Y, Li H, Xing G, Li D, Peng R, He F, Zhang L. 2013. The HECT type ubiquitin ligase NEDL2 is degraded by anaphase-promoting complex/cyclosome (APC/C)-Cdh1, and its tight regulation maintains the metaphase to anaphase transition. *J Biol Chem* 288:35637–35650. doi:10.1074/jbc.M113.472076.

Lüscher B, Vervoorts J. 2012. Regulation of gene transcription by the oncoprotein MYC. *Gene* 494:145–160. doi:10.1016/j.gene.2011.12.027.

Ma L, Robinson LN, Towle HC. 2006. ChREBP·Mlx is the principal mediator of glucose-induced gene expression in the liver. *J Biol Chem* 281:28721–28730. doi:10.1074/jbc.M601576200.

Ma L, Sham YY, Walters KJ, Towle HC. 2007. A critical role for the loop region of the basic helix-loop-helix/ leucine zipper protein Mlx in DNA binding and glucose-regulated transcription. *Nucleic Acids Res* 35:35–44. doi:10.1093/nar/gkl987.

Martin D, Galisteo R, Ji Y, Montaner S, Gutkind JS. 2008. An NF-κB gene expression signature contributes to Kaposi's sarcoma virus vGPCR-induced direct and paracrine neoplasia. *Oncogene* 27:1844–1852. doi:10.1038/sj.onc.1210817.

Mattila J, Havula E, Suominen E, Teesalu M, Surakka I, Hynynen R, Kilpinen H, Väänänen J, Hovatta I, Käkelä R, Ripatti S, Sandmann T, Hietakangas V. 2015. Mondo-Mlx Mediates Organismal Sugar Sensing through the Gli-Similar Transcription Factor Sugarbabe. *Cell Rep* 13:350–364. doi:10.1016/j.celrep.2015.08.081.

McFerrin LG, Atchley WR. 2011. Evolution of the Max and Mlx networks in animals. *Genome Biol Evol* 3:915–937. doi:10.1093/gbe/evr082.

Meroni G, Cairo S, Merla G, Messali S, Brent R, Ballabio A, Reymond A. 2000. Mlx, a new Max-like bHLHZip family member: the center stage of a novel transcription factors regulatory pathway? *Oncogene* 19:3266–77. doi:10.1038/sj.onc.1203634.

Meroni G, Reymond A, Alcalay M, Borsani G, Tanigami A, Tonlorenzi R, Lo Nigro C, Messali S, Zollo M, Ledbetter DH, Brent R, Ballabio A, Carrozzo R. 1997. Rox, a novel bHLHZip protein expressed in quiescent cells that heterodimerizes with Max, binds a non-canonical E box and acts as a transcriptional repressor. *EMBO J* 16:2892–2906. doi:10.1093/emboj/16.10.2892.

Mitra P. 2018. Transcription regulation of MYB: a potential and novel therapeutic target in cancer. *Ann Transl Med* 6:443–443. doi:10.21037/atm.2018.09.62.

Mortazavi A, Williams BA, McCue K, Schaeffer L, Wold B. 2008. Mapping and quantifying mammalian transcriptomes by RNA-Seq. *Nat Methods* 5:621–8. doi:10.1038/nmeth.1226.

Nau MM, Brooks BJ, Battey J. 1986. L-Myc, a New Myc-Related Gene Amplified and Expressed in Human Small Cell Lung Cancer. *Lung Cancer* 2:254.

Naugler WE, Karin M. 2008. NF-κB and Cancer — Identifying Targets and Mechanisms. *Curr Opin Genet Dev* 18:19–26. doi:10.1016/j.gde.2008.01.020.

Nilsson JA, Maclean KH, Keller UB, Pendeville H, Baudino TA, Cleveland JL. 2004. Mnt loss triggers Myc transcription targets, proliferation, apoptosis, and transformation. *Mol Cell Biol* 24:1560–1569. doi:10.1128/MCB.24.4.1560.

O'Shea JM, Ayer DE. 2013. Coordination of Nutrient Availability and Utilization by MAX- and MLX-Centered Transcription Networks. *Cold Spring Harb Perspect Med* 3:a014258.

Ogawa H, Ishiguro K, Gaubatz S, Livingston DM, Nakatani Y. 2002. A Complex with Chromatin Modifiers That Occupies E2F- and Myc-Responsive Genes in G0 Cells A Complex with Chromatin Modifiers That Occupies E2F- and Myc-Responsive Genes in G0 Cells. *Science (80-)* 296:1132–1136.

Olmsted JB, Carlson K, Klebe R, Ruddle F, Rosenbaum J. 2006. Isolation of Microtubule Protein from Cultured Mouse Neuroblastoma Cells. *Proc Natl Acad Sci* 65:129–136. doi:10.1073/pnas.65.1.129.

Orian A, Grewal SS, Knoepfler PS, Edgar BA, Parkhurst SM, Eisenman RN. 2005. Genomic binding and transcriptional regulation by the Drosophila Myc and Mnt transcription factors. *Cold Spring Harb Symp Quant Biol* 70:299–307. doi:10.1101/sqb.2005.70.019.

Orian A, van Steensel B, Delrow J, Bussemaker HJ, Li L, Sawado T, Williams E, Loo LWM, Cowley SM, Yost C, Pierce S, Edgar BA, Parkhurst SM, Eisenman RN. 2003. Genomic binding by the Drosophila Myc, Max, Mad/Mnt transcription factor network. *Genes Dev* 17:1101–1114. doi:10.1101/gad.1066903.ing.

Pai SY, Ho IC. 2002. c-Rel delivers a one-two punch in Th1 cell differentiation. *J Clin Invest* 110:741–742. doi:10.1172/JCI0216552.

Pantaleo MA, Urbini M, Indio V, Ravegnini G, Nannini M, De Luca M, Tarantino G, Angelini S, Gronchi A, Vincenzi B, Grignani G, Colombo C, Fumagalli E, Gatto L, Saponara M, Ianni M, Paterini P, Santini D, Pirini MG, Ceccarelli C, Altimari A, Gruppioni E, Renne SL, Collini P, Stacchiotti S, Brandi G, Casali PG, Pinna AD, Astolfi A, Biasco G. 2017. Genome-Wide Analysis Identifies MEN1 and MAX Mutations and a Neuroendocrine-Like Molecular Heterogeneity in Quadruple WT GIST. *Mol Cancer Res* 15:553–562. doi:10.1158/1541-7786.MCR-16-0376.

Paoli L De, Cerri M, Monti S, Rasi S, Spina V, Bruscaggin A, Greco M, Ciardullo C, Famà R, Cresta S, Maffei R, Ladetto M, Martini M, Laurenti L, Forconi F, Marasca R, Larocca LM, Bertoni F, Gaidano G, Rossi D. 2013. MGA, a suppressor of MYC, is recurrently inactivated in high risk chronic lymphocytic leukemia. *Leuk Lymphoma* 54:1087–1090. doi:10.3109/10428194.2012.723706.

Peterson CW, Stoltzman CA, Sighinolfi MP, Han KS, Ayer DE. 2010. Glucose Controls Nuclear Accumulation, Promoter Binding, and Transcriptional Activity of the MondoA-Mlx Heterodimer. *Mol Cell Biol* 30:2887–2895. doi:10.1128/mcb.01613-09.

Pierce SB, Yost C, Anderson SAR, Flynn EM, Delrow J, Eisenman RN. 2008. Drosophila growth and development in the absence of dMyc and dMnt. *Dev Biol* 315:303–316. doi:10.1016/j.ydbio.2007.12.026.

Pierce SB, Yost C, Britton JS, Loo LWM, Flynn EM, Edgar BA, Eisenman RN. 2004. dMyc is required for larval growth and endoreplication in Drosophila. *Development* 131:2317–2327. doi:10.1242/dev.01108.

Pimentel-Muiños FX, Mazana J, Fresno M. 1995. Biphasic control of nuclear factor-χB activation by the T cell receptor complex: role of tumor necrosis factor α. *Eur J Immunol* 25:179–186. doi:10.1002/eji.1830250130.

Poole CJ, van Riggelen J. 2017. MYC—master regulator of the cancer epigenome and transcriptome. *Genes (Basel)* 8. doi:10.3390/genes8050142.

Popov N, Wahlström T, Hurlin PJ, Henriksson M. 2005. Mnt transcriptional repressor is functionally regulated during cell cycle progression. *Oncogene* 24:8326–8337. doi:10.1038/sj.onc.1208961.

Prendergast GC, Lawe D, Ziff E. 1991. Association of Myn, the Murine Homolog of Max, with c-Myc Stimulates Methylation-Sensitive DNA Binding and Ras Cotransformation. *Cell* 65:395–407.

Priebe MK, Dewert N, Amschler K, Erpenbeck L, Heinzerling L, Schön MP, Seitz CS, Lorenz VN. 2018. c-Rel is a cell cycle modulator in human melanoma cells. *Exp Dermatol* 00:1–8. doi:10.1111/ exd.138486153.

Prochownik E V., VanAntwerp ME. 1993. Differential patterns of DNA binding by myc and max proteins. *Proc Natl Acad Sci* 90:960–964. doi:10.1073/pnas.90.3.960.

Quintanilla A. 2013. MYC oncoprotein role in the regulation of transcription, differentiation and senescence. *PhD Diss*. Universidad de Cantabria.

Ran FA, Hsu PD, Wright J, Agarwala V, Scott DA, Zhang F. 2013. Genome engineering using the CRISPR-Cas9 system. *Nat Protoc* 8:2281–2308. doi:10.1007/978-1-4939-1862-1_10.

Rechsteiner M, Rogers SW. 1996. PEST sequences and regulation by proteolysis. *Trends Biochem Sci* 21:267–271. doi:10.1016/S0968-0004(96)10031-1.

Reddy A, Zhang J, Davis NS, Moffitt AB, Love CL, Waldrop A, Leppa S, Pasanen A, Meriranta L, Karjalainen-Lindsberg M-L, Norgaard P, Pedersen M, Gang AO, Hogdall E, Heavican TB, Lone W, Iqbal J, Qin Q, Li G, Kim SY, Healy J, Richards KL, Fedoriw Y, Bernal-Mizrachi L, Koff JL, Staton AD, Flowers CR, Paltiel O, Goldschmidt N, Calaminici M, Clear A, Gribben J, Nguyen E, Czader MB, Ondrejka SL, Collie A, Hsi ED, Tse E, Au-Yeung RKH, Kwong Y-L, Srivastava G, Choi WWL, Evens AM, Pilichowska M, Sengar M, Reddy N, Li S, Chadburn A, Gordon LI, Jaffe ES, Levy S, Rempel R, Tzeng T, Happ LE, Dave T, Rajagopalan D, Datta J, Dunson DB, Dave SS. 2017. Genetic and Functional Drivers of Diffuse Large B Cell Lymphoma. *Cell* 171:481–494. doi:10.1016/j.cell.2017.09.027.

Rickman DS, Schulte JH, Eilers M. 2018. The expanding world of N-MYC-driven tumors. *Cancer Discov* 8:150–164. doi:10.1158/2159-8290.CD-17-0273.

Robledo M. 2012. MAX and MYC: A Heritable Breakup. *Cancer Res* 72:1–7. doi:10.1158/0008-5472.CAN-11-3891.

Romero OA, Torres-Diz M, Pros E, Savola S, Gomez A, Moran S, Saez C, Iwakawa R, Villanueva A, Montuenga LM, Kohno T, Yokota J, Sanchez-Cespedes M. 2014. MAX inactivation in small cell lung cancer disrupts MYC-SWI/SNF programs and is synthetic lethal with BRG1. *Cancer Discov* 4:292–303. doi:10.1158/2159-8290.CD-13-0799.

Romieu-Mourez R, Kim DW, Shin SM, Demicco EG, Landesman-Bollag E, Seldin DC, Cardiff RD, Sonenshein GE. 2003. Mouse Mammary Tumor Virus c-rel Transgenic Mice Develop Mammary Tumors. *Mol Cell Biol* 23:5738–5754. doi:10.1128/mcb.23.16.5738-5754.2003.

Roussel MF, Ashmun RA, Sherr CJ, Eisenman RN, Ayer DE. 1996. Inhibition of Cell Proliferation by the Mad1 Transcriptional Repressor. *Mol Cell Biol* 16:2796–2801.

Sakamuro D, Eviner V, Elliott KJ, Showe L, White E, Prendergast GC. 1995. c-Myc induces apoptosis in epithelial cells by both p53-dependent and p53-independent mechanisms. *Oncogene* 11:2411–2418.

Saksena S, Sun J, Chu T, Emr SD. 2007. ESCRTing proteins in the endocytic pathway. *Trends Biochem Sci* 32:561–573. doi:10.1016/j.tibs.2007.09.010.

Sans CL, Satterwhite DJ, Stoltzman CA, Breen KT, Ayer DE. 2006. MondoA-Mlx Heterodimers Are Candidate Sensors of Cellular Energy Status: Mitochondrial Localization and Direct Regulation of Glycolysis. *Mol Cell Biol* 26:4863–4871. doi:10.1128/mcb.00657-05.

Santamaría D, Barrière C, Cerqueira A, Hunt S, Tardy C, Newton K, Cáceres JF, Dubus P, Malumbres M, Barbacid M. 2007. Cdk1 is sufficient to drive the mammalian cell cycle. *Nature* 448:811–815. doi:10.1038/nature06046.

Schaub FX, Dhankani V, Berger AC, Trivedi M, Richardson AB, Shaw R, Zhao W, Zhang X, Ventura A, Liu Y, Ayer DE, Hurlin PJ, Cherniack AD, Eisenman RN, Bernard B, Grandori C, TCGA. 2018. Pan-cancer Alterations of the MYC Oncogene and Its Proximal Network across the Cancer Genome Atlas. *Cell Syst* 6:282-300.e2. doi:10.1016/j.cels.2018.03.003.

Schneider A, Peukert K, Eilers M, Hanel F. 1997. Association of Myc with the zinc-finger protein Miz-1 defines a novel pathway for gene regulation by Myc. *Curr Top Microbiol Immunol* 224:137–146.

Schneider U, Schwenk HU, Bornkamm G. 1977. Characterization of EBV-genome negative “null” and “T” cell lines derived from children with acute lymphoblastic leukemia and leukemic transformed non-Hodgkin lymphoma. *Int J cancer* 19:621–626.

Schreiber-Agus N, Chin L, Chen K, Torres R, Rao G, Guida P, Skoultchi A, Depinho RA. 1995. An Amino-Terminal Domain of Mxi1 Mediates Anti-Myc Oncogenic Activity and Interacts with a Homolog of the Yeast Transcriptional Repressor SIN3. *Cell* 80:777–786.

Schwab M, Alitalo K, Klempnauer KH, Varmus HE, Bishop JM, Gilbert F, Brodeur G, Goldstein M, Trent J. 1983. Amplified DNA with limited homology to myc cellular oncogene is shared by human neuroblastoma cell lines and a neuroblastoma tumour. *Nature* 305:245–248. doi:10.1038/305245a0.

Sears RC. 2004. The Life Cycle of C-Myc. *Cell Cycle* 3:1133–1137.

Seitz V, Butzhammer P, Hirsch B, Hecht J, Gütgemann I, Ehlers A, Lenze D, Oker E, Sommerfeld A, von der Wall E, König C, Zinser C, Spang R, Hummel M. 2011. Deep sequencing of MYC DNA-Binding sites in Burkitt lymphoma. *PLoS One* 6. doi:10.1371/journal.pone.0026837.

Sen R, Baltimore D. 1986a. Inducibility of κ immunoglobulin enhancer-binding protein NF-κB by a posttranslational mechanism. *Cell* 47:921–928. doi:10.1016/0092-8674(86)90807-X.

Sen R, Baltimore D. 1986b. Multiple nuclear factors interact with the immunoglobulin enhancer sequences. *Cell* 46:705–716.

Sheiness D, Bishop JM. 1979. DNA and RNA from uninfected vertebrate cells contain nucleotide sequences related to the putative transforming gene of avian myelocytomatosis virus. *J Virol* 31:514–21.

Shih HM, Liu Z, Towle HC. 1995. Two CACGTG motifs with proper spacing dictate the carbohydrate regulation of hepatic gene transcription. *J Biol Chem* 270:21991–21997. doi:10.1074/jbc.270.37.21991.

Shim H, Chun YS, Lewis BC, Dang C V. 1998. A unique glucose-dependent apoptotic pathway induced by c-Myc. *Proc Natl Acad Sci* 95:1511–1516.

Shim H, Dolde C, Lewis BC, Wu C-S, Dang G, Jungmann RA, Dalla-Favera R, Dang C V. 1997. c-Myc transactivation of LDH-A: Implications for tumor

metabolism and growth. *Proc Natl Acad Sci* 94:6658–6663.

Slotta C, Schlüter T, Ruiz-Perera LM, Kadhim HM, Tertel T, Henkel E, Hübner W, Greiner JFW, Huser T, Kaltschmidt B, Kaltschmidt C. 2017. CRISPR/Cas9-mediated knockout of c-REL in HeLa cells results in profound defects of the cell cycle. *PLoS One* 12:1–19. doi:10.1371/journal.pone.0182373.

Sommer A, Waha A, Tonn J, Sörensen N, Hurlin PJ, N ER, Lüscher B, Pietsch T. 1999. Analysis of the MAX-binding protein MNT in human medulloblastomas. *Int J cancer* 82:810–816.

Stacchini A, Aragno M, Vallario A, Alfarano A, Circosta P, Gottardi D, Faldella A, Rege-cambrin G, Thunberg U, Nilsson K, Caligaris-cappio F. 1999. MEC1 and MEC2: two new cell lines derived from B-chronic lymphocytic leukaemia in prolymphocytoid transformation. *Leuk Res* 23:127–136.

Stanton LW, Schwab M, Bishop JM. 1986. Nucleotide sequence of the human N-myc gene. *Proc Natl Acad Sci* 83:1772–1776. doi:10.1073/pnas.83.6.1772.

Steiger D, Furrer M, Schwinkendorf D, Gallant P. 2008. Max-independent functions of Myc in Drosophila melanogaster. *Nat Genet* 40:1084–1091. doi:10.1038/ng.178.

Stoltzman CA, Peterson CW, Breen KT, Muoio DM, Billin AN, Ayer DE. 2008. Glucose sensing by MondoA:Mlx complexes: A role for hexokinases and direct regulation of thioredoxin-interacting protein expression. *Proc Natl Acad Sci* 105:6912–6917. doi:10.1073/pnas.0712199105.

Subramanian A, Subramanian A, Tamayo P, Tamayo P, Mootha VK, Mootha VK, Mukherjee S, Mukherjee S, Ebert BL, Ebert BL, Gillette M a, Gillette M a, Paulovich A, Paulovich A, Pomeroy SL, Pomeroy SL, Golub TR, Golub TR, Lander ES, Lander ES, Mesirov JP, Mesirov JP. 2005. Gene set enrichment analysis: a knowledge-based approach for interpreting genome-wide expression profiles. *Proc Natl Acad Sci U S A* 102:15545–50. doi:10.1073/pnas.0506580102.

Sullivan JC, Kalaitzidis D, Gilmore TD, Finnerty JR. 2007. Rel homology domain-containing transcription factors in the cnidarian Nematostella vectensis. *Dev Genes Evol* 217:63–72. doi:10.1007/s00427-006-0111-6.

Sun S. 2017. The non-canonical NF-κB pathway in immunity and inflammation. *Nat Rev Immunol* 17:545–558. doi:10.1038/nri.2017.52.

Sun SC, Ganchi PA, Ballard DW, Greene WC. 1993. NF-kappa B controls expression of inhibitor I kappa B alpha: evidence for an inducible autoregulatory pathway. *Science* 259:1912–5. doi:10.1126/science.8096091.

Takahashi K, Yamanaka S. 2006. Induction of Pluripotent Stem Cells from Mouse Embryonic and Adult Fibroblast Cultures by Defined Factors. *Cell* 126:663–676. doi:10.1016/j.cell.2006.07.024.

Terragni J, Nayak G, Banerjee S, Medrano J, Graham JR, Brennan JF, Sepulveda S, Cooper GM. 2011. The E-box Binding Factors Max/Mnt, MITF, and USF1 Act Coordinately with FoxO to Regulate Expression of

Proapoptotic and Cell Cycle Control Genes by Phosphatidylinositol 3-Kinase/ Akt/Glycogen Synthase Kinase 3 Signaling. *J Biol Chem* 286:36215–36227. doi:10.1074/jbc.M111.246116.

Toyo-oka K, Bowen TJ, Hirotsune S, Li Z, Jain S, Ota S, Lozach LE, Bassett IG, Lozach J, Rosenfeld MG, Glass CK, Eisenman R, Ren B, Hurlin P, Wynshaw-Boris A. 2006. Mnt-Deficient Mammary Glands Exhibit Impaired Involution and Tumors with Characteristics of Myc Overexpression. *Cancer Res* 66:5565–6894. doi:10.1158/0008-5472.CAN-05-2683.

Toyo-oka K, Hirotsune S, Gambello MJ, Zhou Z, Olson L, Rosenfeld MG, Eisenman R, Hurlin P, Wynshaw-Boris A. 2004. Loss of the Max-interacting protein Mnt in mice results in decreased viability, defective embryonic growth and craniofacial defects: relevance to Miller-Dieker syndrome. *Hum Mol Genet* 13:1057–1067. doi:10.1093/hmg/ddh116.

Trapnell C, Pachter L, Salzberg SL. 2009. TopHat: Discovering splice junctions with RNA-Seq. *Bioinformatics* 25:1105–1111. doi:10.1093/bioinformatics/btp120.

Trapnell C, Roberts A, Goff L, Pertea G, Kim D, Kelley DR, Pimentel H, Salzberg SL, Rinn JL, Pachter L. 2012. Differential gene and transcript expression analysis of RNA-seq experiments with TopHat and Cufflinks. *Nat Protoc* 7:562–78. doi:10.1038/nprot.2012.016.

Tu WB, Helander S, Pilstål R, Hickman KA, Lourenco C, Jurisica I, Raught B, Wallner B, Sunnerhagen M, Penn LZ. 2015. Myc and its interactors take shape. *Biochim Biophys Acta - Gene Regul Mech* 1849:469–483. doi:10.1016/j.bbagrm.2014.06.002.

Van Doorn R, Dijkman R, Vermeer MH, Out-Luiting JJ, Van Der Raaij-Helmer EMH, Willemze R, Tensen CP. 2004. Aberrant expression of the tyrosine kinase receptor EphA4 and the transcription factor twist in Sézary syndrome identified by gene expression analysis. *Cancer Res* 64:5578–5586. doi:10.1158/0008-5472.CAN-04-1253.

Vaque JP, Fernandez-Garcia B, Garcia-Sanz P, Ferrandiz N, Bretones G, Calvo F, Crespo P, Marin MC, Leon J. 2008. c-Myc Inhibits Ras-Mediated Differentiation of Pheochromocytoma Cells by Blocking c-Jun Up-Regulation. *Mol Cancer Res* 6:325–339. doi:10.1158/1541-7786.mcr-07-0180.

Vastrik I, Kaipainen A, Penttila T-L, Lymboussakis A, Alitalo R, Parvinen M, Alitalo K. 1995. Expression of the mad Gene during Cell Differentiation In Vivo and Its Inhibition of Cell Growth In Vitro. *J Cell Biol* 128:1197–1208.

Vennstrom B, Sheiness D, Zabielski J, Bishop JM. 1982. Isolation and characterization of c-myc, a cellular homolog of the oncogene (v-myc) of avian myelocytomatosis virus strain 29. *J Virol* 42:773–9.

Vermeer MH, Van Doorn R, Dijkman R, Mao X, Whittaker S, Van Voorst Vader PC, Gerritsen MJP, Geerts ML, Gellrich S, Söderberg O, Leuchowius KJ, Landegren U, Out-Luiting JJ, Knijnenburg J, Ijszenga M, Szuhai K, Willemze R, Tensen CP. 2008. Novel and highly recurrent chromosomal alterations in

Sézary Syndrome. *Cancer Res* 68:2689–2698. doi:10.1158/0008-5472.CAN-07-6398.

Visekruna A, Volkov A, Steinhoff U. 2012. A key role for NF-κb transcription factor c-rel in T-lymphocyte-differentiation and effector functions. *Clin Dev Immunol* 2012. doi:10.1155/2012/239368.

Vita M, Henriksson M. 2006. The Myc oncoprotein as a therapeutic target for human cancer. *Semin Cancer Biol* 16:318–330. doi:10.1016/j.semcancer.2006.07.015.

Vo BHT, Wolf E, Kawauchi D, Gebhardt A, Rehg JE, Finkelstein D, Walz S, Murphy BL, Youn YH, Han YG, Eilers M, Roussel MF. 2016. The Interaction of Myc with Miz1 Defines Medulloblastoma Subgroup Identity. *Cancer Cell* 29:5–16. doi:10.1016/j.ccell.2015.12.003.

Wahlström T, Henriksson M. 2007. Mnt Takes Control as Key Regulator of the Myc/Max/Mxd Network. *Adv Cancer Res* 61–80. doi:10.1016/S0065-230X(06)97003-1.

Walker W, Zhou ZQ, Ota S, Wynshaw-Boris A, Hurlin PJ. 2005. Mnt-Max to Myc-Max complex switching regulates cell cycle entry. *J Cell Biol* 169:405–413. doi:10.1083/jcb.200411013.

Wang T, Wang G, Hao D, Liu X, Wang D, Ning N, Li X. 2015. Aberrant regulation of the LIN28A/LIN28B and let-7 loop in human malignant tumors and its effects on the hallmarks of cancer. *Mol Cancer* 14:1–13. doi:10.1186/s12943-015-0402-5.

Washkowitz AJ, Schall C, Zhang K, Wurst W, Floss T, Mager J, Papaioannou VE. 2015. Mga is essential for the survival of pluripotent cells during peri-implantation development 1:31–40. doi:10.1242/dev.111104.

Wei R, Qiu X, Wang S, Li Y, Wang Y, Lu K, Fu Y, Xing G, He F, Zhang L. 2015. NEDL2 is an essential regulator of enteric neural development and GDNF/Ret signaling. *Cell Signal* 27:578–586. doi:10.1016/j.cellsig.2014.12.013.

Wernicke CM, Richter GHS, Beinvogl BC, Plehm S, Schlitter AM, Bandapalli OR, Prazeres da Costa O, Hattenhorst UE, Volkmer I, Staege MS, Esposito I, Burdach S, Grunewald TGP. 2012. MondoA is highly overexpressed in acute lymphoblastic leukemia cells and modulates their metabolism, differentiation and survival. *Leuk Res* 36:1185–1192. doi:10.1016/j.leukres.2012.05.009.

Wheatley SP, Altieri DC. 2019. Survivin at a glance. *J Cell Sci* 132:jcs223826. doi:10.1242/jcs.223826.

Wilde BR, Ayer DE. 2015. Interactions between Myc and MondoA transcription factors in metabolism and tumourigenesis. *Br J Cancer* 113:1529–1533. doi:10.1038/bjc.2015.360.

Wu N, Zheng B, Shaywitz A, Dagon Y, Tower C, Bellinger G, Shen CH, Wen J, Asara J, McGraw TE, Kahn BB, Cantley LC. 2013. AMPK-Dependent Degradation of TXNIP upon Energy Stress Leads to Enhanced Glucose Uptake via GLUT1. *Mol Cell* 49:1167–1175.

doi:10.1016/j.molcel.2013.01.035.

Yancopoulos GD, Nisent PD, Tesfaye A, Kohl NE, Goldfarb MP, Alt FW. 1985. N-myc can cooperate with ras to transform normal cells in culture. *Proc Natl Acad Sci U S A* 82:5455–5459.

Yang G, Hurlin PJ. 2017. MNT and Emerging Concepts of MNT-MYC Antagonism. *Genes (Basel)* 8. doi:10.3390/genes8020083.

Yang H, Li TWH, Ko KS, Xia M, Lu SC. 2009. Switch from Mnt-Max to Myc-Max induces p53 and cyclin D1 expression and apoptosis during cholestasis in mouse and human hepatocytes. *Hepatology* 49:860–870. doi:10.1002/hep.22720.

Yang M, Yang S-L, Herrlinger S, Liang C, Dzieciatkowska M, Hansen KC, Desai R, Nagy A, Niswander L, Moss EG, Chen J-F. 2015. Lin28 promotes the proliferative capacity of neural progenitor cells in brain development. *Development* 142:1616–1627. doi:10.1242/dev.120543.

Yang W, Wei J, Guo T, Shen Y, Liu F. 2014. Knockdown of miR-210 decreases hypoxic glioma stem cells stemness and radioresistance. *Exp Cell Res* 326:22–35. doi:10.1016/j.yexcr.2014.05.022.

Yuneva M, Zamboni N, Oefner P, Sachidanandam R, Lazebnik Y. 2007. Deficiency in glutamine but not glucose induces MYC-dependent apoptosis in human cells. *J Cell Biol* 178:93–105. doi:10.1083/jcb.200703099.

Zervos AS, Gyuris J, Brent R. 1993. Mxi1, a Protein That Specifically interacts with Max to bind Myc-Max recognition sites. *Cell* 72:223–232.

Zhang Z, Sun H, Dai H, Walsh RM, Imakura M, Schelter J, Burchard J, Dai X, Chang AN, Diaz RL, Marszalek JR, Bartz SR, Carleton M, Cleary MA, Linsley PS, Grandori C. 2009. MicroRNA miR-210 modulates cellular response to hypoxia through the MYC antagonist MNT. *Cell Cycle* 8:2756–2768. doi:10.4161/cc.8.17.9387.

Zhou J, Yu Q, Chng WJ. 2011. TXNIP (VDUP-1, TBP-2): A major redox regulator commonly suppressed in cancer by epigenetic mechanisms. *Int J Biochem Cell Biol* 43:1668–1673. doi:10.1016/j.biocel.2011.09.005.

Resumen en castellano

8. Resumen en castellano

8.1. Introducción

MNT, perteneciente a la familia MXD, se considera un antagonista y modulador de MYC, una de las oncoproteínas más frecuentemente alteradas en cáncer. La actividad de MYC es muy amplia al regular procesos como el ciclo celular, la diferenciación, el crecimiento celular, el metabolismo o la apoptosis (Grandori et al., 2000; Kalkat et al., 2017). Tanto MYC como las proteínas MXDs son factores de transcripción de tipo hélice-lazo-hélice/cremallera de leucina (bHLHLZ) que heterodimerizan con MAX, se unen a secuencias específicas en el ADN denominadas E-boxes, generalmente activando (MYC-MAX) o reprimiendo (MXD-MAX) la transcripción de genes diana (Delgado and León, 2010; Hurlin et al., 2004; Vita and Henriksson, 2006; Yang and Hurlin, 2017). Las proteínas MXDs reprimen la transcripción gracias a su dominio SID, a través del que interaccionan con los correpresores SIN3A y SIN3B, que a su vez reclutan diversas proteínas con actividad histona deacetilasa. De esta manera, son capaces de compactar la cromatina e impedir así el acceso de la maquinaria de transcripción (Ayer et al., 1995; Grzenda et al., 2009; Halleck et al., 1995; Heinzel et al., 1997; Laherty et al., 1997).

MNT destaca entre el resto de las proteínas MXDs por varias razones. Primero, es el único homólogo de la familia MXD en *Drosophila melanogaster* (Loo et al., 2005), el mayor en tamaño y con expresión más ubicua. La falta de MNT en ratones resulta en defectos craneofaciales, deficiencias en el desarrollo embriónico y muerte a los pocos días del nacimiento (Hurlin et al., 2003; Toyo-oka et al., 2004), mientras que la deficiencia en *Mxd1*, *Mxd2* o *Mxd3* no afecta a la viabilidad (Hurlin and Huang, 2006). La pérdida de MNT suele provocar un fenotipo muy similar al de la sobreexpresión de MYC: mayor proliferación, susceptibilidad a la transformación por RAS y predisposición a la apoptosis (Link et al., 2012; Nilsson et al., 2004). Además, un reciente estudio muestra que la

deleción de *MNT* en cáncer tiene una frecuencia del 10% (Schaub et al., 2018). Sin embargo, la deficiencia de MNT en otros modelos disminuye la tumorogénesis dependiente de MYC. Esto es debido a la función pro-supervivencia de MNT, que contrarresta la apoptosis causada por un exceso de MYC y mantiene la viabilidad de las células tumorales (Campbell et al., 2017).

Hasta ahora, las funciones de MNT siempre se han asociado a su actividad con MAX. Sin embargo, desde que se describieron tumores y líneas celulares deficientes en *MAX* (Burnichon et al., 2012; Comino-Méndez et al., 2011; Hopewell and Ziff, 1995; Romero et al., 2014), se abrió la posibilidad de que existieran funciones de MNT aún desconocidas e independientes de MAX. Nuestros resultados previos parten de la línea celular UR61, derivada la línea celular PC12 de feocromocitoma de rata y que expresa una forma no funcional de la proteína MAX a causa de una deleción (Hopewell and Ziff, 1995).

Por una parte, se llevó a cabo un análisis proteómico previo en nuestro laboratorio (Mª Carmen Lafita y el grupo de Alex von Kriegsheim en *Conway Institute of Biomolecular and Biomedical Research*, Dublín) de inmunoprecipitados de MNT en UR61. En seis experimentos independientes se obtuvieron cinco proteínas, una de las cuales era REL, miembro de la familia NF-κB, para su posterior estudio en esta tesis. Las proteínas NF-κB se encuentran presentes en casi todos los tipos celulares y están implicados en múltiples procesos biológicos, tales como inflamación, inmunidad, diferenciación, crecimiento celular y apoptosis. REL se encuentra alterado en diferentes tipos de tumores, principalmente de tipo linfoide pero también en tumores sólidos (Gilmore and Gerondakis, 2011; Hunter et al., 2016).

Por otra parte, se ha descrito que MLX, una proteína similar a MAX, puede interaccionar con MXD1, MXD4 y MNT (Billin et al., 1999; Meroni et al., 2000). MLX también es un factor de transcripción de tipo bHLHLZ y está implicado en estrés metabólico y respuesta a nutrientes junto con MLXIP y MLXIPL (Carroll et al., 2015; Diolaiti et al., 2015). En estudios previos de nuestro grupo, se observó que MNT era necesario para la óptima proliferación de células UR61, carentes de MAX, y que regulaba la expresión de un grupo de genes (Lafita-Navarro, Tesis

2015). Al ser todo ello en ausencia de MAX, nos planteamos si MNT lo estaba llevando a cabo interaccionando con MLX. Otra posibilidad era que estuviera formando homodímeros, tal y como había detectado Meroni *et al.*, (1997) por ensayos de doble híbrido y co-inmunoprecipitaciones *in vitro*.

8.2. Objetivos

Desde su descubrimiento, varios estudios han demostrado la importancia de MNT para la homeostasis celular y, más concretamente, para la actividad de MYC. Sin embargo, poco se sabe sobre la regulación de MNT o sobre sus interacciones con otras proteínas al margen de MAX. Esta tesis tiene por tanto el objetivo de expandir el conocimiento que tenemos sobre MNT y su papel en la red proximal de MYC.

MNT como regulador de la vía NF-κB

1) Confirmar la interacción entre MNT y REL en diferentes líneas celulares humanas, de rata y de ratón.
2) Investigar si otras proteínas NF-κB también forman parte del complejo con MNT.
3) Estudiar el dominio de MNT implicado en la interacción con REL y la localización subcelular de los complejos.
4) Analizar el impacto de la interacción MNT-REL sobre la actividad de REL en la vía de señalización de NF-κB.

Funciones de MNT más allá de su interacción con MAX

1) Estudiar la formación de heterodímeros MNT-MLX u homodímeros MNT-MNT.
2) Comprobar si MNT y MLX tienen algún papel en la proliferación y regulación génica, incluyendo su unión directa al ADN.
3) Analizar la regulación de MNT a nivel transcripcional y post-transcripcional.

Regulación transcripcional por MNT

1) Determinar nuevas dianas de MNT por medio del análisis del transcriptoma de las células HAP1 *knockout* para MNT.
2) Analizar el papel de MAX y de MLX en la regulación de nuevas dianas de MNT.

8.3. Resultados y discusión

8.3.1. MNT como regulador de la vía NF-κB

En esta primera parte, estudiamos la interacción entre MNT y REL que había sido detectada previamente en nuestro laboratorio por estudios de co-inmunoprecipitación y posterior proteómica (Lafita-Navarro, Tesis 2015). Primero, confirmamos la interacción en líneas celulares de ratón (Neuro-2a), rata (U7/UR61, C6) y humanas (LoVo y CEM). Esta interacción es independiente de MAX y es detectada tanto en el citoplasma como en el núcleo. Posteriormente, observamos que el silenciamiento de *MNT* provoca la translocación de REL al núcleo, la activación de la vía de señalización NF-κB y el aumento de dos dianas de REL: IκBα and BCL-XL. Por el contrario, la sobreexpresión de MNT provoca la represión de la vía de señalización NF-κB y la disminución de los niveles de mRNA de *NFKBIA* (IκBα) y *BCL2L1* (BCL-XL). Finalmente, detectamos la unión de MNT y de REL al gen *NFKBIA* (IκBα) por ensayos de inmunoprecipitación de cromatina. Además, el pico máximo de unión de ambas proteínas coincide en +171/+343 con respecto al punto de inicio de la transcripción. Estos resultados indican que MNT es un represor de la vía NF-κB y, más concretamente, de REL. Por un lado, MNT puede estar reteniendo los dímeros de REL inactivos en el citoplasma y, por otro, formando complejos represores en aquellos genes que normalmente son activados por REL. De esta manera, hemos podido confirmar una nueva función de MNT, independiente de MAX, que establece una nueva conexión entre las vías oncogénicas de MYC y de NF-κB.

8.3.2. Funciones de MNT más allá de su interacción con MAX

En esta segunda parte, estudiamos cómo funciona MNT en las células UR61, deficientes en MAX. Nuestros resultados confirman que MNT puede formar homodímeros y heterodímeros con MLX a través del dominio bHLHLZ. La inducción de MAX en las células UR61 desplaza el equilibrio hacia dímeros MNT-MAX, lo que puede indicar una preferencia de MNT por MAX. Además, observamos una disminución en la proliferación de las células al silenciar *MNT* y *MLX*, señalando el importante papel que tienen estas dos proteínas en la supervivencia de las células UR61. Asimismo, demostramos que MNT es capaz de regular la expresión génica en ausencia de MAX por unión directa al ADN. En concreto, MNT regula genes relacionados con la proliferación y los mecanismos de reparación del ADN, como *BRCA1*, *CDK1*, *BIRC5*/*Survivin*, *ERCC6*, *FBXO32*. Por último, estudiamos la regulación de MNT. Por una parte, nuestros resultados muestran la represión directa por MNT de su propio promotor. La E-box no canónica CATGTG, a -788 pb del punto de inicio de la transcripción, es la que está implicada en la regulación de MNT. Aunque esta autoregulación negativa de MNT es detectada en células sin MAX, la represión se intensifica con la inducción de MAX. Por otra parte, los niveles de MNT en UR61 son altos y no es posible su sobreexpresión a nivel de proteína. Analizando su secuencia de aminoácidos, encontramos tres secuencias de degradación PEST. Después, estudiamos la expresión de diversos mutantes con deleciones en MNT y observamos niveles de expresión más altos en los mutantes carentes de estas secuencias. Por tanto, confirmamos que existe una autoregulación de MNT también a nivel de proteína. Teniendo en cuenta todos estos datos, podemos decir que los niveles de MNT están muy controlados, lo que es indicativo del papel clave que tiene MNT en la homeostasis celular.

8.3.3. Regulación transcripcional por MNT

En esta tercera parte nos hemos basado en el modelo celular de las HAP1, que derivan de la línea de leucemia mieloide crónica KBM-7 (Essletzbichler et al., 2014). Al ser unas células casi haploides, son adecuadas para la producción de mutantes *knockout* (KO) con la tecnología del CRISPR/Cas9 (Ran et al., 2013). Una vez obtuvimos las células MNT KO y *wild type* (WT) de Horizon, decidimos

analizar los niveles de MNT, MAX, MLX y MYC, junto con su proliferación. Curiosamente, observamos una disminución de MYC y una mayor tasa de proliferación de las células MNT KO. Este fenotipo había sido observado anteriormente en modelos de ratón (Hurlin et al., 2003; Toyo-oka et al., 2004). Después, llevamos a cabo experimentos de RNA-seq y obtuvimos 460 genes alterados por la eliminación de *MNT*; alrededor de la mitad de ellos estaban aumentados y la otra mitad, disminuidos. El análisis ontológico reveló que los genes afectados por la depleción de *MNT* estaban relacionados con proliferación, diferenciación, desarrollo, neurogénesis, respuesta a estímulos y adhesión. Tras validar el RNA-seq por RT-qPCR, decidimos silenciar *MAX* y *MLX* y analizar los efectos de estas dos proteínas en la expresión génica. De esta manera, clasificamos los genes en regulados por MNT-MAX, MNT-MLX o MNT-MNT/? (homodímeros MNT-MNT o MNT unido a una proteína desconocida). Finalmente, con nuestros datos y los ChIP-seqs publicados en la base de datos ENCODE, pudimos definir varias dianas directas de MNT: *LIN28A*, *WIPI1*, *FOXG1*, *HECW2*, *MYB* y *CHMP4C*.

Finalmente, podemos concluir que nuestro trabajo contribuye a la profundización en nuestro conocimiento sobre MNT, sus funciones y sus interacciones. MNT regula múltiples procesos para la correcta homeostasis celular y tiene un papel clave en la red proximal de MYC, uniendo las ramas de MAX y de MLX. El estudio de las funciones específicas de cada uno de los miembros de la red y de cómo afectan a las funciones de MYC podrá sin duda conducir al desarrollo de estrategias para contrarrestar la tumorogénesis llevada a cabo por MYC.

8.4. Conclusiones

1) MNT interacciona con REL en líneas celulares de ratón (Neuro-2a), de rata (U7/UR61, C6) y de humano (LoVo, CEM), tanto en el núcleo como en el citoplasma, independientemente de MAX.

2) El silenciamiento de MNT provoca la translocación de REL al núcleo, la activación de la vía de señalización de NF-κB y el aumento de los niveles de dos dianas de REL: IκBα and BCL-XL.
3) MNT reprime *NFKBIA* (que codifica para IκBα) por medio de la unión directa a regiones reguladoras de su gen. El pico máximo de unión se detecta en +171/+343 con respecto al punto de inicio de la transcripción y coincide con el pico de unión de REL en el gen *NFKBIA.*
4) MNT forma homodímeros y heterodímeros con MLX en células UR61 a través del dominio bHLH.
5) Los dímeros MNT-MLX se localizan tanto en el citoplasma como en el núcleo.
6) MNT y MLX son necesarios para la proliferación óptima de las células en ausencia de MAX.
7) MNT regula la expresión de genes implicados en ciclo celular y reparación del ADN en ausencia de MAX.
8) MNT se une directamente a *BIRC5*, *CDK1* and *BRCA1* (para activar su transcripción) y a *FBXO32*, *CCNG2* and *ERCC6* (para reprimir su transcripción).
9) MNT se une a *E-boxes* y a motivos de unión de factores de transcripción de tipo *forkhead* en ausencia de MAX.
10) MNT autorregula negativamente su promotor a través de la *E-box* 2 (CATGTG) situada a -788 del punto de inicio de la transcripción, en colaboración con MAX.
11) MNT se encuentra en exceso en las células deficientes en MAX y no es posible llevar a cabo su sobreexpresión.
12) Las células HAP1 *knockout* para MNT proliferan más rápido, incluso a pesar de tener niveles más bajos de MYC.
13) MNT regula la transcripción génica tanto como un activador como un represor, en complejos MNT-MAX, MNT-MLX o MNT-MNT/?, afectando a múltiples procesos celulares, incluyendo desarrollo, proliferación, diferenciación o respuesta a estímulos externos.

Annexes

9. Annexes

Annex 1. ChIP-seq results. The table shows the genes and regions detected in the ChIP-seq experiments (in triplicate) with a q-value <0.7. Chrom, chromosome.

Gene	Chrom	Start	End	TSS distance	Signal	q-value	Annotation
AABR07003040.1	chr1	94473713	94474035	-19692	141.86198	0.00001	Intergenic
MCM7	chr12	19312805	19313475	876	105.2951	0.00001	intron (ENSRNOT00000001825. intron 1 of 13)
YTHDC2	chr1	180971723	180972393	1168512	49.84661	0.00001	Intergenic
CCNG2	chr14	16275925	16276657	-223	499.62541	0.00001	promoter-TSS (ENSRNOT00000002876)
FOXK1	chr14	16275925	16276657	-35451	192.85369	0.00001	Intergenic
RIOK2	chr1	82452065	82452735	-143	115.75299	0.00001	promoter-TSS (ENSRNOT00000017165)
CDC40	chr9	41337486	41338156	16	128.25274	0.00001	promoter-TSS (ENSRNOT00000087740)
PHF21B	chr1	180738768	180739438	28364	110.59105	0.00001	intron (ENSRNOT00000017906. intron 2 of 12)
AABR07035428.2	chr12	19328514	19329184	17579	115.50543	0.00001	intron (ENSRNOT00000001466. intron 2 of 8)
CDK12	chr12	14200676	14200946	-649	131.03918	0.00001	promoter-TSS (ENSRNOT00000082668)
RPS6KA5	chr6	124735773	124736443	-330	113.89653	0.00001	promoter-TSS (ENSRNOT00000091693)
AABR07064998.2	chr10	11205633	11206303	8528	98.78731	1.14956E-05	Intergenic
KLHL24	chr13	89445422	89446092	-10343	101.2998	1.71845E-05	Intergenic
TNRC6B	chr7	121930127	121930797	-153	85.87448	2.70396E-05	promoter-TSS (ENSRNOT00000033975)
HBP1	chr6	51257652	51258322	-362	86.06352	3.93079E-05	promoter-TSS (ENSRNOT00000012004)
KDM5B	chr10	86156624	86157294	-2633	88.85319	5.37023E-05	Intergenic
LOC103690980	chr1	54058156	54058826	-3695	21.96606	6.73184E-05	Intergenic
GABARAPL1	chr20	40913271	40913941	-353	82.66174	8.09128E-05	promoter-TSS (ENSRNOT00000077356)
LOC100911356	chr13	90513902	90514572	-99	80.84637	9.42048E-05	promoter-TSS (ENSRNOT00000088996)
CDC40	chr1	46329360	46330030	-69	88.46051	0.000108611	promoter-TSS (ENSRNOT00000087740)
YTHDC2	chr6	103938301	103938971	1401239	83.42893	0.000123613	Intergenic
RF00002	chr7	2201465	2202135	20153	80.45633	0.000140917	Intergenic
MCM7	chr12	19313004	19313674	677	73.05478	0.000158173	promoter-TSS (ENSRNOT00000001827)
TNRC6B	chr7	121930333	121931003	30	66.555	0.000174939	promoter-TSS (ENSRNOT00000033975)
TCP11L2	chr7	24893820	24894490	-8380	79.92627	0.00019055	Intergenic
CCNG2	chr6	103798975	103799645	-223	75.17918	0.00020692	promoter-TSS (ENSRNOT00000002876)
FBXO32	chr7	98098039	98098709	-106	80.31343	0.000224979	promoter-TSS (ENSRNOT00000010361)
CYP2B1	chr7	98098238	98098908	116213	22.85698	0.00024348	Intergenic

FCGR2B	chr20	48503654	48504324	-11942	69.35571	0.000264378	Intergenic
LOC683469	chr16	15111110	15111780	140	111.42867	0.000284299	exon (ENSRNOT00000060703. exon 1 of 4)
ZDBF2	chr9	70041233	70041903	-18115	39.51652	0.000304983	Intergenic
TMEM242	chr1	180692356	180693026	-13	76.29343	0.000324734	promoter-TSS (ENSRNOT00000046311)
VOM2R37	chr1	99094686	99095356	40956	71.98416	0.000343835	intron (ENSRNOT00000056515. intron 4 of 4)
KMT5B	chr1	219001037	219001707	528	75.31798	0.000362686	intron (ENSRNOT00000022486. intron 1 of 11)
YTHDC2	chr1	180692621	180693291	1447614	39.92178	0.000380706	Intergenic
AABR07020651.1	chr13	33592719	33593389	-555749	71.01038	0.000400596	Intergenic
VOM2R37	chr1	261090347	261091017	40607	74.08927	0.000421532	intron (ENSRNOT00000056515. intron 4 of 4)
ERCC6	chr17	11757325	11757995	-94	75.48635	0.000447244	promoter-TSS (ENSRNOT00000088529)
KLHL24	chr11	84643306	84643976	-10137	68.63935	0.000478866	Intergenic
FRAT2	chr11	84643512	84644182	-245	23.3752	0.000509283	promoter-TSS (ENSRNOT00000072055)
JADE1	chr2	128463555	128464225	2666	71.17905	0.000540268	intron (ENSRNOT00000018872. intron 1 of 10)
CNPY4	chr1	1154969	1155639	-108	71.86791	0.000571608	promoter-TSS (ENSRNOT00000033288)
RF00100	chr7	125677717	125678387	89652	64.84703	0.000605207	Intergenic
TRIB1	chr2	49293013	49293683	0	85.17743	0.00063833	promoter-TSS (ENSRNOT00000005885)
LOC500684	chr1	59129473	59130143	-3514	71.46528	0.000672414	Intergenic
AABR07001599.1	chr1	54194237	54194907	-67003	67.95892	0.000707325	Intergenic
PSMG3	chr12	16898649	16899319	-41	70.48702	0.000759004	promoter-TSS (ENSRNOT00000001716)
AABR07072837.1	chr16	8733606	8734276	115155	65.08933	0.000810198	Intergenic
FAM168B	chr20	48503860	48504530	-323	55.92799	0.000862675	promoter-TSS (ENSRNOT00000039480)
B4GALT7	chr17	9558369	9559039	-70	66.42193	0.000922618	promoter-TSS (ENSRNOT00000036223)
TICRR	chr1	141391129	141391799	202	55.81323	0.000998125	exon (ENSRNOT00000031783. exon 1 of 22)
GPR19	chr13	51381421	51382091	-10151	64.86881	0.001086841	Intergenic
AABR07044408.2	chr20	4908400	4909070	-1330	58.00027	0.001172757	intron (ENSRNOT00000082497. intron 3 of 7)
FBXO32	chr4	163293036	163293706	-305	66.1557	0.001258143	promoter-TSS (ENSRNOT00000010361)
YTHDC2	chr1	180738996	180739666	1447879	80.77813	0.00134206	Intergenic
NLRP5	chr1	71522380	71523050	-35925	41.05807	0.001424138	Intergenic
YTHDC2	chr7	99273997	99274667	1401467	71.32363	0.001508499	Intergenic
PIM3	chr7	129861410	129862080	1418	59.23681	0.001603877	intron (ENSRNOT00000085835. intron 2 of 3)
LOC102547056	chr7	99954157	99954827	-25628	65.3391	0.001698674	Intergenic
TFAP4	chr4	168666489	168667159	-258	59.35772	0.001799633	promoter-TSS (ENSRNOT00000006979)
RF00100	chr2	49293212	49293882	89851	24.84731	0.001908816	Intergenic
AABR07020651.1	chr13	33475503	33476173	-672965	42.61725	0.002017744	Intergenic
AABR07020651.1	chr13	33475950	33476620	-672518	39.04096	0.002127086	Intergenic
EXOSC5	chr12	14279432	14280102	-69	59.9738	0.002233161	promoter-TSS (ENSRNOT00000027995)

NLRP5	chr1	71522174	71522844	-35719	57.67713	0.002337707	Intergenic
GTF2A1	chr6	115351084	115351754	1262	61.47071	0.002443222	intron (ENSRNOT00000005873. intron 1 of 8)
PPM1D	chr10	72950754	72951424	41539	62.73382	0.002561675	Intergenic
AABR07055191.1	chr7	507126	507796	91836	57.4641	0.002679705	Intergenic
CDK5RAP1	chr3	149870122	149870792	-44	56.23081	0.002823397	promoter-TSS (ENSRNOT00000021418)
AABR07055191.1	chr7	507341	508011	92051	21.58931	0.002965384	Intergenic
AABR07008309.1	chr2	52814728	52815398	31681	55.90037	0.003170881	Intergenic
AABR07052589.1	chr1	99095035	99095705	-326	59.13497	0.003371631	promoter-TSS (ENSRNOT00000081267)
GABARAPL1	chr4	163293250	163293920	-139	53.76585	0.00359703	promoter-TSS (ENSRNOT00000077356)
MSX2	chr3	64852433	64853103	73798	66.28574	0.003818968	Intergenic
AABR07056118.1	chr7	20244905	20245575	-17440	33.27867	0.004125304	Intergenic
RGD1561114	chr18	41909267	41909937	-10152	50.33628	0.004483777	Intergenic
RGD1560718	chr1	54042364	54043034	-6631	69.79567	0.004875936	Intergenic
HARBI1	chr3	80614247	80614917	-355	49.58747	0.005264935	promoter-TSS (ENSRNOT00000065462)
H2AFV	chr14	86706689	86707359	-398	93.27539	0.005673173	promoter-TSS (ENSRNOT00000082893)
NPTN	chr8	63367659	63368329	-11093	51.70575	0.006073639	Intergenic
FCGR2B	chr13	89445627	89446297	-12147	81.88358	0.006483044	Intergenic
YIPF4	chr6	22138194	22138864	-243	51.16993	0.006883051	promoter-TSS (ENSRNOT00000007607)
LRRC55	chr3	72574884	72575554	27329	51.48408	0.007345223	Intergenic
AABR07035428.2	chr12	14200707	14201377	17348	59.71487	0.007797978	intron (ENSRNOT00000001466. intron 2 of 8)
UBTF	chr10	90265983	90266653	-1301	58.43918	0.008284189	Intergenic
STARD13	chr12	1107296	1107966	87960	52.35659	0.00876482	intron (ENSRNOT00000001446. intron 1 of 13)
NPAS4	chr1	220264833	220265503	604	51.97184	0.009234662	intron (ENSRNOT00000027119. intron 1 of 7)
SMG7	chr13	70321869	70322539	-452	52.52221	0.009715675	promoter-TSS (ENSRNOT00000092336)
AC117971.2	chr7	19667621	19668291	172813	39.32676	0.01033913	Intergenic
AABR07001599.1	chr1	54184192	54184862	-56958	59.38015	0.010968267	Intergenic
AABR07018078.1	chr15	38709374	38710044	275	33.12022	0.011584892	intron (ENSRNOT00000074738. intron 1 of 8)
AABR07018078.1	chr15	38709701	38710371	-52	28.54126	0.01219596	promoter-TSS (ENSRNOT00000074738)
AABR07072837.1	chr20	40913486	40914156	114940	23.2056	0.012801091	Intergenic
PPM1D	chr10	72950964	72951634	41749	40.05863	0.013414578	Intergenic
SELENOW	chr1	77301728	77302398	233618	46.3042	0.014049601	Intergenic
ZMIZ1	chr16	1750582	1751252	1726	53.35757	0.014718651	intron (ENSRNOT00000014004. intron 1 of 23)
SETDB2	chr15	39680176	39680846	24697	52.78306	0.015386435	Intergenic
STARD13	chr12	1107512	1108182	87744	41.88815	0.016051957	intron (ENSRNOT00000001446. intron 1 of 13)
LOC683469	chr16	15111317	15111987	-67	45.20156	0.016733855	promoter-TSS (ENSRNOT00000060703)
LOC103690980	chr1	54059171	54059841	-2680	50.97429	0.017407203	Intergenic
RF00002	chr7	2113554	2114224	108064	62.04688	0.018070327	Intergenic

AABR07038886.1	chrX	63460760	63461430	-23031	59.49312	0.018748261	intron (ENSRNOT00000048127. intron 7 of 9)
RGD1566337	chr2	194753267	194753937	122360	45.98072	0.019425714	Intergenic
BRCA1	chr10	89455019	89455689	-673	47.67085	0.0201037	promoter-TSS (ENSRNOT00000028109)
VOM2R9	chr1	56002976	56003646	-107675	47.04095	0.020971573	Intergenic
RGD1566337	chr2	194768846	194769516	106781	31.99474	0.02183861	Intergenic
RF00619	chr8	49186038	49186708	-15483	56.46441	0.022690549	Intergenic
RGD1566337	chr2	194753479	194754149	122148	30.14443	0.023533688	Intergenic
LOC103690980	chr1	54058954	54059624	-2897	71.406	0.024373113	Intergenic
HMGA1	chr20	7138481	7139151	2809	56.94055	0.025206991	intron (ENSRNOT00000000580. intron 3 of 3)
RGD1566337	chr2	194769205	194769875	106422	51.80844	0.02602963	Intergenic
TACO1	chr10	94259818	94260488	-44	48.49478	0.026850291	promoter-TSS (ENSRNOT00000063973)
MSX2	chr17	11759645	11760315	76118	61.04175	0.027684456	Intergenic
AABR07060519.1	chr4	77447806	77448476	-1517	71.21372	0.028504734	Intergenic
AABR07001207.1	chr1	38786656	38787326	48516	54.12794	0.02932115	Intergenic
PCID2	chr16	81757234	81757904	598	46.49768	0.030216141	promoter-TSS (ENSRNOT00000092551)
TREM1	chr9	14795920	14796590	13192	35.94014	0.031099399	intron (ENSRNOT00000049193. intron 1 of 3)
TREM1	chr9	14796225	14796895	12887	30.47532	0.031975769	intron (ENSRNOT00000049193. intron 1 of 3)
NDUFC2	chr1	162364427	162365097	-5039	45.74886	0.032848156	Intergenic
NDUFC2	chr1	162364628	162365298	-4838	22.17121	0.033709398	Intergenic
MRPL3	chr8	113603484	113604154	286	53.20523	0.034558668	intron (ENSRNOT00000017280. intron 1 of 9)
RPL18	chr1	101700460	101701130	-1180	45.21348	0.035434067	Intergenic
TREM1	chr9	14795693	14796363	13419	34.77309	0.036343019	intron (ENSRNOT00000049193. intron 1 of 3)
CDC25C	chr18	27550205	27550875	-316	51.928	0.037277176	promoter-TSS (ENSRNOT00000037368)
CDC25C	chr18	27550406	27551076	-517	34.61044	0.038203926	promoter-TSS (ENSRNOT00000037368)
FLT1	chr12	9140371	9141041	106398	50.05784	0.039147046	intron (ENSRNOT00000001248. intron 14 of 29)
BRD3	chr3	6025139	6025809	-7877	53.71638	0.040081134	intron (ENSRNOT00000084491. intron 1 of 12)
GPAT4	chr16	73609296	73609966	-6318	49.05042	0.041001713	Intergenic
POTEM	chr16	22100886	22101556	15613	45.18363	0.042100475	intron (ENSRNOT00000078734. intron 3 of 3)
HTT	chr14	81279360	81280030	-25058	46.23735	0.043185306	intron (ENSRNOT00000015894. intron 10 of 15)
TMEM101	chr10	90095254	90095924	507	15.76812	0.044262914	exon (ENSRNOT00000081539. exon 2 of 4)
TMEM101	chr10	90095737	90096407	24	37.12887	0.045328568	promoter-TSS (ENSRNOT00000081539)
FCGR2B	chr13	89445826	89446496	-12346	18.69553	0.046383979	Intergenic
SELENOW	chr1	77301266	77301936	234080	27.50438	0.047434246	Intergenic
AABR07059198.1	chr4	8317599	8318269	61323	50.53929	0.048496679	Intergenic

RF00001	chr10	76492260	76492930	-954	48.17227	0.049617514	promoter-TSS (ENSRNOT00000070730)
STAT3	chr10	88842224	88842894	-326	49.69294	0.050740764	promoter-TSS (ENSRNOT00000026760)
AABR07025272.1	chr16	31323558	31324228	-22013	40.53565	0.051855879	Intergenic
GALR1	chr18	79272865	79273535	-14630	46.91985	0.053015883	Intergenic
CYP2B1	chr7	99274196	99274866	116412	36.38855	0.054177131	Intergenic
RF00002	chr2	436776	437446	-27187	44.56362	0.055333992	Intergenic
AABR07010672.1	chr2	147015512	147016182	9017	37.69849	0.056534298	Intergenic
RGD1561114	chr18	41908263	41908933	-9148	34.85485	0.057754523	Intergenic
RGD1561114	chr18	41908463	41909133	-9348	16.48493	0.058965638	Intergenic
AABR07044408.2	chr20	4906498	4907168	-3232	32.31656	0.060242086	intron (ENSRNOT00000082497. intron 3 of 7)
AC117971.2	chr7	19741089	19741759	99345	42.06498	0.061507348	Intergenic
AC117971.2	chr7	19741486	19742156	98948	23.00879	0.062760587	Intergenic
LOC102556187	chr6	32923692	32924362	42140	49.21752	0.064032138	Intergenic
AABR07000639.1	chr1	20659859	20660529	77111	43.88361	0.065312153	Intergenic
SLBP	chr14	82356516	82357186	-65	50.38805	0.066578959	promoter-TSS (ENSRNOT00000040229)
VPS52	chr20	5441259	5441929	112	45.1531	0.0678419	promoter-TSS (ENSRNOT00000037499)
RPS18	chr20	5441508	5442178	-33	18.30675	0.069094583	promoter-TSS (ENSRNOT00000037499)
AABR07044408.3	chr20	4903285	4903955	-2442	47.96866	0.070335892	intron (ENSRNOT00000082497. intron 3 of 7)
AABR07020651.1	chr13	33570678	33571348	-577790	30.78465	0.071608075	Intergenic
AABR07026565.2	chr16	83848477	83849147	-4149	43.55749	0.072887659	TTS (ENSRNOT00000032918)
POTEM	chr16	22100636	22101306	15863	51.44588	0.074155608	intron (ENSRNOT00000078734. intron 3 of 3)
CNPY4	chr12	19328714	19329384	92	30.07372	0.075422166	promoter-TSS (ENSRNOT00000033288)
LOC365791	chr2	137390918	137391588	13743	49.14647	0.076678039	intron (ENSRNOT00000090907. intron 6 of 20)
AABR07001100.1	chr1	38024112	38024782	-34440	22.1122	0.07803025	Intergenic
AABR07001100.1	chr1	38024463	38025133	-34791	36.73648	0.079371393	Intergenic
CEP250	chr3	151517564	151518234	9538	18.19461	0.080757711	intron (ENSRNOT00000055251. intron 10 of 29)
CEP250	chr3	151517882	151518552	9856	21.92452	0.082130223	intron (ENSRNOT00000055251. intron 10 of 29)
AABR07044397.1	chr20	4665532	4666202	11167	54.24702	0.083496448	intron (ENSRNOT00000061027. intron 6 of 7)
STPG2	chr2	244497315	244497985	-24049	42.63433	0.08485765	Intergenic
AABR07037307.1	chrX	18211837	18212507	48814	25.53123	0.086209872	Intergenic
TXNDC11	chr10	4601679	4602349	23545	35.0067	0.087626003	intron (ENSRNOT00000003332. intron 4 of 11)
LOC102551100	chr3	92145223	92145893	50444	24.26132	0.089035254	Intergenic
LOC102551100	chr3	92145463	92146133	50684	18.30459	0.090433221	Intergenic
USP49	chr9	15370131	15370801	4899	34.67345	0.091880214	intron (ENSRNOT00000018550. intron 1 of 6)
MRPL3	chr8	113603707	113604377	509	30.29603	0.09335466	intron (ENSRNOT00000017280. intron 1 of 9)

AABR07002845.1	chr1	86811240	86811910	-7961	42.62292	0.094841846	Intergenic
USPL1	chr12	6956613	6957283	-34	40.28789	0.096314129	promoter-TSS (ENSRNOT00000001210)
BORCS8	chr16	21028848	21029518	-49	66.43373	0.097824131	promoter-TSS (ENSRNOT00000041221)
CCPG1	chr8	79660286	79660956	-36	39.42697	0.099342938	promoter-TSS (ENSRNOT00000089949)
RGD1560718	chr1	54043674	54044344	-7941	45.39796	0.100846307	Intergenic
ACVR1	chr3	44515345	44516015	7250	32.08571	0.102337075	intron (ENSRNOT00000006963. intron 1 of 10)
AABR07063599.1	chr6	36582330	36583000	148669	38.80732	0.103825732	Intergenic
AABR07063599.1	chr6	36582531	36583201	148468	32.14693	0.10530088	Intergenic
AABR07006038.1	chr1	214988416	214989086	16390	24.25222	0.106789856	intron (ENSRNOT00000088263. intron 1 of 1)
AABR07006038.1	chr1	214988209	214988879	16597	43.50945	0.108265229	intron (ENSRNOT00000088263. intron 1 of 1)
AABR07001734.1	chr1	55756034	55756704	48971	54.31549	0.109726367	Intergenic
STX18	chr14	77482839	77483509	9736	42.14681	0.111175733	intron (ENSRNOT00000008410. intron 1 of 10)
SMPDL3A	chr20	40829099	40829769	50507	39.28369	0.11263309	Intergenic
PCTP	chr10	77523962	77524632	-12265	42.91245	0.114074349	Intergenic
OLR1197	chr8	40266918	40267588	4422	44.19033	0.115501068	Intergenic
FGF8	chr1	265469367	265469697	29299	47.08488	0.11693136	Intergenic
AABR07027039.1	chr17	11787153	11787823	64047	41.54954	0.118358649	Intergenic
ARHGAP26	chr18	32087970	32088640	119444	36.1573	0.119771641	intron (ENSRNOT00000018843. intron 4 of 23)
RBMS2	chr7	2592579	2593249	-4071	21.29832	0.121171086	Intergenic
RBMS2	chr7	2592375	2593045	-3867	41.98764	0.122555837	Intergenic
TMEM220	chr10	53533391	53534061	-37263	49.53787	0.123938147	Intergenic
ZDBF2	chr9	70039232	70039902	-20116	36.6284	0.125323351	Intergenic
RPS6KA5	chr6	124735982	124736652	-539	56.10978	0.126702446	promoter-TSS (ENSRNOT00000091693)
AABR07026339.1	chr16	72588872	72589542	-107740	24.40548	0.128077252	Intergenic
CDK12	chr10	86156827	86157497	-446	16.5422	0.129442532	promoter-TSS (ENSRNOT00000082668)
RF00026	chr15	108812527	108813197	10811	44.32389	0.130827788	intron (ENSRNOT00000018918. intron 4 of 7)
UBTF	chr10	90266191	90266861	-1509	21.12087	0.132212647	Intergenic
KDM5B	chr13	51383994	51384664	-60	42.90754	0.133597706	promoter-TSS (ENSRNOT00000087025)
LOC500876	chr7	100303561	100304231	79001	26.64946	0.134968991	Intergenic
RAB11FIP4	chr10	66908793	66909463	-33270	40.52296	0.136336456	intron (ENSRNOT00000089538. intron 50 of 57)
RF00026	chr15	108812728	108813398	10610	32.45569	0.13771841	intron (ENSRNOT00000018918. intron 4 of 7)
ARL15	chr2	45700999	45701669	32365	45.45529	0.139091631	intron (ENSRNOT00000071353. intron 1 of 3)
VOM2R9	chr1	56001576	56002246	-106275	37.09363	0.140456228	Intergenic
YTHDC2	chr1	181286471	181287141	853764	39.78443	0.141817231	Intergenic
ZDHHC7	chr19	52759399	52760069	-9427	44.29964	0.143194059	Intergenic

AGFG2	chr12	22082506	22083176	776	43.96141	0.144583589	intron (ENSRNOT00000077711. intron 1 of 12)
RF00026	chr4	177995315	177995985	72085	45.61466	0.146001057	Intergenic
YTHDC2	chr1	181293703	181294373	846532	15.17243	0.147407303	Intergenic
MTRR	chr1	37774728	37775398	30966	42.35722	0.148829835	Intergenic
RF00066	chr14	87941136	87941806	200427	34.15902	0.150240839	Intergenic
STARD13	chr12	1209561	1210231	-14305	42.61632	0.151639031	Intergenic
RAD51B	chr6	102684285	102684955	207584	44.53301	0.153026273	Intergenic
RPL18	chr1	101700670	101701340	-970	35.04478	0.154402383	promoter-TSS (ENSRNOT00000028555)
AABR07011278.1	chr2	160887674	160888344	596559	34.06527	0.155766837	Intergenic
AABR07001734.1	chr1	55753361	55754031	46298	41.06458	0.157147328	exon (ENSRNOT00000089548. exon 4 of 4)
GTPBP2	chr9	17207410	17208080	-751	43.71647	0.158536768	promoter-TSS (ENSRNOT00000026195)
TDRD3	chr15	70803340	70804010	13550	42.63925	0.15993702	intron (ENSRNOT00000012440. intron 7 of 10)
AABR07070486.1	chr8	72310334	72311004	25597	42.34552	0.161332179	Intergenic
POTEM	chr16	22105288	22105958	11211	47.61771	0.162719649	intron (ENSRNOT00000078734. intron 3 of 3)
POTEM	chr16	22105487	22106157	11012	19.52487	0.16409978	intron (ENSRNOT00000078734. intron 3 of 3)
LOC499542	chr2	61747525	61748195	10057	31.42507	0.165487045	Intergenic
TTC17	chr3	83271158	83271828	35288	44.07554	0.166864519	intron (ENSRNOT00000014088. intron 10 of 24)
RF00001	chr9	26775312	26775982	1280	44.61279	0.168231377	Intergenic
EZH1	chr10	89117056	89117726	12948	44.21249	0.169588735	intron (ENSRNOT00000027640. intron 9 of 19)
LOC500684	chr6	103938504	103939174	-3717	40.03171	0.170952714	Intergenic
RGD1563680	chr3	107177921	107178591	35494	41.80701	0.172310602	intron (ENSRNOT00000006177. intron 1 of 10)
RF00003	chr4	62734611	62735281	-30770	22.47252	0.173692873	intron (ENSRNOT00000014832. intron 17 of 42)
ARHGAP11A	chr3	105297940	105298610	-167	41.00069	0.175064868	promoter-TSS (ENSRNOT00000010994)
RF00026	chr10	63296613	63297283	-7889	39.79422	0.176448918	Intergenic
SLC37A2	chr8	39781308	39781978	-47049	25.19005	0.177827941	intron (ENSRNOT00000040901. intron 10 of 12)
RF00325	chr6	23445640	23446310	2786	43.45538	0.179223106	intron (ENSRNOT00000035320. intron 12 of 18)
OLIG3	chr1	14680521	14681191	-116910	44.89101	0.180631713	Intergenic
GTF2A1	chr6	115352642	115353312	-296	40.76059	0.182030432	promoter-TSS (ENSRNOT00000005873)
AABR07072979.1	chr4	31943386	31944056	-44546	45.32177	0.183420554	Intergenic
RF00015	chr12	46863012	46863682	-3	43.68909	0.184802142	promoter-TSS (ENSRNOT00000084988)
PSMA8	chr18	6155656	6156326	41290	44.39554	0.186173987	intron (ENSRNOT00000044541. intron 4 of 6)
PSMA8	chr18	6155858	6156528	41492	23.53425	0.187537879	intron (ENSRNOT00000044541. intron 4 of 6)
BRCA1	chr10	89455257	89455927	-911	40.43882	0.188893929	promoter-TSS (ENSRNOT00000028109)

DDX55	chr12	37468689	37469359	-89	41.17471	0.190258908	promoter-TSS (ENSRNOT00000001387)
RF00560	chr2	5836235	5836905	18866	40.83053	0.191618308	Intergenic
OSBPL2	chr3	175493047	175493717	-316	40.11184	0.192991864	promoter-TSS (ENSRNOT00000087356)
AABR07026137.1	chr16	65168822	65169492	-9006	43.83871	0.194362287	Intergenic
SGO1	chr9	4408131	4408801	-12603	43.77972	0.195731174	Intergenic
AABR07068949.1	chr8	2960458	2961128	-113978	44.06365	0.197114694	Intergenic
BRD3	chr3	6025374	6026044	-8112	27.18302	0.198495196	intron (ENSRNOT00000084491. intron 1 of 12)
AABR07037307.1	chrX	18212299	18212969	49276	43.58759	0.199867877	Intergenic
MCM8	chr3	125478005	125478675	7789	43.92424	0.20123059	intron (ENSRNOT00000028898. intron 7 of 18)
CDRT4	chr10	49385604	49386274	17625	46.89529	0.202617989	intron (ENSRNOT00000004392. intron 1 of 1)
AC108295.1	chr3	72424247	72424917	-21046	20.40558	0.204005088	intron (ENSRNOT00000033427. intron 8 of 11)
AC108295.1	chr3	72423804	72424474	-20603	27.98905	0.205382294	intron (ENSRNOT00000033427. intron 8 of 11)
AC108295.1	chr3	72424010	72424680	-20809	21.19563	0.206750229	intron (ENSRNOT00000033427. intron 8 of 11)
PRPF31	chr1	64162209	64162879	-83	56.69445	0.208138299	promoter-TSS (ENSRNOT00000089713)
RFX7	chr8	79239885	79240555	80850	32.94742	0.209520248	intron (ENSRNOT00000086841. intron 2 of 8)
TMEM100	chr10	77602989	77603659	65984	41.42083	0.210904089	Intergenic
MICAL1	chr20	46192151	46192821	-7495	42.88688	0.212279961	Intergenic
ABRAXAS2	chr1	204874747	204875417	13516	43.1005	0.213646115	intron (ENSRNOT00000023214. intron 4 of 8)
RF00003	chr6	75622373	75623043	251	38.99899	0.21501512	TTS (ENSRNOT00000080461)
KDM5A	chr4	152892138	152892808	85	41.64601	0.216376953	promoter-TSS (ENSRNOT00000075895)
ARL13B	chr7	957773	958443	230057	40.01584	0.217735378	Intergenic
MRGPRX3	chr1	103315304	103315974	7837	41.09048	0.219088206	intron (ENSRNOT00000019051. intron 1 of 1)
RF00100	chr10	21527541	21528211	-140846	42.95519	0.220430659	Intergenic
EVX2	chr3	61583959	61584629	-2696	44.6211	0.221766529	Intergenic
EVX2	chr3	61584165	61584835	-2902	25.6424	0.223092515	Intergenic
RDH14	chr6	36200085	36200755	90150	37.22685	0.224412477	Intergenic
AABR07001734.1	chr1	55756233	55756903	49170	40.36103	0.225728294	Intergenic
INSM2	chr6	76367815	76368485	-15296	42.45229	0.227036666	Intergenic
OTOS	chr9	99881811	99882481	-60192	38.86717	0.22833527	Intergenic
AABR07030501.1	chr10	90778122	90778792	-5819	44.03974	0.229627025	Intergenic
RGD1565784	chr10	14542795	14543465	-70	48.84929	0.230911201	promoter-TSS (ENSRNOT00000047111)
AABR07027235.1	chr17	20562136	20562806	-56853	44.96364	0.232195608	Intergenic
AABR07061902.2	chr4	151937421	151938091	48437	42.08587	0.233471568	Intergenic
PDE4A	chr8	22188638	22189308	-627	42.38075	0.234747513	promoter-TSS (ENSRNOT00000061100)
EFCAB1	chr11	90050276	90050946	183675	43.36616	0.236027714	Intergenic
PTPRG	chr15	13301405	13302075	-73133	30.8811	0.237301782	Intergenic

AABR07020651.1	chr13	33593029	33593699	-555439	47.26255	0.238577784	Intergenic
HAGH	chr10	14216423	14217093	603	25.13201	0.23985678	promoter-TSS (ENSRNOT00000019767)
HAGH	chr10	14216104	14216774	284	26.97703	0.241127642	promoter-TSS (ENSRNOT00000019767)
AABR07035813.1	chr12	23103532	23104202	-26572	23.92431	0.24239854	Intergenic
AABR07030040.1	chr10	63702268	63702938	5995	44.73366	0.243660426	intron (ENSRNOT00000005100. intron 5 of 13)
AABR07035813.1	chr12	23103232	23103902	-26872	30.84457	0.244914219	Intergenic
LOC100912282	chr7	144391163	144391833	-69258	30.50143	0.246164827	Intergenic
B4GALT7	chr17	9557934	9558604	355	31.04011	0.247471961	intron (ENSRNOT00000083492. intron 1 of 6)
AABR07026915.1	chr17	4763849	4764519	53653	42.00228	0.248772861	Intergenic
YTHDC2	chr1	180926059	180926729	1214176	27.8022	0.250066779	Intergenic
OLIG3	chr1	14807972	14808642	10541	42.52161	0.2513709	Intergenic
TMTC1	chr4	182867899	182868569	-23943	42.14295	0.252669022	Intergenic
RFXANK	chr16	21029074	21029744	-187	42.6359	0.253962153	promoter-TSS (ENSRNOT00000041221)
CDK5RAP1	chr3	149870326	149870996	-248	52.64201	0.255256612	promoter-TSS (ENSRNOT00000021418)
CDK5RAP1	chr3	149870525	149871195	-447	16.70976	0.256543491	promoter-TSS (ENSRNOT00000021418)
PTPRG	chr15	13301606	13302276	-73334	23.67834	0.257832702	Intergenic
MYL10	chr12	22998297	22998967	22885	37.9087	0.259115266	Intergenic
SIK3	chr8	50306629	50307299	-3441	27.83552	0.26038922	Intergenic
KLF9	chr1	240908037	240908707	-111	33.81445	0.261663412	promoter-TSS (ENSRNOT00000019367)
AABR07024439.1	chr16	42155	42825	3439	46.23418	0.262932941	Intergenic
CECR2	chr4	153216833	153217503	-614	35.21268	0.264195855	promoter-TSS (ENSRNOT00000015499)
AABR07001207.1	chr1	38786176	38786846	48996	36.95927	0.265450776	Intergenic
AABR07056200.1	chr7	21234888	21235558	-30490	44.29807	0.266703675	Intergenic
YTHDC2	chr1	180972145	180972815	1168090	86.86198	0.267948296	Intergenic
YTHDC2	chr1	181014454	181015124	1125781	53.29261	0.269194387	Intergenic
LYSMD4	chr1	128046092	128046762	-152895	40.17272	0.2704388	intron (ENSRNOT00000055877. intron 19 of 22)
EHF	chr3	93238303	93238973	-22143	16.97553	0.271682084	Intergenic
AABR07068053.1	chr9	80048682	80049352	-19247	42.58345	0.272921029	Intergenic
AABR07068053.1	chr9	80048886	80049556	-19043	15.0579	0.274154261	Intergenic
AC110102.2	chr4	44688638	44689308	-25089	41.72711	0.275381017	Intergenic
ERGIC2	chr4	182573732	182574402	20164	34.39535	0.276610715	intron (ENSRNOT00000079291. intron 10 of 12)
ERGIC2	chr4	182573527	182574197	20369	41.78626	0.27783375	intron (ENSRNOT00000079291. intron 10 of 12)
ADRA1A	chr15	43348639	43349309	50180	40.82661	0.279053195	intron (ENSRNOT00000012736. intron 1 of 1)
BTG1	chr7	37787196	37787866	-25300	29.66325	0.280265732	Intergenic
BTG1	chr7	37787405	37788075	-25091	21.46141	0.281471871	Intergenic
TTLL9	chr3	148457475	148458145	9078	37.81	0.282671485	intron (ENSRNOT00000083812. intron 3 of 14)
AABR07039256.1	chrX	73074581	73075251	12484	41.71115	0.283870982	Intergenic

LOC365791	chr2	137349873	137350543	-19068	33.16023	0.285068349	intron (ENSRNOT00000090907. intron 8 of 20)
MTMR14	chr4	145194656	145195326	-79	38.90496	0.28626747	promoter-TSS (ENSRNOT00000010723)
EXOSC5	chr1	82455347	82456017	3213	41.06529	0.287459721	intron (ENSRNOT00000028026. intron 1 of 5)
AABR07011057.1	chr2	156939456	156940126	95692	29.56122	0.288648962	Intergenic
UBL3	chr12	7864536	7865206	-1067	29.66256	0.289832445	Intergenic
STARD13	chr12	1107718	1108388	87538	22.44147	0.291008048	intron (ENSRNOT00000001446. intron 1 of 13)
AABR07011057.1	chr2	156938927	156939597	96221	28.58462	0.292177656	Intergenic
RRM2B	chr7	76811846	76812516	-31364	17.87964	0.293348587	intron (ENSRNOT00000009115. intron 36 of 54)
RRM2B	chr7	76811622	76812292	-31140	39.12752	0.294512003	intron (ENSRNOT00000009115. intron 36 of 54)
TNNI3K	chr2	261229589	261230259	107239	38.98591	0.295677311	intron (ENSRNOT00000030341. intron 16 of 24)
AABR07013425.1	chr2	236939711	236940381	-116901	46.30904	0.29683766	Intergenic
YTHDC2	chr1	180702682	180703352	1437553	32.92821	0.297995016	Intergenic
AFF4	chr10	38708348	38709018	16472	39.11802	0.299150684	intron (ENSRNOT00000009440. intron 1 of 20)
SAMD4A	chr15	23844838	23845508	52242	25.85892	0.30029977	intron (ENSRNOT00000089226. intron 6 of 11)
YTHDC2	chr1	180702381	180703051	1437854	34.55832	0.301444941	Intergenic
TTC28	chr12	51716189	51716859	-13794	38.29206	0.302593782	Intergenic
TSC22D1	chr15	58530668	58531338	-23371	40.38992	0.303735112	Intergenic
CBL	chr8	48557330	48558000	7057	41.45115	0.304869515	intron (ENSRNOT00000067902. intron 1 of 15)
AABR07001599.1	chr1	54146988	54147658	-19754	30.25511	0.306014496	Intergenic
AABR07001599.1	chr1	54146746	54147416	-19512	38.30946	0.307155998	Intergenic
RF00001	chr15	46029117	46029787	-10091	36.42182	0.308292529	intron (ENSRNOT00000066864. intron 1 of 10)
AABR07030034.1	chr10	63527049	63527719	23850	36.00821	0.309421865	Intergenic
OLR392	chr2	209617430	209618100	-35138	34.98077	0.310547473	Intergenic
ESR1	chr1	41311413	41312083	-11446	38.39566	0.311673588	intron (ENSRNOT00000082133. intron 1 of 2)
AABR07015966.1	chr14	88348663	88349333	165005	35.75353	0.312792982	Intergenic
NECTIN2	chr1	80670797	80671467	-4547	41.0805	0.313908445	Intergenic
NECTIN2	chr1	80670997	80671667	-4747	16.14251	0.315017732	Intergenic
RF00100	chr13	9937666	9938336	-299809	31.67806	0.316120747	Intergenic
ANAPC11	chr10	109774816	109775486	273	37.61317	0.317220321	promoter-TSS (ENSRNOT00000054955)
RF00026	chr4	128802610	128803280	62984	21.15406	0.318320054	Intergenic
RF00026	chr4	128802393	128803063	63201	37.29373	0.319414039	Intergenic
AABR07001734.1	chr1	55753564	55754234	46501	27.81184	0.320502189	exon (ENSRNOT00000089548. exon 4 of 4)
MIR802	chr11	33618066	33618736	48145	32.82631	0.32158516	Intergenic
AABR07016141.1	chr14	94548479	94549149	-41951	37.7953	0.322665847	Intergenic

SNX24	chr18	48282288	48282958	80895	43.42386	0.323744203	intron (ENSRNOT00000023507. intron 1 of 6)
BRINP3	chr13	63078136	63078806	-448015	28.07601	0.324820178	Intergenic
BRINP3	chr13	63078374	63079044	-447777	27.91074	0.325889974	Intergenic
MTMR9	chr15	46740947	46741617	-22030	38.36343	0.326956518	Intergenic
TMEM220	chr10	53533619	53534289	-37035	19.10638	0.328017489	Intergenic
ALG5	chr2	143932369	143933039	-35	36.13159	0.329075083	promoter-TSS (ENSRNOT00000086214)
FGD6	chr7	35010525	35011195	58849	23.64981	0.330133807	exon (ENSRNOT00000077666. exon 4 of 21)
MUM1	chr7	12337262	12337932	8878	36.42007	0.331192124	intron (ENSRNOT00000060708. intron 6 of 12)
AABR07000137.1	chr1	1415690	1416360	-23696	15.62408	0.332250773	Intergenic
PTPRM	chr9	115257319	115257989	124791	38.93705	0.333304364	intron (ENSRNOT00000056366. intron 4 of 32)
POLQ	chr11	66658538	66659208	36480	41.38872	0.334359756	intron (ENSRNOT00000063995. intron 9 of 29)
AABR07018457.1	chr15	58777093	58777763	51163	41.74989	0.335412312	Intergenic
NDOR1	chr3	2474567	2475237	11	47.31102	0.336461208	promoter-TSS (ENSRNOT00000014445)
FOSL2	chr6	25780564	25781234	-163904	40.13961	0.33750639	intron (ENSRNOT00000005855. intron 7 of 11)
FOSL2	chr6	25780769	25781439	-164109	25.11107	0.338546244	intron (ENSRNOT00000005855. intron 7 of 11)
AABR07005838.2	chr1	202882990	202883660	53758	43.76074	0.339583046	Intergenic
AABR07012426.1	chr2	195065905	195066575	27048	35.54269	0.340618318	Intergenic
RF00066	chr13	53999749	54000419	-100144	23.56796	0.341651239	Intergenic
RGD1306941	chr9	63970795	63971465	-95449	41.64273	0.342685714	Intergenic
AABR07044173.1	chr19	61546843	61547513	36296	40.188	0.343717781	Intergenic
SULT2A2	chr1	76584107	76584777	29837	54.13816	0.344745019	intron (ENSRNOT00000041367. intron 3 of 5)
AABR07001599.1	chr1	54176181	54176851	-48947	40.15342	0.345772938	Intergenic
LRRC55	chr3	72575083	72575753	27130	34.01583	0.346803922	Intergenic
RF00026	chr1	147838350	147839020	-9856	42.89636	0.347834776	intron (ENSRNOT00000074103. intron 7 of 9)
AC117971.2	chr7	19667972	19668642	172462	37.85553	0.348862268	Intergenic
RF00181	chr15	88364697	88365367	-75050	40.86949	0.349884739	Intergenic
KIF11	chr1	256034529	256035199	-1002	22.71073	0.350909398	Intergenic
AABR07031221.1	chr18	4648048	4648718	48358	23.94613	0.351928955	Intergenic
AABR07022053.1	chr13	104552384	104553054	83782	25.46132	0.352950661	Intergenic
AABR07027799.1	chr17	44320864	44321534	99397	47.08527	0.353972074	Intergenic
ADAM34L	chr16	51530459	51531129	-199658	30.91757	0.354989085	Intergenic
AABR07020835.1	chr13	43172846	43173516	-212273	20.41749	0.356001641	Intergenic
AABR07035175.1	chr12	5882411	5883081	-59470	41.55707	0.357008043	Intergenic
AABR07020835.1	chr13	43172504	43173174	-212615	39.71057	0.358010694	Intergenic
NR1H5	chr2	205454546	205455216	-3490	41.86567	0.359009549	Intergenic
SLC12A8	chr11	70525850	70526520	-26985	43.11551	0.360005387	intron (ENSRNOT00000002435. intron 7 of 8)

RF00002	chr7	2121437	2122107	100181	24.58253	0.360996507	Intergenic
CEP68	chr14	104535827	104536497	-12865	37.44795	0.361985355	Intergenic
NLRP1A	chr10	57766748	57767418	-27974	34.58841	0.362971896	intron (ENSRNOT00000037546. intron 1 of 14)
TRIM16	chr10	49238833	49239503	7438	44.56281	0.36395526	intron (ENSRNOT00000065335. intron 1 of 5)
ERO1A	chr15	19650485	19651155	4561	18.7531	0.364937086	intron (ENSRNOT00000009404. intron 1 of 15)
ERO1A	chr15	19650217	19650887	4829	39.59818	0.365913135	intron (ENSRNOT00000009404. intron 1 of 15)
HUS1	chr14	89214126	89214796	-5636	29.29639	0.366886727	Intergenic
GZMF	chr15	35191862	35192532	3528	43.60587	0.367856132	intron (ENSRNOT00000044840. intron 1 of 4)
EPHB4	chr12	22411274	22411944	6371	40.84774	0.368823003	intron (ENSRNOT00000072208. intron 3 of 16)
AABR07016141.1	chr14	94369468	94370138	-220962	22.14093	0.369786456	Intergenic
SMAD7	chr18	71315182	71315852	-80313	22.59928	0.370745595	Intergenic
SMAD7	chr18	71315683	71316353	-79812	27.46217	0.371700376	Intergenic
RGS18	chr13	62051200	62051870	-460396	15.67857	0.37265075	Intergenic
ZFP365	chr20	22086594	22087264	26705	41.24385	0.373601834	TTS (ENSRNOT00000057992)
LIFR	chr2	56418949	56419619	-7083	34.88109	0.374550171	Intergenic
LIFR	chr2	56419154	56419824	-6878	21.28434	0.375493134	Intergenic
HTT	chr14	81279580	81280250	-25278	40.77724	0.37643587	intron (ENSRNOT00000015894. intron 10 of 15)
AC117971.2	chr7	19628286	19628956	212148	40.747	0.377374022	Intergenic
STPG2	chr2	244497517	244498187	-23847	29.87006	0.378308413	Intergenic
AC117971.2	chr7	19628568	19629238	211866	33.43939	0.379239006	Intergenic
VOM2R37	chr1	99095993	99096663	39649	32.2807	0.380171888	intron (ENSRNOT00000056515. intron 4 of 4)
AKAP12	chr1	40862821	40863491	-16591	35.55599	0.381100045	intron (ENSRNOT00000060767. intron 2 of 3)
AABR07035437.1	chr12	14873244	14873914	-166921	30.5759	0.38202431	intron (ENSRNOT00000089775. intron 4 of 46)
BRPF3	chr20	6043809	6044479	-5142	40.16977	0.382944644	Intergenic
VOM2R37	chr1	99095487	99096157	40155	17.88427	0.383860125	intron (ENSRNOT00000056515. intron 4 of 4)
MEIS1	chr14	103150528	103151198	170407	22.50471	0.384772478	Intergenic
RF00003	chr9	71678018	71678688	19454	40.75897	0.385685223	Intergenic
CCDC92B	chr10	61413524	61414194	-7775	18.62671	0.386597463	intron (ENSRNOT00000077649. intron 1 of 5)
CCDC92B	chr10	61413752	61414422	-7547	16.39032	0.387505615	exon (ENSRNOT00000092490. exon 2 of 4)
CCT6A	chr12	30501445	30502115	54	29.0656	0.388412323	promoter-TSS (ENSRNOT00000090466)
ARHGEF37	chr18	56849491	56850161	20975	39.01156	0.389318463	intron (ENSRNOT00000087188. intron 3 of 12)
USP40	chr9	95066032	95066702	42372	38.98602	0.390219529	intron (ENSRNOT00000035338. intron 27 of 29)

AABR07068306.1	chr9	97405377	97406047	-20709	32.7787	0.391117276	Intergenic
EPB41L4A	chr18	26628639	26629309	27905	40.95108	0.392012576	intron (ENSRNOT00000038247. intron 7 of 17)
AABR07053870.1	chr3	131731113	131731783	121857	15.05405	0.392904497	Intergenic
AABR07053870.1	chr3	131730911	131731581	121655	39.74528	0.393792101	Intergenic
RGD1561699	chr14	15422069	15422739	4298	45.91843	0.394676256	Intergenic
TIAM2	chr1	44292209	44292879	-18969	41.25456	0.395558754	Intergenic
DDX31	chr3	7422758	7423428	273	39.09361	0.39643866	promoter-TSS (ENSRNOT00000088339)
LEO1	chr8	82369138	82369808	-11284	19.11065	0.39731412	Intergenic
AABR07008594.1	chr2	65945037	65945707	-74487	22.50381	0.398186929	Intergenic
AABR07066188.1	chr9	4627166	4627836	6076	47.99776	0.399061656	Intergenic
NR1H5	chr2	205454785	205455455	-3729	23.8181	0.39993462	Intergenic
RGD1311251	chr8	58006464	58007134	23243	35.60556	0.400804879	intron (ENSRNOT00000009562. intron 8 of 9)
ZFP955A	chr7	15787368	15788038	2256	37.43047	0.401670558	exon (ENSRNOT00000073235. exon 2 of 2)
AABR07058210.1	chr7	105074820	105075490	-26852	37.97686	0.402536253	Intergenic
AABR07035083.1	chr12	4132844	4133514	-37681	16.23578	0.403396383	Intergenic
GABRR3	chr11	43081948	43082618	17129	35.31464	0.404258351	intron (ENSRNOT00000002281. intron 2 of 8)
AC126899.1	chr19	44434377	44435047	-38102	37.16466	0.405117496	Intergenic
SPATA19	chr8	28590897	28591567	136270	35.0788	0.405975663	Intergenic
RF00026	chr7	100090838	100091508	27435	24.51339	0.406830964	Intergenic
AABR07001207.1	chr1	38788697	38789367	46475	16.14867	0.407682435	Intergenic
AABR07009373.2	chr2	94821735	94822405	46879	36.38803	0.408530984	intron (ENSRNOT00000091734. intron 2 of 2)
JAZF1	chr4	83053446	83054116	83746	39.26844	0.409374701	intron (ENSRNOT00000039580. intron 1 of 4)
NHLRC3	chr2	142532647	142533317	153595	37.62612	0.410215438	Intergenic
AABR07059198.1	chr4	8317798	8318468	61522	21.28259	0.411053168	Intergenic
TARS2	chr2	197878773	197879443	-966	23.84583	0.411888816	promoter-TSS (ENSRNOT00000087052)
RF00560	chr2	145957674	145958344	-73129	43.71686	0.412723312	Intergenic
CD300E	chr10	103637523	103638193	-18775	44.34164	0.413556642	Intergenic
ARL16	chr10	109645256	109645926	-6537	40.28279	0.414387837	intron (ENSRNOT00000054966. intron 6 of 21)
AABR07044408.2	chr20	4906881	4907551	-2849	58.20608	0.415214967	intron (ENSRNOT00000082497. intron 3 of 7)
AABR07033357.1	chr11	18083784	18084454	-370025	16.55357	0.416040874	Intergenic
AABR07033357.1	chr11	18083575	18084245	-370234	40.94862	0.416862664	Intergenic
SOX6	chr1	185738479	185739149	65637	35.24207	0.417681269	intron (ENSRNOT00000048020. intron 2 of 15)
OLR505	chr3	73771281	73771951	8366	40.43475	0.418497627	Intergenic
ASAP1	chr7	104717876	104718546	31341	29.50874	0.41931365	intron (ENSRNOT00000079981. intron 7 of 22)
AABR07025973.1	chr16	56977832	56978502	-53840	37.55585	0.420127394	Intergenic

CRK	chr10	63837780	63838450	8308	37.48417	0.420936902	intron (ENSRNOT00000006407. intron 1 of 2)
AABR07035864.1	chr12	25898847	25899517	-52775	39.0767	0.421743114	Intergenic
AABR07000137.1	chr1	1382582	1383252	9412	41.24877	0.422546005	Intergenic
MYBPC3	chr3	79962485	79963155	22259	30.98017	0.423347501	exon (ENSRNOT00000079394. exon 33 of 35)
MYBPC3	chr3	79962690	79963360	22464	29.84595	0.424144656	intron (ENSRNOT00000017360. intron 31 of 33)
AABR07013718.1	chr2	252972787	252973457	-100720	24.74921	0.4249394	Intergenic
AABR07013718.1	chr2	252973190	252973860	-101123	15.36227	0.425731711	Intergenic
AABR07052608.1	chr3	65909623	65910293	-11657	25.88964	0.426523535	Intergenic
AABR07071287.1	chr8	107750711	107751381	51566	21.40747	0.427311912	intron (ENSRNOT00000019536. intron 13 of 21)
GAS1	chr17	4845957	4846627	-497	42.88763	0.42809879	promoter-TSS (ENSRNOT00000073271)
RNF217	chr1	28210540	28211210	-91047	38.71662	0.428885141	Intergenic
EMID1	chr14	85405469	85406139	-7272	39.37936	0.429668979	Intergenic
TOM1L2	chr10	46721110	46721780	-535	41.79131	0.430452268	promoter-TSS (ENSRNOT00000067866)
RF00100	chr6	30338041	30338711	105633	39.74827	0.431231026	Intergenic
AABR07063511.1	chr6	32692721	32693391	-92978	39.5055	0.432010199	Intergenic
RAI14	chr2	60734173	60734843	-51057	39.49238	0.432786794	Intergenic
APOB	chr6	33249503	33250173	73012	40.99665	0.433559793	Intergenic
AC098190.1	chr2	6080192	6080862	-198990	19.67821	0.434332172	Intergenic
AABR07027872.1	chr17	47889227	47889897	18951	41.75111	0.435102922	Intergenic
AABR07039256.1	chrX	73074795	73075465	12270	40.86517	0.435872029	Intergenic
RF01296	chr3	142589532	142590202	132363	32.155	0.436639479	Intergenic
RGD1561667	chr1	55235076	55235746	15638	51.69435	0.437405259	Intergenic
DNAJB12	chr20	29444573	29445243	-602	35.63217	0.438168346	promoter-TSS (ENSRNOT00000044805)
FAM167A	chr15	46636838	46637508	23363	38.84029	0.438929732	intron (ENSRNOT00000015055. intron 3 of 3)
INTS4	chr1	162444759	162445429	-2586	38.38439	0.439687379	Intergenic
AABR07065486.1	chr6	130750652	130751322	-40267	36.22255	0.440443292	Intergenic
AABR07065486.1	chr6	130750880	130751550	-40039	26.58384	0.441195425	Intergenic
LMOD3	chr4	129618339	129619009	468	37.53382	0.441945789	intron (ENSRNOT00000047453. intron 1 of 3)
ADCY2	chr1	37420919	37421589	-86022	36.13434	0.442692333	Intergenic
SUB1	chr2	62039005	62039675	-4712	23.54845	0.443437074	Intergenic
KNG1	chr11	81444988	81445658	-702	39.06264	0.444178977	promoter-TSS (ENSRNOT00000078131)
RF00334	chr4	183486346	183487016	36535	36.34903	0.444919049	intron (ENSRNOT00000071407. intron 17 of 21)
SMPDL3A	chr20	40884490	40885160	105898	33.64674	0.445655222	Intergenic
SDC4	chr3	160879973	160880643	10882	33.2143	0.446390558	intron (ENSRNOT00000019386. intron 1 of 4)
AABR07032862.1	chr18	86239198	86239868	40147	38.66309	0.44712196	intron (ENSRNOT00000076159. intron 33 of 35)
RF00026	chr9	58134825	58135495	139053	38.62591	0.447851466	Intergenic

AC117971.2	chr7	19670707	19671377	169727	40.23774	0.448578031	Intergenic
OLIG3	chr1	14808181	14808851	10750	26.24092	0.449302671	Intergenic
USP8	chr3	119203484	119204154	30001	40.02167	0.450024336	exon (ENSRNOT00000015124. exon 10 of 19)
USP8	chr3	119203683	119204353	30200	17.7357	0.450744047	intron (ENSRNOT00000015124. intron 10 of 18)
AC109942.1	chr7	15271732	15272402	-7544	39.31891	0.451461791	Intergenic
RF00100	chr12	6361140	6361810	-12699	38.60211	0.452179636	Intergenic
ZC3HC1	chr4	57702025	57702695	4253	20.08635	0.452895494	intron (ENSRNOT00000013604. intron 2 of 9)
RF00001	chr15	87177985	87178655	-43414	39.58284	0.453608308	Intergenic
AC128582.1	chr8	80156129	80156799	-293490	40.42716	0.454320151	Intergenic
AABR07066677.1	chr9	12329471	12330141	-16311	22.64994	0.455027873	Intergenic
MYH8	chr10	53833391	53834061	14908	37.67922	0.455733548	intron (ENSRNOT00000057260. intron 22 of 33)
ZFP827	chr19	32461576	32462246	67054	34.66332	0.456437166	intron (ENSRNOT00000015929. intron 6 of 12)
ZFP827	chr19	32461775	32462445	66855	21.04674	0.457137659	intron (ENSRNOT00000015929. intron 6 of 12)
AABR07012426.1	chr2	195066154	195066824	27297	26.15949	0.457835011	Intergenic
AABR07066677.1	chr9	12330219	12330889	-15563	15.59378	0.458530258	Intergenic
AABR07066677.1	chr9	12360463	12361133	14681	32.52158	0.45922339	Intergenic
AABR07027128.1	chr17	14932690	14933360	16039	34.72215	0.45991651	Intergenic
PDE5A	chr2	226969787	226970457	69503	37.61649	0.460606434	intron (ENSRNOT00000019638. intron 7 of 20)
PTPRB	chr7	59323507	59324177	-2676	29.50695	0.461294206	intron (ENSRNOT00000085073. intron 12 of 12)
PTPRB	chr7	59323708	59324378	-2475	26.52662	0.461979814	intron (ENSRNOT00000085073. intron 12 of 12)
VOM2R24	chr8	3957100	3957770	46158	37.46989	0.462664311	Intergenic
AABR07070173.1	chr8	55966929	55967599	57392	25.13457	0.463345554	Intergenic
PDE5A	chr2	226969999	226970669	69715	25.74376	0.464024595	intron (ENSRNOT00000019638. intron 7 of 20)
EEA1	chr7	37140932	37141602	39876	24.59404	0.46470142	intron (ENSRNOT00000087297. intron 12 of 29)
EEA1	chr7	37141154	37141824	40098	24.29395	0.465374947	exon (ENSRNOT00000029764. exon 11 of 28)
ASCC3	chr20	55378855	55379525	125504	37.95091	0.466047304	intron (ENSRNOT00000057016. intron 13 of 41)
XPO1	chr14	108004580	108005250	-2809	21.68977	0.466720632	Intergenic
CDCA7	chr3	59152702	59153372	-243	40.61047	0.467392781	promoter-TSS (ENSRNOT00000002066)
SELENOW	chr1	77202457	77203127	332889	38.418	0.468064819	Intergenic
LOC102555038	chr12	3747378	3748048	-59743	19.48606	0.468735666	Intergenic
WEE1	chr1	174751344	174752014	-16281	36.54032	0.46940315	Intergenic
AABR07066060.1	chr9	1095003	1095673	5061	27.88129	0.470068338	intron (ENSRNOT00000086927. intron 1 of 1)

LOC299277	chr6	127882143	127882813	4062	25.21976	0.470731217	intron (ENSRNOT00000057298. intron 3 of 3)
RF00026	chr2	210908259	210908929	-5257	22.46567	0.471391774	intron (ENSRNOT00000026710. intron 3 of 8)
SLC12A1	chr3	117457942	117458612	35573	40.46481	0.472052172	intron (ENSRNOT00000008857. intron 15 of 26)
PC	chr1	219758810	219759480	-38	30.86416	0.472710229	promoter-TSS (ENSRNOT00000086155)
CMSS1	chr11	45214316	45214986	-89417	36.43496	0.473365933	Intergenic
RF00001	chr3	137388531	137389201	-224259	40.45664	0.474019273	Intergenic
ROCK2	chr6	42164924	42165594	-15635	38.30803	0.474671329	Intergenic
CHD1L	chr2	199761464	199762134	10097	26.4966	0.475322092	intron (ENSRNOT00000043937. intron 5 of 24)
MEIKIN	chr10	39733894	39734564	7722	32.48081	0.475972652	intron (ENSRNOT00000036822. intron 4 of 8)
MEIKIN	chr10	39734093	39734763	7921	22.29917	0.47662081	intron (ENSRNOT00000036822. intron 4 of 8)
NINJ2	chr4	152622801	152623471	-7333	38.97742	0.477267652	Intergenic
AABR07072065.1	chr1	269596584	269597254	-251991	32.59809	0.477912071	Intergenic
GALNT5	chr3	43968677	43969347	-56288	30.53329	0.478555156	Intergenic
AGFG2	chr12	22082792	22083462	1062	30.88395	0.479195797	intron (ENSRNOT00000077711. intron 1 of 12)
AABR07072065.1	chr1	269596959	269597629	-252366	17.21859	0.47983398	Intergenic
GALNT5	chr3	43968876	43969546	-56089	23.71859	0.480470801	Intergenic
FCGR1A	chr2	198442558	198443228	-3439	41.18348	0.481104036	intron (ENSRNOT00000082450. intron 1 of 5)
TMEM229A	chr4	52393674	52394344	-43385	41.26326	0.481735887	Intergenic
SPNS3	chr10	59086982	59087652	25471	19.90228	0.482366346	intron (ENSRNOT00000041886. intron 7 of 10)
BMPR1B	chr2	247674141	247674811	-227594	39.06255	0.482994294	Intergenic
RF00066	chr14	87941398	87942068	200165	22.38982	0.483624173	Intergenic
AABR07070077.1	chr8	47765939	47766609	13783	33.42918	0.484252643	Intergenic
AABR07070077.1	chr8	47765692	47766362	13536	26.85185	0.484878581	Intergenic
SLCO2A1	chr8	111415223	111415893	-79773	35.06414	0.485503092	Intergenic
TSN	chr13	34251266	34251936	49	34.40878	0.486125049	promoter-TSS (ENSRNOT00000068524)
CD2AP	chr9	20809299	20809969	44338	39.62093	0.486745562	intron (ENSRNOT00000016291. intron 3 of 17)
RAB11FIP4	chr10	66909128	66909798	-32935	42.74078	0.487363499	intron (ENSRNOT00000089538. intron 50 of 57)
AABR07025272.1	chr16	31323768	31324438	-22223	17.96096	0.487978851	Intergenic
TCF23	chr6	26743092	26743762	27737	38.9841	0.488593854	Intergenic
AABR07001734.1	chr1	55755643	55756313	48580	32.22159	0.48920738	Intergenic
LRP2BP	chr16	49438065	49438735	14994	39.19072	0.489820548	intron (ENSRNOT00000041617. intron 8 of 8)
MT1M	chr20	3665632	3666302	-11507	15.37424	0.490431097	Intergenic
MT1M	chr20	3665344	3666014	-11795	21.29246	0.491040146	Intergenic
TPBPA	chr17	4160426	4161096	-4280	33.21157	0.491647687	Intergenic

AABR07043598.1	chr19	30533111	30533781	55541	32.72739	0.492252579	Intergenic
AABR07018038.1	chr15	36861954	36862624	-3259	20.05669	0.492854811	intron (ENSRNOT00000076667. intron 18 of 19)
AABR07018038.1	chr15	36862234	36862904	-2979	22.58914	0.493456643	intron (ENSRNOT00000076667. intron 19 of 19)
AABR07033271.1	chr11	14606315	14606985	61045	37.29203	0.494055798	Intergenic
AABR07032724.3	chr18	78009707	78010377	-267426	29.79499	0.494654541	Intergenic
AABR07032724.3	chr18	78009936	78010606	-267197	26.8791	0.495252869	Intergenic
AABR07005886.1	chr1	204175564	204176234	83748	34.68963	0.495847354	Intergenic
SEL1L2	chr3	134474383	134475053	-12065	33.02847	0.49644141	Intergenic
SEL1L2	chr3	134474707	134475377	-12389	28.65316	0.497032743	Intergenic
LRRC63	chr15	57135190	57135860	34869	38.06213	0.497624782	intron (ENSRNOT00000079097. intron 8 of 10)
RF00026	chr20	45555930	45556600	61828	39.89646	0.498215231	intron (ENSRNOT00000000713. intron 4 of 12)
RF00001	chr18	11608979	11609649	-30887	36.80965	0.498802935	Intergenic
TAGAP	chr1	47491701	47492371	10916	26.8029	0.499391332	Intergenic
TAGAP	chr1	47491265	47491935	11352	25.89694	0.49997697	Intergenic
CPNE8	chr7	131889613	131890283	-91712	22.37342	0.500562142	Intergenic
PGAP1	chr9	61225518	61226188	-90890	37.44526	0.50114569	Intergenic
ALKAL2	chr6	49833289	49833959	8155	39.45371	0.501726454	intron (ENSRNOT00000006921. intron 4 of 4)
CKAP4	chr7	24971470	24972140	32307	36.63971	0.502306734	Intergenic
FUT10	chr16	64649788	64650458	66101	43.08362	0.502885369	exon (ENSRNOT00000071166. exon 4 of 5)
AABR07034456.1	chr11	72533853	72534523	41098	39.72909	0.503462352	Intergenic
RF00100	chr14	50676522	50677192	128501	24.3497	0.504036515	Intergenic
RF00100	chr14	50676323	50676993	128700	31.2895	0.504610171	Intergenic
AABR07001018.1	chr1	33767707	33768377	-26761	39.66883	0.505182154	Intergenic
RF00001	chr9	26775567	26776237	1025	41.85998	0.505752455	TTS (ENSRNOT00000070299)
AABR07001662.1	chr1	54956023	54956693	-72796	49.85121	0.506319904	Intergenic
AABR07058815.1	chr7	138416811	138417481	7191	40.64553	0.506886821	intron (ENSRNOT00000077822. intron 1 of 2)
AABR07012426.1	chr2	195066463	195067133	27606	16.87258	0.507450868	Intergenic
TNIK	chr2	113960985	113961655	-23326	38.457	0.508014373	Intergenic
RF00560	chr8	99942202	99942872	11571	31.23834	0.508576162	Intergenic
PAK7	chr3	129381348	129382018	-24192	35.25276	0.509136227	Intergenic
LOC100912097	chr1	148918859	148919529	56701	32.98242	0.509696909	Intergenic
AABR07072065.1	chr1	269597458	269598128	-252865	17.03627	0.510254684	Intergenic
ALKAL2	chr6	49833502	49834172	8368	36.44001	0.510811893	intron (ENSRNOT00000006921. intron 4 of 4)
AABR07066188.1	chr9	4627453	4628123	6363	38.75655	0.511366178	Intergenic
RF00002	chr7	22260383	22261053	193299	15.02309	0.511919885	Intergenic
RF00002	chr7	22260768	22261438	192914	17.12574	0.512471833	Intergenic
YTHDC2	chr1	181294857	181295527	845378	24.2865	0.513022012	Intergenic
AABR07052263.1	chr3	43790712	43791382	96949	38.11153	0.5135716	Intergenic

EPG5	chr18	74325946	74326616	26350	37.60684	0.514119409	intron (ENSRNOT00000078403. intron 10 of 43)
ARHGAP42	chr8	7465666	7466336	-39390	26.06917	0.514665433	Intergenic
ARHGAP42	chr8	7465204	7465874	-38928	24.01278	0.51521085	Intergenic
TREM1	chr9	14801070	14801740	8042	38.12187	0.515755657	intron (ENSRNOT00000049193. intron 1 of 3)
TTC17	chr3	83270871	83271541	35575	18.57264	0.51630104	intron (ENSRNOT00000014088. intron 10 of 24)
MRS2	chr17	42084909	42085579	20868	39.16784	0.51684581	exon (ENSRNOT00000024196. exon 25 of 25)
HMBS	chr8	48674832	48675502	-419	40.67761	0.517388772	promoter-TSS (ENSRNOT00000014127)
KLF9	chr1	240929877	240930547	21729	26.49955	0.517931112	intron (ENSRNOT00000019367. intron 1 of 1)
OLR1345	chr9	99693647	99694317	-13003	38.82124	0.518470439	Intergenic
OLIG3	chr1	14680731	14681401	-116700	16.00182	0.519010328	Intergenic
BAIAP2L1	chr12	12239610	12240280	12850	41.07283	0.519548386	intron (ENSRNOT00000092610. intron 1 of 12)
YTHDC2	chr1	180925765	180926435	1214470	42.28482	0.520084607	Intergenic
MSX2	chr17	11757529	11758199	74002	24.75199	0.520620182	Intergenic
AABR07071368.2	chr8	111992244	111992914	-4869	15.94533	0.521153909	Intergenic
AABR07004992.1	chr1	173327471	173328141	52470	43.56338	0.521686982	Intergenic
AABR07063599.1	chr6	36582734	36583404	148265	20.10577	0.522218196	Intergenic
AABR07052750.1	chr3	71653574	71654244	-10686	15.23193	0.522748746	Intergenic
AABR07001662.1	chr1	54955761	54956431	-72534	44.36614	0.523277426	Intergenic
RPL32	chr4	147718821	147719491	-84	39.2497	0.523805435	promoter-TSS (ENSRNOT00000090620)
AABR07004061.1	chr1	123796005	123796675	-173241	37.54712	0.524331561	Intergenic
RF00026	chr8	73322446	73323116	39694	32.87487	0.524857008	Intergenic
RAB11FIP4	chr10	66912487	66913157	-29576	26.74302	0.525379351	intron (ENSRNOT00000089538. intron 51 of 57)
RAB11FIP4	chr10	66912192	66912862	-29871	18.89435	0.525902215	intron (ENSRNOT00000089538. intron 51 of 57)
SLCO1A6	chr4	176362801	176363471	18341	29.35357	0.526423175	exon (ENSRNOT00000048367. exon 8 of 14)
SLCO1A6	chr4	176362599	176363269	18543	32.66785	0.526942224	intron (ENSRNOT00000048367. intron 8 of 13)
AABR07012039.1	chr2	183291200	183291870	-40607	37.05822	0.527459356	Intergenic
AABR07012039.1	chr2	183291399	183292069	-40806	23.12017	0.527975779	Intergenic
MIR125B1	chr8	45881065	45881735	83140	26.58601	0.528491492	Intergenic
MIR125B1	chr8	45880629	45881299	82704	22.79744	0.52900649	Intergenic
LEO1	chr8	82374015	82374685	-6407	36.71194	0.529518332	Intergenic
LEO1	chr8	82374304	82374974	-6118	27.80668	0.530029449	Intergenic
ATG7	chr4	146700049	146700719	101971	40.12363	0.530538616	intron (ENSRNOT00000067532. intron 17 of 17)
NFKB2	chr1	265997217	265997887	-55450	19.97737	0.531048272	intron (ENSRNOT00000086041. intron 5 of 40)
SGCD	chr10	32528939	32529609	-57820	17.94003	0.53155597	Intergenic

RF00619	chr1	245880592	245881262	-10118	41.28352	0.532062928	intron (ENSRNOT00000023762. intron 12 of 14)
RGD1566337	chr2	194945602	194946272	-69975	39.14376	0.532570369	Intergenic
RGD1565355	chr4	13991210	13991880	-10216	38.87209	0.53307584	Intergenic
RF00100	chr9	14241934	14242604	-20256	36.73965	0.533580562	Intergenic
B3GNT7	chr9	93335381	93336051	9433	21.95487	0.534084532	Intergenic
B3GNT7	chr9	93335181	93335851	9233	35.8457	0.534587747	Intergenic
AABR07004130.1	chr1	126315859	126316529	87212	38.18253	0.535088971	Intergenic
ZFP266	chr8	21516284	21516954	2394	38.39512	0.535590666	exon (ENSRNOT00000085060. exon 6 of 6)
RBM24	chr17	18717799	18718469	-35258	35.43691	0.536090363	Intergenic
LOC680288	chr13	37696248	37696918	986	27.92506	0.536588054	TTS (ENSRNOT00000045263)
PLPP1	chr2	44712854	44713524	49065	37.19416	0.537084971	intron (ENSRNOT00000066098. intron 2 of 5)
HINFP	chr8	48640572	48641242	-6110	40.40759	0.537579873	TTS (ENSRNOT00000030745)
APP	chr11	24737337	24738007	-95814	20.62765	0.538073991	Intergenic
PAPOLA	chr6	129581207	129581877	-27532	16.46426	0.538567324	intron (ENSRNOT00000083626. intron 12 of 18)
RF00001	chr13	73005951	73006621	-7370	40.39456	0.539058626	intron (ENSRNOT00000093410. intron 2 of 8)
APP	chr11	24737657	24738327	-96134	24.44561	0.539549134	Intergenic
PAPOLA	chr6	129581008	129581678	-27731	39.42789	0.540037602	intron (ENSRNOT00000083626. intron 12 of 18)
PELO	chr2	47216117	47216787	52173	30.11949	0.540525267	intron (ENSRNOT00000086114. intron 2 of 28)
EHBP1	chr14	107168465	107169135	-8466	38.75016	0.541012127	Intergenic
MRPL21	chr1	218531730	218532400	20	47.95239	0.541496932	promoter-TSS (ENSRNOT00000018487)
RXFP2	chr12	6034913	6035583	43163	17.20734	0.541982171	intron (ENSRNOT00000001197. intron 13 of 17)
RXFP2	chr12	6035371	6036041	42705	23.79739	0.542465346	intron (ENSRNOT00000001197. intron 13 of 17)
CNIH1	chr15	23583079	23583749	-3019	38.26035	0.542946453	Intergenic
AABR07042780.1	chr19	7385010	7385680	-862648	26.2169	0.543427986	Intergenic
AABR07042780.1	chr19	7385588	7386258	-862070	19.1784	0.543907441	Intergenic
METTL17	chr15	28278638	28279308	-8051	34.74171	0.544386065	Intergenic
METTL17	chr15	28278848	28279518	-7841	28.86882	0.544862602	Intergenic
AABR07057590.1	chr7	79320309	79320979	136316	20.08319	0.5453383	Intergenic
AABR07057590.1	chr7	79320102	79320772	136523	35.58534	0.545813157	Intergenic
PLD5	chr13	94290332	94291002	-1334	36.73405	0.546285911	intron (ENSRNOT00000005332. intron 1 of 9)
TCF4	chr18	65238868	65239538	-46115	36.90355	0.546757816	intron (ENSRNOT00000081797. intron 3 of 18)
IPCEF1	chr1	43609560	43610230	28266	38.80843	0.547228868	intron (ENSRNOT00000024460. intron 4 of 8)
MNX1	chr4	2436002	2436672	-55066	39.14824	0.547699066	Intergenic

GM10642	chr8	77068617	77069287	-19517	17.82482	0.548168405	intron (ENSRNOT00000078685. intron 2 of 8)
AABR07027501.1	chr17	34558525	34559195	-12592	41.13389	0.548636882	Intergenic
GM10642	chr8	77068410	77069080	-19724	35.55083	0.549103232	intron (ENSRNOT00000078685. intron 2 of 8)
CCDC189	chr1	199036754	199037424	178	50.12688	0.549568713	promoter-TSS (ENSRNOT00000025499)
PIN1	chr8	21666454	21667124	-2447	25.05649	0.550032055	Intergenic
CCDC90B	chr1	157058741	157059411	-344519	26.33451	0.55049452	intron (ENSRNOT00000055401. intron 12 of 21)
CCDC90B	chr1	157058502	157059172	-344758	32.98443	0.550957374	intron (ENSRNOT00000055401. intron 12 of 21)
FAR2	chr4	182489022	182489692	6163	31.24343	0.551418078	intron (ENSRNOT00000002528. intron 1 of 11)
RFX7	chr8	79240124	79240794	81089	35.44183	0.551877896	intron (ENSRNOT00000086841. intron 2 of 8)
RFX7	chr8	79240349	79241019	81314	31.32387	0.552336826	intron (ENSRNOT00000086841. intron 2 of 8)
RF00026	chr15	17141454	17142124	-90607	32.87386	0.552796138	Intergenic
RF00100	chr1	184686769	184687439	191617	38.81839	0.553253283	Intergenic
RF00100	chr2	151402254	151402924	-43589	38.33501	0.553709532	Intergenic
FAM3C	chr4	49492050	49492720	-52518	38.91193	0.554164881	Intergenic
ADAM10	chr8	77193450	77194120	86249	30.31233	0.554618051	intron (ENSRNOT00000083255. intron 6 of 15)
ADAM10	chr8	77193725	77194395	86524	22.37535	0.555071591	intron (ENSRNOT00000083255. intron 6 of 15)
AABR07019443.1	chr15	106025180	106025850	-36392	35.58976	0.555522943	Intergenic
LOC102554127	chr13	41494134	41494804	125183	31.16755	0.555974663	Intergenic
RF00017	chr14	50519797	50520467	152339	42.27633	0.556424187	Intergenic
LOC102554127	chr13	41494341	41495011	125390	21.22211	0.556872793	Intergenic
DUSP16	chr4	168495581	168496251	21261	38.2384	0.557320477	intron (ENSRNOT00000009151. intron 3 of 5)
TMTC1	chr4	182858641	182859311	-14685	15.52916	0.557767236	Intergenic
RGD1561667	chr1	55235542	55236212	16104	30.65552	0.558213069	Intergenic
PSMG3	chr12	16895849	16896519	-2841	39.78421	0.558659258	Intergenic
RMI2	chr10	4860433	4861103	49537	41.69852	0.559104516	Intergenic
RPS4X	chr4	35772821	35773491	-42557	35.37	0.559550129	Intergenic
AABR07042999.1	chr19	15887892	15888562	44358	36.86605	0.559993518	Intergenic
TMEM126B	chr1	156180669	156181339	-81027	40.6114	0.560437259	Intergenic
MCAM	chr8	48503168	48503838	30679	22.40363	0.560878768	exon (ENSRNOT00000067902. exon 7 of 16)
MCAM	chr8	48503472	48504142	30983	28.1848	0.561320625	intron (ENSRNOT00000067902. intron 6 of 15)
OLFML2A	chr3	23226132	23226802	2988	37.25058	0.561760243	intron (ENSRNOT00000018853. intron 1 of 7)
SEC11A	chr1	142781578	142782248	-22031	33.5727	0.562198911	Intergenic
LOC108353037	chr15	53677043	53677713	-181384	27.35354	0.562636626	Intergenic
DAD1	chr15	32887803	32888473	-43	37.48612	0.563073385	promoter-TSS (ENSRNOT00000012233)

AABR07005838.2	chr1	202953947	202954617	124715	19.64566	0.563507888	Intergenic
AABR07035437.1	chr12	14731580	14732250	-25257	28.80297	0.563942727	intron (ENSRNOT00000089775. intron 4 of 46)
AABR07035437.1	chr12	14731366	14732036	-25043	36.46686	0.564376601	intron (ENSRNOT00000089775. intron 4 of 46)
MKL1	chr7	122385110	122385780	18222	31.41788	0.564808209	intron (ENSRNOT00000088814. intron 1 of 13)
MKL1	chr7	122384844	122385514	18488	29.40307	0.565240146	intron (ENSRNOT00000088814. intron 1 of 13)
RF00003	chr15	38133053	38133723	-28818	37.71746	0.565669809	intron (ENSRNOT00000063962. intron 4 of 12)
RF00003	chr15	38133256	38133926	-29021	15.51944	0.566098495	intron (ENSRNOT00000063962. intron 4 of 12)
MC4R	chr18	62664974	62665644	-50584	43.84787	0.566527505	Intergenic
NUMB	chr6	107296560	107297230	28450	38.28937	0.566955536	intron (ENSRNOT00000042594. intron 2 of 10)
PHF12	chr10	64859980	64860650	1817	33.36804	0.567381276	intron (ENSRNOT00000056234. intron 2 of 14)
AABR07056118.1	chr7	20248869	20249539	-13476	42.7376	0.567807337	Intergenic
DEPDC5	chr14	83218386	83219056	350	49.69239	0.568232409	intron (ENSRNOT00000067694. intron 1 of 41)
BET1	chr4	29112519	29113189	-20101	20.28652	0.568655181	Intergenic
RF00108	chr1	194916538	194917208	496	40.98125	0.569078267	TTS (ENSRNOT00000080729)
SINHCAF	chr4	183417921	183418591	-589	27.28807	0.569499045	promoter-TSS (ENSRNOT00000089160)
SINHCAF	chr4	183418363	183419033	-1031	28.17777	0.569920134	intron (ENSRNOT00000083310. intron 1 of 6)
LOC100362344	chr4	184193693	184194363	-97222	24.28502	0.570338908	Intergenic
SULT2A2	chr1	76584333	76585003	29611	19.31128	0.570756676	intron (ENSRNOT00000041367. intron 3 of 5)
LOC100362344	chr4	184194022	184194692	-97551	16.22614	0.571173434	Intergenic
ARRDC4	chr1	129739581	129740251	36360	26.28687	0.571589181	Intergenic
IKBKE	chr13	48133332	48134002	-77273	37.78979	0.57200523	intron (ENSRNOT00000086928. intron 4 of 21)
BRAT1	chr12	16020626	16021296	6920	38.40834	0.572418946	intron (ENSRNOT00000064726. intron 6 of 12)
AABR07044836.1	chr20	23017987	23018657	9289	21.51333	0.572832962	Intergenic
AABR07044836.1	chr20	23018188	23018858	9088	15.13416	0.573244637	Intergenic
AABR07044836.1	chr20	23017774	23018444	9502	36.89621	0.573656607	Intergenic
OPCML	chr8	29461623	29462293	8315	16.44602	0.57406623	intron (ENSRNOT00000090643. intron 1 of 7)
OPCML	chr8	29461360	29462030	8052	15.98231	0.574476146	intron (ENSRNOT00000090643. intron 1 of 7)
RF00026	chr20	45556132	45556802	62030	29.26027	0.57488503	intron (ENSRNOT00000000713. intron 4 of 12)
RF00100	chr12	2303302	2303972	-3576	41.01002	0.575292881	Intergenic
COL26A1	chr12	22864866	22865536	30182	35.70456	0.575699696	intron (ENSRNOT00000059530. intron 1 of 14)

TANGO6	chr19	38884672	38885342	38719	42.66904	0.576105472	intron (ENSRNOT00000030768. intron 7 of 17)
RF00340	chr1	200128405	200129075	28120	28.38494	0.576510206	intron (ENSRNOT00000027644. intron 10 of 15)
BNIP2	chr8	76400393	76401063	355	37.38452	0.576915225	intron (ENSRNOT00000081072. intron 1 of 8)
MED17	chr8	13834938	13835608	-105	38.25651	0.577317869	promoter-TSS (ENSRNOT00000014435)
AABR07053402.1	chr3	104696227	104696897	-21105	17.81345	0.577720795	Intergenic
AABR07053402.1	chr3	104696028	104696698	-20906	39.31071	0.57812267	Intergenic
AABR07053402.1	chr3	104695599	104696269	-20477	18.72493	0.578522161	Intergenic
FLRT3	chr3	135259429	135260099	-563110	35.89679	0.578923261	Intergenic
EIF4G2	chr1	175950469	175951139	-55294	34.6754	0.579321972	Intergenic
EIF4G2	chr1	175950669	175951339	-55494	20.06567	0.579719622	Intergenic
GALK2	chr3	118142463	118143133	-1798	41.29181	0.580116209	intron (ENSRNOT00000083356. intron 1 of 9)
CEP55	chr1	256747664	256748334	2711	37.49069	0.580513067	intron (ENSRNOT00000022133. intron 2 of 8)
EEF2K	chr1	190777437	190778107	-2464	40.77319	0.58090886	Intergenic
AABR07027799.1	chr17	44388825	44389495	31436	39.782	0.581304922	Intergenic
VOM2R64	chr12	21095124	21095794	-17920	27.5033	0.581701254	Intergenic
VOM2R64	chr12	21095372	21096042	-18168	25.95915	0.582096516	Intergenic
SLC38A2	chr7	138100487	138101157	19	38.77297	0.582490706	promoter-TSS (ENSRNOT00000039002)
CACNA1E	chr13	72023643	72024313	39369	46.75894	0.582885162	intron (ENSRNOT00000090544. intron 2 of 43)
SMG8	chr10	74387504	74388174	948	25.45482	0.583277199	exon (ENSRNOT00000008107. exon 1 of 4)
RF00049	chr2	52255858	52256528	2918	42.0832	0.583670845	intron (ENSRNOT00000033627. intron 6 of 21)
AABR07027567.1	chr17	36956414	36957084	364	41.32764	0.584062066	intron (ENSRNOT00000024854. intron 1 of 5)
BCL2L11	chr3	120619608	120620278	-106963	22.92133	0.584453549	intron (ENSRNOT00000021740. intron 14 of 19)
BCL2L11	chr3	120619092	120619762	-107479	20.03982	0.584843948	intron (ENSRNOT00000021740. intron 14 of 19)
ZC3H8	chr3	121479907	121480577	8298	27.44429	0.58523326	exon (ENSRNOT00000023845. exon 3 of 9)
AABR07054753.1	chr3	168681371	168682041	38208	26.6816	0.585622831	Intergenic
AABR07054753.1	chr3	168681726	168682396	38563	26.54094	0.586011313	Intergenic
CDC42EP3	chr6	2002695	2003365	-60058	39.6763	0.586400052	Intergenic
CDC42EP3	chr6	2002904	2003574	-60267	17.93321	0.586786346	Intergenic
RF00026	chr4	71157607	71158277	-6801	37.99256	0.587172896	Intergenic
RF00066	chr13	53999366	54000036	-99761	37.39563	0.587558347	Intergenic
AABR07030501.1	chr10	90778379	90779049	-6076	25.31565	0.58794405	Intergenic
KCTD3	chr13	107393996	107394666	77512	28.97823	0.588328653	intron (ENSRNOT00000004992. intron 65 of 72)
MAJIN	chr1	221554263	221554933	-3495	23.47628	0.588712151	Intergenic
MAJIN	chr1	221554057	221554727	-3701	36.00016	0.589094543	Intergenic

NDUFS4	chr2	46477879	46478549	-2011	35.80935	0.589477184	Intergenic
ELMOD2	chr19	24477081	24477751	9980	39.7342	0.589858714	intron (ENSRNOT00000031614. intron 5 of 8)
PRPF8	chr10	63634767	63635437	-117	39.37557	0.590237774	promoter-TSS (ENSRNOT00000005016)
AABR07006436.1	chr1	233538742	233539412	131087	27.60559	0.590618437	intron (ENSRNOT00000019174. intron 2 of 6)
RF00405	chr20	11941278	11941948	-7379	24.41315	0.590996624	Intergenic
LRGUK	chr4	61245079	61245749	-174595	21.32557	0.591373691	intron (ENSRNOT00000075621. intron 18 of 21)
LRGUK	chr4	61245351	61246021	-174323	23.62764	0.591750999	intron (ENSRNOT00000075621. intron 18 of 21)
RF00026	chr4	66283113	66283783	3192	36.32187	0.592127185	intron (ENSRNOT00000007544. intron 1 of 1)
CDC42EP3	chr6	1991384	1992054	-48747	22.9749	0.592502245	Intergenic
SNX11	chr10	84639048	84639718	-272	41.91292	0.592877542	promoter-TSS (ENSRNOT00000011474)
CTRB1	chr19	43913868	43914538	-3146	32.70823	0.593253078	Intergenic
AABR07060145.1	chr4	59075019	59075689	-60938	37.03232	0.593627484	Intergenic
CTRB1	chr19	43914090	43914760	-3368	30.21621	0.594000759	Intergenic
AABR07006978.1	chr1	275127793	275128463	-122306	20.04016	0.5943729	Intergenic
AABR07006978.1	chr1	275127575	275128245	-122088	29.83948	0.594745274	Intergenic
UTP18	chr10	81289009	81289679	298514	41.02921	0.595115141	intron (ENSRNOT00000075163. intron 6 of 8)
IFNGR2	chr11	31702834	31703504	8830	36.5366	0.595486609	intron (ENSRNOT00000002779. intron 2 of 6)
AABR07007409.1	chr2	13104347	13105017	-49467	24.08855	0.595855565	Intergenic
AABR07007409.1	chr2	13104106	13104776	-49226	35.51695	0.59622475	Intergenic
AABR07020651.1	chr13	33593593	33594263	-554875	15.60296	0.596592789	Intergenic
TNPO1	chr2	29132028	29132698	-11259	19.15742	0.596961056	Intergenic
DTD1	chr3	138815641	138816311	45361	35.54624	0.597328175	intron (ENSRNOT00000066986. intron 4 of 4)
AABR07020651.1	chr13	33593985	33594655	-554483	22.18608	0.597694143	Intergenic
TNPO1	chr2	29132404	29133074	-11635	23.04877	0.598058958	Intergenic
ZFP68	chr12	18170817	18171487	18493	30.50515	0.598422618	Intergenic
ZFP68	chr12	18170577	18171247	18253	29.79682	0.598785121	Intergenic
ZFP68	chr12	18171059	18171729	18735	20.44521	0.599147843	Intergenic
SULT2B1	chr1	101731740	101732410	9366	17.93014	0.599509404	intron (ENSRNOT00000067430. intron 1 of 6)
RF00026	chr9	58258512	58259182	262740	35.78552	0.599869802	Intergenic
OCLN	chr2	30567249	30567919	9007	16.77428	0.600230417	intron (ENSRNOT00000024674. intron 1 of 8)
AABR07058608.1	chr7	127500414	127501084	-65823	38.00714	0.600589866	Intergenic
CLNK	chr14	76627291	76627961	-29685	37.4119	0.600948146	Intergenic
DCDC5	chr3	97531005	97531675	181886	38.86128	0.601306641	Intergenic
CTBS	chr2	252310501	252311171	4962	37.07467	0.601663963	intron (ENSRNOT00000020972. intron 3 of 6)

CTBS	chr2	252310705	252311375	5166	20.73989	0.602020112	intron (ENSRNOT00000020972. intron 3 of 6)
ZFP68	chr12	18187419	18188089	35095	35.8	0.602375084	Intergenic
PLEKHA5	chr4	174669550	174670220	-22446	38.16478	0.602730266	intron (ENSRNOT00000042291. intron 3 of 31)
ANK3	chr20	20075196	20075866	-29516	20.31577	0.603084268	Intergenic
MED30	chr7	92175148	92175818	-59114	35.25107	0.603438479	Intergenic
GCNT3	chr8	76475440	76476110	-23221	34.7753	0.603791507	Intergenic
MAP4K3	chr6	3310651	3311321	44353	28.04049	0.604143351	intron (ENSRNOT00000078044. intron 16 of 33)
MAP4K3	chr6	3310388	3311058	44616	35.23381	0.604494008	intron (ENSRNOT00000078044. intron 16 of 33)
AABR07017527.1	chr15	25206715	25207385	73234	23.80784	0.604844868	Intergenic
POLN	chr14	81872599	81873269	14191	39.95662	0.605194538	intron (ENSRNOT00000058067. intron 1 of 22)
DDX20	chr2	208111433	208112103	40411	38.46142	0.605544411	intron (ENSRNOT00000051835. intron 2 of 6)
RXFP2	chr12	6035624	6036294	42452	15.99938	0.605893091	intron (ENSRNOT00000001197. intron 13 of 17)
AABR07012384.1	chr2	194716155	194716825	158504	33.93808	0.606240575	intron (ENSRNOT00000070843. intron 1 of 1)
YPEL1	chr11	88197311	88197981	-17104	39.7199	0.606588259	Intergenic
STMN4	chr15	43033698	43034368	26125	23.57253	0.606934745	Intergenic
STMN4	chr15	43033474	43034144	25901	32.17106	0.607281428	Intergenic
AABR07012384.1	chr2	194716435	194717105	158784	29.47654	0.607625512	intron (ENSRNOT00000070843. intron 1 of 1)
TP53BP1	chr3	113198442	113199112	33013	35.20906	0.60796979	intron (ENSRNOT00000019025. intron 11 of 27)
VOM1R64	chr9	101225367	101226037	2856	20.46717	0.608312863	Intergenic
KCTD6	chr15	18477007	18477677	16024	36.43079	0.60865613	intron (ENSRNOT00000010260. intron 14 of 14)
VOM1R64	chr9	101225168	101225838	2657	29.89276	0.608998187	Intergenic
OLR1382	chr10	12822826	12823496	-5024	15.07465	0.609339034	Intergenic
OLR1382	chr10	12822624	12823294	-4822	37.06901	0.609680072	Intergenic
AABR07010476.1	chr2	137147953	137148623	5263	36.93045	0.610019896	TTS (ENSRNOT00000083443)
GPX8	chr2	44916879	44917549	-10184	39.47448	0.610358504	Intergenic
RCBTB2	chr15	55029670	55030340	-4028	38.06121	0.610695894	Intergenic
MECOM	chr2	117301007	117301677	153427	37.86078	0.61103347	Intergenic
AC129049.2	chr1	273618460	273619130	-1646	36.90267	0.611371233	Intergenic
OPA1	chr11	74715381	74716051	77957	38.335	0.611706366	Intergenic
SPAG17	chr2	201939662	201940332	-260800	48.43836	0.612043091	Intergenic
RF00026	chr1	143504382	143505052	8126	36.32907	0.612377182	intron (ENSRNOT00000087785. intron 1 of 8)
DYNC1H1	chr6	134948823	134949493	-9696	36.6921	0.612711455	Intergenic
LRRC75B	chr20	14062414	14063084	8210	34.6918	0.613045911	Intergenic
AABR07005596.1	chr1	189803220	189803890	5495	35.71531	0.613379137	intron (ENSRNOT00000091780. intron 1 of 1)

DLAT	chr8	55075988	55076658	11509	23.08651	0.613711131	intron (ENSRNOT00000032152. intron 7 of 13)
ST6GAL1	chr11	81002213	81002883	-21126	27.26057	0.614043304	Intergenic
ST6GAL1	chr11	81001901	81002571	-20814	34.48489	0.614375658	Intergenic
MAFG	chr10	109811101	109811771	-113	38.50348	0.614706775	promoter-TSS (ENSRNOT00000054970)
ACSM2	chr1	189385884	189386554	21931	33.1895	0.615036655	intron (ENSRNOT00000084260. intron 7 of 14)
AABR07030040.1	chr10	63691549	63692219	-4724	31.77518	0.615366713	intron (ENSRNOT00000005100. intron 5 of 13)
ACSM2	chr1	189385672	189386342	21719	33.27613	0.615695529	intron (ENSRNOT00000084260. intron 7 of 14)
CYP3A62	chr12	18704455	18705125	25001	16.49911	0.616024521	intron (ENSRNOT00000087229. intron 11 of 12)
AABR07052750.1	chr3	71653299	71653969	-10961	18.21695	0.616353689	Intergenic
AABR07036010.1	chr12	30501798	30502468	127	37.63197	0.616680193	promoter-TSS (ENSRNOT00000093591)
SPAG5	chr10	65556372	65557042	3810	25.01419	0.617008291	TTS (ENSRNOT00000056217)
WLS	chr2	266270556	266271226	-44145	39.44864	0.617333721	Intergenic
BTBD11	chr7	24136469	24137139	-34043	15.22321	0.617659321	intron (ENSRNOT00000044331. intron 17 of 30)
BTBD11	chr7	24135960	24136630	-33534	15.93731	0.617985094	intron (ENSRNOT00000044331. intron 17 of 30)
DPY19L2	chr8	25805887	25806557	23347	35.09472	0.618309615	intron (ENSRNOT00000071884. intron 6 of 21)
LOC102553774	chr8	103011475	103012145	-123070	17.4309	0.618632882	intron (ENSRNOT00000011358. intron 14 of 15)
LOC102553774	chr8	103011275	103011945	-123270	37.18964	0.618956317	intron (ENSRNOT00000011358. intron 14 of 15)
AABR07001662.1	chr1	54980641	54981311	-97414	38.68306	0.619278496	Intergenic
AABR07001662.1	chr1	54980879	54981549	-97652	33.81832	0.619600843	Intergenic
RF00026	chr3	22079478	22080148	31688	37.07086	0.61992193	intron (ENSRNOT00000025443. intron 18 of 20)
AC112866.1	chr1	193755986	193756656	-55648	33.35409	0.620243183	Intergenic
RF00026	chr1	147838554	147839224	-9652	30.90831	0.620563174	intron (ENSRNOT00000074103. intron 7 of 9)
AC112866.1	chr1	193756188	193756858	-55850	20.38142	0.62088333	Intergenic
STXBP6	chr6	65273470	65274140	45722	37.16753	0.621202221	intron (ENSRNOT00000005618. intron 1 of 5)
LOC685680	chr11	60158537	60159207	18742	24.35743	0.621519845	intron (ENSRNOT00000033595. intron 3 of 5)
RF00026	chr2	47385654	47386324	88904	19.09302	0.621837631	Intergenic
RF00026	chr2	47385446	47386116	88696	25.73306	0.622154147	Intergenic
LEO1	chr8	82373576	82374246	-6846	16.63346	0.62246939	Intergenic
SKOR2	chr18	73115449	73116119	-42189	30.00738	0.622786228	Intergenic
SKOR2	chr18	73115653	73116323	-41985	21.40783	0.623100357	Intergenic
GTF3A	chr12	9876772	9877442	-12316	20.4148	0.623414645	Intergenic
GTF3A	chr12	9876573	9877243	-12117	31.17126	0.623727655	Intergenic
TMTC1	chr4	182985963	182986633	-142007	33.95253	0.624040822	Intergenic

SFT2D1	chr1	53003306	53003976	10825	17.79174	0.624354146	intron (ENSRNOT00000049831. intron 5 of 7)
FOXK1	chr12	14295257	14295927	-51276	40.46599	0.624666189	Intergenic
APBA2	chr1	125514526	125515196	147581	18.67033	0.62497695	intron (ENSRNOT00000022049. intron 5 of 13)
RF00560	chr2	107870087	107870757	-241391	39.19446	0.625287864	Intergenic
RF00015	chr18	64395486	64396156	68093	40.48744	0.625597493	Intergenic
AABR07027263.1	chr17	21810090	21810760	-24377	17.20843	0.625907276	Intergenic
ALS2	chr9	66027044	66027714	6492	27.34722	0.62621577	intron (ENSRNOT00000035209. intron 1 of 33)
ACVR1C	chr3	44380553	44381223	-38533	32.41112	0.626524415	Intergenic
ALS2	chr9	66027356	66028026	6180	15.98557	0.62683177	intron (ENSRNOT00000035209. intron 1 of 33)
GSS	chr3	151082300	151082970	23922	29.90443	0.627137832	intron (ENSRNOT00000025657. intron 9 of 12)
ACVR1C	chr3	44380755	44381425	-38735	27.6572	0.627444042	Intergenic
GSS	chr3	151082053	151082723	24169	23.19023	0.627750403	intron (ENSRNOT00000025657. intron 9 of 12)
SERPINB6B	chr17	32809579	32810249	-26487	35.89016	0.62805402	Intergenic
ZBTB10	chr2	94619061	94619731	110912	34.65275	0.628359232	Intergenic
ERAP1	chr2	1107770	1108440	-302829	33.07222	0.628663144	Intergenic
SH3TC2	chr18	57340245	57340915	54258	31.99877	0.628965755	intron (ENSRNOT00000026174. intron 14 of 16)
RF00001	chr9	81052603	81053273	1001	22.37225	0.629268511	TTS (ENSRNOT00000070156)
PSRC1	chr2	211183212	211183882	6991	18.02629	0.629569964	exon (ENSRNOT00000027263. exon 34 of 34)
PSRC1	chr2	211182860	211183530	6639	23.5995	0.629871561	TTS (ENSRNOT00000027263)
RF00001	chr9	81052974	81053644	1372	23.98371	0.630173302	Intergenic
ALDOA	chr1	198231231	198231901	778	28.66814	0.630473737	intron (ENSRNOT00000088473. intron 1 of 8)
AABR07013288.4	chr2	231927015	231927685	-14444	19.32992	0.630772862	exon (ENSRNOT00000014695. exon 16 of 20)
AABR07067210.1	chr9	35154863	35155533	6996	37.85453	0.631072129	Intergenic
AABR07013288.4	chr2	231926812	231927482	-14647	37.68923	0.631370084	intron (ENSRNOT00000014695. intron 15 of 19)
TMTC3	chr7	39949513	39950183	267208	26.82413	0.63166818	Intergenic
EPB41L5	chr13	35642222	35642892	26411	37.93287	0.631966417	intron (ENSRNOT00000042862. intron 6 of 22)
PROSER3	chr1	89005970	89006640	736	32.30102	0.632263338	intron (ENSRNOT00000032363. intron 1 of 10)
PROSER3	chr1	89006173	89006843	533	26.92563	0.632558943	intron (ENSRNOT00000032363. intron 1 of 10)
AABR07005977.1	chr1	210567875	210568545	-50483	37.45443	0.632854686	intron (ENSRNOT00000031734. intron 9 of 11)
TAB2	chr1	2185036	2185706	-111475	19.7902	0.633149109	Intergenic
GPC6	chr15	102160407	102161077	-4009	37.93478	0.633443669	Intergenic
ALG8	chr1	162340864	162341534	-852	36.85952	0.633736907	promoter-TSS (ENSRNOT00000016478)

RBM28	chr4	56396904	56397574	40903	42.03954	0.634030281	Intergenic
PEX1	chr4	27697807	27698477	-105	36.88665	0.63432379	promoter-TSS (ENSRNOT00000038136)
SLC25A19	chr10	104204409	104205079	-25221	24.70914	0.634617436	intron (ENSRNOT00000005347. intron 3 of 5)
JAZF1	chr4	83160164	83160834	-22972	17.22157	0.634908293	Intergenic
AABR07068163.1	chr9	86793140	86793810	18082	37.48657	0.635200747	Intergenic
SLC25A19	chr10	104204167	104204837	-24979	28.13816	0.635491872	intron (ENSRNOT00000005347. intron 3 of 5)
PTK2	chr7	114551711	114552381	21854	35.16188	0.635781666	intron (ENSRNOT00000011219. intron 3 of 30)
RF00015	chr15	20208729	20209399	-22675	19.87068	0.636071592	Intergenic
RGS22	chr7	74894274	74894944	7388	36.82466	0.636360186	intron (ENSRNOT00000039378. intron 2 of 27)
CAST	chr2	1512784	1513454	-1528	42.08427	0.63664891	intron (ENSRNOT00000062055. intron 2 of 28)
ZXDC	chr4	122300856	122301526	18912	37.54691	0.636937766	intron (ENSRNOT00000038244. intron 8 of 10)
AABR07013676.2	chr2	249576536	249577206	-46772	36.21244	0.637226752	Intergenic
TK2	chr19	930941	931611	14073	39.70674	0.637512934	intron (ENSRNOT00000017269. intron 6 of 9)
AABR07059140.1	chr4	4549315	4549985	47627	34.60917	0.637800712	Intergenic
RF00100	chr13	16129066	16129736	-190817	48.60631	0.638087152	Intergenic
RTTN	chr18	86075550	86076220	4223	15.60904	0.63837225	intron (ENSRNOT00000064901. intron 5 of 11)
AABR07042652.1	chr19	1350245	1350915	95138	38.84945	0.638657476	Intergenic
SPATS2L	chr9	64777571	64778241	32855	32.45485	0.638941357	intron (ENSRNOT00000021527. intron 3 of 11)
RF00015	chr14	87004010	87004680	-39339	37.68243	0.639226837	Intergenic
COX5A	chr8	62304003	62304673	5980	35.87633	0.639510972	intron (ENSRNOT00000025525. intron 1 of 4)
CASP3	chr16	48830261	48830931	32608	36.01052	0.639795233	Intergenic
FOXC1	chr17	33706468	33707138	244681	33.56347	0.640078147	intron (ENSRNOT00000023691. intron 7 of 10)
AABR07035475.1	chr12	16536368	16537038	-122925	26.73417	0.640361186	intron (ENSRNOT00000001709. intron 10 of 17)
EPB41L3	chr9	117598384	117599054	15099	35.73455	0.640642874	intron (ENSRNOT00000088647. intron 2 of 20)
SRPK1	chr20	5875913	5876583	-10394	38.63423	0.640924687	Intergenic
AABR07035475.1	chr12	16535840	16536510	-123453	19.92187	0.641206624	intron (ENSRNOT00000001709. intron 10 of 17)
AABR07052263.1	chr3	43535648	43536318	-158115	36.13924	0.641487207	Intergenic
MEMO1	chr6	22371871	22372541	9722	15.8475	0.641767914	intron (ENSRNOT00000008687. intron 2 of 7)
MEMO1	chr6	22371640	22372310	9491	30.6256	0.642047265	intron (ENSRNOT00000008687. intron 2 of 7)
EPHB3	chr11	83579245	83579915	-32906	39.91358	0.642325258	Intergenic
AABR07068066.2	chr9	80584769	80585439	84214	32.11818	0.642604851	Intergenic

AABR07026938.1	chr17	5961978	5962648	85711	36.86683	0.642883086	intron (ENSRNOT00000042145. intron 16 of 17)
TMEM126B	chr1	156180887	156181557	-80809	24.13254	0.643159961	Intergenic
ITM2C	chr9	92901715	92902385	-14419	39.22961	0.643438436	Intergenic
LOC100911649	chr16	12746196	12746866	-4521	35.93679	0.643715549	Intergenic
SAMD13	chr2	252507361	252508031	-1725	31.01525	0.643992782	Intergenic
SNX3	chr20	47262248	47262918	8919	38.04736	0.644268651	intron (ENSRNOT00000074532. intron 5 of 5)
FAM168B	chr9	41337688	41338358	-525	31.36352	0.644544638	promoter-TSS (ENSRNOT00000039480)
AABR07057877.1	chr7	91698882	91699552	57648	36.68224	0.644820743	Intergenic
AABR07051626.2	chr3	18303623	18304293	-11362	17.19037	0.645095482	Intergenic
AABR07051626.2	chr3	18303418	18304088	-11567	36.72644	0.645368851	Intergenic
GPR150	chr2	2802038	2802708	12317	31.59693	0.645643822	Intergenic
RF00026	chr8	62485831	62486501	-1092	34.07371	0.645917424	intron (ENSRNOT00000026492. intron 1 of 6)
MNT	chr10	61684289	61684959	-617	41.09961	0.646189653	promoter-TSS (ENSRNOT00000092606)
MNT	chr10	61684490	61685160	-416	16.57051	0.646463486	promoter-TSS (ENSRNOT00000003933)
APOLD1	chr4	168732761	168733431	-19037	37.6397	0.646734457	Intergenic
BARX2	chr8	32923904	32924574	93615	32.27188	0.647007031	Intergenic
AABR07026339.1	chr16	72775690	72776360	79078	33.63011	0.647278229	intron (ENSRNOT00000048602. intron 9 of 9)
RF00026	chr8	87062603	87063273	83278	36.889	0.647549541	intron (ENSRNOT00000077071. intron 51 of 65)
SRRM3	chr12	23908666	23909336	16740	19.70179	0.647819475	intron (ENSRNOT00000001957. intron 1 of 14)
RF00091	chr10	110990549	110991219	28205	35.52946	0.648089522	Intergenic
GMCL1	chr4	118511159	118511829	22772	42.94741	0.648359681	intron (ENSRNOT00000024414. intron 9 of 13)
USPL1	chr12	6951297	6951967	5282	41.08753	0.648628459	intron (ENSRNOT00000072129. intron 3 of 8)
RLN1	chr1	247487015	247487685	-1148	35.7548	0.648897349	Intergenic
AABR07057877.1	chr7	91699083	91699753	57447	27.84157	0.649164856	Intergenic
PCNT	chr20	12985181	12985851	40730	38.23325	0.649432472	intron (ENSRNOT00000048218. intron 13 of 41)
KCNIP2	chr1	265650254	265650924	-77180	19.32571	0.649700199	intron (ENSRNOT00000054703. intron 22 of 25)
LOC306079	chr15	62676467	62677137	155849	37.33569	0.649968037	Intergenic
AABR07032171.1	chr18	50697554	50698224	-75198	36.46217	0.650234487	Intergenic
TMTC1	chr4	182966090	182966760	-122134	34.09343	0.650499549	Intergenic
SEMA6D	chr3	116725276	116725946	-174267	25.24579	0.650764719	Intergenic
SEMA6D	chr3	116725719	116726389	-173824	19.31041	0.651029997	Intergenic
RF00026	chr10	63301800	63302470	-2702	36.20998	0.651293884	Intergenic
AABR07031590.1	chr18	21247559	21248229	83948	38.47154	0.651557878	Intergenic
TFEC	chr4	44037588	44038258	98892	34.72576	0.651821978	Intergenic
TFEC	chr4	44037796	44038466	98684	20.32478	0.652084684	Intergenic

PPP1R1C	chr3	66753300	66753970	80389	33.26751	0.652347496	intron (ENSRNOT00000081338. intron 4 of 4)
GRIN2A	chr10	6164669	6165339	234706	24.69599	0.652610414	Intergenic
GRIN2A	chr10	6164469	6165139	234506	35.86715	0.652871935	Intergenic
RDH14	chr6	36289781	36290451	179846	37.71154	0.65313356	Intergenic
RF00003	chr2	73648209	73648879	-182284	36.40747	0.653393786	Intergenic
AABR07015729.1	chr14	72800864	72801534	-87839	21.72723	0.653654116	Intergenic
MYOM2	chr16	79670367	79671037	1017	40.42835	0.653913043	intron (ENSRNOT00000015908. intron 1 of 36)
AABR07015729.1	chr14	72800623	72801293	-88080	21.48185	0.654172073	Intergenic
AABR07035471.1	chr12	15943183	15943853	17347	26.64445	0.654431206	intron (ENSRNOT00000001654. intron 2 of 3)
GUCY2G	chr1	276134452	276135122	93787	31.74546	0.654688934	Intergenic
CHN1	chr3	60567370	60568040	44219	39.46294	0.654948271	intron (ENSRNOT00000068745. intron 2 of 8)
PLS1	chr8	103608358	103609028	220	32.35402	0.655204694	intron (ENSRNOT00000013209. intron 1 of 14)
MTMR3	chr14	84815255	84815925	4825	37.20399	0.655462726	intron (ENSRNOT00000057501. intron 1 of 18)
MYRFL	chr7	59869649	59870319	12093	36.04806	0.65571935	intron (ENSRNOT00000068774. intron 4 of 30)
SETDB2	chr15	39680555	39681225	24318	35.75017	0.655976075	Intergenic
RGD1561667	chr1	55226666	55227336	7228	45.49114	0.6562329	Intergenic
LOC102547963	chr16	5357971	5358641	276067	37.71378	0.656488314	intron (ENSRNOT00000048043. intron 10 of 36)
AABR07039245.1	chrX	73027329	73027999	4497	36.85978	0.65674534	Intergenic
AABR07052263.1	chr3	43535363	43536033	-158400	28.61362	0.656999441	Intergenic
SLC28A1	chr1	142973236	142973906	22477	31.09174	0.657255153	intron (ENSRNOT00000077441. intron 8 of 16)
CBL	chr8	48557538	48558208	6849	25.23311	0.657510965	intron (ENSRNOT00000067902. intron 1 of 15)
AABR07070151.1	chr8	54351938	54352608	289352	32.60815	0.657765362	Intergenic
RGD1305938	chr2	53826975	53827645	-135	38.58112	0.658019858	promoter-TSS (ENSRNOT00000078158)
FOXN3	chr6	123716612	123717282	-139252	38.57173	0.658272936	Intergenic
CD3EAP	chr1	80270974	80271644	-308	38.99628	0.658526111	promoter-TSS (ENSRNOT00000034266)
NETO1	chr18	83515839	83516509	44832	34.15187	0.658779384	intron (ENSRNOT00000019384. intron 4 of 10)
ATP5S	chr6	92034540	92035210	-22932	39.74169	0.659031237	intron (ENSRNOT00000006473. intron 6 of 9)
TSC22D1	chr15	58552402	58553072	-1637	37.02431	0.659283186	Intergenic
OLR1326	chr8	43739241	43739911	6031	27.17487	0.659535232	Intergenic
SCP2D1	chr3	139223978	139224648	249442	34.17257	0.659785854	Intergenic
MYO16	chr16	84957616	84958286	-18628	34.28131	0.660036572	Intergenic
LOC100909977	chr11	54099843	54100513	-37461	39.09127	0.660287385	Intergenic
RF00026	chr9	58135026	58135696	139254	19.82878	0.660536772	Intergenic
MIR6326	chr10	62296955	62297625	-2049	34.45459	0.660786254	Intergenic

AC117065.2	chr12	16299461	16300131	1655	15.26157	0.66103583	intron (ENSRNOT00000060444. intron 6 of 18)
AC117065.2	chr12	16299223	16299893	1893	19.21437	0.6612855	intron (ENSRNOT00000060444. intron 6 of 18)
PCDHA6	chr18	30014622	30015292	-2961	25.05722	0.661533741	intron (ENSRNOT00000084132. intron 1 of 3)
PCDHA6	chr18	30014423	30015093	-3160	35.81061	0.661782075	intron (ENSRNOT00000084132. intron 1 of 3)
AABR07045086.1	chr20	33671215	33671885	-73140	36.08709	0.662028979	Intergenic
RF00015	chr14	86437851	86438521	12994	37.28807	0.662275974	exon (ENSRNOT00000083394. exon 4 of 23)
IRAK4	chr7	135805681	135806351	2318	38.29176	0.662523061	intron (ENSRNOT00000007932. intron 1 of 11)
AABR07063755.1	chr6	46320229	46320899	301789	36.09511	0.662770241	Intergenic
FARS2	chr17	29354625	29355295	5862	33.41298	0.663015986	intron (ENSRNOT00000080031. intron 1 of 5)
FARS2	chr17	29354859	29355529	5628	23.87694	0.663261823	intron (ENSRNOT00000080031. intron 1 of 5)
AABR07030919.1	chr10	109418543	109419213	-1308	37.29374	0.663506222	Intergenic
ZFP84	chr1	87709702	87710372	13032	33.14106	0.663750712	exon (ENSRNOT00000028158. exon 4 of 4)
CCDC14	chr11	69277435	69278105	39078	42.93843	0.663995292	Intergenic
ZFP84	chr1	87709906	87710576	13236	22.95971	0.664238432	exon (ENSRNOT00000028158. exon 4 of 4)
NUP205	chr4	62691263	62691933	-12181	38.74479	0.664481662	Intergenic
RPRD1B	chr3	154501212	154501882	-5488	19.30549	0.664724981	Intergenic
RPRD1B	chr3	154501697	154502367	-5003	18.62042	0.664966857	Intergenic
AABR07061158.1	chr4	107552899	107553569	-109381	34.80436	0.665208822	Intergenic
ADRA1A	chr15	43348847	43349517	50388	27.9537	0.665450874	intron (ENSRNOT00000012736. intron 1 of 1)
DRD2	chr8	53666517	53667187	-11925	21.3087	0.665693015	Intergenic
GPR45	chr9	49856714	49857384	19181	17.59816	0.66593371	exon (ENSRNOT00000079239. exon 11 of 12)
POLE	chr12	52447546	52448216	4159	35.88705	0.666174493	intron (ENSRNOT00000067453. intron 3 of 48)
RGD1566337	chr2	194751540	194752210	124087	44.38886	0.666413828	Intergenic
RGD1566337	chr2	194751739	194752409	123888	20.66922	0.666654784	Intergenic
TFEC	chr4	44163360	44164030	-26880	35.44757	0.666894292	Intergenic
RYK	chr8	111358978	111359648	32880	18.91204	0.667132349	intron (ENSRNOT00000067203. intron 2 of 14)
EGFLAM	chr2	56655983	56656653	23637	28.90483	0.667372028	intron (ENSRNOT00000016722. intron 1 of 21)
RYK	chr8	111359509	111360179	33411	20.10641	0.667610256	intron (ENSRNOT00000067203. intron 3 of 14)
RF00554	chr18	49546284	49546954	-22057	39.80924	0.667848569	Intergenic
OLR1090	chr7	15702435	15703105	4123	24.80639	0.668085429	intron (ENSRNOT00000042742. intron 1 of 1)
OTOR	chr3	137239011	137239681	85260	33.93693	0.668323912	Intergenic

YTHDC2	chr1	181198334	181199004	941901	22.35831	0.66856094	Intergenic
AABR07001662.1	chr1	54956246	54956916	-73019	37.77388	0.668798053	Intergenic
SMPDL3A	chr20	40829977	40830647	51385	38.88539	0.669033709	Intergenic
STARD13	chr12	1229030	1229700	-33774	34.0752	0.669269448	Intergenic
RF00026	chr18	37458562	37459232	-25524	22.05437	0.66950527	Intergenic
AABR07020983.1	chr13	50702997	50703667	11318	38.91952	0.669741175	intron (ENSRNOT00000076984. intron 2 of 2)
CPEB2	chr14	72623233	72623903	-243238	34.20649	0.669975621	Intergenic
AABR07013676.2	chr2	249576743	249577413	-46979	30.09927	0.670210149	Intergenic
INPP5F	chr1	200088598	200089268	51184	31.07712	0.670444759	exon (ENSRNOT00000027630. exon 8 of 20)
INPP5F	chr1	200088342	200089012	50928	29.71848	0.670677906	intron (ENSRNOT00000027630. intron 7 of 19)
PINX1	chr15	47181598	47182268	-29650	35.50565	0.670911135	Intergenic
RF00413	chr19	12646125	12646795	-28042	17.71707	0.671144445	intron (ENSRNOT00000090886. intron 6 of 14)
RF00413	chr19	12645912	12646582	-28255	31.9863	0.67137629	intron (ENSRNOT00000090886. intron 6 of 14)
RF00100	chr14	50676760	50677430	128263	25.55572	0.671609762	Intergenic
SIK3	chr8	50355863	50356533	45793	20.03938	0.671840221	intron (ENSRNOT00000073507. intron 1 of 24)
AABR07027368.1	chr17	26689677	26690347	-82084	16.01294	0.672072306	Intergenic
UCHL3	chr3	171141186	171141856	-6866	28.7938	0.672302924	Intergenic
CFAP20	chr19	10008991	10009661	-15621	39.04932	0.672533621	intron (ENSRNOT00000016386. intron 11 of 11)
AABR07027368.1	chr17	26689955	26690625	-81806	16.44992	0.672764396	Intergenic
RF00560	chr4	125381490	125382160	-46273	36.16901	0.672993702	Intergenic
SEL1L2	chr3	134373612	134374282	32629	22.03234	0.673223086	intron (ENSRNOT00000033562. intron 2 of 18)
AABR07007765.1	chr2	27569327	27569997	-1488	36.08739	0.673452547	Intergenic
RF00026	chr19	44345662	44346332	46158	29.58576	0.673682087	Intergenic
RF00026	chr19	44345351	44346021	45847	18.06606	0.673910154	Intergenic
AABR07021527.1	chr13	76577155	76577825	-18091	18.69129	0.674138298	intron (ENSRNOT00000039210. intron 2 of 21)
WNT16	chr4	49293128	49293798	-75833	34.49993	0.674366519	intron (ENSRNOT00000038566. intron 16 of 22)
AABR07006436.1	chr1	233539059	233539729	130770	19.6566	0.674594817	intron (ENSRNOT00000019174. intron 2 of 6)
PHF19	chr3	13992998	13993668	-15109	16.77091	0.674821638	Intergenic
PHF19	chr3	13992792	13993462	-14903	36.61506	0.675048536	Intergenic
LDB2	chr14	70789032	70789702	8647	24.71905	0.675275511	intron (ENSRNOT00000083871. intron 1 of 8)
LDB2	chr14	70788832	70789502	8447	31.56323	0.675501006	intron (ENSRNOT00000083871. intron 1 of 8)
CCL20	chr9	88878740	88879410	-39358	36.18603	0.675728132	Intergenic
RF00001	chr9	18668481	18669151	-67235	18.33792	0.675953778	intron (ENSRNOT00000061014. intron 5 of 8)

CYB5R3	chr7	124045776	124046446	-4517	35.32303	0.676177943	Intergenic
RGS10	chr1	199831892	199832562	-8841	34.13374	0.67640374	Intergenic
AABR07044167.1	chr19	60559169	60559839	-383038	23.87545	0.676628054	intron (ENSRNOT00000078559. intron 22 of 24)
RF00003	chr18	43118033	43118703	473005	18.07179	0.676852442	Intergenic
RF00003	chr18	43117772	43118442	473266	35.74673	0.677075345	Intergenic
PROSER1	chr2	142686464	142687134	75	38.60962	0.677299882	promoter-TSS (ENSRNOT00000014614)
WWC2	chr16	47404934	47405604	36501	30.96388	0.677522933	intron (ENSRNOT00000017966. intron 1 of 22)
BARHL1	chr3	7464456	7465126	33764	36.00431	0.677744497	intron (ENSRNOT00000064323. intron 17 of 19)
COBL	chr14	92547914	92548584	29687	17.45604	0.677967694	intron (ENSRNOT00000086154. intron 1 of 15)
PRKACA	chr19	25092763	25093433	-1991	37.66208	0.678189404	TTS (ENSRNOT00000006964)
AABR07009224.1	chr2	89863561	89864231	-365501	19.87871	0.678411186	Intergenic
SLC22A25	chr1	224666230	224666900	31949	28.12516	0.67863304	intron (ENSRNOT00000024234. intron 6 of 9)
SLC22A25	chr1	224665849	224666519	32330	24.08109	0.678853404	intron (ENSRNOT00000024234. intron 6 of 9)
DOCK8	chr1	243060077	243060747	1540	21.97163	0.679073839	intron (ENSRNOT00000092734. intron 1 of 2)
DOCK8	chr1	243059877	243060547	1340	33.05171	0.679294346	intron (ENSRNOT00000092734. intron 1 of 2)
GPR139	chr1	188814535	188815205	80353	35.60888	0.679514925	Intergenic
AABR07005779.1	chr1	198910686	198911356	-890	26.75229	0.67973401	promoter-TSS (ENSRNOT00000055002)
SRRM3	chr12	23887345	23888015	38061	25.83201	0.679953166	intron (ENSRNOT00000001957. intron 3 of 14)
SRRM3	chr12	23887628	23888298	37778	25.99707	0.680172392	intron (ENSRNOT00000001957. intron 3 of 14)
HELB	chr7	64850175	64850845	36938	33.97085	0.680390122	intron (ENSRNOT00000064448. intron 22 of 23)
DBR1	chr8	107831595	107832265	5506	21.88242	0.680609489	intron (ENSRNOT00000019769. intron 4 of 7)
RGD1563680	chr3	107178144	107178814	35717	20.42524	0.68082736	intron (ENSRNOT00000006177. intron 1 of 10)
DBR1	chr8	107831925	107832595	5836	27.95321	0.681043732	intron (ENSRNOT00000019769. intron 4 of 7)
RF00560	chr4	56503061	56503731	-8605	22.80873	0.681261741	Intergenic
RF00560	chr4	56502859	56503529	-8807	36.48127	0.681478251	Intergenic
AABR07020835.1	chr13	43363471	43364141	-21648	34.97522	0.68169483	Intergenic
PHLDA3	chr13	52596506	52597176	7924	23.48489	0.681911477	Intergenic
AABR07026441.1	chr16	76654642	76655312	95359	35.57884	0.682126623	Intergenic
AABR07026441.1	chr16	76654844	76655514	95157	19.90333	0.682343408	Intergenic
SLIT2	chr14	66965961	66966631	12203	36.88152	0.68255869	intron (ENSRNOT00000005477. intron 5 of 36)
CENPV	chr10	48833289	48833959	27278	18.87062	0.682772467	Intergenic

OXR1	chr7	80577780	80578450	-46895	20.95096	0.682987885	intron (ENSRNOT00000081948. intron 3 of 16)
MYO1D	chr10	68117594	68118264	24935	35.83055	0.683201797	intron (ENSRNOT00000004609. intron 1 of 21)
MYO1D	chr10	68117800	68118470	24729	23.64276	0.683415776	intron (ENSRNOT00000004609. intron 1 of 21)
USP10	chr19	52589509	52590179	23237	34.4612	0.683629822	intron (ENSRNOT00000022432. intron 3 of 14)
USP10	chr19	52589715	52590385	23443	27.56103	0.683842361	intron (ENSRNOT00000022432. intron 3 of 14)
ZSCAN4F	chr7	17852395	17853065	6923	33.32241	0.684056541	exon (ENSRNOT00000030164. exon 3 of 3)
ZSCAN4F	chr7	17852594	17853264	6724	20.54739	0.684269212	exon (ENSRNOT00000030164. exon 3 of 3)
FAT1	chr16	50538625	50539295	-37039	38.1652	0.684480374	Intergenic
RF00560	chr9	85312851	85313521	-7644	38.36021	0.684693177	Intergenic
RAPGEF5	chr6	145433809	145434479	-112451	38.44231	0.684904469	Intergenic
POP4	chr1	94680062	94680732	-10936	36.51179	0.685115826	Intergenic
RF00425	chr14	105840577	105841247	-65769	39.00918	0.685327249	Intergenic
AABR07008259.1	chr2	49858483	49859153	1263	36.57383	0.685537158	intron (ENSRNOT00000082762. intron 1 of 1)
EVI5L	chr12	2597869	2598539	-5366	15.66489	0.685748711	intron (ENSRNOT00000001367. intron 4 of 11)
EVI5L	chr12	2597590	2598260	-5087	38.73344	0.68595717	intron (ENSRNOT00000001367. intron 4 of 11)
WASF3	chr12	10338248	10338918	-3084	15.34726	0.686167272	intron (ENSRNOT00000092340. intron 2 of 4)
S100A10	chr2	193970739	193971409	78485	18.5284	0.686377439	Intergenic
WASF3	chr12	10337923	10338593	-2759	16.51901	0.686586089	intron (ENSRNOT00000092340. intron 2 of 4)
BEST1	chr1	226058288	226058958	-8694	34.98631	0.686793221	Intergenic
AABR07021612.2	chr13	81462530	81463200	-19728	25.23679	0.687001998	Intergenic
AABR07021612.2	chr13	81462902	81463572	-19356	29.10849	0.687209255	Intergenic
RTTN	chr18	86123591	86124261	7871	21.64826	0.687416576	intron (ENSRNOT00000076159. intron 5 of 35)
RTTN	chr18	86123388	86124058	7668	33.59155	0.687623958	intron (ENSRNOT00000076159. intron 5 of 35)
PHTF2	chr4	10890920	10891590	67974	40.0546	0.687831403	intron (ENSRNOT00000066739. intron 7 of 17)
HELZ	chr10	95744704	95745374	-25115	45.21138	0.688037327	Intergenic
ZNHIT6	chr2	251415909	251416579	-37400	25.59343	0.688243312	intron (ENSRNOT00000019210. intron 59 of 63)
KITLG	chr7	42263538	42264208	-5911	19.67387	0.688449359	Intergenic
ZNHIT6	chr2	251416345	251417015	-36964	21.50679	0.688653882	intron (ENSRNOT00000019210. intron 59 of 63)
AABR07069791.3	chr8	40056795	40057465	-19317	39.51738	0.688860052	Intergenic
RF00156	chr15	101511741	101512411	6882	21.77168	0.689064697	Intergenic
RF00560	chr16	46971887	46972557	-85136	18.73023	0.689269402	Intergenic

RF00004	chr1	232671913	232672583	21245	18.67052	0.689472581	Intergenic
RF00560	chr16	46972250	46972920	-84773	18.98767	0.689677408	Intergenic
RF00004	chr1	232672247	232672917	21579	15.72532	0.689880707	Intergenic
FAT4	chr2	125745860	125746530	-5935	32.22506	0.690084066	Intergenic
SH3BGRL2	chr8	91040735	91041405	-29003	35.6685	0.690287486	Intergenic
AABR07030040.1	chr10	63702467	63703137	6194	37.86049	0.690489375	intron (ENSRNOT00000005100. intron 5 of 13)
POLG	chr1	141196709	141197379	-9013	30.97223	0.690692913	Intergenic
ADRA1B	chr10	29409255	29409925	41054	34.68766	0.690894921	intron (ENSRNOT00000087937. intron 17 of 17)
AABR07038886.1	chrX	63462250	63462920	-21541	52.52775	0.691096988	intron (ENSRNOT00000048127. intron 7 of 9)
DNER	chr9	92129400	92130070	-64333	33.79041	0.691299114	intron (ENSRNOT00000093357. intron 4 of 12)
ST8SIA4	chr9	103146541	103147211	60314	23.88658	0.691499706	intron (ENSRNOT00000026010. intron 4 of 4)
RF00334	chr3	46853457	46854127	-29148	34.90966	0.691700357	intron (ENSRNOT00000087439. intron 3 of 15)
AABR07007839.1	chr2	30110180	30110850	16094	22.93747	0.691901066	Intergenic
AABR07032593.1	chr18	72986821	72987491	-65555	34.86975	0.692101834	Intergenic
SCG5	chr3	105250172	105250842	28955	34.06778	0.69230266	exon (ENSRNOT00000010679. exon 3 of 6)
ELOVL3	chr1	265876016	265876686	-7004	44.21867	0.692503543	Intergenic
MYH11	chr10	796131	796801	32036	36.51708	0.692702891	intron (ENSRNOT00000084608. intron 4 of 40)
AC115181.1	chr10	14153890	14154560	17342	22.34758	0.692902295	Intergenic
AC115181.1	chr10	14153442	14154112	16894	28.68874	0.693101757	Intergenic
GTF2A1	chr6	115351284	115351954	1062	21.61481	0.69329968	intron (ENSRNOT00000005873. intron 1 of 8)
SAMD4B	chr1	85339130	85339800	1660	35.49816	0.69349766	intron (ENSRNOT00000093716. intron 2 of 12)
AABR07010944.1	chr2	155530203	155530873	-25302	36.70935	0.693697293	Intergenic
MAB21L1	chr2	145148823	145149493	-25718	25.8347	0.693895386	Intergenic
NCEH1	chr2	112901116	112901786	-12924	38.52533	0.694091938	intron (ENSRNOT00000017805. intron 1 of 4)
POLQ	chr11	66695165	66695835	-147	36.78938	0.694290144	promoter-TSS (ENSRNOT00000063995)
RPS15A	chr1	187573042	187573712	192367	24.31219	0.694486807	Intergenic
AKAP13	chr1	136962201	136962871	-51736	33.24553	0.694685126	Intergenic
CNNM2	chr1	266608022	266608692	77880	31.58082	0.694881901	intron (ENSRNOT00000054699. intron 1 of 7)
THBS1	chr3	109863033	109863703	1248	37.43998	0.695078732	intron (ENSRNOT00000070912. intron 25 of 48)
SIAH2	chr2	148918341	148919011	-26776	16.7511	0.695274017	Intergenic
AC119473.1	chr7	117811323	117811993	13721	25.65135	0.695470959	intron (ENSRNOT00000052227. intron 3 of 11)
SELENOW	chr1	77202958	77203628	332388	19.85671	0.695666355	Intergenic

AABR07056438.1	chr7	25617780	25618450	32029	33.61341	0.695861806	intron (ENSRNOT00000082493. intron 1 of 1)
SELENOW	chr1	77202758	77203428	332588	39.81805	0.696057312	Intergenic
PDLIM3	chr16	49558194	49558864	15785	34.55022	0.696251269	intron (ENSRNOT00000017568. intron 3 of 6)
BCL2L11	chr3	120893192	120893862	164839	24.21885	0.696446885	Intergenic
CAR12	chr8	72437525	72438195	32112	35.03265	0.696640951	intron (ENSRNOT00000023952. intron 2 of 10)
RF00045	chr4	54635078	54635748	300149	34.3948	0.696835071	intron (ENSRNOT00000056996. intron 6 of 8)
PIWIL2	chr15	52124540	52125210	-8874	37.84658	0.69702764	Intergenic
BCL2L11	chr3	120892965	120893635	164612	25.43648	0.697221868	Intergenic
GFPT1	chr4	118938957	118939627	87173	24.87511	0.697414544	Intergenic
TNFSF4	chr13	79282198	79282868	12560	36.4094	0.697607273	intron (ENSRNOT00000003969. intron 1 of 2)
GFPT1	chr4	118938718	118939388	86934	32.40447	0.697800056	Intergenic
ULK2	chr10	48100026	48100696	29016	25.83746	0.697991285	intron (ENSRNOT00000003792. intron 11 of 27)
FANCL	chr14	110682343	110683013	6588	21.54325	0.698182566	intron (ENSRNOT00000029513. intron 1 of 13)
ULK2	chr10	48099795	48100465	29247	24.65851	0.698373899	intron (ENSRNOT00000003792. intron 11 of 27)
VPS13C	chr8	73888063	73888733	205511	26.55237	0.698565285	Intergenic
VPS13C	chr8	73888310	73888980	205758	20.49613	0.698756724	Intergenic
GABRG2	chr10	26934956	26935626	243963	32.90754	0.698946605	Intergenic
FOXN3	chr6	123513387	123514057	63973	33.63558	0.699138148	intron (ENSRNOT00000006604. intron 1 of 6)
XPO4	chr15	37927693	37928363	-1313	41.39892	0.699328134	Intergenic
MRPL48	chr1	165606013	165606683	27	37.55053	0.69951817	promoter-TSS (ENSRNOT00000024290)
AABR07013750.1	chr2	254542843	254543513	-6504	22.83937	0.699706648	Intergenic
AABR07013750.1	chr2	254542355	254543025	-6992	20.15118	0.699896787	Intergenic

Annex 2. RNA-seq results of MNT KO versus WT HAP1. The genes differentially regulated upon MNT knockout obtained by Cufflinks, DESeq2 and RNA eXpress with a q-value <0.05 and a 0.7< log_2 ratio <-0.7.

	Cufflinks		DESeq2		RNA eXpress	
	log2(Ratio)	q Value	log2(Ratio)	q Value	log2(Ratio)	q value
ABCA1	1.4	0.00149243	1.24	9.86E-04	1.34	1.30E-08
ABCB1	-1.12	0.0199651	-0.99	3.36E-02	-1.09	3.06E-07
ACVR2B	1.14	0.00149243	1.01	2.86E-02	1.07	0.000352
ADAMTS17	2.4	0.00687371	1.46	3.80E-02	1.95	0.000115
AFF3	2.19	0.00149243	1.59	4.72E-03	2.01	2.21E-11
AGPAT4	1.47	0.00149243	1.35	1.30E-03	1.49	1.78E-08
AHR	-1.68	0.00149243	-1.4	1.59E-03	-1.51	0.0000461
AJUBA	1.57	0.00149243	1.35	6.20E-04	1.48	3.14E-09
AKNAD1	-2.3	0.00149243	-1.64	1.83E-03	-1.96	1.46E-09
ALDH1A2	-7.93	0.00149243	-6.44	0.00E+00	-7.12	0
ALX4	2.8	0.00149243	2.29	0.00E+00	2.68	4.12E-21
AMER2	2.61	0.00274009	1.85	3.84E-04	2.1	0.0000156
ANKRD1	3.33	0.00149243	2.49	0.00E+00	2.82	9.82E-10
APOBEC3C	3.22	0.00149243	1.92	9.86E-04	2.61	4.65E-09
APOBEC3G	2.75	0.00593146	1.5	3.32E-02	1.83	0.00334
APOLD1	1.81	0.00149243	1.55	6.60E-04	1.6	0.000344
ARHGAP31	-1.28	0.00593146	-1.12	2.29E-02	-1.25	0.00000177
ARID5B	-1.26	0.00149243	-1.1	6.19E-03	-1.17	0.00000444
ARNTL	-2.7	0.00149243	-2.28	0.00E+00	-2.55	5.12E-14
ASH2L	-1.63	0.00149243	-1.45	5.80E-05	-1.59	8.50E-17
ATP10A	-1.66	0.00149243	-1.36	6.88E-03	-1.55	0.00000148
ATP10D	-1.68	0.00149243	-1.48	4.40E-05	-1.49	0.000127
ATRNL1	1.59	0.0255771	1.52	2.38E-03	1.73	4.91E-07
B2M	-1.29	0.00149243	-1.13	7.23E-03	-1.21	0.0000422
BAALC	-1.76	0.0173329	-1.29	4.48E-02	-1.64	2.06E-08
BCAS3	1.73	0.00274009	1.41	5.28E-03	1.59	0.0000177
BCHE	1.61	0.00149243	1.38	2.22E-03	1.51	0.00000275
BCL11B	-2.49	0.00149243	-1.94	1.70E-05	-2.22	1.26E-09
BHLHE22	-3.6	0.00149243	-2.55	0.00E+00	-3.27	2.08E-21
BMP2	-11.97	0.00149243	-4.78	0.00E+00	-6.19	3.51E-42
BMP7	3.3	0.00149243	2.59	0.00E+00	3.11	4.80E-30
BTBD11	-4.2	0.00149243	-3.06	0.00E+00	-3.78	9.38E-32
BTN3A3	-2.38	0.00149243	-2.01	5.00E-06	-2.32	8.89E-18
BVES	1.92	0.00149243	1.65	5.30E-05	1.83	2.40E-12
C16orf45	-2.72	0.00274009	-1.63	1.14E-02	-2.18	0.00000784
C2orf72	-2.9	0.00149243	-1.59	1.79E-02	-2.22	0.00000877
C5	2.25	0.0038637	1.5	1.61E-02	1.93	0.0000013
CABYR	1.63	0.0125503	1.17	4.15E-02	1.41	2.32E-09

CADM1	-4.25	0.0125503	-1.96	1.31E-03	-3.26	1.17E-11
CADM2	3.54	0.00149243	2.46	0.00E+00	2.98	2.94E-17
CADPS2	4.31	0.00149243	3.56	0.00E+00	3.95	1.00E-38
CALB1	-2.39	0.0038637	-1.58	1.53E-02	-2.18	1.52E-07
CALD1	1.47	0.00149243	1.3	2.19E-03	1.34	0.000358
CAV1	1.9	0.00274009	1.38	2.41E-02	1.72	0.00000137
CCDC109B	-1.26	0.00149243	-1.09	1.74E-02	-1.19	0.0000125
CCDC80	1.91	0.00149243	1.62	3.00E-05	1.74	8.49E-10
CCND2	2.19	0.00149243	1.89	1.00E-06	1.99	2.19E-09
CDH2	1.6	0.00149243	1.4	3.84E-04	1.49	4.47E-07
CDH3	3.42	0.0038637	1.52	3.13E-02	2.35	0.0000109
CDH9	3.2	0.00149243	1.76	4.78E-03	2.48	6.94E-08
CECR1	5.29	0.0166826	2.53	5.00E-06	3.77	6.87E-15
CELF2	1.97	0.00149243	1.6	9.38E-04	1.7	0.0000582
CHD1L	-1.59	0.00149243	-1.34	2.29E-04	-1.47	1.22E-21
CHI3L2	-1.82	0.00149243	-1.38	7.15E-03	-1.47	0.00415
CHL1	-8.66	0.00149243	-5.82	0.00E+00	-7.03	0
CHMP4C	-11.82	0.00149243	-3.69	0.00E+00	-5.49	2.12E-31
CHRNA9	9.3	0.00149243	1.56	1.65E-02	3.6	6.30E-11
CHST2	-3.2	0.00149243	-2.25	1.00E-05	-2.84	2.51E-14
CLDN1	-4.36	0.00149243	-3.6	0.00E+00	-3.14	1.02E-08
CNKSR3	-1.29	0.00149243	-1.12	1.16E-02	-1.24	2.94E-10
CNNM2	1.39	0.0398267	1.15	4.52E-02	1.36	2.12E-07
CNRIP1	1.85	0.00149243	1.5	1.98E-03	1.76	3.92E-11
CNTN1	-5.48	0.00149243	-3.93	0.00E+00	-4.74	1.26E-35
CNTN3	4.03	0.00149243	2.6	0.00E+00	3.38	2.34E-16
COCH	1.23	0.00593146	1.08	1.31E-02	1.18	8.80E-08
COL19A1	2.09	0.00149243	1.8	2.00E-06	1.98	4.45E-15
COL24A1	2.05	0.00149243	1.61	1.52E-03	1.89	5.01E-09
COL4A5	4.04	0.00149243	3.57	0.00E+00	3.84	0
COL4A6	3.99	0.00149243	3.42	0.00E+00	3.75	1.40E-45
COL5A2	2.8	0.00149243	2.49	0.00E+00	2.62	1.61E-22
COL9A1	2.91	0.00149243	1.89	6.72E-04	2.43	3.92E-10
CPE	-3.54	0.00149243	-3.1	0.00E+00	-3.4	0
CROT	-3.08	0.00149243	-2.67	0.00E+00	-3.02	3.17E-26
CRYM	-2.52	0.00149243	-1.86	2.29E-04	-2.12	9.74E-07
CSMD3	1.97	0.00149243	1.6	1.01E-04	1.73	2.75E-07
CSRNP3	1.88	0.00149243	1.56	6.81E-04	1.64	0.0000538
CTGF	1.94	0.00853121	1.45	1.49E-02	1.8	1.70E-07
CTSF	2.13	0.00149243	1.74	6.80E-05	1.91	5.29E-08
CXCL14	-2.45	0.00149243	-1.7	3.46E-03	-2.25	3.08E-12
CXXC4	2.05	0.00149243	1.71	4.51E-04	1.94	4.17E-08
CYR61	2.95	0.00149243	2.32	0.00E+00	2.43	2.30E-08
CYYR1	3.68	0.00149243	2.88	0.00E+00	3.17	1.78E-16
DAAM1	1.82	0.00149243	1.6	8.00E-06	1.75	3.93E-17

DCAF12L2	2.77	0.00149243	2.08	1.60E-05	2.5	1.19E-13
DDAH1	1.22	0.00149243	1.09	1.07E-02	1.17	0.0000131
DLC1	2.76	0.00149243	2.27	0.00E+00	2.57	8.23E-21
DLL1	-3.95	0.0141407	-1.97	1.14E-03	-3.01	2.29E-09
DNAJB9	1.48	0.00149243	1.25	1.03E-02	1.33	0.000542
DNAJC15	3.93	0.00149243	2.85	0.00E+00	3.23	7.08E-14
DPYSL3	-2.27	0.00149243	-1.76	3.34E-04	-2.11	3.29E-14
DTNA	5.44	0.00149243	4.25	0.00E+00	5.14	0
DUSP6	2.33	0.00149243	1.66	4.15E-03	2.11	7.85E-08
DYNC1I1	-1.23	0.00687371	-1.08	2.87E-02	-1.19	0.00000436
EFEMP1	4.6	0.00149243	3.69	0.00E+00	4.21	2.45E-43
EFNB2	1.68	0.00149243	1.42	1.75E-03	1.61	2.23E-10
EFR3B	-1.92	0.00149243	-1.37	2.55E-02	-1.58	0.00108
EFS	11.03	0.00149243	3.56	0.00E+00	5.18	1.49E-26
EGFEM1P	1.7	0.00853121	1.41	7.78E-03	1.48	0.00266
EGLN3	1.71	0.00149243	1.39	6.43E-03	1.55	0.0000346
ELAVL2	1.84	0.00149243	1.6	9.30E-05	1.7	2.39E-07
EMP1	2.99	0.00149243	2.43	0.00E+00	2.66	2.16E-14
ENOX1	3.43	0.00149243	2.47	0.00E+00	3.09	1.98E-21
EPB41L4B	-2.11	0.00149243	-1.86	0.00E+00	-2	1.89E-14
EPDR1	-2.05	0.00149243	-1.66	3.25E-04	-1.97	7.27E-18
EPHA3	2.62	0.00149243	2.2	0.00E+00	2.25	2.37E-08
EPHA7	2.12	0.00149243	1.78	2.00E-05	1.87	9.90E-07
EPHB6	-4.6	0.0304062	-2.35	3.20E-05	-2.94	3.27E-07
ERBB4	2.75	0.00149243	2.18	1.00E-06	2.58	3.68E-21
ESRRG	1.48	0.00149243	1.23	1.53E-02	1.35	0.0000507
ETV6	1.69	0.00149243	1.37	4.98E-03	1.55	4.51E-08
EYA2	-9.18	0.00149243	-1.51	2.21E-02	-3.31	8.36E-09
F11R	-1.41	0.00149243	-1.22	3.94E-03	-1.32	0.0000134
FA2H	-2.63	0.00149243	-1.79	9.87E-04	-2.03	0.000062
FAAH2	-3.44	0.00149243	-2.18	3.90E-05	-2.82	1.11E-12
FABP3	1.52	0.0160387	1.39	4.81E-02	1.66	0.00514
FAM102B	-1.62	0.00149243	-1.37	1.57E-03	-1.49	0.00000773
FAM111A	-1.28	0.00149243	-1.1	1.53E-02	-1.18	0.000919
FAM124A	-1.76	0.00149243	-1.44	1.21E-03	-1.63	8.53E-08
FAM127B	3.7	0.00149243	1.96	1.01E-03	-2.86	2.19E-07
FAM155A	4.67	0.00149243	2.3	5.20E-05	4.28	2.05E-40
FAM213A	1.42	0.0077109	1.19	1.31E-02	1.37	7.60E-13
FAM227A	1.89	0.00687371	1.43	1.50E-02	1.66	0.000108
FAM84A	-3.04	0.00149243	-1.96	5.59E-04	-2.43	2.63E-07
FAM84B	1.74	0.00149243	1.52	1.19E-04	1.67	1.36E-12
FAT1	1.15	0.00149243	1.03	8.49E-03	1.09	0.0000924
FBN1	2.46	0.00149243	2.16	0.00E+00	2.24	1.89E-11
FBXO32	3.47	0.00149243	2.82	0.00E+00	3.3	6.49E-33
FBXO43	-2.63	0.00853121	-1.5	3.22E-02	-2.02	0.000215

FER	1.31	0.00149243	1.14	3.21E-02	1.16	0.011
FERMT1	-1.87	0.00149243	-1.66	1.00E-06	-1.82	2.12E-31
FEZ1	1.33	0.00149243	1.15	8.28E-03	1.26	1.42E-07
FLT1	-1.77	0.0101596	-1.39	4.30E-03	-1.57	0.0000015
FLVCR2	-1.54	0.00488984	-1.38	3.15E-03	-1.57	5.42E-11
FMNL2	-1.14	0.00149243	-1	4.28E-02	-1.1	0.000344
FOLH1	-8.1	0.00149243	-5.66	0.00E+00	-6.56	0
FOXA1	-1.81	0.00149243	-1.55	1.38E-04	-1.72	3.21E-11
FOXA2	-9.43	0.00149243	-1.65	9.34E-03	-3.73	8.92E-12
FOXG1	4.62	0.00149243	2.67	0.00E+00	3.8	5.72E-19
FREM2	1.37	0.00149243	1.23	2.22E-03	1.22	0.0039
FRMD4A	-1.53	0.0387375	-2.85	0.00E+00	-4.43	1.01E-19
FRMD6	-2.1	0.00149243	-1.82	1.00E-06	-2	1.10E-17
FRY	-1.69	0.00274009	-1.43	8.65E-04	-1.61	2.55E-13
FSIP2	1.35	0.0381873	1.39	4.04E-02	1.71	0.000403
FUT9	-10.32	0.00149243	-5.15	0.00E+00	-5.51	1.28E-27
FZD10	-9.15	0.00149243	-1.76	4.57E-03	-3.82	2.02E-12
GABRQ	-4	0.0173329	-1.65	1.38E-02	-2.4	0.0000236
GADL1	3.53	0.00149243	2.78	0.00E+00	2.85	2.94E-10
GALNT5	-1.33	0.0147595	-1.15	2.15E-02	-1.31	3.85E-08
GAP43	4.55	0.00149243	2.68	0.00E+00	3.64	2.94E-18
GCNT4	1.95	0.00149243	1.59	7.99E-04	1.75	0.00000148
GJA1	3.07	0.00149243	2.67	0.00E+00	2.93	9.52E-30
GJB6	-3.62	0.00149243	-2.41	2.00E-06	-3.01	7.51E-14
GLCCI1	1.66	0.00149243	1.45	1.16E-03	1.56	0.00000595
GLIS3	4.12	0.00149243	3.03	0.00E+00	3.65	1.75E-31
GLT8D2	1.76	0.0109536	2.04	2.26E-04	-0.839	0.000122
GPC3	1.5	0.00149243	1.33	1.29E-04	1.44	1.35E-12
GPM6B	1.06	0.0101596	1.02	4.75E-02	1.1	0.000859
GPR19	3.2	0.00149243	2.59	0.00E+00	2.99	4.96E-26
GPR37	-2.51	0.00149243	-1.76	2.04E-03	-2.29	1.19E-10
GRAMD1C	-2.36	0.00149243	-1.92	1.80E-05	-2.19	2.05E-12
GTSF1	-3.14	0.00149243	-2.72	0.00E+00	-2.99	1.89E-41
GUCY1A3	-1.35	0.0117547	-1.17	9.70E-03	-1.27	0.0000138
GXYLT2	-3.11	0.00149243	-2.18	3.20E-05	-2.86	3.78E-17
HBP1	1.75	0.00274009	1.56	1.90E-05	1.7	4.85E-14
HCLS1	-3.32	0.00149243	-2	4.78E-04	-2.34	0.0000252
HDX	5.08	0.00149243	3.12	0.00E+00	4.07	1.30E-20
HECW2	-4.3	0.0038637	-2.31	2.40E-05	-3.31	4.39E-17
HLA-A	-1.88	0.00149243	-1.59	9.80E-05	-1.71	0.0000476
HLA-C	-2.48	0.00149243	-1.67	1.18E-04	-1.82	0.00000277
HLA-E	-1.36	0.00149243	-1.09	4.58E-02	-1.22	0.00391
HMGA2	-0.95	0.0368945	1.13	1.95E-02	1.21	0.000486
HOPX	-4.09	0.00274009	-1.45	4.24E-02	-2.59	0.00000587
HOXC9	-3.72	0.00149243	-2.46	2.00E-06	-3.08	2.88E-14

HOXD13	1.15	0.00938137	1.01	4.35E-02	1.11	0.0000149
HPGD	-1.69	0.00149243	-1.42	3.58E-04	-1.45	0.00183
HRASLS5	-1.91	0.00149243	-1.68	7.00E-06	-1.85	4.55E-17
HSD17B3	-1.59	0.0409013	1.98	9.38E-04	2.67	3.71E-07
HTR7	-3.15	0.00149243	-2.43	0.00E+00	-2.92	4.95E-24
IAH1	-2.82	0.00149243	-2.37	0.00E+00	-2.65	5.50E-29
ID1	-3.15	0.00149243	-2.43	0.00E+00	-2.92	4.95E-24
IFI16	-11.25	0.00149243	-3.72	0.00E+00	-5.43	2.28E-30
IFIT1	2.1	0.00149243	1.87	5.00E-06	2.03	2.94E-10
IGFBP5	2.27	0.00149243	1.94	2.00E-06	1.94	0.00000566
IL12RB2	-1.61	0.0160387	-1.27	3.36E-02	-1.51	0.00000907
IL20RA	-2.84	0.00149243	-2.16	8.00E-06	-2.68	5.72E-20
IL7R	3.59	0.00149243	2.39	3.00E-06	2.75	2.01E-08
INHBB	-3.46	0.0077109	-1.52	3.15E-02	-2.47	0.000001
IRS1	2.09	0.00274009	1.51	8.59E-03	1.9	6.03E-09
ITGB8	1.89	0.00149243	1.53	1.54E-03	1.64	0.0000944
ITM2C	-1.81	0.00149243	-1.35	2.26E-02	-1.48	0.00718
ITPR1	-1.41	0.00149243	-1.25	2.74E-03	-1.36	3.38E-08
ITPR2	-1.68	0.00149243	-1.49	2.80E-05	-1.58	2.63E-08
JAM2	1.8	0.00149243	1.61	6.10E-05	1.79	1.22E-12
KCNH8	-2.31	0.0038637	-1.61	8.22E-03	-2	0.00000586
KCNK1	-2.49	0.00149243	-2.06	0.00E+00	-2.35	7.73E-22
KCNK2	-2.39	0.00149243	-1.99	0.00E+00	-2.13	7.13E-09
KCNMB4	1.85	0.00149243	1.55	3.04E-04	1.73	4.75E-11
KCNQ5	-9.07	0.00149243	-2.75	0.00E+00	-4.69	1.16E-20
KCTD12	-4.1	0.00149243	-3.42	0.00E+00	-3.79	1.29E-35
KIAA1324L	-1.92	0.00149243	-1.64	5.30E-05	-1.81	3.56E-11
KIAA1456	4.27	0.00149243	3.59	0.00E+00	4.02	1.67E-30
KIFAP3	1.72	0.00149243	1.49	9.30E-05	1.62	1.47E-10
KIT	-2.48	0.00149243	-1.93	4.90E-05	-2.12	0.00000113
KLHL14	-3.27	0.00274009	-2.03	3.58E-04	-2.73	4.51E-10
KLHL24	1.13	0.00149243	1.01	2.86E-02	1.05	0.00308
KLHL41	-2.62	0.00149243	-1.78	3.03E-03	-2.35	1.18E-07
KLHL5	1.36	0.00149243	1.16	2.00E-02	1.22	0.00223
KLRB1	-3.94	0.0077109	-2.19	1.37E-04	-3.29	5.37E-13
KY	-4.56	0.00938137	-2.61	2.00E-06	-3.74	7.02E-14
LAMA2	3.68	0.00149243	3.25	0.00E+00	3.29	1.51E-21
LAMA4	-3.82	0.00149243	-3.11	0.00E+00	-3.43	3.98E-24
LAMB1	1.19	0.00149243	1.05	1.54E-02	1.12	0.0000567
LIMCH1	1.06	0.00149243	0.95	3.68E-02	1.04	0.00000314
LIN28A	6.53	0.00149243	5.98	0.00E+00	6.5	0
LIN7A	-1.59	0.00149243	-1.36	1.10E-03	-1.5	3.54E-11
LINC00649	-2.03	0.00488984	-1.39	2.42E-02	-1.92	1.47E-10
LIPH	-1.87	0.00938137	-1.42	1.66E-02	-1.74	0.00000115
LMO3	1.48	0.00149243	1.28	2.25E-02	1.25	0.0296

LOC100505817	-2.9	0.00488984	-1.71	8.49E-03	-2.37	0.00000819
LOC100506990	1.16	0.0368945	1.09	3.91E-02	1.26	2.91E-08
LOC729739	3.03	0.00488984	1.72	6.36E-03	2.38	4.05E-07
LOX	1.71	0.00149243	1.62	5.06E-04	1.72	0.0000099
LPL	-4.22	0.00149243	-2.78	0.00E+00	-3.02	5.72E-09
LPPR4	-5.5	0.00593146	-3.1	0.00E+00	-4.21	4.31E-21
LPPR5	-5.88	0.00274009	-3.98	0.00E+00	-4.52	7.60E-24
LRFN5	4.06	0.00149243	2.45	6.00E-06	3.2	2.54E-11
LRRC1	-1.17	0.00149243	-1.02	2.28E-02	-1.12	0.0000246
LRRN3	1.55	0.00149243	1.37	1.76E-03	3.21	5.39E-23
LY96	-3	0.00149243	-2.28	1.00E-06	-2.78	9.61E-20
LYPD6	1.18	0.0133444	1.01	4.54E-02	1.13	2.00E-07
MACF1	1.29	0.00149243	1.13	5.19E-03	1.23	7.56E-07
MAF	-2.43	0.00149243	-2.04	0.00E+00	-2.12	2.08E-08
MAL2	-3.93	0.0246626	-1.6	1.81E-02	-2.69	5.80E-07
MAN1C1	-2.54	0.0038637	-1.44	3.36E-02	-2.1	0.00000129
MAP2	1.63	0.00149243	1.43	2.70E-04	1.54	1.87E-08
MAPK10	4.01	0.00149243	2.41	7.00E-06	3.31	4.60E-15
MARC1	14.3	0.00149243	6.45	0.00E+00	7.74	0
MB21D1	-7.01	0.0038637	-4.87	0.00E+00	-5.76	0
MCTP2	-9.27	0.00149243	-2.18	1.64E-04	-4.22	7.24E-16
ME1	1.19	0.00149243	1.03	3.33E-02	1.11	0.00028
MEST	3.45	0.00274009	2.93	0.00E+00	3.24	1.01E-38
MET	-1.89	0.00149243	-1.66	2.00E-06	-1.8	5.31E-16
METTL7A	2.55	0.00149243	2.2	0.00E+00	2.45	1.34E-38
MGARP	-4.19	0.00149243	-2.48	3.00E-06	-3.42	3.28E-18
MICAL2	1.84	0.0077109	1.78	2.00E-05	1.68	0.000309
MOBP	-6.12	0.00149243	-5.18	0.00E+00	-5.47	0
MPDZ	1.7	0.00149243	1.52	2.00E-05	1.65	6.11E-15
MR1	-3.61	0.00149243	-2.53	1.00E-06	-3.43	1.41E-20
MSRB3	1.41	0.00149243	1.18	1.11E-02	1.32	1.68E-07
MSX1	-1.63	0.0324913	-1.32	8.51E-03	-1.48	0.0000141
MYB	-2.58	0.00149243	-2.2	0.00E+00	-2.43	4.71E-20
MYBPC1	-3.59	0.00149243	-3.03	0.00E+00	-3.4	0
MYO3B	-2.24	0.00488984	-1.43	3.59E-02	-1.89	0.00000981
MYOF	2.7	0.00149243	2.33	0.00E+00	2.43	3.31E-12
MYOM1	-1.89	0.00149243	-1.49	3.14E-03	-1.76	5.01E-09
MYRIP	-3.11	0.0133444	-2.54	0.00E+00	-2.93	6.37E-30
NAV3	1.68	0.00149243	1.46	4.36E-04	1.52	0.0000204
NDST4	4.15	0.00274009	2.5	3.00E-06	3.48	2.34E-18
NEBL	2.24	0.00149243	1.83	2.30E-05	2.01	1.05E-08
NECAB1	-2.34	0.00149243	-1.74	1.60E-05	-1.87	3.01E-07
NEDD4L	-1.93	0.00149243	-1.7	4.00E-06	-1.89	4.44E-27
NEDD9	1.69	0.00149243	1.47	5.80E-05	1.54	3.58E-07
NEK3	-2.45	0.00149243	-1.56	1.57E-02	-1.92	0.000123

NELL2	1.17	0.00149243	1.02	1.49E-02	1.12	7.32E-11
NES	1.19	0.00149243	1.06	9.21E-03	1.16	4.35E-11
NFIL3	-1.46	0.00687371	-1.21	1.45E-02	-1.39	6.96E-10
NHSL1	1.09	0.00938137	0.96	4.23E-02	1.07	9.89E-08
NID2	-1.55	0.0038637	-1.43	5.18E-03	-1.6	0.0000133
NKX2-4	-3.3	0.00149243	-2.2	8.20E-05	-3.05	6.63E-13
NKX3-1	-1.66	0.0101596	-1.31	1.53E-02	-1.57	4.70E-11
NLRC5	-5.08	0.00274009	-2.17	2.16E-04	-2.81	0.00000206
NOG	2.47	0.00149243	1.75	1.03E-03	1.97	0.0000453
NOV	-3.49	0.00149243	-2.62	0.00E+00	-2.85	4.03E-10
NPY1R	-3.04	0.00149243	-2.53	0.00E+00	-2.76	5.26E-18
NQO1	2.14	0.00149243	1.91	0.00E+00	2	6.52E-12
NR1D2	1.26	0.00149243	1.09	1.55E-02	1.19	0.0000312
NR2F2	1.35	0.0109536	1.19	2.51E-02	1.34	0.0000521
NR3C1	-4.09	0.00149243	-2.86	0.00E+00	-3.56	2.62E-20
NR5A2	-3.11	0.00149243	-2.63	0.00E+00	-2.76	5.11E-16
NRIP1	2.98	0.00149243	2.53	0.00E+00	2.73	2.67E-17
NRXN1	-3.67	0.00149243	-1.96	8.91E-04	-2.81	7.91E-11
NUAK1	1.5	0.00149243	1.31	7.12E-04	1.43	8.49E-10
OLFM3	2.2	0.0038637	1.52	1.50E-02	1.79	0.000417
PACRG	-4.25	0.0250604	-1.88	2.53E-03	-2.91	1.47E-08
PAG1	1.57	0.0173329	1.21	3.59E-02	1.44	0.00000996
PAK3	-1.34	0.0038637	-1.09	1.81E-02	-1.2	5.16E-07
PARM1	1.27	0.00149243	1.13	4.62E-03	1.21	0.00000922
PBX3	-1.79	0.00149243	-1.53	1.43E-04	-1.69	1.09E-09
PCDH11X	2.03	0.00149243	1.67	2.30E-04	1.77	0.0000127
PCDH7	4.36	0.00149243	3.48	0.00E+00	4.07	2.80E-45
PCDHB2	-3.45	0.00149243	-1.98	6.81E-04	-2.81	5.32E-12
PCDHB5	1.79	0.00149243	1.48	9.87E-04	1.71	7.40E-14
PDCD4	1.6	0.00149243	1.43	1.64E-04	1.52	1.27E-08
PDE10A	-5.89	0.00149243	-4.07	0.00E+00	-4.96	2.95E-38
PDE1B	-9.45	0.00149243	-1.98	8.73E-04	-3.61	1.37E-10
PDE3A	4.7	0.00149243	3.6	0.00E+00	4.31	1.12E-44
PDE4B	3.06	0.00149243	2.44	0.00E+00	2.71	1.18E-17
PDE5A	-1.23	0.00149243	-1.23	7.88E-03	-1.35	0.000157
PDGFRA	3.43	0.00149243	3.02	0.00E+00	3.12	4.26E-22
PDK4	3.85	0.00593146	1.72	8.39E-03	2.77	5.15E-08
PEG10	1.39	0.00149243	1.24	2.34E-03	1.27	0.000334
PER2	1.46	0.00687371	1.19	1.78E-02	1.36	1.82E-08
PGR	-3.11	0.00149243	-2.23	7.00E-06	-2.64	7.56E-10
PHKA1	-1.11	0.00149243	-0.99	2.10E-02	-1.07	0.0000253
PI15	7.04	0.00149243	5.22	0.00E+00	5.45	6.68E-34
PIK3AP1	-2.5	0.00149243	-2.23	0.00E+00	-2.4	1.62E-24
PITX2	9.96	0.00149243	1.61	1.24E-02	3.61	5.54E-11
PLAT	2.16	0.00274009	1.56	2.37E-02	2.24	0.0000424

PLCE1	-1.72	0.00149243	-1.53	3.60E-05	-1.63	1.92E-08
PLEKHG1	1.21	0.00149243	1.08	1.40E-02	1.15	0.0000939
PLXDC2	-1.88	0.00149243	-1.66	3.30E-05	-1.73	3.52E-10
PMP22	1.09	0.0038637	0.96	3.24E-02	1.06	8.55E-09
PODXL	1.13	0.00149243	1	2.00E-02	1.11	4.08E-12
POF1B	-5.34	0.00149243	-4.8	0.00E+00	-5.15	0
POSTN	7.62	0.00149243	4.75	0.00E+00	5.31	5.28E-28
PPARG	-1.22	0.0206826	-1.06	4.23E-02	-1.21	5.35E-09
PPFIA2	1.61	0.00149243	1.41	1.34E-03	1.44	0.000285
PPP1R14C	-3.39	0.00149243	-2.57	0.00E+00	-3.09	1.18E-21
PPP1R1C	-4.21	0.00149243	-1.9	2.01E-03	-2.85	4.03E-09
PPP2R2B	4.33	0.00149243	3.37	0.00E+00	3.74	3.26E-23
PRAME	-1.76	0.0147595	-1.33	3.23E-02	-1.53	0.000497
PREX2	2.14	0.00149243	1.79	4.00E-06	1.95	2.92E-11
PROM1	-5.23	0.00149243	-4.58	0.00E+00	-5.02	0
PROX1	-2.03	0.00488984	-1.61	1.11E-03	-1.79	0.00000281
PRRG4	-2.21	0.00149243	-1.85	7.00E-06	-2.11	2.92E-15
PRSS35	3.01	0.00149243	2.63	0.00E+00	2.85	5.19E-30
PRTG	1.7	0.00149243	1.39	3.34E-03	1.54	0.00000641
PSMB9	-3.27	0.00274009	-1.55	2.59E-02	-2.34	0.0000161
PTCHD1	-4.07	0.00149243	-2.44	1.50E-05	-4.01	4.68E-14
PTGER3	2.55	0.0324913	2.15	0.00E+00	2.22	1.09E-08
PTPN13	1.33	0.00149243	1.17	9.21E-03	1.19	0.00267
PTPRD	-1.11	0.00149243	-0.97	2.21E-02	-1.04	0.0000159
PXDN	-9.28	0.00149243	-3.04	0.00E+00	-5	1.10E-24
RAB32	2.65	0.00149243	2.09	2.00E-06	2.41	1.94E-15
RAPGEF4	-1.4	0.0147595	-1.19	1.34E-02	-1.33	8.10E-09
RBMS3	3.35	0.00149243	2.68	0.00E+00	2.97	8.94E-14
RELN	4.09	0.00149243	3.67	0.00E+00	3.32	9.97E-14
REPS2	1.88	0.00149243	1.65	7.00E-06	1.8	8.52E-17
RIMS2	-7.54	0.0101596	-4.9	0.00E+00	-5.91	6.17E-44
RMST	-2.13	0.00274009	-1.68	2.07E-03	-1.92	0.0000334
RND3	4.7	0.00149243	3.71	0.00E+00	4.15	3.58E-30
RNF128	-9.75	0.00149243	-2.05	5.46E-04	-3.85	1.98E-12
RNF152	-2.15	0.00274009	-1.71	5.13E-04	-2.07	1.74E-15
RNF165	-9	0.00149243	-1.36	4.94E-02	-3.36	3.06E-09
RNF182	1.31	0.00149243	1.12	2.80E-02	1.17	0.00312
ROBO2	1.18	0.00149243	1.02	2.15E-02	1.13	2.49E-08
RORA	-2	0.00149243	-1.8	1.00E-06	-1.95	9.25E-13
RPS3A	1.21	0.0403658	1.06	1.28E-02	1.15	0.0000882
RPS6KA5	1.35	0.0109536	1.11	3.95E-02	1.26	0.0000236
RPS6KA6	3.66	0.00149243	3.08	0.00E+00	3.33	2.67E-24
RYR2	-4.16	0.00149243	-3.07	0.00E+00	-3.43	1.49E-15
SAMD12	-2.49	0.00149243	-2.06	7.00E-06	-2.4	4.84E-13
SAMD5	3.65	0.00149243	2.92	0.00E+00	3.28	1.43E-21

SAMHD1	-1.17	0.00149243	-1.06	9.25E-03	-1.15	6.30E-11
SCARA3	-10.14	0.00149243	-2.7	1.00E-06	-3.7	5.75E-11
SCN9A	1.85	0.00149243	1.62	2.20E-05	1.53	0.00146
SEMA3D	-1.75	0.00149243	-1.48	4.15E-04	-0.853	0.00000241
SEMA6D	3.98	0.00149243	2.74	0.00E+00	3.5	2.69E-19
SEPP1	-3.88	0.00853121	-1.87	2.60E-03	-1.48	0.00206
SERINC5	-1.06	0.00687371	-0.93	4.63E-02	-3.12	1.21E-10
SERPINB9	-1.32	0.00149243	-1.17	2.07E-03	-1.28	1.12E-10
SFRP1	1.77	0.00149243	1.5	4.58E-04	1.68	2.01E-10
SH3D19	1.49	0.00149243	1.2	3.79E-03	1.29	5.16E-07
SHISA3	1.52	0.00149243	1.35	1.20E-03	1.39	0.000105
SHROOM3	3.42	0.00149243	2.96	0.00E+00	3.28	0
SLC16A6	1.55	0.0109536	1.47	1.11E-03	1.64	2.95E-07
SLC16A7	-2.31	0.00149243	-2.07	1.20E-05	-2.4	1.82E-10
SLC16A9	1.26	0.00149243	1.08	2.98E-02	1.16	0.00101
SLC19A3	2.55	0.00149243	1.69	4.25E-03	2.26	3.17E-10
SLC1A3	1.72	0.00149243	1.51	1.08E-03	1.27	3.40E-08
SLC25A26	1.24	0.0363245	1.15	8.16E-03	-1.14	0.00339
SLC2A4	3.13	0.00149243	2.19	2.70E-05	2.73	1.18E-11
SLC35F1	-1.25	0.0077109	-1.04	4.16E-02	2	2.43E-09
SLC44A5	-1.05	0.00593146	1.81	3.20E-05	1.52	0.00088
SLC4A4	-4.18	0.00149243	-2.51	2.00E-06	-3.23	2.26E-12
SLC7A3	1.73	0.00149243	1.33	2.06E-02	1.52	0.00088
SLC8A1	3.18	0.00149243	2.72	0.00E+00	2.79	6.56E-14
SLCO5A1	3.18	0.00149243	1	4.49E-02	1.06	0.00182
SLFN12	3.66	0.00149243	2.74	0.00E+00	3.18	4.81E-16
SLFN5	1.44	0.00488984	1.24	9.21E-03	1.39	0.0000023
SLIT2	-1.17	0.0160387	-1.02	3.18E-02	-1.15	3.65E-08
SNCAIP	3.73	0.00149243	3.07	0.00E+00	3.39	2.33E-27
SNTB1	-4.49	0.00149243	-3.83	0.00E+00	-4.72	6.22E-30
SNTG2	-4.32	0.0038637	-2.61	1.00E-06	-3.69	2.23E-16
SNX19	3.9	0.00274009	2.16	1.88E-04	3.07	4.76E-10
SOAT1	-1.21	0.00149243	-1.04	2.90E-02	-1.13	0.000306
SOSTDC1	5.61	0.0077109	3.45	0.00E+00	4.72	1.76E-32
SOX21	-1.28	0.0109536	-1.07	3.57E-02	-1.16	0.000664
SOX4	-1.78	0.00149243	-1.59	4.00E-06	-1.73	3.72E-18
SPARC	4.59	0.00149243	4.08	0.00E+00	4.45	0
SPOCK3	-11.13	0.00149243	-3.51	0.00E+00	-4.88	1.04E-21
SSBP2	1.25	0.0447681	1.12	1.28E-02	1.21	0.00000766
ST18	-4.41	0.00149243	-3.68	0.00E+00	-4.06	3.15E-43
ST8SIA4	-2.87	0.00149243	-2.36	0.00E+00	-2.6	8.18E-12
STAC	-4.47	0.00149243	-3.1	0.00E+00	-3.91	2.03E-24
STX18	-1.34	0.00149243	-1.26	1.61E-03	-1.37	8.25E-08
SULF1	3.95	0.00149243	2.86	0.00E+00	3.53	3.20E-17
SULF2	1.72	0.00149243	1.52	5.07E-04	1.72	6.11E-15

SYT1	-5.72	0.00149243	-4.88	0.00E+00	-5.23	0
TACC1	-1.71	0.00149243	-1.51	1.30E-05	-1.64	2.65E-18
TAF4B	1.17	0.00149243	1.02	2.87E-02	1.1	0.000104
TAL1	-5.22	0.00149243	-4.25	0.00E+00	-4.79	0
TAP1	-1.86	0.00149243	-1.47	2.65E-03	-1.62	0.000113
TBC1D23	-1.31	0.00149243	-1.11	2.15E-02	-1.2	0.000663
TBX5-AS1	-1.32	0.0219152	-1.12	1.32E-02	-1.21	0.0000448
TCEAL2	-4.85	0.00149243	-3.18	0.00E+00	-3.99	1.93E-20
TCEAL8	-14.97	0.00149243	-6.2	0.00E+00	-7.32	0
TCF24	-2.45	0.00149243	-1.89	6.80E-05	-2.12	5.17E-07
TDGF1	1.46	0.0226048	1.23	2.29E-02	1.47	1.97E-10
TENM1	2.24	0.00149243	1.96	0.00E+00	2.1	7.25E-13
TFDP2	1.4	0.00149243	1.25	7.80E-04	1.36	1.56E-13
THBS1	4.7	0.00149243	3.68	0.00E+00	3.89	7.03E-20
TLL1	-9.07	0.00149243	-2.75	0.00E+00	-4.33	2.42E-16
TM4SF1	-1.52	0.00687371	-1.26	1.51E-02	-1.45	2.99E-07
TMC5	-2.38	0.00149243	-2.16	6.60E-05	-2.93	1.72E-16
TMEFF2	-1.82	0.00149243	-1.48	9.44E-04	-1.68	8.87E-10
TMEM155	9.37	0.00149243	1.59	1.33E-02	3.65	2.87E-11
TMEM169	2.5	0.00149243	1.76	1.63E-03	2.28	4.89E-12
TMEM200A	-5.39	0.00149243	-3.72	0.00E+00	-4.62	1.53E-34
TMEM35	1.73	0.00274009	1.37	9.03E-03	1.63	3.68E-10
TMEM47	-3.21	0.00149243	-2.61	0.00E+00	-2.71	6.62E-11
TMTC1	6.14	0.00149243	5.35	0.00E+00	5.64	0
TNFRSF21	-1.54	0.00938137	-1.28	1.48E-02	-1.49	2.28E-09
TNFSF10	-2.91	0.00149243	-1.61	1.53E-02	-2.2	0.0000337
TNIK	1.83	0.00488984	1.55	7.00E-05	1.74	4.12E-18
TP53INP1	-1.58	0.0101596	-4.73	0.00E+00	-5.87	4.33E-35
TPM2	5.28	0.00149243	3.36	0.00E+00	3.98	8.54E-19
TRDN	-4.2	0.00149243	-2.11	3.58E-04	-3.34	1.04E-12
TRIM24	1.18	0.00149243	1.05	1.22E-02	1.15	1.20E-07
TRIM7	-1.62	0.0173329	-1.36	1.21E-02	-1.63	1.73E-11
TRIML2	2.95	0.00149243	2.55	0.00E+00	2.8	8.36E-27
TRPC4	-5.35	0.00149243	-3.32	0.00E+00	-4.12	2.50E-18
TRPM6	3.03	0.00149243	2.37	0.00E+00	2.73	8.34E-16
TSC1	1.16	0.0038637	0.98	2.98E-02	1.05	0.000197
TSHZ1	-1.94	0.0077109	-1.38	2.84E-02	-1.74	3.99E-07
TSPAN7	-3.59	0.0077109	-1.63	1.55E-02	-2.7	3.65E-08
TXLNB	1.98	0.00853121	1.36	4.46E-02	1.77	0.00000278
UACA	1.86	0.00149243	1.62	4.60E-05	1.72	1.73E-07
UGT2B4	10.71	0.00149243	2.85	0.00E+00	4.63	4.71E-20
UNC79	-3.23	0.00149243	-2.31	3.00E-06	-2.92	8.13E-20
UNG	1.4	0.00149243	1.24	8.72E-04	1.36	1.37E-14
VCAN	3.84	0.00149243	3.38	0.00E+00	3.55	1.09E-33
VEGFC	2.67	0.00149243	2.04	3.00E-05	2.43	1.34E-11

VGLL3	1.69	0.00149243	1.36	7.80E-03	1.45	0.000751
VIM	1.69	0.00149243	1.51	6.00E-06	1.64	1.34E-18
VIT	3.71	0.00149243	2.39	6.00E-06	2.64	8.11E-07
VSNL1	3.07	0.00149243	2.36	7.00E-06	3.11	4.84E-16
WIPI1	3.24	0.00149243	2.67	0.00E+00	2.99	2.06E-21
YPEL5	1.19	0.00488984	1.03	2.13E-02	1.2	0.00152
ZBTB20	-2.14	0.00149243	-2.05	0.00E+00	-1.87	3.28E-12
ZEB1	1.62	0.00149243	1.41	1.04E-03	1.49	0.0000238
ZMAT4	-3.8	0.0186365	-1.45	4.25E-02	-2.8	1.05E-07
ZNF365	-3.18	0.00149243	-1.53	2.89E-02	-2.52	7.07E-08
ZNF426	-6.37	0.00149243	-4.94	0.00E+00	-5.55	0
ZNF440	2.61	0.00149243	2.11	1.00E-06	2.3	1.09E-09
ZNF532	2.29	0.00149243	1.73	6.96E-04	2.13	1.05E-12
ZNF544	-5.27	0.00149243	-6.13	0.00E+00	-7.14	0
ZNF788	-4.56	0.00149243	-2.25	8.80E-05	-3.06	2.67E-08
ZYG11A	1.75	0.00149243	1.51	1.26E-04	1.66	5.96E-12

Annex 3. GSEA analysis of RNA-seq data of MNT KO *versus* WT HAP1. The pathways with a p-value <0.05 are shown in the table.

KEGG PATHWAYS					
NAME	**SIZE**	**ES**	**NES**	**NOM p-value**	**FDR q-value**
Bladder cancer	42	0.54	1.43	0	1.00
P53 signaling pathway	68	0.42	1.38	0	1.00
O-glycan_biosynthesis	27	0.44	1.33	0	1.00
Protein export	23	0.40	1.31	0	1.00
Melanoma	71	0.42	1.29	0	1.00
Ascorbate and aldarate metabolism	25	0.42	1.26	0	0.80
Regulation of autophagy	34	0.41	1.22	0	0.81
Steroid hormone biosynthesis	55	0.37	1.21	0	0.77
RNA degradation	57	0.35	1.18	0	0.90
Drug metabolism cytochrome p450	72	0.36	1.17	0	0.79
Pantothenate and coA biosynthesis	16	-0.69	-1.64	0	0.12
Nitrogen metabolism	23	-0.60	-1.58	0	0.10
Proximal tubule bicarbonate reclamation	23	-0.60	-1.55	0	0.13
Maturity onset diabetes of the young	25	-0.70	-1.54	0	0.11
Type I diabetes mellitus	43	-0.66	-1.50	0	0.15
Leishmania infection	72	-0.46	-1.42	0	0.30
Long term depression	70	-0.42	-1.41	0	0.28
Asthma	30	-0.68	-1.38	0	0.31
Cell adhesion molecules cams	133	-0.40	-1.35	0	0.37
Cytokine cytokine receptor interaction	260	-0.40	-1.32	0	0.42
Hematopoietic cell lineage	87	-0.47	-1.32	0	0.39
Glycosphingolipid biosynthesis lacto and neolacto series	26	-0.46	-1.32	0	0.38
Allograft rejection	37	-0.67	-1.29	0	0.44
Neuroactive ligand receptor interaction	272	-0.39	-1.27	0	0.44
Leukocyte transendothelial migration	116	-0.37	-1.26	0	0.43
Autoimmune thyroid disease	52	-0.50	-1.22	0	0.49
C2 REACTOME PATHWAYS					
NAME	**SIZE**	**ES**	**NES**	**NOM p-value**	**FDR q-value**
NaCl dependent neurotransmitter transporters	17	0.71	1.65	0	0.15
Signaling by robo receptor	29	0.52	1.64	0	0.1
Amine compound SLC transporters	27	0.60	1.63	0	0.16
Darpp 32 events	24	0.56	1.57	0	0.29
Synthesis of bile acids and bile salts via 7alpha hydroxycholesterol	15	0.61	1.54	0	0.34
Adherens junctions' interactions	27	0.55	1.53	0	0.35
Metabolism of non-coding RNA	48	0.48	1.50	0	0.38
Insulin synthesis and processing	20	0.54	1.46	0	0.49
Destabilization of mRNA by tristetraprolin TTP	17	0.51	1.44	0	0.52
Collagen formation	58	0.46	1.44	0	0.48
Destabilization of mRNA by BRF1	17	0.51	1.39	0	0.66

G0 and early G1	23	0.42	1.38	0	0.67
Signaling by FGFR mutants	43	0.47	1.35	0	0.79
Unblocking of NMDA receptor glutamate binding and activation	15	0.49	1.32	0	0.87
Amine derived hormones	15	0.56	1.30	0	0.91
Regulation of glucokinase by glucokinase regulatory protein	27	0.39	1.29	0	0.89
PI3K cascade	68	0.35	1.29	0	0.85
Fatty acyl coA biosynthesis	18	0.41	1.29	0	0.87
NEP/NS2 interacts with the cellular export machinery	27	0.41	1.25	0	0.83
Triglyceride biosynthesis	38	0.43	1.24	0	0.82
Transport of mature mRNA derived from an intronless transcript	32	0.38	1.18	0	0.89
Nuclear signaling by ERBB4	38	-0.60	-1.65	0	0.15
Tight junction interactions	29	-0.59	-1.62	0	0.14
Transport of vitamins nucleosides and related molecules	31	-0.58	-1.60	0	0.22
Interferon gamma signaling	60	-0.60	-1.60	0	0.19
Regulation of beta cell development	30	-0.61	-1.60	0	0.22
Ion channel transport	54	-0.57	-1.56	0	0.24
Netrin1 signaling	38	-0.51	-1.53	0	0.27
Ion transport by P-type ATPases	33	-0.59	-1.51	0	0.30
Gap junction assembly	18	-0.78	-1.49	0	0.35
Glutamate neurotransmitter release cycle	15	-0.54	-1.48	0	0.36
Apoptotic cleavage of cellular proteins	39	-0.43	-1.45	0	0.42
Semaphorin interactions	65	-0.47	-1.44	0	0.42
Neurotransmitter release cycle	34	-0.59	-1.42	0	0.48
The role of NEF in HIV1 replication and disease pathogenesis	27	-0.53	-1.40	0	0.52
Ligand gated ion channel transport	21	-0.57	-1.39	0	0.59
Peptide ligand binding receptors	183	-0.42	-1.39	0	0.56
Ca-dependent events	29	-0.59	-1.38	0	0.54
Integrin alphaIIb beta3 signaling	27	-0.54	-1.38	0	0.52
Gap junction trafficking	27	-0.60	-1.38	0	0.52
Amine ligand binding receptors	37	-0.45	-1.37	0	0.52
PKA-mediated phosphorylation of CREB	17	-0.61	-1.36	0	0.52
Other semaphorin interactions	15	-0.64	-1.35	0	0.56
Incretin synthesis secretion and inactivation	20	-0.53	-1.35	0	0.56
Membrane trafficking	124	-0.36	-1.34	0	0.55
Striated muscle contraction	27	-0.54	-1.32	0	0.62
Nitric oxide stimulates guanylate cyclase	25	-0.48	-1.31	0	0.61
A tetrasaccharide linker sequence is required for GAG synthesis	25	-0.63	-1.30	0	0.68
G alpha q signalling events	180	-0.36	-1.29	0	0.68
Platelet aggregation plug formation	36	-0.47	-1.29	0	0.65
Class A1 rhodopsin like receptors	295	-0.34	-1.22	0	0.80
GPCR ligand binding	396	-0.34	-1.21	0	0.81
Platelet homeostasis	76	-0.38	-1.20	0	0.80
Degradation of the extracellular matrix	29	-0.58	-1.13	0	0.79

C2 BIOCARTA PATHWAYS					
NAME	**SIZE**	**ES**	**NES**	**NOM p-value**	**FDR q-value**
TOB1	19	0.57	1.47	0	1.0
ATM	20	0.52	1.43	0	0.84
VEGF	29	-0.58	-1.63	0	0.18
TH1TH2	19	-0.69	-1.56	0	0.29
CCR3	23	-0.54	-1.49	0	0.38
GCR	19	-0.54	-1.47	0	0.42
NO1	30	-0.42	-1.29	0	0.83
ECM	24	-0.41	-1.22	0	0.96
C2 HALLMARK PATHWAYS					
NAME	**SIZE**	**ES**	**NES**	**NOM p-value**	**FDR q-value**
UV RESPONSE DN	144	0.44	15.10	0	0.10
ANGIOGENESIS	36	0.43	13.48	0	0.13
TGF BETA SIGNALING	54	0.42	13.14	0	0.16
EPITHELIAL MESENCHYMAL TRANSITION	200	0.32	12.03	0	0.32
PANCREAS BETA_CELLS	40	-0.61	-15.03	0	0.28
IL6 JAK STAT3 SIGNALING	87	-0.47	-14.11	0	0.18
ALLOGRAFT REJECTION	200	-0.42	-12.90	0	0.49
UV RESPONSE UP	157	-0.41	-12.83	0	0.41
ANDROGEN RESPONSE	101	-0.36	-12.63	0	0.38
INTERFERON ALPHA RESPONSE	95	-0.49	-12.46	0	0.37
INTERFERON GAMMA RESPONSE	199	-0.38	-1.15	0	0.61
APOPTOSIS	161	-0.34	-11.46	0	0.56

Publications